Defining the patho-physiological roles of the receptor GPR35

Amlan Ganguly

B.Pharm (Hons), M.Pharm (Thesis)

A thesis submitted

in fulfilment of the requirements for the degree of

Doctor of Philosophy

School of Molecular Biosciences

College of Medical, Veterinary and Life Sciences

University of Glasgow

January 2024

Supervised by Professor Graeme Milligan

Abstract

G-protein-coupled receptors (GPCRs) have tremendous potential as therapeutic targets for a wide range of disorders since they mediate most of our physiological responses to hormones, neurotransmitters, and environmental stimuli. GPR35 is a rhodopsin-like class A GPCR first identified over two decades ago. Even though GPR35 is currently a poorly characterised orphan receptor, it has significant therapeutic utilities for various ailments, including fatty liver disease, inflammatory bowel problem and different malignancies.

The pharmacology of the GPR35 orthologues in humans and rodents varies significantly and in human orthologue, there are 2 isoforms that are transcribed and translated from 3 variants of the human GPR35 gene. Although the pharmacology of the two human GPR35 isoforms is similar, agonist response efficacy is significantly lower in the longer isoform compared to the shorter one. From experimental studies, it was found that amino acid cysteine at position 27 of long isoform of GPR35 (hGPR35b) acted as a dampener of hGPR35b efficacy. Mutation of this cysteine to serine resulted in the efficacy of hGPR35b being equivalent to hGPR35a. In order to gain a deeper comprehension of the function of the N-terminal extension of hGPR35b, 10 further mutants containing cysteine in place of different residues were produced in the Cys27Ser hGPR35b backbone. Based on the findings, it was clear that almost all of the mutants showed G protein activation and arrestin-3 recruitment activity almost identical to hGPR35b after cysteine was added.

For investigating the post-translational states of GPR35, novel phospho-site-specific antibodies were developed and employed. After conducting immunoblotting and immunocytochemical experiments with these phosphorylation specific antisera, it was clearly visible that these antisera acted as useful biosensors for assessing the activation status of the human and mouse orthologues of GPR35. Furthermore, these antibodies only recognised fully matured versions of GPR35 and might serve as helpful instruments for assessing target involvement in drug discovery and target validation operations.

To pinpoint the specific contribution of individual GRK in GPR35 phosphorylation, a variety of complementary techniques, such as the production of genome-edited

cell lines lacking the GRK isoforms GRK2, GRK3, GRK5, and GRK6, which are widely expressed, restoration of function using certain GRKs as well as the development and use of both selective small molecule GRK inhibitors were employed. The availability of cell lines generated from 293 lacking expression of several GRKs revealed that, whereas agonist-induced receptor-arrestin interactions were unaffected by the absence of either GRK2 or GRK3, they were nearly completely prevented by the absence of both GRK5 and GRK6. Furthermore, reconstitution investigations using individual GRK isoforms were made possible by the ΔGRK2/3/5/6 HEK293 cells, which demonstrated that GRK5 and GRK6 functioned nearly equally well. My experimental results were supported by a molecular level and mechanistic investigation that used the 'Alphafold' deep learning algorithm and revealed that GRK5 and GRK6 interacted with hGPR35a more strongly and effectively than GRK2 and GRK3. Upon comparing the efficacies of GRK2/3 blockers and GRK5/6 inhibitors, it was clearly evident that agonist-induced interactions between human GPR35a and arrestin-2 or arrestin-3, as well as the identification of agonist-mediated phosphorylation of the human and mouse orthologue in immunoblotting and immunocytochemistry investigations, were effectively inhibited by GRK5/6 blockers. For further ensuring the predominant contribution of GRK5/6, hGPR35a phosphorylation was conducted in ΔGRK2/3/5/6 293 cells with transient introduction of GRK2/3/5/6. Immunoblotting using anti-hGPR35a $pSer^{300}$-$pSer^{303}$ revealed that the presence of GRK5 and, in particular, GRK6 increased the phosphorylation of these sites, but GRK2 and GRK3 had no appreciable impact.

Finally, the luciferase-based complementation assay also demonstrated that GRK5 and GRK6 could interact with GPR35 in a significant way, thereby supporting my recent findings.

In conclusion, the outcome of this thesis provides a clear insight into the isoform variation in human orthologues of GPR35. Moreover, this research project gives a clear idea about the phosphorylation and indeed, regulation of GPR35, a receptor that is currently gaining a lot of attention as a potential new therapeutic target for conditions like ulcerative colitis, inflammatory bowel diseases, fatty liver diseases, and different cancers. The outcomes of this research project will

certainly aid in the discovery of novel therapeutics targeting the orphan receptor GPR35.

Table of Contents

Contents

List of Tables

List of Figures

Acknowledgement

First and foremost, I would like to give the Almighty my sincere appreciation for enabling me to complete this research project and finally write up the outcome thesis in order to earn the degree of Doctor of Philosophy in Molecular Pharmacology.

I am very much grateful to my erudite supervisor, **Prof Graeme Milligan**, for his excellent supervision, constant encouragement, sympathetic cooperation, constructive criticism as well as enthusiastic guidance at all stages of this thesis work. I am again thankful to him for providing me all the cutting-edge facilities in the amazing lab at the Advanced Research Centre (ARC) of the University of Glasgow to carry out the research work.

I would also like to thank my supervisor, **Dr. Brian Hudson**, for his aid with arranging experiments, technical support, advice on BRET based investigations and criticism of both my research efforts and thesis.

I express my deepest sense of appreciation and respect to **Prof Andrew B Tobin** for his thoughtful suggestions and appreciation during lipid meeting and weekly lab meeting.

It gives me immense pleasure to express sincere appreciation and gratefulness to **Dr. Tezz Quon.** I have learnt a lot from Tezz regarding experimental techniques, fundamental of cloning and molecular biology, data analysis and also writing. I have always enjoyed scientific discussion and future direction of experiments with Tezz.

I am also very much grateful to **Laura Jenkins** for her excellent training in cell culture, BRET assay, western blot, immunocytochemistry. Without the help of Laura, it would not be possible for me to learn the techniques and conduct the laboratory experiments.

I am also thankful to **Dr Sara Marsango**, **Dr. Li Chuing Lin**, **Dr John Pediani**, **Dr. Richard Ward, Dr. Natasja Barki** for their constant support and help. I would also

like to thank all my friends in the lab, **Yueming Li**, **Pietro Cocchiara**, **Domonkos Dedeo** for their support and make the lab environment enjoyable.

My family has played a significant role in my professional development. I remember my father, **Prithwish Kumar Ganguly**, who loved me more than himself. He is nor more in the world, but I believe, only because of his blessing, I was able to do research in a foreign country. I am highly grateful to my mother **Madhabi Rani Chanda**, who has sacrificed a lot for me during my PhD journey and is waiting for my early return. I always like to thank my wife **Mowsume Bhattacharjee**, for constantly encouraging me throughout the long PhD time.

Last but not the least, I want to thank the Commonwealth Scholarship Commission (CSC) for funding my PhD and the University of Glasgow to carry out my research in a modern well-equipped laboratory.

Amlan Ganguly

Author's Declaration

"I declare that, except where explicit reference is made to the contribution of others, this thesis is the result of my own work and has not been submitted for any other degree at the University of Glasgow or any other institution."

Signature

Printed name: Amlan Ganguly

Definitions/Abbreviations

AP-2	Adaptor protein 2
Arr	Arrestin
BRET	Bioluminescent resonance energy transfer
BSA	Bovine serum albumin
C-terminus	Carboxy terminus
DAPI	4´, 6-diamidino-2-phenylindole
DMSO	Dimethyl sulfoxide
dNTP	Deoxynucleoside triphosphate
DNA	Deoxyribonucleic acid
DMEM	Dulbecco's modified eagle's medium
Dox	Doxycycline
ECL	Extracellular loop
$EC_{50/80}$	Effective concentration at 50/80% maximal response
EDTA	Ethylenediamine tetraacetic acid
ELISA	Enzyme-linked immunosorbent assay
ERK	Extracellular signal-regulated kinase
eYFP	Enhanced yellow fluorescent protein
FBS	Fetal bovine serum
FDA	Food and Drug Administration
G protein	Guanine nucleotide-binding protein
GDP	Guanosine diphosphate
GPCR	G protein-coupled receptor
GPR35	G protein-coupled receptor 35
GRK	G protein-coupled receptor kinase
GTP	Guanosine 5´- triphosphate
GWAS	Genome-wide association study
Gαi	Gα inhibitory
Gαs	Gα stimulatory
H	Human
HA	Haemagglutinin
HEK 293	Human embryonic kidney
IBD	Inflammatory bowel disease

ICL	Intracellular loop
LB	Luria Bertani
LPA	Lysophosphatidic acid
M	Mouse
MAPK	Mitogen-activated protein kinase
mRNA	Messenger ribonucleic acid
N-terminus	Amino terminus
PBS	Phosphate-buffered saline
PDE5	cGMP-specific phosphodiesterase type 5
PCR	Polymerase chain reaction
PDM	Phosphorylation-deficient mutant
PFA	Paraformaldehyde
PKA	cAMP-dependent protein kinase
PKC	Protein kinase C
PSC	Primary sclerosing cholangitis
PTx	Bordetella pertussis Toxin
qRT-PCR	Quantitative real-time polymerase chain reaction
RGS	Regulators of G protein signalling
Rluc	Renilla luciferase
RNA	Ribonucleic acid
RPM	Revolutions per minute
SDS-PAGE	Sodium dodecyl sulphate polyacrylamide gel electrophoresis
SNP	Single nucleotide polymorphism
TMD	Transmembrane Domain
TBST	Tris-buffered saline (TBS) Tween
UV	Ultraviolet
WT	Wild type

List of Publications

Quon, T., Lin, L.C., **Ganguly, A**., Tobin, A.B. and Milligan, G., 2020. Therapeutic opportunities and challenges in targeting the orphan G protein-coupled receptor GPR35. ACS Pharmacology & Translational Science, 3(5), pp.801-812.

Divorty, N., Jenkins, L., **Ganguly, A**., Butcher, A.J., Hudson, B.D., Schulz, S., Tobin, A.B., Nicklin, S.A. and Milligan, G., 2022. Agonist-induced phosphorylation of orthologues of the orphan receptor GPR35 functions as an activation sensor. Journal of Biological Chemistry, 298(3).

Ganguly, A., Quon, T., Jenkins, L., Joseph, B., Al-awar, R., Chevigne, A., Tobin, A.B., Uehling, D.E., Hoffmann, C., Drube, J and Milligan, G., 2023. G protein-receptor kinases 5/6 are the key regulators of G protein-coupled receptor 35-arrestin interactions, Journal of Biological Chemistry, 299(10).

Abstracts:

Pharmacology 2022, British Pharmacological Society annual meeting, September 2022.

Investigation of the pharmacology of the two isoforms of human GPR35. **Amlan Ganguly**, Tezz Quon, Amanda E. Mackenzie, Graeme Milligan. (Poster communication)

6th ERNEST meeting, March 2022.

The role of disulphide bonds in the extracellular domain of isoforms of human GPR35. **Amlan Ganguly**, Tezz Quon, Amanda E. Mackenzie, Graeme Milligan. (Poster communication)

Chapter 1 Introduction

1.1 G protein-coupled receptors

The G protein-coupled receptor (GPCR) superfamily of cell surface proteins represent the largest family of transmembrane receptors and currently serve as the target for nearly 30% of all Food and Drug Administration approved small molecule drugs (Sriram and Insel, 2018) (Santos et al., 2017). GPCRs are membrane bound receptors that respond to a variety of stimuli including hormones, odorants, pheromones, peptides, chemokines, metabolites, neurotransmitters, ions (Lefkowitz, 2007) and transduce these extracellular signals into cellular response through effector proteins. GPCRs have thus been the subject of significant research for many years and play crucial roles in a wide variety of physiological functions. The seven-transmembrane α-helical fold shared by members of the GPCR family gives it its distinctive appearance, and the transmembrane bundles of family members are quite similar. Other structural characteristics include an extracellular domain consisting of the N-terminal region and three flexible extracellular loops (ECLs) and an intracellular domain consisting of three intracellular loops (ICLs) and a C-terminal tail. These highly fluctuating areas contribute significantly to the ligand-binding and signalling selectivity of each receptor (Katritch et al., 2012).

According to research, the gene families that code for GPCRs were present in the last common eukaryotic ancestor around 1.2 billion years ago, providing evidence of the ancient roots of GPCR superfamily (Gurevich and Gurevich, 2008, De Mendoza et al., 2014). About 800 receptors have been identified in the human genome as a result of the evolution of GPCRs from a common ancestor, making GPCRs the largest family of cell membrane receptors (Fredriksson et al., 2003, Venter et al., 2001).

The binding complex between GPCR and ligands experiences significant alterations in conformation during activation to enable a heterotrimeric G-protein coupling, that in turn influences a variety of intracellular signalling pathways, having an impact on physiology. Since pharmacological modification of GPCRs can be used to modify GPCR regulation, activation, and downstream signalling in both health and illness, these receptors are often considered effective therapeutic targets in a range of clinical illnesses. So, it should come as no surprise that GPCR research remains a key component in translational medicine initiatives. In order

to achieve this, many 'druggable' GPCRs exist, and clinical medicine frequently makes use of ligands that either block or activate the receptor.

1.1.1 GPCRs in drug discovery

GPCRs and their ligands are frequently associated with pathophysiology and disease as a result of their widespread use in physiological processes. This makes the family a valuable source of therapeutic targets, together with their accessibility to the cell membrane (Rask-Andersen et al., 2011). The transmembrane characteristics of GPCRs also make them appropriate pharmacological targets since drugs do not need to cross the plasma membrane to reach their receptors (Sriram and Insel, 2018). It should therefore not be astonishing that many drug research programmes continue to focus on GPCRs.

Though GPCRs are the most useful targets for therapeutic molecules, the majority of approved drugs only target a small subset of the GPCR family, which includes the histamine H1 receptor, the 5-HT_{2A} serotonin receptor, the M1, M2, and M3 muscarinic receptors, the α_{1A} and α_{2A} adrenergic receptors, and the dopamine D_2 receptor (Garland, 2013). Less than one third of the 365 non-olfactory GPCRs are now used as pharmacological targets. More than 120 of these GPCRs are orphans, meaning they do not yet have a corresponding endogenous ligand associated with them (Alexander et al., 2015). These orphan receptors frequently have unclear physiological roles and are poorly characterised. However, many orphan GPCRs are assumed to have important therapeutic roles due to the significance of GPCR signal transduction in various physiological processes. Therefore, these receptors constitute a reservoir of previously untapped prospective therapeutic targets, and continuous research efforts are being made to deorphanise these receptors and define their roles in various diseases.

A ‘classical pharmacology’ ligand-based strategy was historically used to identify GPCR drug targets. In this technique, lead compounds were made by extracting physiologically active molecules, such as from tissue extracts, and using them to assist in discovering targets. This tactic was used on some of the most successful therapeutic GPCR targets, like the ß-adrenergic receptors, which ß blockers later targeted once it was established in 1948 that they were adrenaline receptors (Wachter and Gilbert, 2012). However, due to improvements in homology

screening methods and the subsequent publishing of the human genome database, substantial pool of orphan receptor targets came into existence, and a new approach to drug development was evolved (Lander, 2011). The goal of 'reverse pharmacology' is to identify the receptor target initially and then test for endogenous and artificial ligands using the cloned receptor (Lecca and Abbracchio, 2008). The pharmacological characteristics and biological role of the receptor can then be studied using these tool molecules (Kolar et al., 2017). The reverse pharmacology approach has also aided in discovering new endogenous ligands and yet-to-be-identified transmitter systems, such as identifying orexins and their receptors as regulators of wakefulness and appetite (Sakurai et al., 1998). Following on from these early successes, the technique continues to yield potential new pharmacological targets, such as the free fatty acid receptor 1 (FFA1), previously the orphan GPR40, which is now a sought-after therapeutic target in type 2 diabetes (Li et al., 2016).

Understanding an orphan GPCR's coupling and signalling patterns is helpful when creating screening assays for deorphanisation. Successful deorphanisation and surrogate ligand screenings have been achieved using G protein and second messenger activity tests such as guanosine triphosphate (GTP)-γS, cyclic adenosine monophosphate (cAMP), and intracellular calcium ($[Ca^{2+}]$ i) assays (Jenkins et al., 2010). Elements of the cycle of desensitisation and internalisation have also been utilised in screening attempts, specifically the translocation of the adaptor protein arrestin (Neetoo-Isseljee et al., 2013). In order to appropriately interpret screens for orphan receptors, it is crucial to comprehend how these mechanisms differ among GPCRs.

Now a days, modern technology is being used to deorphanise poorly characterised receptors by using the reverse pharmacology concept. A recent increase in high-quality crystal structures has made it possible to perform in silico homology modelling, which, when combined with virtual screening is an effective way to find artificial ligands for orphan receptors that have little or no molecules available to study their function (Ngo et al., 2016). Using this technique, very effective synthetic 'surrogate' ligands for orphan receptors like GPR17 have been discovered., which is thought to be a potential target for neurodegenerative illness (Eberini et al., 2011).

1.1.2 GPCR structure

GPCRs typically span the surface of almost all eukaryotic cells and are located within the lipid-rich plasma membrane in their inactive state. The relatively hydrophobic transmembrane domains (TMDs) of GPCRs are structurally stabilised by these conditions. Both extracellular domains and the transmembrane helices' structural design offer adaptable spaces for GPCR ligand attachment. Extracellular and intracellular loops (E/ICL) that cross the cell membrane link the seven helices (Kobilka, 2007). Within the seven transmembrane helices and connecting loops, the core area is bounded by an intracellular carboxyl (C)-terminus and an exterior amino (N)-terminus (Figure 1.1). Sequence alignments show that the C and N-termini, together with the third intracellular loop between the fifth and sixth TMDs, are the most variable areas (Kobilka, 2007). The length and function of GPCR termini can vary, and they are frequently an indication of the classification of GPCR.

Several highly conserved sections within the TMDs have also been identified by analysis of the GPCR protein structure, and as anticipated from such conservation, these regions are crucial for receptor shape and function (Teller et al., 2001). The key "DRY" motif is perhaps the most well-known of these. This amino acid sequence, also known as glutamic acid/aspartic acid-arginine-tyrosine (i.e., E/DRY), is found at the intersection of the bottom of the third TMD and second ICL of the "rhodopsin-like" family of GPCRs (Ballesteros et al., 1998). Due to its remarkable conservation, scientists have looked into its structural and functional characteristics inside GPCRs, and the data clearly suggests that it plays a crucial role in the regulation of G-protein coupling, constitutive activity, and conformational stability (Rovati et al., 2007). An unprecedented improvement in knowledge of the organisational structure of GPCR family members has been made possible by recent rapid advancements in the capacity to acquire the atomic-level X-ray structures of individual GPCRs and stabilise them.

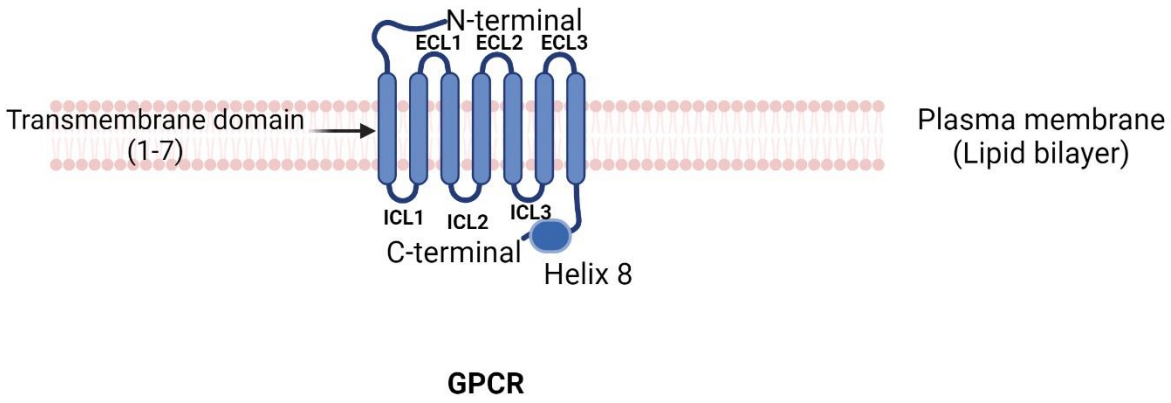

Figure 1.1 A distinctive membrane-spanning structural motif of a G protein-coupled receptor GPCRs are membrane-integral proteins that share a seven-alpha-helical structural domain motif. Along with having seven α-helical, hydrophobic transmembrane (TM) domains, the GPCR structure is connected by a series of three extracellular loops (ECl 1-3) and three intracellular loops (ICL 1-3), which are bordered by an extracellular amino (N) terminus and an intracellular carboxyl (C) terminus. Helix 8 lies parallel to the cytoplasmic membrane surface and connects the membrane domain of the receptor with its C-terminal tail. This figure was created with BioRender.com.

1.1.3 GPCR subfamily classification

Even though numerous acknowledged techniques for categorising GPCRs based on evolutionary and sequence preservation are employed here, the two most accepted techniques are employed here. Initially, functional characteristics and sequence are used to categorise six classes of GPCR, designated as class A through class F (Attwood and Findlay, 1994). Class A refers to the 'rhodopsin-like' family of receptors and it is the most prevalent subgroup. Class B includes the adhesion and secretin receptors, and class C accommodates the metabotropic glutamate receptors, γ-aminobutyric (GABA) receptors, calcium sensing receptors and a family of taste receptors. Class C receptors in rodents also include pheromone receptors for taste type 1 and vasopressin (V2) which are absent in humans (Alexander et al., 2019). The final class of receptors to exist in humans is class F, the frizzled/smoothened family of GPCRs. Class D and class E consist of the fungal pheromone and cyclic adenosine monophosphate (cAMP) receptors, respectively, possessing a sequence sufficiently different to be considered separate classes of receptor family than the class A (Attwood and Findlay, 1994).

Another approach to GPCR classification, known as the GRAFS system, has evolved over time. After phylogenetic sequencing of the human genome, this method separates receptors into five classes based on a phylogenetic tree: glutamate (G), rhodopsin (R), adhesion (A), frizzled/taste2 (F), and secretin (S) (Figure 1.2).

There is very little to no sequence homology among these five groupings (Fredriksson et al., 2003). Recently, this technique proved successful in separating secretin from adhesion GPCRs, which were both classified as class B in the previous classification scheme. The GRAFS system, which is now the most widely used system, will be utilised throughout my thesis.

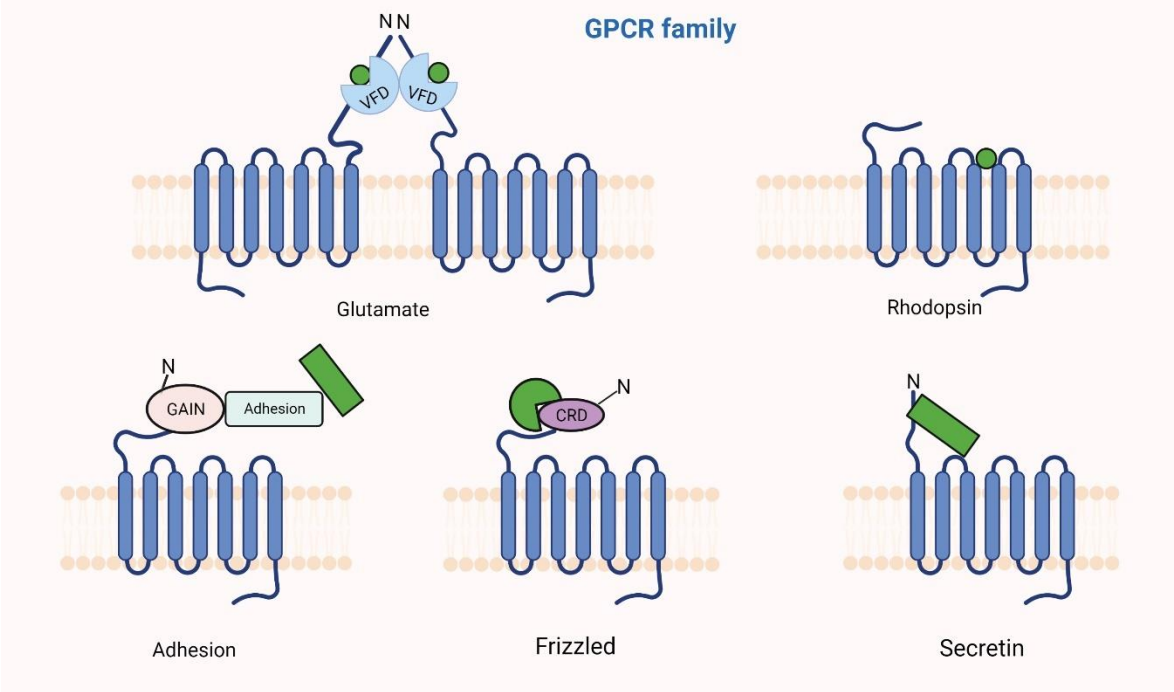

Figure 1.2 Classification of G protein coupled receptors based on structural similarities
GPCRs have a common structure consisting of seven α-helical transmembrane domains, intracellular C-terminus that is relatively conserved, and an extracellular N-terminus which is highly diverse. Glutamate receptors exist as constitutive dimers and possess a large Venus flytrap domain (VFD) in the N-terminus to facilitate ligand binding. Conversely, Rhodopsin-like receptors have a small N-terminus as the ligand binding pocket lies deep within the seven transmembrane domains. Adhesion GPCRs feature a GPCR autoproteolysis-inducing (GAIN) domain which acts to catalyse the N-terminus permitting non-covalent association of the adhesion domain, to which ligands bind. Frizzled receptors contain cysteine-rich domains (CRD) to enable ligand binding, whereas ligands bind to secretin receptors via hormone peptide binding domains within long N-terminus. Green shapes represent the modes of ligand interaction with each receptor subtype. This figure was created with BioRender.com.

At least 140 of the 800 GPCRs found in mammalian systems are orphan receptors (Levoye et al., 2006). These receptors are a subset of GPCRs that lack classification because their activating ligands are unknown. When endogenous ligands are found, generally through cell signalling assays, orphan receptors are deorphanised. This is accomplished either by comparing the function and sequence to receptors that have already undergone this process or by looking at the expression correlations between the receptor and ligand (Tang et al., 2012).

Characterising orphan GPCRs is crucial because they might serve as therapeutic and pharmacological targets.

1.1.4 Structural characteristics of GPCR subfamily

According to structural research, the N-terminal domains and various ligand binding compartments are the most significant points of differences within receptor subfamilies. To enable various ligand binding modalities, the seven transmembrane domains also take on distinct conformations in various receptors (Basith et al., 2018, Zhang et al., 2015).

The Venus flytrap domain (VFD) is a large extracellular domain found on glutamate receptors that houses the orthosteric ligand binding pocket to the TMDs (Kunishima et al., 2000). In all receptors in this family except for the $GABA_B$ receptor, a cysteine rich domain (CRD) connects the VFDs to the TMDs. The rhodopsin-like receptor family consists of 719 members, making up 80% of all GPCRs; structurally, this family possesses the typical seven TMDs forming a ligand binding pocket in addition to an eighth helix with an apalmitoylated cysteine at the C terminal tail (Hu et al., 2017, Yang et al., 2021). Adhesion receptor family members own a long extracellular N terminus with a conserved region close to TMD1 playing a permissive role in ligand binding; this region constitutes two components: a region rich in serine and threonine residues, and an integrated GPCR autoproteolysis-inducing (GAIN) domain contains a GPCR proteolysis site (GPS) (Harmar, 2001, Prömel et al., 2013). The frizzled/taste2 receptor family controls cell proliferation and fate during development through the mediation of signals from secreted glycoproteins called Wnt, binding to conserved cysteine residues on the N-terminus (Fredriksson et al., 2003). The secretin family of receptors encompass 15 receptor subtypes in humans, with the ligands being polypeptide hormones such as glucagon, secretin and glucagon-like peptides (Harmar, 2001). The N-terminus contains conserved residues key for ligand binding to the receptor (Fredriksson et al., 2003).

1.1.5 GPCR crystallisation

Massive efforts have been made to obtain the atomic structures of GPCRs in both their active (R*) and inactive (R) states in order to better understand the links

between GPCR structure and function. These structures offer a lot of information regarding the crucial residues that regulate GPCR flexibility, facilitating the conformational changes that take place when the ligand is bound, the receptor is activated, and then G-protein coupling occurs (Nakamura et al., 2013). Since the discovery of the crystal structure of the first GPCR, bovine Rhodopsin, (Palczewski et al., 2000) more than 20 years ago, a growing body of structural data regarding class A receptors has become accessible (Stevens et al., 2013). Included in this are the high-resolution structural identities of the $ß_2$AR in 2007 and the CXCR4 chemokine receptor in 2010 (Rasmussen et al., 2007, Wu et al., 2010). Despite this progress, early attempts to trap the GPCR in an active state were frequently unsuccessful due to the activated GPCR's conformational instability within a lipid-rich, hydrophobic membrane (Kobilka, 2007, Kobilka and Schertler, 2008). However, with the creation of highly specific antibodies and GPCR stabilising ligands, this has been improved remarkably (Maeda and Schertler, 2013). In 2011, the first descriptions of the agonist-bound, active states of the $ß_2$AR, A_{2A}-adenosine, and rhodopsin receptors were published (Rasmussen et al., 2011, Standfuss et al., 2011). These findings offered highly desired comparative structural information about the basic conformational status, ligand selectivity, and conserved domains that are crucial for amplifying the R* state of rhodopsin-like/class A GPCRs (Maeda and Schertler, 2013). The two leading experts in this subject, Professors Brian Kobilka and Robert Lefkowitz, won the 2012 Nobel Prize in Chemistry for their outstanding contributions to GPCR research, which is the most significant achievement.

1.2 GPCR signalling

1.2.1 GPCR activation

GPCRs are vital for maintaining homeostasis by controlling a variety of physiological signalling activities. They are also crucial for triggering responses to pathogenic stimuli in the extracellular environment. In the case of Class, A GPCRs, the signal is started when a ligand binds to the orthosteric binding site, which is a binding pocket inside the helix bundle. Significant conformational changes are brought about by the ligand binding in both the intracellular domain and the transmembrane helix bundle. Crystal structures of the ligand-bound rhodopsin, $ß_2$ adrenergic receptor have demonstrated that these modifications are shared by all

Class A GPCRs (Rasmussen et al., 2011). The intracellular domain of the receptor can be translocated to and bound to by cytoplasmic effector proteins, which then controls the signalling cascades within cells.

1.2.2 G protein-mediated signalling

It is currently understood that GPCR signalling is a complex network regulated by a variety of variables and feeding into a vast array of effector pathways. The heterotrimeric G proteins, the first of these effectors to be characterised, are, however, where the superfamily derives its name. The majority of GPCRs primarily use this family of guanine nucleotide-binding proteins as signalling effectors in the cytoplasm. When they are inactive and bound to GDP, their α, ß, and γ subunits combine to form a heterotrimeric complex. Lipid modifications on the α and γ subunits serve as the complex's anchors to the plasma membrane (Vögler et al., 2008). After the ligand binds to the GPCR and stabilises its active state, the Gα subunit connects to the intracellular domain of the receptor. Gα binds to the cytoplasmic ends of transmembrane helices 5 and 6 in the case of Class A GPCRs (Rasmussen et al., 2011). As a result, the Gα subunit undergoes a conformational shift that enhances GDP/GTP exchange, activating the G protein and enabling the Gα subunit to separate from the receptor and the ßγ dimer (Chung et al., 2011). When both the Gα and Gßγ subunits are active, they can control their own signalling pathways via a variety of second messengers until the Gα subunit's intrinsic GTPase activity hydrolyses GTP into GDP (Sprang et al., 2007). This ends the signal and permits the inactive heterotrimer to reassociate. A family of GTPase activating proteins known as regulators of G protein signalling (RGS), which mediates early termination of the signal, can quicken the GTPase activity of Gα (Woodard et al., 2015). This GDP/GTP cycle can be used to repeatedly activate and deactivate G proteins until either desensitisation mechanisms prevent additional Gα protein binding or ligand dissociation puts the GPCR back in its inactive state. Each of the α, ß, and γ isoforms of the G protein family has a distinct downstream signalling profile and tissue distribution (Wettschureck and Offermanns, 2005). G proteins can interact with a variety of GPCRs, while GPCRs can engage in interactions with a variety of G family members thereby making the GPCR biology more complex. Therefore, the signalling response to a stimulus in each individual cell is dependent on the availability of the GPCR, its interacting G protein subunits, and

their cytoplasmic effector proteins. The Gα protein family can be divided into several subfamilies, each of which has a distinctive signalling profile (Figure 1.3).

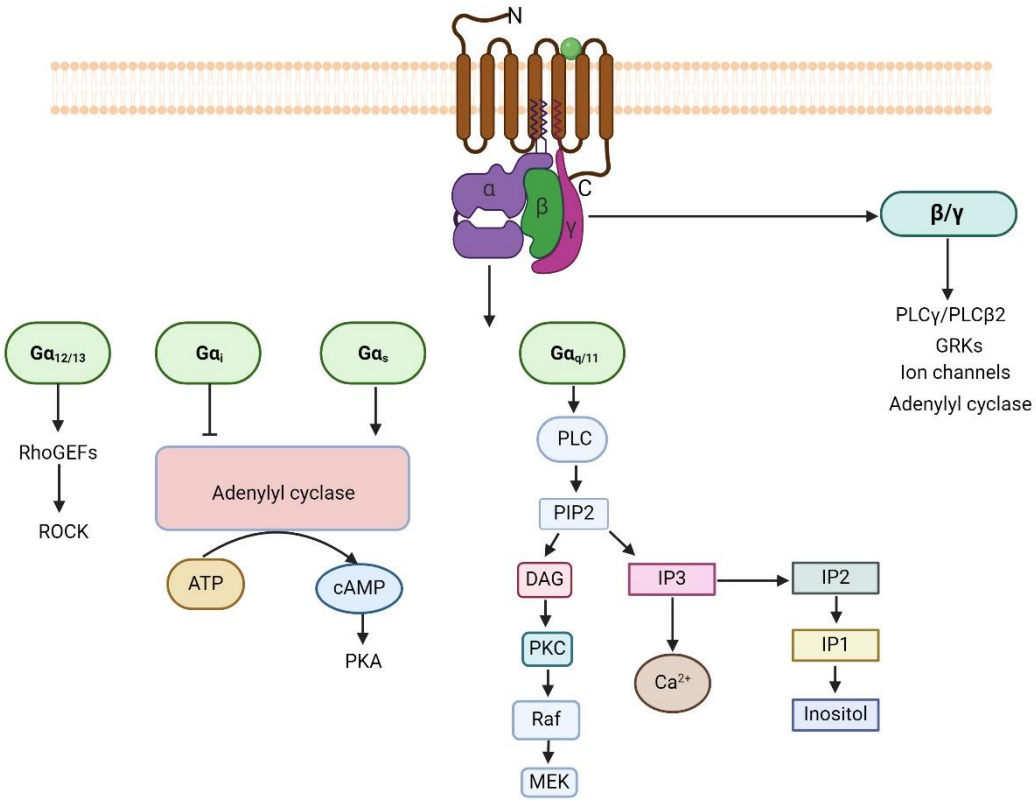

Figure 1.3 G protein-mediated signalling pathways of GPCR
Heterotrimeric G proteins form a coupling with G protein-coupled receptors. Following agonist stimulation, the Gα subunit is made more capable of switching from GDP to GTP, which enables the Gα and Gβγ subunits to separate and activate downstream effectors. The four families of Gα subunits are $G\alpha_s$, $G\alpha_{i/o}$, $G\alpha_q$, and $G\alpha_{12/13}$. The $G\alpha_s$ and $G\alpha_{i/o}$ families control the activity of adenylate cyclase, whereas the $G\alpha_{12/13}$ family stimulates Rho GTPases. The $G\alpha_q$ subunit activates phospholipase-C signalling, increases intracellular Ca^{2+} through IP3, which is quickly broken down to IP2, IP1, and then inositol via the inositol phosphate route. The MAPK signalling pathway receives input from the PLC pathway as well. Furthermore, adenylyl cyclase and Rho GTPases are just a few of the effectors that Gβγ subunits can activate. This figure was created with BioRender.com.

1.2.2.1 The $G\alpha_s$ sub-family

The ubiquitously produced Gα 'stimulatory' ($G\alpha_s$) subunits transmit messages by raising intracellular levels of the second messenger cAMP. The transmembrane enzyme adenylate cyclase, which changes adenosine triphosphate (ATP) into cAMP, is activated and bound by active $G\alpha_s$ as it diffuses within the plasma membrane. cAMP has a variety of biological actions depending on the cell type in question, including hormone release, smooth muscle relaxation, activation of neurons, and stimulation of glycogenolysis and lipolysis (Wettschureck and

Offermanns, 2005). cAMP-dependent protein kinase (PKA) is the mediator of these actions.

1.2.2.2 The $G\alpha_{i/o}$ sub-family

There are eight members of the Gα 'inhibitory' ($G\alpha_{i/o}$) subfamily, which exerts its actions by reducing intracellular cAMP and by regulating several ion channels. The most prevalent and widely dispersed $G\alpha_{i/o}$ proteins in most tissues are $G\alpha_{i/1}$, $G\alpha_{i/2}$, and $G\alpha_{i/3}$. By blocking different isoforms of adenylate cyclase, they reduce cAMP. Restricted expression is present in other $G\alpha_{i/o}$ family members, such as $G\alpha_o$ in neurons and $G\alpha_z$ in platelets. It is believed that they mainly exert their actions indirectly by releasing their βγ subunits (Wettschureck and Offermanns, 2005). The cellular actions of $G\alpha_{i/o}$ proteins are mostly antagonistic to those of $G\alpha_s$ because they function by lowering cAMP.

1.2.2.3 The $G\alpha_{q/11}$ sub-family

Similar to the $G\alpha_{i/o}$ subfamily, the $G\alpha_{q/11}$ subfamily has members that are both widespread and tissue specific. $G\alpha_q$ and $G\alpha_{11}$ are both widely expressed, whereas $G\alpha_{14}$ is only found in certain organs, such as the kidney, lung, and spleen, and $G\alpha_{16}$ is only present in hematopoietic cells (Wettschureck and Offermanns, 2005). As this protein family is not PTX sensitive like the $G\alpha_{i/o}$ family, it is possible to characterise this pathway using assays that target downstream signalling proteins. All of these do so by enlisting and activating phospholipase C-β, which catalyses the conversion of phosphatidylinositol 4,5-bisphosphate into inositol 1,4,5-trisphosphate (IP3) and diacylglycerol, to transmit their signals (DAG) (Wettschureck and Offermanns, 2005, Litosch, 2016). IP3 facilitates the release of intracellular calcium, whereas DAG triggers protein kinase C (PKC). RhoA can also be activated by $G\alpha_{q/11}$ via p63RhoGEF (Litosch, 2016). These numerous effectors carry out a variety of signalling tasks that lead to activities such as synaptic transmission, cellular hypertrophy, and smooth muscle contraction (Wettschureck and Offermanns, 2005).

1.2.2.4 The $G\alpha_{12/13}$ sub-family

The $G\alpha_{12}$/ $G\alpha_{13}$ family of proteins, the last G-protein family discovered in 1991, is still poorly understood for a number of reasons (Strathmann and Simon, 1991).

Although being widely expressed, $G\alpha_{12}$ and $G\alpha_{13}$ commonly couple to GPCRs that also activate other Gα subunits. As there are no specific inhibitors of $G\alpha_{12}$/ $G\alpha_{13}$, it has been challenging to pinpoint their precise signalling functions. The RhoA-mediated effects on the actin cytoskeleton are the functions of $G\alpha_{12}$ and $G\alpha_{13}$ that are most understood. Four Rho guanine nucleotide exchange factors (RhoGEFs) are bound and activated by $G\alpha_{12}$/ $G\alpha_{13}$, thereby promoting the exchange of RhoA GDP/GTP (Siehler, 2009). Numerous downstream pathways are set off by RhoA, and these pathways alter cell polarity, shape, adhesion, migration, and hypertrophy (Siehler, 2009, Worzfeld et al., 2008).

1.2.2.5 Gβγ signalling

GPCRs can signal through the Gβγ complex in addition to the four Gα sub-families, which frequently supports the Gα-mediated response. After being dissociated by GPCR, the Gβγ subunit has complete control over a variety of its own targets including the G protein-regulated inward rectifier K^+ channel, phospholipase C-β, and adenylate cyclase (Clapham and Neer, 1997). Most tissues express $G\alpha_{i/0}$ subunits more than any other Gα subunit, hence Gβγ complexes generated from heterotrimers containing $G\alpha_{i/0}$ subunits are assumed to be the main source of Gβγ mediated signalling (Wettschureck and Offermanns, 2005).

1.2.3 GPCR desensitisation

GPCRs have a variety of mechanisms for desensitisation, which is a reduction in response intensity brought on by ongoing or recurrent stimulation. These mechanisms allow for the highly controlled termination of the agonist-induced response, and they are carried out by cytoplasmic proteins that interact with ICLs and C-terminal tail of the receptor (Tobin, 2008). Desensitisation mechanisms therefore rely on the expression of different cytoplasmic mediators as well as the amino acid sequence of GPCRs.

1.2.3.1 Heterologous desensitisation by effector kinases

The term "heterologous desensitisation" describes how effector kinases desensitise receptors. This can happen as a result of ligand binding to a receptor other than the one that will ultimately become desensitised since it is not dependent on agonist occupancy and is not receptor specific. Some receptors can be

phosphorylated on serine and threonine residues at consensus locations in the ICLs and C-terminal tail by PKA and PKC. Due to this, the G protein binding site is disrupted, and the receptor is cut off from the G protein-mediated response (Tobin, 2008).

1.2.3.2 Homologous desensitisation by arrestins

Agonist-occupied, activated GPCRs undergo homologous desensitisation, which happens more quickly than heterologous desensitisation (Lohse, 1993). The ICLs and C-terminal tails of agonist-bound GPCRs are phosphorylated by G protein-coupled receptor kinases (GRKs) at serine and threonine residues that are different from those phosphorylated by effector kinases (Seibold et al., 2000). Contrary to heterologous desensitisation, the receptor cannot be released from the G protein by GRKs alone (Benovic et al., 1987). Instead, GRK-mediated phosphorylation causes the adaptor protein arrestin to be drawn to and bind to the GPCR, where it facilitates desensitisation by sterically impeding the Gα subunit's ability to connect (Gimenez et al., 2012). The arrestins are a family of four proteins of which arrestin-2 and arrestin-3 are expressed universally and are responsible for homologous desensitisation of the majority of non-visual GPCRs. Arrestin-1 (visual arrestin) and arrestin-4 (cone arrestin) are only expressed in the retina (Luttrell and Lefkowitz, 2002). The immediate result of arrestin-2/arrestin-3 binding to the GPCR is steric inhibition of additional Gα-GDP binding to the agonist-occupied receptor because the arrestin-2/arrestin-3 and Gα binding surfaces overlap (Figure 1.4) (Szczepek et al., 2014). This quickly turns off G protein-dependent signalling that has been activated (Benovic et al., 1987, Lohse, 1993).

Arrestin-2/arrestin-3's secondary desensitising role is to trigger clathrin's internalisation of an agonist-occupied receptor. Clathrin and the adaptor protein 2 complex (AP2) are brought to the plasma membrane by receptor-bound arrestin-2/arrestin-3 to begin the development of clathrin-coated pits (Figure 1.4) (Goodman Jr et al., 1996, Laporte et al., 1999). As a result, the agonist-occupied receptor is internalised. There are two possible arrestin-2/arrestin-3-mediated internalisation mechanisms. The arrestin-2/arrestin-3 either dissociates before endocytosis or remains in complex with the receptor and colocalises to the endosome, depending on the GPCR implicated (Zhang et al., 1999). The GRK-

mediated phosphorylation of serine and threonine residues in the C-terminal tail determines this, at least in part (Gimenez et al., 2012). The destiny of the endocytosed receptor is determined by both sorting signals in the receptor intracellular domain and the stability of the association with arrestin-2/arrestin-3; It might either be targeted for destruction by ubiquitination or recycled back to the plasma membrane (Marchese and Trejo, 2013). Prior to endocytosis, receptors that separate from arrestin-2/arrestin-3, can resume spatially compartmentalised G protein-dependent signalling (Tsvetanova and Von Zastrow, 2014, Calebiro et al., 2009). However, relatively recent studies suggest that this might also be possible for GPCRs that have been internalised and bound to arrestin-2/arrestin-3, leading to endosomal compartment-mediated G protein signalling (Thomsen et al., 2016). The G protein-dependent response is further spatiotemporally regulated by these characteristics of the internalisation cycle.

1.2.3.3 G protein-independent signalling

Arrestin has recently gained recognition as a critical mediator of signalling in its own right, in addition to its role in desensitisation and internalisation of the receptor. Without triggering G protein activation, arrestin can be attracted to agonist occupied GPCRs at the plasma membrane, where it can serve as a scaffold for cytoplasmic signalling proteins (Figure 1.4) (Wei et al., 2003, Shenoy et al., 2006). Essentially, this function is non-canonical and a number of significant pathways, including the Src-family kinases, extracellular signal-regulated kinase (ERK), c-jun N-terminal kinase (JNK), mitogen-activated protein kinases (MAPK), and phosphodiesterases, have been demonstrated to bind to and be activated by arrestin when it is coupled to GPCRs (Shenoy et al., 2006, Houslay and Baillie, 2005, DeWire et al., 2007). Compared to G protein-dependent responses, this arrestin-mediated signalling has a slower onset and a longer duration, increasing the temporal regulation and variability of GPCR signalling (Shenoy et al., 2006). It has been demonstrated that arrestin-mediated signalling has physiological significance in vivo in a variety of situations, including growth, the central nervous system, and the cardiovascular system (Luttrell and Gesty-Palmer, 2010). As a result, it is crucial to take into account the arrestin signalling pathway while developing new drugs, both as a target of interest and as a conduit for harmful off-target effects.

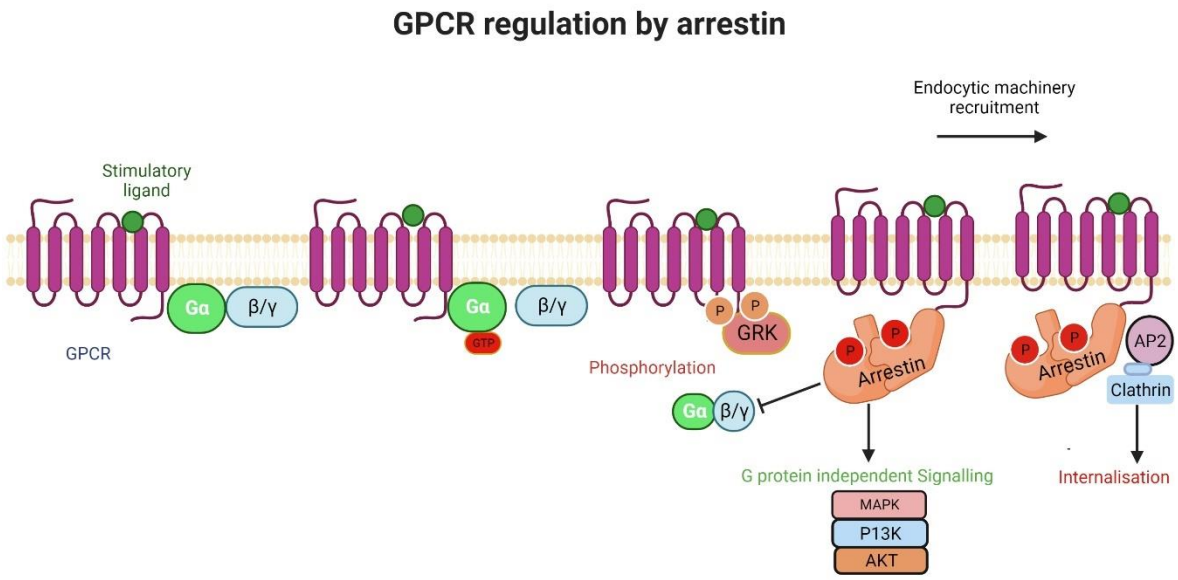

Figure 1.4 Desensitisation, internalisation, and signalling of receptors by arrestin
GRKs phosphorylate intracellular residues of the active GPCR after agonist binding and G protein signalling. Arrestin is attracted to the receptor, which sterically prevents G protein activation and binding. In order to start the internalisation of the receptor into clathrin coated pits, arrestin is also recruited by adaptor proteins like AP-2 and clathrin. Moreover, arrestin functions in G protein independent signalling as a scaffold protein. This figure was created with BioRender.com.

1.2.4 Interaction of GRKs with GPCR

The majority of transmembrane receptors belong to the G protein-coupled receptor (GPCR) family, and GPCR kinases (GRKs) and ß-arrestins carefully control the signal transduction of these receptors. As GRKs are soluble proteins, so they need specific mechanisms to move them close to membrane embedded GPCRs. It has been demonstrated that binding to active GPCRs causes GRKs to become allosterically active (Palczewski et al., 1991). The precise mechanism of this interaction between GPCRs and GRKs has not yet been identified for each receptor, but it is clear from x-ray crystallography and cryo-EM structure of GPCRs-GRKs that this interaction primarily occurs through the insertion of an N-terminal α-helix of GRKs into the cytoplasmic cavity of the GPCR. Although structural data is not always conclusive, this manner of GRK-binding is very appealing because G proteins and arrestins both probe for active GPCR conformations in a similar way (Cato et al., 2021). GRK-binding causes the intracellular phosphorylation of activated GPCRs in a cellular setting. GRK mediated GPCR phosphorylation decreased but did not completely cease G protein-based signalling. Another group of players was therefore suspected. These athletes were actually arrestins (Gurevich and Gurevich, 2019).

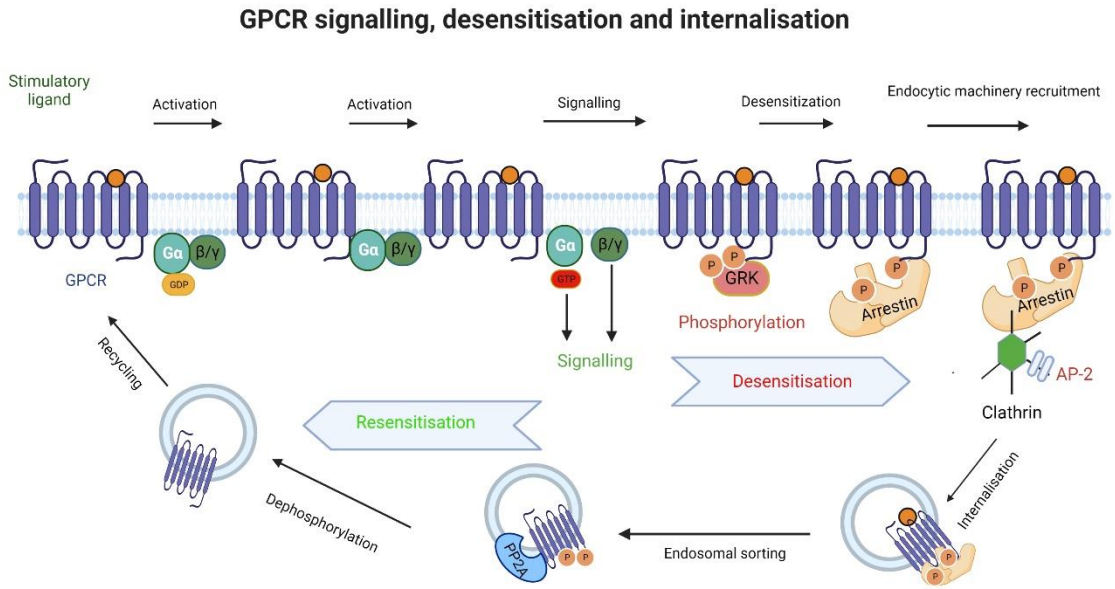

Figure 1.5 GPCR signalling and regulation
GPCRs are cell surface proteins that are primarily localised in plasma membrane. Agonist binding activates GPCRs. Active receptor binds inactive (GDP-liganded) heterotrimeric G protein consisting of α-, β-, and γ-subunits. The nucleotide pocket of the G protein α subunit is opened by receptor engagement allowing bound GDP to be released and more plentiful cytoplasmic GTP to bind. GTP bound G protein detaches from GPCR as a distinct α-subunit-GTP and a dimer of β and γ. They can both initiate signalling by interaction with various effectors. Specialised GPCR kinases that phosphorylate many GPCRs at the C-terminus recognise active GPCRs. Arrestins bind to active, phosphorylated GPCRs and, through direct contacts, activate the coated pit, clathrin, and clathrin adaptor AP-2, which facilitates the internalisation of the receptor. In the acidic environment of the endosome, the loss of agonist causes the internalised receptor to become inactive. This promotes arrestin dissociation, which allows the phosphatases to access receptor-attached phosphates (possibly PP2A). The dephosphorylated receptor can be recycled back to the plasma membrane and reused. The idea of the figure was adopted from (Karnam et al., 2021).This figure was created with BioRender.com.

1.2.5 Tissue specific GPCR signalling and phosphorylation barcode

GPCRs are usually phosphorylated by several kinases, predominantly by GRK family of kinases. Usually, ligand binding to a GPCR results in multiple possible signalling fates and therefore choosing the most specific outcome is crucial. According to a novel paradigm, the phosphorylation pattern, or ‘barcode’ may affect how cells react to receptor activation. Different kinases can encourage the internalisation of the receptor, desensitisation of the receptor, or G protein- or arrestin-mediated signalling in different ways (Ren et al., 2005, Nobles et al., 2011). The presence of phospho-acceptor residues in the GPCR sequence determines the potential phosphorylation pattern of the intracellular domain of the GPCR, although other kinases or the expression of the relevant GRKs may also play a role. Based on this logic, the cell type-specific signalling hypothesis was developed,

which postulates that the specificity of the GPCR signalling profile is regulated by the kinases produced in a certain cell type (Tobin, 2008, Liggett, 2011). For therapeutically important GPCRs including the dopamine and muscarinic receptors, cell type specific GRK activity has been shown in vivo (Gurevich et al., 2016, Walker et al., 2004). This demonstrates that GPCRs can potentially carry out various tasks in various tissues, cell types, or physiological and pathological contexts. Therefore, it will be advantageous to use GPCRs as pharmacological targets if we can comprehend how this phosphorylation barcode relates to specific GPCRs.

1.2.6 Ligand-specific GPCR signalling

A ligand's pharmacological characteristics determine how it will interact with a receptor. Affinity, efficacy, and drug potencies are among the characteristics of drugs that can be measured. Biased ligands are those ligands that bind to a receptor in a way that stabilises a conformation that selectively activates a certain signalling pathway. Certain G protein coupling specificities may be favoured by ligand-specific receptor conformations, which may also promote arrestin-mediated signalling or regulate the pace of receptor internalisation or recycling (Maudsley et al., 2005). In drug discovery, biased GPCR ligands hold significant promise for improving response specificity and minimising off-target side effects brought on by erroneous activation of harmful pathways (Whalen et al., 2011). In order to achieve this, biased ligands are being investigated as therapeutics for a variety of applications, with G protein-biased agonists of the μ-opioid receptor serving as analgesics and ß-arrestin-biased agonists of the angiotensin II receptor serving as treatments for heart failure showing the greatest promise (DeWire et al., 2013, Luttrell et al., 2015). It is known that ligand-specific signalling, namely G protein versus arrestin bias, is linked to receptor phosphorylation. As a result, different ligand-receptor conformations encourage phosphorylation by various GRKs to determine the signalling response (Nobles et al., 2011). To fully utilise the potential of this ‘functional selectivity’ for drug development applications, understanding the phosphorylation of therapeutically relevant GPCRs and how these influences downstream signalling is crucial.

1.3 G protein-coupled receptor 35

A class A G protein-coupled receptor (GPCR) called GPR35 was first discovered more than 20 years ago (O'Dowd et al., 1998) and formally recognised as a receptor for the tryptophan metabolite kynurenic acid in 2006 (Wang et al., 2006). GPR35 still officially remains as a poorly characterised 'orphan receptor' and research on the type of endogenous ligand(s) that activate GPR35 is still quite active today (Milligan, 2023). However, understanding the functions and regulation of this receptor has been significantly hampered by the marked differences in the potency of many synthetic agonists between human GPR35 and both the rat and mouse orthologues, as well as the unusually small number of antagonist ligands that are currently on the market (Milligan, 2023). In addition, the antagonists that have been described so far have little affinity for rat and mouse, thereby making them suitable only for 'human-specific' form of the receptor (Quon et al., 2020). Recently, the first atomic-level structure of a human GPR35-G protein complex determined by cryoelectron microscopy (cryoEM) was published, with a global resolution of 3.2 Å (Duan et al., 2022). Although GPR35 is poorly characterised and the use of preclinical disease models has historically been constrained due to significant pharmacological variations between human and rodent orthologues of the receptor and a lack of antagonists with affinity for mouse and rat GPR35, some remarkable advancements and tool compounds have already come into the spotlight to tackle these issues. Improved ligands, new transgenic knock-in mouse lines, and thorough analyses of the disease relevance of single-nucleotide polymorphisms (SNPs) have all contributed to a greater understanding of the central functions of GPR35 and sparked efforts towards proof-of-concept studies that specifically target disease (Milligan, 2023).

1.3.1 GPR35 discovery and fundamental characteristics

When human genomic DNA was amplified using GPR1 degenerate primers, a genomic DNA homology screen was conducted to find GPR35 for the first time (O'Dowd et al., 1998). A single open reading frame was discovered to encode a 309 amino acid protein in this preliminary research. This protein most closely resembled the hydroxycarboxylic acid receptor HM74 (30%) and the lysophosphatidic acid (LPA) receptor 4 (32%), often referred to as P2Y9/GPR23. The novel GPR35 gene was located on human chromosome 2q37.3 by this

investigation. In a later investigation, GPR35 was found to have two splice variants: the previously known short isoform, GPR35a, and a multi-exon version, GPR35b, with a 31 amino acid N-terminal extension (Okumura et al., 2004). Even though this study discovered GPR35b enrichment in gastric cancer samples, it is yet unknown what function this long variation serves. Humans are the only species known to harbour GPR35b. Rat GPR35 is 306 amino acids long, while mouse GPR35 has 307 amino acids. Both proteins share 85% similarity with each other and 72% with that of humans GPR35a (Taniguchi et al., 2006). GPR35a and GPR35b have similar pharmacological properties, as evidenced by the equal potency of agonists on both isoforms in G protein and arrestin-based experiments (Guo et al., 2008, MacKenzie et al., 2014, Marti-Solano et al., 2020). Given that all isoforms share the same subcellular location, the N-terminal extension on GPR35b does not seem to influence expression or trafficking (Guo et al., 2008).

GPR35 shares the same basic structure as the majority of Class A GPCRs, consisting of seven transmembrane helices, a brief N-terminal domain, and a cytosolic helix 8 that comes before a brief C-terminal tail. The amino acid sequence of transmembrane helices is highly conserved, despite differences in the ECLs, ICLs, and C-terminal tail between the human and rodent orthologues. There are seven naturally occurring variants of the GPR35 protein in humans due to non-synonymous, coding region single nucleotide polymorphisms (SNPs) in the gene. Only one of these, V76M (minor allele frequency 0.02), significantly affects ligand binding (MacKenzie et al., 2014). Interestingly, although the molecular relevance of these correlations is uncertain, the T108M and S294R polymorphisms have been linked to disease (Quon et al., 2020, Sun et al., 2008, Ellinghaus et al., 2013).

1.3.2 Suggested endogenous ligands of GPR35

Determining the upstream and downstream signalling events of GPR35 activation is essential for understanding the receptor's function. For this, several endogenous molecules have been discovered to have GPR35 agonist activity over time. Although some papers have asserted that they are endogenous ligands, each of these claims has been refuted for a variety of reasons. So that the International Union of Basic and Clinical Pharmacology continues to formally designate GPR35 as an orphan receptor (Davenport et al., 2013).

1.3.2.1 Kynurenic acid

The first naturally occurring substance to be identified as having GPR35 agonist action (Wang et al., 2006, Quon et al., 2020) was kynurenic acid (Mackenzie and Milligan, 2017), a by-product of tryptophan metabolism with primarily central and peripheral nervous system-based signalling effects. With potency in the high micromolar range, it is commonly recognised that kynurenic acid competitively inhibits all three ionotropic glutamate receptors (Schwarcz et al., 2012). Many in vitro and ex vivo tests have supported the fundamental findings, but as with other GPR35 activators, the efficacy of kynurenic acid varies among human, mouse, and rat orthologues (Wang et al., 2006, Jenkins et al., 2011). In fact, it has been questioned if kynurenic acid is the primary endogenous agonist due to the very modest potency of the compound reported by several researchers at (especially human) GPR35 (De Giovanni et al., 2022, Jenkins et al., 2011). There are numerous other known molecular targets for kynurenic acid (Joisten et al., 2021, Roth et al., 2021), and recent research has shown that it is around 20-fold more potent at activating the GPCR hydroxycarboxylic acid receptor (HCAR) 3 than GPR35 (Kapolka et al., 2020). Moreover, it can inhibit the adenosine A_{2B} receptor by functioning as a negative allosteric modulator (NAM) or blocker (Kapolka et al., 2020). Kynurenic acid has been used extensively in both ex vivo and in vivo studies, with the expectation that effects will reflect activation of GPR35, despite these examples showing that simple small molecules derived from intermediary metabolism (and many such molecules are in fact carboxylic acids) can have multiple targets (Milligan, 2023). These include early studies showing that kynurenic acid was able to induce interactions between monocytes and human umbilical vein endothelial cells by occupying GPR35 to a significant proportion (Barth et al., 2009, Milligan, 2023). One of the most recent studies found that phagocytosis, inflammatory responses, and macrophage cytokine production are all influenced by kynurenic acid-GPR35 signalling (Miyamoto et al., 2023). This group was also inspired to look into the possible function of this axis in the complex communication between the gut and the brain, particularly in the setting of multiple sclerosis, as there is a significant abundance of kynurenic acid and remarkable expression of GPR35 in the gastrointestinal tract (Miyamoto et al., 2023).

1.3.2.2 Lysophosphatidic acid

Due to its resemblance to other LPA receptors, GPR35 has also been investigated as an LPA receptor. Oka et al. have demonstrated that LPA caused Ca^{2+} response, activation of RhoA and ERK, as well as internalisation of GPR35 in GPR35-transfected cells (Oka et al., 2010). In vector-transfected control cells, LPA also caused a brief activation of RhoA, which was ascribed to the other LPA receptors. LPA is a bioactive phospholipid derivate that can be generated both intracellularly and extracellularly. It can activate six known GPCRs, LPAR1-6 (Ye and Chun, 2010). GPR35 deletion blocked the LPA-induced Ca^{2+} signalling in bone marrow-derived macrophages (BMDMs) in a more recent investigation by Schneditz and colleagues. Yet the authors speculated that the absence of GPR35 would affect LPA signalling via the other LPA receptors (Schneditz et al., 2019). Although there is no definitive evidence and direct link between GPR35 and LPA, the LPA/GPR35 axis has been demonstrated in both mouse and zebrafish, where LPA caused macrophage movement that was dependent on GPR35 as well as the induction of the cytokine TNF, which was accompanied by activation of the NF-kB and ERK pathways. However, it is currently unclear whether GPR35 modulates LPA signalling via interacting with and altering the activity of its receptors or by directly binding to LPA.

1.3.2.3 CXCL17

It has also been suggested that CXCL17, whose expression is linked to mucosal regions, is an endogenous agonist of GPR35 (Maravillas-Montero et al., 2015, Lee et al., 2013). According to Maravillas-Montero et al., GPR35-transfected cells move towards CXCL17 (Maravillas-Montero et al., 2015, Burkhardt et al., 2012). In contrast to kynurenic acid, CXCL17 functioned on GPR35 at nanomolar concentrations that are within a physiological range, hence the scientists advised changing GPR35's name to CXCR8. However, later research revealed that in GPR35-expressing cells, CXCL17 failed to elicit migratory or signalling responses (Binti Mohd Amir et al., 2018, Park et al., 2018). Furthermore, kynurenic acid and zaprinast lessened the effects of CXCL17 in a mouse model of neuropathic pain, providing more evidence that CXCL17 receptors are of separate entity other than GPR35 (Rojewska et al., 2019). Moreover, a contradicting element of CXCL17 biology for GPR35 was discovered in a recent work (Giblin and Pease, 2023) and

this group ultimately questioned the notion of chemokine as modelling of CXCL17 using a variety of platforms failed to establish a chemokine-like fold.

1.3.2.4 5-Hydroxyindoleacetic acid (5-HIAA)

The serotonin metabolite 5-hydroxyindoleacetic acid (5-HIAA) has recently been proposed as a high-potency endogenous activator of GPR35 (De Giovanni et al., 2022, De Giovanni et al., 2023a) and has later been noted by another scientist (Im, 2023). This is an intriguing option because serotonin is found in high concentrations in the intestine and colon, 5-HIAA is a significant metabolite, and GPR35 expression is highest in the lower gut. De Giovanni et al. provided convincing evidence that kynurenic acid and the potent synthetic GPR35 agonist lodoxamide could both stimulate chemotaxis in murine WEHI-231 B lymphoma cells that had been genetically modified to express a version of GPR35 that was fused to a green fluorescent protein (GFP) (De Giovanni et al., 2022). Nevertheless, lysophosphatidic acid (LPA) administration did not have this impact, despite a small number of research suggesting that at least some species of LPA can activate GPR35 in the past (Kaya et al., 2020). Serotonin was unable to encourage migration of GPR35-GFP-transduced WEHI-231 cells, while 5-HIAA was able to do so in a concentration-dependent manner with a clear peak between 10 and 100 nM, supporting the idea that 5-HIAA may directly activate GPR35. This idea was also strengthened by the findings of neutrophil attachment assays, where 5-HIAA promoted this for cells from wild-type mice but not GPR35 knock-out mice. Using the WEHI-231 cell model once more, it was discovered that 1 μM 5-HIAA was just as effective as 10 μM lodoxamide, indicating that it functions as a highly effective and potent agonist (De Giovanni et al., 2022). For both mouse and human GPR35, such effects were seen. This study provides significant support for the importance of 5-HIAA and may be the most thorough exploration of the potential coupling of a new endogenous ligand with GPR35 (De Giovanni et al., 2022, De Giovanni et al., 2023a). The same group of researchers in a separate study claimed that the 5-HIAA-GPR35 axis is an eosinophil chemoattractant receptor system that regulates the clearance of a deadly fungal pathogen, with implications for the use of serotonin metabolism inhibitors in the treatment of fungal infections (De Giovanni et al., 2023b). Direct measurements of activation of each human and rodent orthologue of GPR35 following their transfection into and confirmation of expression in more conventional cell lines that are extensively employed for

pharmacological and functional characterisation of GPCRs were, however, absent from the study. As a result, even if the findings of De Giovanni et al. (De Giovanni et al., 2022) are intriguing and seem convincing, outside verification is still needed.

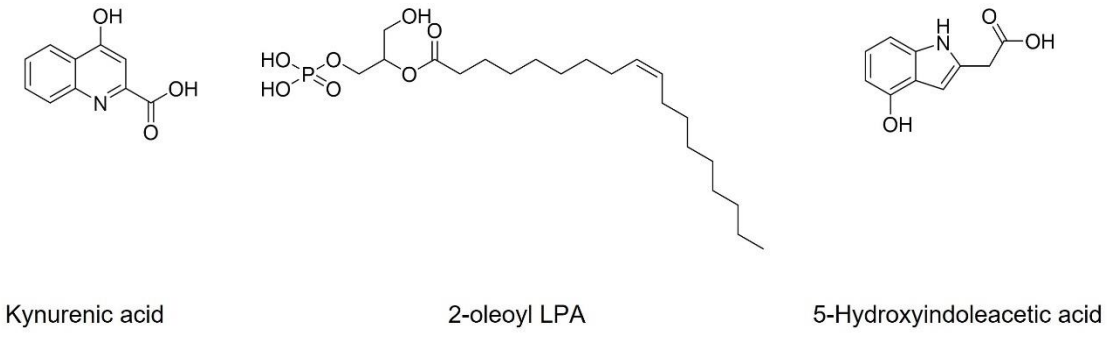

Kynurenic acid 2-oleoyl LPA 5-Hydroxyindoleacetic acid

Figure 1.6 Structures of potential GPR35 endogenous ligands
Structures were drawn by ChemDraw software.

1.3.3 Synthetic ligands of GPR35

Although substantial progress has been made in identifying the suspected endogenous GPR35 activators, the introduction of synthetic agonists has helped to shed light on the molecular mechanisms behind GPR35 activation. They have proven effective as tool compounds and assisted research into the pharmacology and operation of the GPR35 (Divorty et al., 2015).

1.3.3.1 Synthetic agonists of GPR35

Among all the surrogate ligands of GPR35, the first substantially characterised synthetic agonist was zaprinast which is a cyclic guanosine monophosphate-specific phosphodiesterase inhibitor (Taniguchi et al., 2006). Similar to its potency as an inhibitor of cGMP-phosphodiesterase subtypes, it has modest potency against GPR35. Zaprinast, however, continues to be a commonly used tool chemical for in vitro and even ex vivo research (Quon et al., 2020), while being of little use in explicitly characterising GPR35-mediated effects in vivo. This demonstrates that it exhibits comparatively similar potency at the rat, mouse, and human orthologues of GPR35, with rank order rat > mouse > human. Another synthetic GPR35 agonist is lodoxamide which is a mast cell stabiliser with anti-inflammatory properties. It is normally used in the treatment of allergic conjunctivitis. While

lodoxamide has a high potency for the human and rat GPR35, it has a 100-fold lower potency for the mouse orthologue (MacKenzie et al., 2014, Kim et al., 2019). Lodoxamide, however, has demonstrated protective effects in a mouse model of hepatic fibrosis that were prevented by a GPR35 antagonist (Kim et al., 2019). As there remains concern about the low potency of lodoxamide for mouse GPR35, this condition makes this agonist a poor choice to assess the function of GPR35 in wild-type mice. Another mast cell stabiliser and anti-allergy drug, pemirolast is a relatively potent agonist of rat and mouse orthologues of GPR35. However, this ligand is not particularly potent at the human GPR35. So lodoxamide may, therefore, be used as a 'repurposed' GPR35-targeting drug, however, pemirolast will not. Other important synthetic agonists of GPR35 include cromolyn disodium and pamoic acid which display modest potency as agonists for GPR35. The first clue that several clinically used medications can mediate at least some of their effects via GPR35 was the discovery that cromolyn disodium can activate GPR35 with a lot more efficacy in human than in rodent forms (Yang et al., 2010). The discovery that pamoate salts of numerous drugs activated (at least in humans) GPR35 and that this congener was the defining characteristic of a diverse set of medications that appeared to activate the receptor was a huge surprise (Neubig, 2010). Pamoate also has strong human GPR35 selectivity and frequently functions as a partial agonist. In a recent investigation, (Kim et al., 2023) reported that pamoic acid induced peripheral GPR35 activation may help relieve pruritus and its related conditions. Therefore, careful consideration must be made to the selection of ligands used to evaluate GPR35 function in other species because most of these drugs either have not been evaluated on rodent orthologues or have only been examined on human GPR35-expressing cells, which limits their use in rodent investigations. Doxantrazole, amlexanox, bufrolin and PSB-13253 are some other important synthetic agonists of GPR35.

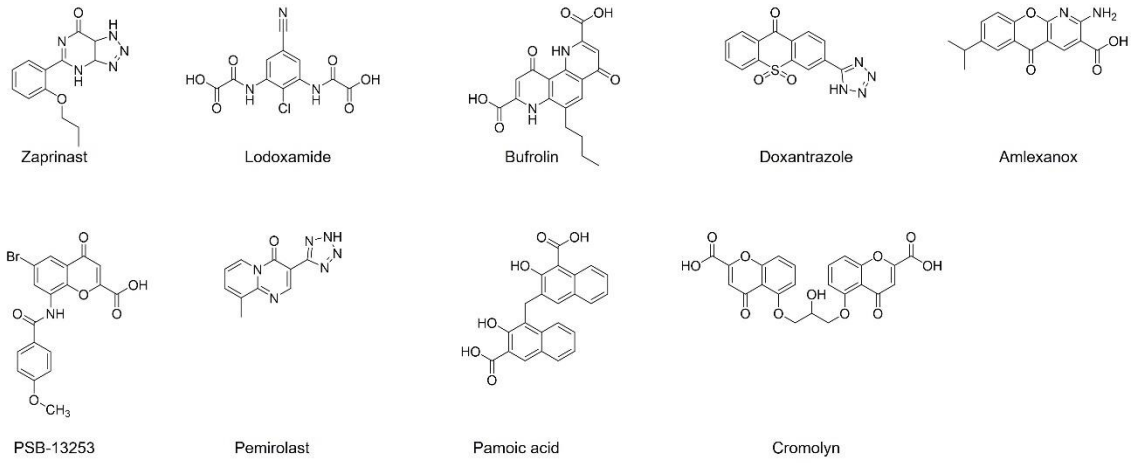

Figure 1.7 GPR35 synthetic agonists with specific chemical structures
Structures were drawn by ChemDraw software.

1.3.3.2 Synthetic antagonists of GPR35

Although antagonist compounds are important for characterising GPCRs, finding and using such tools has been difficult for GPR35. So far, only a few GPR35 antagonists have been characterised; the only two that have been extensively studied in human-derived cells and tissues (McCallum et al., 2015, Boleij et al., 2021) are CID-2745687 (Zhao et al., 2010) and ML145 (CID-2286812) (Heynen-Genel et al., 2010). They cannot, however, be used to describe the functions of GPR35 in either wild-type mice or rats (Jenkins et al., 2012) because they both have no discernible affinity at either rat or mouse GPR35. Although there are some reports on the antagonism of the compounds in mouse model, it is evident that there is still a divergence between the underlying pharmacological research in transfected cells and the application of this substance in various physiological preparations (Quon et al., 2020). To address this problem, Lin et al. (Lin et al., 2021) recently produced and used tissue from a transgenic knock-in mouse strain in which mouse GPR35 was substituted with the comparable human isoform. It was evident that ML145 was able to reverse the capacity of lodoxamide to prevent triglyceride accumulation in these animals' hepatocytes in a concentration-dependent manner and with an IC_{50} commensurate with its reported binding affinity at human GPR35. These transgenic mice may be useful in a variety of disease models where contributions of GPR35 are being evaluated because existing antagonists can inhibit human GPR35 (Quon et al., 2020).

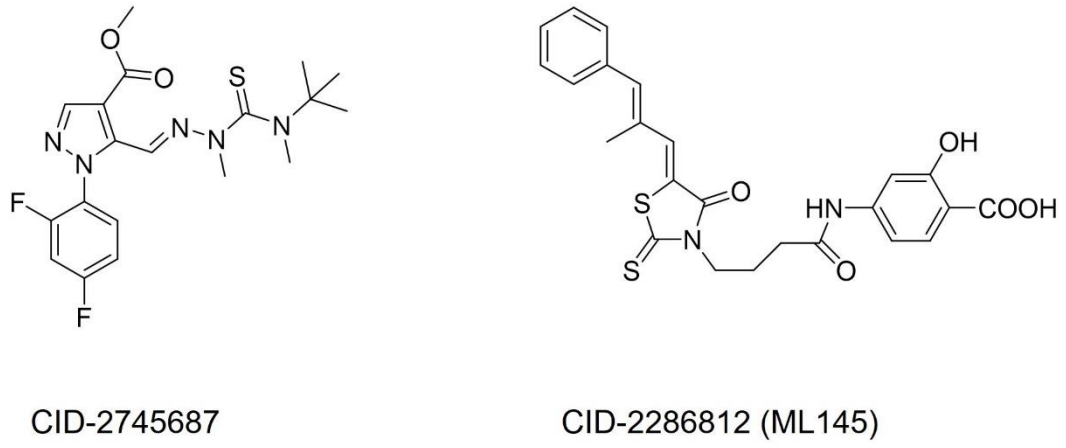

Figure 1.8 Chemical structures of synthetic GPR35 antagonists
Structures were drawn by ChemDraw software.

1.3.4 GPR35 signalling

Studies of downstream signalling and reactions to GPR35 activation have been carried out to characterise the pathways in which the receptor is engaged and, consequently, to understand the physiology and function of the receptor. Some signalling mediators that directly interact with GPR35 have been found, and they shed light on the possible pathways and reactions that could be influenced by pharmacological manipulation.

1.3.4.1 $G\alpha_{i/o}$ mediated signalling of GPR35

In terms of classical GPCR signalling, depending on the cell type and/or background species, GPR35 appears to bind to different Gα subunits. *Bordetella pertussis* toxin, which is known to particularly impair coupling to $G\alpha_{i/o}$ family G proteins, reduced kynurenic acid-induced binding of [^{35}S]-GTPγS generated by human GPR35 heterologously expressed in Chinese hamster ovary cells (Wang et al., 2006). In addition, Ohshiro et al. (Ohshiro et al., 2008) demonstrated that kynurenic acid and zaprinast both inhibited forskolin-induced cyclic adenosine 3′ 5′ monophosphate (cAMP) generation in Chinese hamster ovary cells transfected with rat GPR35, indicating that one or more G proteins from the adenylate cyclase-inhibiting $G\alpha_{i/o}$ family were involved. Rat neurons heterologously expressing human GPR35 have also been found to be sensitive to pertussis toxin, with GPR35-dependent effects on N-type calcium channels (Guo et al., 2008). It is also noteworthy that pre-treatment of the cells with pertussis toxin prevented both

the chemotaxis of THP-1 cells and the elevation of $[Ca^{2+}]_i$ levels in HEK293 cells transfected with the human ortholog of GPR35, according to a recent study demonstrating CXCL17 as a possible GPR35 agonist (Maravillas-Montero et al., 2015).

1.3.4.2 $G\alpha_{12/13}$ mediated signalling of GPR35

More recent investigations have shown $G\alpha_{13}$ connection to GPR35 in addition to $G\alpha_{i/o}$ signalling in GPR35-mediated responses. An activation state-sensing GTP-$G\alpha_{13}$ antibody was used to establish zaprinast-induced activation of $G\alpha_{13}$ in transfected HEK293 cells (Jenkins et al., 2011). The same study also showed that zaprinast can cause increases in $[Ca^{2+}]_i$ in HEK293 cells that have been co-transfected with a chimeric $G\alpha_q/G\alpha_{13}$ G protein subunit in either human or rat GPR35. This effect was unique to the $G\alpha_{13}$ chimaera as opposed to the similar $G\alpha_{12}$ subunit.

Hence, the $G\alpha_{i/o}$ or $G\alpha_{13}$ pathways appear to be predominantly responsible for the conventional G protein-mediated cellular and biological actions of GPR35 (Figure 1.9). The efficiency of G protein coupling may potentially be influenced by additional variables that have not yet been thoroughly investigated, such as ligand bias or Gα subunit expression. In the context of GPR35 as a therapeutic target, the notion of ligand bias is particularly intriguing since once understood, this property could be used to improve the specificity of drug-induced responses (Divorty et al., 2015).

1.3.4.3 Arrestin mediated signalling of GPR35

Upon activation with several agonists, such as kynurenic acid and zaprinast, GPR35 has been shown to directly recruit arrestin-3 in addition to activating G protein-dependent responses (Jenkins et al., 2010). Following this, the receptor is internalised in an agonist-dependent manner, which is likely regulated by arrestin-3 in accordance with the conventional hypothesis for GPCR desensitisation and phosphorylation (Goodman Jr et al., 1996, MacKenzie et al., 2014). Arrestins have now been demonstrated to serve as signalling scaffolds for several GPCRs, engaging with a variety of pathways, most notably the extracellular signal-regulated kinase (ERK1/2) pathway that is independent of G proteins. The other

important routes include the c-Jun N-terminal kinase, protein kinase B, and cAMP pathways (Luttrell and Gesty-Palmer, 2010).

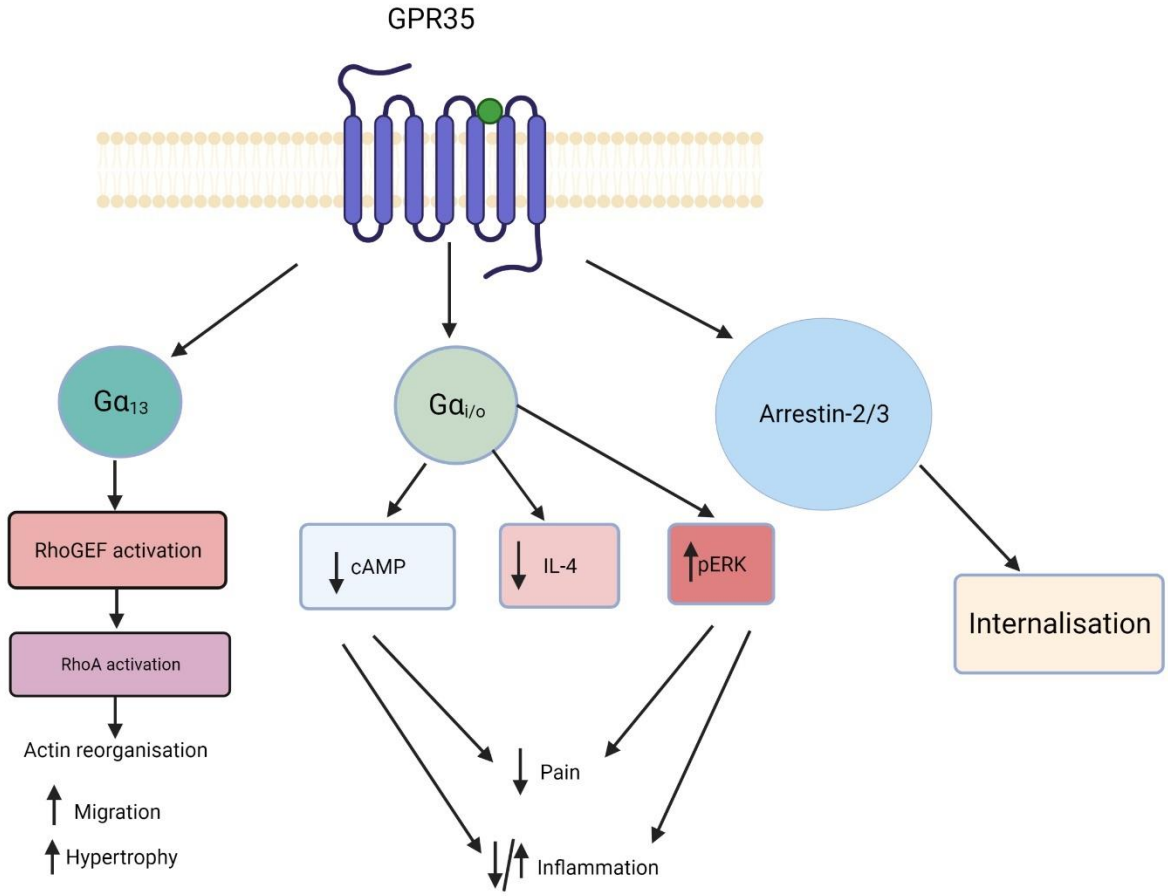

Figure 1.9 GPR35 signalling model
The coupling of GPR35 to $G\alpha_{13}$, $G\alpha_{i/o}$, and arrestin 2/3 has been demonstrated. The signalling mechanisms and physiological effects linked to GPR35 activation are outlined. RhoGEF, Ras homologue guanine nucleotide exchange factor; RhoA, Ras homologue gene family member A; cAMP, 3′-5′-cyclic adenosine monophosphate; IL-4, interleukin-4; ERK, extracellular-signal regulated kinase; Ca^{2+}, calcium. This figure was created with BioRender.com.

1.4 GPR35 as a novel therapeutic target

The physiological function and importance of the orphan receptor GPR35 remain unclear despite the availability of functional ligands and insights into its cellular signalling profile. However, in recent years, GPR35 has been implicated in a range of physiological and pathophysiological conditions. It may have broad therapeutic usefulness given its associations with numerous different disease states. In order to determine whether this receptor has the potential to be a novel therapeutic target, it is crucial to look into the physiological roles of this receptor in both health and disease.

1.4.1 GPR35 expression pattern

The existence of GPR35 transcripts in endogenous tissue was also found by O'Dowd et al., with the rat small intestine displaying the highest levels of expression (O'Dowd et al., 1998). In later research, it was discovered that human GPR35 is expressed at high levels in the pancreas and small intestine (Wang et al., 2006, Leonard and Chu, 2007), as well as in the colon, spleen, and immune cells (monocytes, neutrophils, T cells, and dendritic cells), and at lower levels in the stomach, skeletal muscle, adipose tissue, kidney, liver, and thymus (Taniguchi et al., 2006). Very high GPR35 levels were found in the mouse spleen, while the small intestine, colon, stomach, thymus, and adipose tissue also expressed GPR35 at levels comparable to those found in humans (Wang et al., 2006). High levels of GPR35 expression have been found in the spleen, colon, dorsal root ganglion, and uterus in rats (Taniguchi et al., 2006), while moderate levels have been found in the cerebrum, heart, liver, bladder, and spinal cord (Figure 1.10) (Ohshiro et al., 2008, Mackenzie et al., 2011).

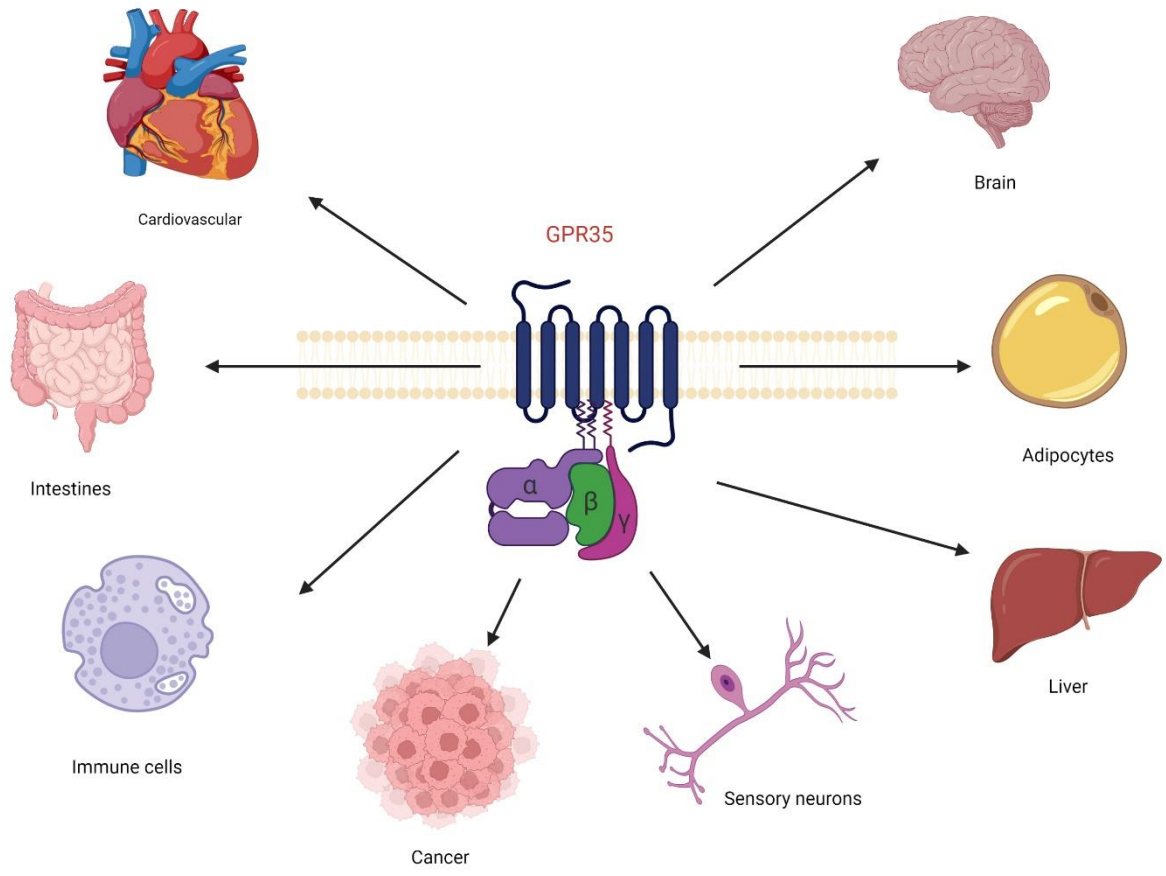

Figure 1.10 Expression pattern of GPR35
GPR35 is expressed in brain, heart, liver, immune cells, adipocytes, intestines, sensory neurones and GPR35 is also associated with cancer. This figure was created with BioRender.com.

1.4.2 GPR35 in metabolic and gastrointestinal disease

Given that GPR35 is highly expressed in the gastrointestinal tract, it is anticipated that the receptor would play a role in maintaining gut homeostasis. From a recent investigation (Wang et al., 2023), it is reported that GPR35-mediated Kynurenic acid sensing is essential for preserving the integrity of the gut barrier against DSS-induced damage in rat colitis model. In fact, GPR35 has been identified as a potential risk factor for chronic inflammatory bowel diseases like IBD and ulcerative colitis. In the first of these reports, a GWAS for early onset IBD (including Crohn's disease and ulcerative colitis) found a GPR35 SNP linked to ulcerative colitis (Imielinski et al., 2009). Although there was no difference in GPR35 expression between tissue from people with IBD and tissue from genetically unrelated controls, the SNP at rs4676410 is an upstream intron variation of GPR35 that encodes a cytosine to thymine substitution. The nearby genes CAPN10 and GPR35 had both previously been associated with disease in a GWAS for type 2 diabetes mellitus prior to the IBD GWAS (Horikawa et al., 2000). In the coding area of GPR35, this investigation found four non-synonymous SNPs; only one, designated ‘UCSNP-38’, encoding a serine to arginine substitution at amino acid position 294, revealed a connection with type 2 diabetes (Divorty et al., 2015). However, further in-depth investigation found no association of type 2 diabetes with GPR35. GPR35 may also play a role in IBD, according to a more recent study on ulcerative colitis and primary sclerosing cholangitis, a chronic cholestatic liver disease (Ellinghaus et al., 2013). Although ulcerative colitis is commonly present in primary sclerosing cholangitis patients, an integrated analysis of GWAS data for both conditions found two GPR35 SNPs to be significantly associated with primary sclerosing cholangitis (Ellinghaus et al., 2013). The first of these was the upstream intron variant rs4676410 that was previously discovered in the IBD GWAS (Imielinski et al., 2009), while the second, rs3749171, encodes a methionine to threonine alteration in the receptor's third transmembrane domain. Due to the high expression of GPR35 and the presence of kynurenic acid in bile and the gastrointestinal tract (Paluszkiewicz et al., 2009), it can be speculated that GPR35 might play significant roles in the regulation of inflammation in these regions, although experimental data is not still evident. Despite being a potential target in the treatment of IBD, there remains a dearth of high and equipotent agonists on both human and mouse GPR35, which limits the in vivo study of GPR35 agonists in mouse model of IBD. Recently, structural modifications to lodoxamide provides

a series of useful ligands that eliminate the species selectivity issues and one compound was proven more effective than the reference drug in alleviating clinical symptoms of DSS-induced IBD in mice (Song et al., 2023).

1.4.3 GPR35 in inflammation and immune health

Several studies have found a connection between GPR35 and the control of inflammation, either through the presence of the receptor on the surface of immune-specific cells or by agonist activation changing the immune response. In one of the earliest investigations on GPR35 agonists, it was discovered that kynurenic acid treatment led to a dose-dependent reduction in tumour necrosis factor (TNF) secretion from GPR35-expressing human peripheral blood mononuclear cells (Wang et al., 2006). Treatment of human invariant natural killer-like T (iNKT) cells with kynurenic acid or zaprinast has revealed further connections between GPR35 and pro-inflammatory effects (Fallarini et al., 2010). By secreting the anti-inflammatory cytokines IL-4, IL-5, and TGFß or the pro-inflammatory cytokine, INFγ, activated iNKT cells, which are involved in the development of dendritic cells, GPR35 can either counteract autoimmunity or worsen it. In a later period, one of the most well-known studies to link GPR35 with immune regulation demonstrates that kynurenic acid treatment of monocytes and neutrophils can result in $ß_2$ integrin-mediated firm arrest to monolayers of human umbilical vein endothelial cells that express intracellular adhesion molecule 1. Treatment with pertussis toxin and administration of short hairpin-RNA targeting GPR35 both inhibited the kynurenic acid-induced adherence of monocytic cells, demonstrating that GPR35 is a direct modulator of leukocyte adhesion (Barth et al., 2009). A recent study (Wu et al., 2023b) also claimed that GPR35 is a versatile receptor that can adopt either pro-inflammatory or anti-inflammatory roles within distinct immune cells and tissues.

As previous research has linked GPR35 to the regulation of inflammation (Mackenzie et al., 2011) and zaprinast, a well-known GPR35 agonist, has been shown to actively relieve inflammatory pain, it is now also having positive effects on the production of new bone via the Wnt/GSK3ß/ß-catenin signalling pathway (Zhang et al., 2021). In another study, gallic acid inhibited the inflammasome process and promoted osteogenic differentiation via regulation of GPR35/GSK3ß/ß-catenin pathway signaling. Pham et al. also hypothesised that

GPR35 might be a novel target in the treatment of periodontitis and their results supported the potential for gallic acid for the prevention and treatment of periodontal disease via GPR35 (Pham et al., 2023). In a separate investigation, the promising effects of kynurenic acid on age-related osteoporosis and osteoblastic differentiation were revealed (Ma et al., 2023) and this effect was dependent on Wnt/ß-catenin signaling. As kynurenic acid is claimed to be the endogenous activator of GPR35, the contribution of kynurenic acid to the treatment of age-related osteoporosis might be mediated by GPR35. A different group of researchers demonstrated that downregulation of kynurenic acid formation may contribute to life span extension, and a role of GPR35 is noted (Oxenkrug and Navrotska, 2023).

GPR35 has been connected to immunological health through dietary consumption and digestion of foods containing tryptophan, such as red meat, fish, eggs, and vegetables, which are broken down to produce serotonin, melanin, kynurenic acid, and nicotinamide, among other things (Thorburn et al., 2014). Via the action of *Escherichia coli* in the gut, kynurenic acid can be released from dietary protein and transferred to the extracellular milieu and circulation where it has wide anti-inflammatory effects (Kuc et al., 2008). In addition to research on the effects of kynurenic acid, Yang et al. showed that GPR35 overexpression occurs in response to IgE antibody exposure (Yang et al., 2010). Cromolyn disodium and nedocromil sodium, two anti-allergic and anti-asthma medications, were found to be effective at GPR35 in the same investigation, and numerous related mast cell stabilisers were also found to be effective (MacKenzie et al., 2014). These results indicate that GPR35 might be implicated in inflammation caused by the innate immune response and that it might be targeted for the treatment of inflammatory diseases or autoimmunity. However, the role of the receptor still needs to be fully understood.

1.4.4 GPR35 in central nervous system and nociception

Following observations of its expression in the rat spinal cord and dorsal root ganglion neurons, GPR35 has also been speculated to have effects on the central nervous system (Moroni et al., 2012). Once more, it was discovered that kynurenic acid and zaprinast reduced forskolin-induced cAMP generation in these neurons in a pertussis toxin-sensitive way, suggesting that the GPR35/$G\alpha_{i/o}$ axis may be a

possible target for the treatment of pain. Pre-treatment with the kynurenic acid precursor L-kynurenine or zaprinast dramatically decreased the number of writhes by 58% and 54%, respectively, in a rat 'writhing test' pain model (Cosi et al., 2011). As a result, GPR35 might be a beneficial anti-nociceptive target, albeit it is unclear whether this will apply to people, especially as there is currently no information available about GPR35 expression in human sensory neurons.

Another example of a connection to the central nervous system can be seen in mouse cortical astrocytes, where GPR35 mRNA was found. Forskolin-induced cAMP generation in these cells was once more decreased by kynurenic acid; however, this effect was reversed by either pre-treatment with the GPR35 antagonist CID-2745687 or GPR35 mRNA suppression by siRNA (Berlinguer-Palmini et al., 2013). It is imperative to reiterate, meanwhile, that CID-2745687 has purportedly been demonstrated to be incredibly selective for the human ortholog of GPR35 (Jenkins et al., 2012), casting doubt on the antagonist's mode of action in a mouse model. Overall, the preliminary research suggests that GPR35, a critical part of the central nervous system and nociception, is still a potential therapeutic target for the management of pain or the prevention of excitotoxic damage, even though these findings are not yet completely confirmed. Very recently, Cheng et al. highlighted the vital role of intestinal GPR35 in depression-like behaviour through microbial metabolic signals to the brain (Cheng et al., 2024).

1.4.5 GPR35 in cardiovascular disease

Although its expression profile does not immediately suggest a role for GPR35 in cardiovascular illness, the receptor has been connected, both directly and indirectly, to a number of cardiovascular dysfunctional processes. An astounding 37.5 mmHg increase in blood pressure was observed in early investigations (Min et al., 2010) on a GPR35 deletion mouse strain when compared to wild-type littermates, suggesting a strong likelihood that GPR35 agonists could lower blood pressure. Unfortunately, this was not confirmed by a later independent investigation employing a different knockout line (Divorty et al., 2018). Despite this, numerous studies have indicated that GPR35 contributes to certain cardiovascular abnormalities (Divorty et al., 2015). In fact, an early result showed a connection between coronary artery calcification and a nonsynonymous GPR35 SNP in the intracellular C-terminal tail (rs3749172, S294R) (Sun et al., 2008).

Although this serine residue is a potential site of agonist-induced phosphorylation, replacing it has not been shown to affect the receptor's function or regulation. By observing increases in cardiac GPR35 expression brought on by hypoxia in mice models of cardiac failure, Ronkainen et al. hypothesised that GPR35 mRNA levels would serve as an early indicator of developing cardiac failure (Ronkainen et al., 2014). In order to determine whether GPR35 ligands may be useful for treating neointima formation in vein graft failure after coronary artery bypass surgery, MacCallum et al. examined the effects of GPR35 activation on cell migration and proliferation. This was done because human vascular smooth muscle and endothelial cells express GPR35 robustly (McCallum et al., 2015). In a scratch-wound test, GPR35 activation had an impact on the migration of vascular smooth muscle that was mediated via the RhoA/Rho kinase signalling axis. The $G\alpha_{12}/G\alpha_{13}$ group of G proteins, which GPR35 actively chooses, are responsible for actively controlling this. Recently, (Li et al., 2021) shaded new light on the functions that GPR35 plays in modulating vascular tone and endothelial function, two processes that are crucial to the pathophysiology of elevated blood pressure. Inhibiting the action of GPR35 may be a useful therapeutic strategy for regaining hemodynamic equilibrium and endothelial cell function. Altogether, a clear road to functional translation, despite several studies addressing the cardiovascular effects of GPR35 activity, appears elusive.

1.4.6 GPR35 in energy homeostasis and fatty liver disease

Energy homeostasis includes biological processes that control metabolism, energy intake, and energy expenditure. Although little is known about it, some data suggests that GPR35 and its ligands may be able to control this process. As previously mentioned, the expression of GPR35 is mostly found in the stomach, small intestine, and colon of the gastrointestinal (GI) tract along with immune cells (Milligan, 2011). Kynurenic acid concentrations in the GI tract, particularly in the small intestine, are also substantial (Turski et al., 2013). With the secretion of peptide hormones like cholecystokinin (CCK), which promotes pancreatic enzyme synthesis by sending signals to the central nervous system, the GI tract actively regulates energy balance (Boguszewski and van der Lely, 2015). In GI vagal afferents, GPR35 is expressed with the CCK1 receptor and GPR65, a possible proton sensing receptor. As a result, GPR35 may function as a component of the gut-brain signalling pathway that controls energy balance (Egerod et al., 2018).

Energy homeostasis also depends on lipid metabolism. Adipose tissue, the liver, and skeletal muscle are the primary organs involved in lipid metabolism. Obesity is ultimately caused by an imbalance between the oxidation of free fatty acids by the liver and skeletal muscle and fat accumulation by adipose tissue. The serum levels of kynurenine are said to be higher in obese persons (Mangge et al., 2014). While not being a direct activator of GPR35 (Wang et al., 2006), kynurenine is a precursor of kynurenic acid, the blood concentrations of which are elevated in Zucker fatty rats, a popular rat model of obesity that also lacks leptin receptors (Oxenkrug et al., 2016). Hence, it is plausible that metabolites of the kynurenine pathway, such as kynurenic acid, may contribute to the burden of obesity.

Cirrhosis and hepatocellular carcinoma are two prominent chronic liver diseases that can develop from hepatic steatosis. It is characterised by a build-up of lipid in the liver that is aided by an imbalance in energy homeostasis. GPR35 agonist lodoxamide (potent for rat and human but not for mouse) has been demonstrated to decrease lipid formation in the human HepG2 cell model and, more interestingly, considering the pharmacological characteristics of this ligand, in mouse primary hepatocytes (Nam et al., 2019). It has been demonstrated that lodoxamide reduces the amount of key lipogenic transcription factor, sterol regulatory element-binding protein-1c, hence inhibiting SREBP-1c-induced lipid synthesis. As a result, it was postulated that activating GPR35 may have therapeutic value in managing hepatic steatosis. Before publicly promoting this, however, there is still much that has to be evaluated. Although intriguing, as previously mentioned, lodoxamide is at least 100 times less active at the mouse GPR35 than at the orthologues in either humans or rats, and little is known regarding the ligand's absorption, pharmacokinetics, and pharmacodynamic properties. Hence, it is uncertain if this dose would be adequate to occupy mouse GPR35 significantly. However, based on these investigations, Lin et al. verified that lodoxamide can inhibit liver X-receptor-mediated lipid accumulation in the more commonly used human HepG2 hepatoma cell line (Lin et al., 2021). This gave them the confidence to utilise genome editing technique to create HepG2 clones deficient in GPR35 expression. They observed greater baseline lipid levels in these mutants and a lack of response to lodoxamide until human GPR35a was briefly restored. Although the moderately potent GPR35 agonist bufrolin was able to reduce liver X-receptor-induced lipid accumulation in primary hepatocytes from

wild-type mice (Lin et al., 2021), the lack of suitable antagonists with affinity for mouse GPR35 led this group to create a transgenic mouse line in which human GPR35a was used in place of endogenous mouse GPR35. Lodoxamide concentrations that were predicted to bind to human GPR35a were able to restrict the accumulation of lipids in primary hepatocytes from these animals, and one of the GPR35 antagonists that is specific to humans, ML145, inhibited this (Lin et al., 2021). Moreover, the administration of lodoxamide after the start of fat storage could counteract this characteristic (Lin et al., 2021). Recently, in a separate study, GPR35 expression in hepatocytes and its regulatory role in cholesterol homeostasis in nonalcoholic steatohepatitis was clearly depicted (Wei et al., 2023).

As previously mentioned, GPR35 clearly demonstrates selection for $G\alpha_{12}$ and $G\alpha_{13}$ activation over other G proteins (and in fact, for $G\alpha_{13}$ over $G\alpha_{12}$) (Mackenzie et al., 2019). $G\alpha_{12}$ appears to be crucial for hepatic lipid metabolism, although the effect of GPR35 on hepatic steatosis is still unknown (Kim et al., 2018). It has been demonstrated that activation of $G\alpha_{12}$ reduces hepatic steatosis by boosting liver mitochondrial respiration and fatty acid oxidation. Sets of genes associated with lipid catabolism, acyl-CoA metabolism, ketogenesis, and peroxisomal oxidation activities are suppressed by $G\alpha_{12}$ gene knockout. Importantly, the central players in this gene network are PPAR and PGC-1. These data also offer a possible connection between GPR35's role in preserving energy balance and avoiding the onset of hepatic steatosis, however at this point, it is merely a hint. Hence, novel therapeutic approaches for obesity, glucose intolerance, and fatty liver disease may benefit from considering GPR35 ligands.

Given the elevated expression of GPR35 in the gut and the crucial influence of gut microbial ecology in the development of metabolic disorders, (Wu et al., 2023a) investigated whether variations in GPR35 could impact the composition of gut microbes. Here, it is shown that a global or host intestinal epithelial cells (IEC) specific GPR35 deletion causes a dysbiotic gut microbiome in mice. Most importantly, this is shown to be causally related to the susceptibility to metabolic syndrome generated by a high-fat diet.

1.4.7 GPR35 in cancer

Although GPR35 expression has been associated with a number of malignancies, including gastric, breast, and colon cancers, its function is still unclear (Okumura et al., 2004, Ali et al., 2019, Guo et al., 2017, Wang et al., 2018). Despite GPR35 expression in breast cancer tissues has a high correlation with advanced histological grades (Guo et al., 2017), and ligands such as kynurenic acid can decrease cell proliferation in such malignancies (Walczak et al., 2011), the role of this receptor in cancer is not still directly manifested. Also, it has been noted that individuals with colon cancer whose lymph nodes exhibit high amounts of hGPR35b have brief disease-free survival periods (Ali et al., 2019). In another study (Mackiewicz et al., 2023), high GPR35 expression were found in surgery tissue samples of colorectal cancer (CRC) and pancreatic adenocarcinoma (PDAC). This strongly indicates the prognostic value of GPR35 testing in patients with an increased risk of CRC or PDAC development and warrants further clinical confirmation. In a separate study (Xiang et al., 2023), neuroglobin, an epigenetically silenced factor, has been claimed to block CRC metastasis via the GPR35. A different team of researchers (Bu et al., 2023) discovered that CXCL17 and its receptor GPR35 were highly present in drug-resistant CRC cells and that CXCL17 deletion inhibited drug resistance, cell migration, invasion, and the growth of CRC. Overexpression of GPR35 in non-small cell lung cancer (NSCLC) is linked to a poor prognosis for patients, and GPR35 knockdown greatly reduces chemoresistance in NSCLC in vitro and in vivo (Wang et al., 2018). These findings suggest that GPR35 may aid in the growth and metastasis of cancer and may even function as a clinical tumour marker. Hence, more research into the role, signalling, and functionality of GPR35 in advanced malignancies is of great interest.

One well-known element that raises the risk of several malignancies, including colon cancer, is Src signalling (Kim et al., 2009). It has been suggested that GPR35 can elevate Na/K-ATPase-mediated ion transport, which in turn activates the epidermal growth factor receptor/Src/Ras/ERK signalling pathway in colon cancer cells (Schneditz et al., 2019). In fact, Schneditz et al. demonstrated that genetic GPR35 depletion could decrease intestinal tumorigenesis in both spontaneous and inflammation-driven colon cancer mouse models, and that a lipid-coupled peptide (pepducin) able to inhibit GPR35 activation specifically also decreased tumour

burden in a mouse model of colitis (Schneditz et al., 2019). Although this characteristic is unlikely to be directly relevant to carcinogenesis, hypoxia is a major characteristic of solid tumours that promotes metastasis and supports tumour recurrence via stimulating cancer stem cell differentiation (Hajizadeh et al., 2019, Zhang et al., 2019). Hypoxia-inducible factor-1 (HIF-1) is known to upregulate GPR35 in certain circumstances, including in cardiac myocytes during the progression of cardiac failure (Kim et al., 2009). The effectiveness of GPR35 antagonists in such circumstances, though untested, may therefore be of interest. One of the GPR35 antagonists CID-2745687 has recently been proven as a promising anti-cancer agent by targeting hyperactivation and overexpression of YAP/TAZ in colorectal cancer (CRC) (Otkur et al., 2023a). In another study (Hashemi and Khorramdelazad, 2023), the chemokine CXCL17, along with its possible receptor GPR35 or CXCR8, were reported to be involved in recruiting myeloid cells, regulating angiogenesis, defending against pathogenic microorganisms, and numerous other mechanisms. Given the paucity of research on the dual function of CXCL17 in human cancers, this study (Hashemi and Khorramdelazad, 2023) has looked into the possible pro- and anti-tumour functions of this chemokine as well as potential future directions for cancer therapy. In another report (Yue et al., 2023) GPR35 expression in group 2 innate lymphoid cells (ILC2s) and its impact on tumour immunity were investigated. The outcomes of this report suggested that GPR35 is essential for controlling the invasion of ILC2 as well as the expression of IL-13 and IL-5, which ultimately can modulate tumour immune responses. Hence ILC2s/GPR35 may be a promising therapeutic target for treating lung adeno carcinoma.

Chronic inflammation and lipid metabolism are relevant to cancer even though they are risk factors rather than direct regulators. As GPR35 activation can control inflammation and improve lipid metabolism, it is possible that GPR35 agonists will suppress the growth and spread of cancer. Despite the concerns raised earlier regarding the probable lack of selectivity of many substances that have low intensity activity at GPR35, molecules like flavonoid glycosides can nevertheless bind to GPR35 and act as agonists (Wang et al., 2019). Very recently, 2 food-derived flavonoids thymonin and eriodictyol were also identified as novel GPR35 agonists (Nakashima et al., 2023). Often used in herbal remedies and shown to inhibit the growth of oral and colon cancer cells (Browning et al., 2005, Nasri et

al., 2017) any effects are more likely to resemble homeopathy than to be a result of direct GPR35 pharmacology.

1.5 Thesis aims

Despite being poorly characterised, the orphan G-protein-coupled receptor 35 (GPR35) is receiving a lot of attention as a potential therapeutic target. The use of preclinical disease models has historically been constrained by significant pharmacological variations between human and rodent orthologues of the receptor and a lack of antagonists with affinity for mouse and rat GPR35 (Milligan, 2023). In addition, in the human form of the receptor, there exist two isoforms that differ from each other in 31 additional amino acids in the N-terminal domain. Although having very comparable pharmacology, the longer isoform's agonist effectiveness is about 70% lower than the shorter one (Marti-Solano et al., 2020). In the case of GPCR regulation, although the contribution of agonist mediated phosphorylation of GPR35 in engaging GRKs and subsequent interaction with arrestin is common but to have a thorough map of the identity of individual posttranslational regulatory sites and the contribution of each modified amino acid to the overall effect is sparse. With the help of mass spectrometry, [^{32}P] labelling, mutagenesis, and phospho-site– specific antisera, a clear insight into GPR35 phosphorylation was achieved (Divorty et al., 2022). In addition, it is also vital to pinpoint the specific contribution of individual GRK in phosphorylation and regulation of this receptor. For this, I used combinations of GRK subtype knock-out cell lines (Drube et al., 2022), and reconstitution of function with individual GRKs, a pSer^{300}-pSer^{303} human GPR35a directed antiserum and a group of selective small molecule GRK inhibitors (Uehling et al., 2021). Finally, I developed a complementation experiment based on split nanoluciferase to directly and methodically reveal the GPR35-GRK interaction pattern.

The aims of this PhD thesis are

In-depth investigation of the pharmacology and signalling of the two isoforms of human GPR35 by site-directed mutagenesis techniques and (Arrestin and G protein based) pharmacological experiments.

Identification of the location and specific sites of GPR35 phosphorylation and characterisation of phosphorylation site specific antisera.

Investigation of the contribution of individual or a group of GRKs in GPR35 phosphorylation.

Measurement of the direct and systematic interaction between different GRKs and GPR35.

The outcomes of this thesis will provide unique and wide-ranging insights into isoform functional distinction of human GPR35 and modes of regulation of the receptor that is currently garnering a lot of attention as a potential new therapeutic target for a variety of illnesses, including cancer, inflammatory bowel disorders, and non-alcoholic steatohepatitis.

Chapter 2 Materials and Methods

2.1 Pharmacological test compounds

Lodoxamide (2-[2-chloro-5-cyano-3-(oxaloamino) anilino]-2-oxoacetic acid): Cayman Chemical (Ann Arbor, MI).

Zaprinast 5-(2-propoxyphenyl)-2,6-dihydrotriazolo[4,5-d] pyrimidin-7-one: Tocris Bioscience (Abingdon, U.K.).

Pamoic acid 4-[(3-carboxy-2-hydroxynaphthalen-1-yl) methyl]-3-hydroxynaphthalene-2-carboxylic acid: Sigma-Aldrich.

Bufrolin 6-butyl-4,10-dioxo-1,7-dihydro-1,7-phenanthroline-2,8-dicarboxylic acid: synthesized in collaboration with Novartis, Horsham, U.K.

Amlexanox 2-amino-5-oxo-7-propan-2-ylchromeno[2,3-b] pyridine-3-carboxylic acid: Tocris Bioscience (Abingdon, U.K.).

Doxantrazole 10,10-dioxo-3-(2H-tetrazol-5-yl) thioxanthen-9-one: Sigma-Aldrich.

Cromolyn 5-[3-(2-carboxy-4-oxochromen-5-yl) oxy-2-hydroxypropoxy]-4-oxochromene-2-carboxylic acid: Sigma-Aldrich.

PSB-13253 6-bromo-8-[(4-methoxybenzoyl) amino]-4-oxochromene-2-carboxylic acid: MedKoo Biosciences, Inc.

CID-2745687 (1-(2,4-difluorophenyl)-5-[[2-[[(1,1-dimethylethyl) amino] thioxomethyl] hydrazinylidene] methyl]-1H-pyrazole-4-carboxylic acid, methyl ester): Tocris Bioscience (Abingdon, U.K.).

Pemirolast 9-methyl-3-(2H-tetrazol-5-yl) pyrido[1,2-a] pyrimidin-4-one: Vistakon Pharmaceuticals.

Compound 101 (3-[[[4-methyl-5-(4-pyridyl)-4H-1,2,4-triazole-3-yl] methyl] amino]-N-[2-(trifuoromethyl) benzyl] benzamidehydrochloride): Takeda Pharmaceutical Company, Tokyo, Japan

Compound 19 ((*S*)-*N*2-(1-(5-chloropyridin-2-yl) ethyl)-*N*4-(5-ethyl-1*H*-pyrazol-3-yl)-5-methoxyquinazoline-2,4-diamine): synthesized in collaboration with David E. Uehling, Drug Discovery Program, Ontario Institute for Cancer Research, Toronto, Ontario, Canada.

Compound 15 ((S)-N4-(3-Ethyl-1H-pyrazol-5-yl)-N2-(1-(5-fluoropyridin-2-yl) ethyl)-5-methoxyquinazoline-2,4-diamine): synthesized in collaboration with David E. Uehling, Drug Discovery Program, Ontario Institute for Cancer Research, Toronto, Ontario, Canada.

Compound 16 (N4-(5-Ethyl-1H-pyrazol-3-yl)-N2-((5-fluoropyridin-2-yl) methyl)-5-methoxyquinazoline-2,4-diamine) : synthesized in collaboration with David E. Uehling, Drug Discovery Program, Ontario Institute for Cancer Research, Toronto, Ontario, Canada.

Compound 17 N2-(4-Chlorobenzyl)-N4-(5-ethyl-1H-pyrazol-3-yl)-5-methoxyquinazoline-2,4-diamine: synthesized in collaboration with David E. Uehling, Drug Discovery Program, Ontario Institute for Cancer Research, Toronto, Ontario, Canada.

Compound 18 N2-(4-Chloro-2-methoxybenzyl)-N4-(5-ethyl-1H-pyrazol-3-yl)-5-methoxyquinazoline-2,4-diamine: synthesized in collaboration with David E. Uehling, Drug Discovery Program, Ontario Institute for Cancer Research, Toronto, Ontario, Canada.

Dimethyl sulfoxide (DMSO), at stock concentrations ranging from 1 to 100 mM, was used to dissolve all pharmacological test substances.

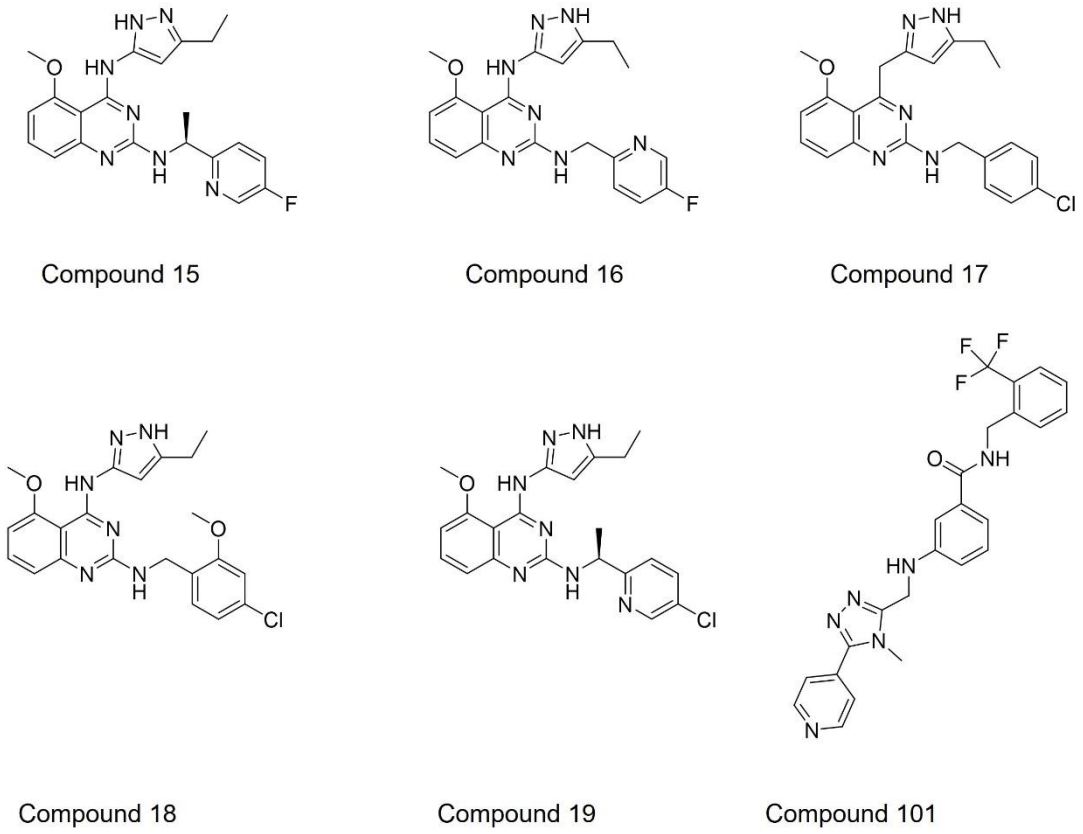

Figure 2.1 Chemical structures of GRK inhibitor compounds
Compounds 15, 16, 17, 18 and 19 are GRK5/6 inhibitors; compound 101 is a GRK2/3 blocker. Structures were drawn by ChemDraw software.

2.2 Chemical reagents

Coelentrazine-h: Thermo Fisher Scientific

Hygromycin-B: Roche, West Sussex, UK

Blasticidin: Life Technologies, Thermo Fischer Scientific, Renfrew, Scotland, UK

Polyethylenimine (PEI) [linear poly (vinyl alcohol) (MW-25000)]: Polysciences, Warrington, PA, USA

cOmplete EDTA-free Protease Inhibitor Cocktail: Roche Diagnostics.

PhosSTOP Phosphatase Inhibitor Cocktail: Roche Diagnostics.

High affinity anti-HA (rat) and anti-HA affinity matrix: Roche Diagnostics.

NuPAGE™ 4 to 12%, Bis-Tris, 1.0–1.5 mm, Mini Protein Gels: Catalog number: NP0321BOX, Thermo Fisher Scientific

Ampicillin stock – 100 mg/ml (make up in distilled water then filter sterilise), working concentration 100 µg/µL

Kanamycin stock 50 mg/ml (make up in distilled water then filter sterilise), working concentration 50 µg/µL

Other cell culture reagents: Thermo Fisher Scientific

2.3 Antibody and antisera

A rabbit phospho-site-specific hGPR35 antiserum pSer^{300}/ pSer^{303}-hGPR35a: (catalogue number 7TM0102C), incorporated the sequence KAHKpSQDpSLCVTL, developed in collaboration with 7TM Antibodies GmbH (Jena, Germany).

A pSer^{298}/pSer^{301}-mGPR35 antiserum (7TM0102B), raised against the sequence TPHKpSQDpSQILSLT, collaboratively created with 7TM Antibodies GmbH (Jena, Germany).

A GPR35 (non-phospho) antibody (cat number 7TM0102N), directed against the distal part of the carboxyl-terminal tail of hGPR35, were created with the assistance of 7TM Antibodies GmbH. (Jena, Germany).

IRDye 800CW donkey anti-rabbit IgG: LI-COR Biosciences

IRDye 800CW donkey anti-goat IgG: LI-COR Biosciences

IRDye 800CW goat anti-rat IgG: LI-COR Biosciences

Horseradish peroxidase anti-mouse (sheep): GE Healthcare

Anti-LgBiT monoclonal antibody (cat number N7100): Promega Corporation

GRK isoform-directed antisera for GRK 2 sc-13143 (C-9): Santa Cruz Biotechnology

GRK isoform-directed antisera for GRK 5 sc-518005 (D-9): Santa Cruz Biotechnology

GRK isoform-directed antisera for GRK 3 CS #80362 (D8G6V): Cell Signalling Technology

GRK isoform-directed antisera for GRK 6 CS #5878 (D1A4): Cell Signalling Technology

2.4 Buffers and solutions

Competent bacteria solution 1: 30 mM CH_3CO_2K, 10 mM $RbCl_2$, 10 mM $CaCl_2$, 50 mM $MnCl_2$, 15% (v/v) glycerol were mixed, and pH was adjusted to 5.8 with acetic acid.

Competent bacteria solution 2: 10 mM 3-morpholinopropane-1-sulfonic acid (MOPS), 10 mM $RbCl_2$, 75 mM $CaCl_2$, 15% (v/v) glycerol were mixed, and pH was fixed at 6.5 with HCl

Hank's balanced salt solution (HBSS): 137 mM NaCl, 5.3 mM KCl, 0.34 mM Na_2HPO_4, 0.44 mM KH_2PO_4, 4 mM $NaHCO_3$, 1.26 mM $CaCl_2$, 0.5 mM $MgCl_2$, 0.4 mM $MgSO_4$ were mixed, and pH was fixed at 7.3

Laemmli buffer (2x): 60 mM Tris, 80 mM sodium dodecyl sulphate (SDS), 50 mM dithiothreitol, 10% (v/v) glycerol, 0.25% (w/v) bromophenol blue

Luria-Broth (LB): 1% Tryptone, 0.5% yeast extract and 10g NaCl = 1L H_2O (pH 7.0) Autoclaving was conducted at 126°C.

Luria-agar (LA): 1% (w/v) Tryptone, 0.5% (w/v) yeast extract, 1% (w/v) NaCl and 1.5% (w/v) Bacto-agar = 1L H_2O (pH 7.0) and autoclaved at 126°C. Agar broth was cooled, 50 mg/mL ampicillin was added, and then 10 cm dishes were filled with solidified agar broth. These dishes were then stored at 4°C.

Lysis buffer (phospholabelling): 20 mM Tris (pH 7.4), 150 mM NaCl, 3 mM ethylenediaminetetraacetic acid (EDTA), 1% (v/v) NP-40, 0.5% (w/v) sodium deoxycholate were mixed properly.

Phosphate-buffered saline (PBS): 137 mM NaCl, 2.7 mM KCl, 1.8 mM KH_2PO_4, 10 mM Na_2HPO_4, pH was fixed at 7.4

Transfer buffer (1L): 14.4 g glycine, 3.03 g Tris, 200 ml methanol, H_20 up to 1000 ml.

Tris-acetate-EDTA (TAE) buffer: 40 mM Tris, 1 mM EDTA (pH 8), 20 mM acetic acid were mixed.

Tris-buffered saline (TBS) 10X (1L): 24 g Tris and 88 g NaCl were dissolved in 900 mL of water and made final volume to 1 L.

This solution was diluted to 1X and then the pH was adjusted to 7.6.

500µl of Tween-20 was added to 500 ml TBS (1X). This was used for washing blots.

After adding 5% BSA to TBS 1X, the solution was used for blocking non-specific bands.

Upon addition of 0.1% Tween-20 and 5% BSA to TBS 1X, this solution was used for antibody dilution.

Tris-EDTA (TE) buffer: 10 mM Tris, 0.1 mM EDTA, pH 7.4

MOPS SDS Running Buffer (20X): NuPAGE™, Catalog number**:** NP0001, Thermo Fisher Scientific. (1X Running Buffer was used for running gel in western blot)

2.5 Generation of DNA constructs and mutagenic plasmids

Generation of the following mutants in each of hGPR35a-eYFP construct, hGPR35b-eYFP construct, hGPR35a- $G\alpha_{13}$ SPASM sensor and hGPR35b- $G\alpha_{13}$ SPASM sensor:

hGPR35a: Cys8Ser, Cys248Ser

hGPR35b: Cys27Ser, Cys39Ser and Cys279Ser

After getting preliminary information from the above mutants, some additional mutants were generated in the Cys27Ser backbone of the long isoform of GPR35 (hGPR35b). In order to use the mutants in the arrestin-3 interaction test, the enhanced yellow fluorescent protein (eYFP) tag was attached with the mutants. To measure G protein activation, the same mutants were also created in GPR35- $G\alpha_{13}$ SPASM sensors. (Table 2.1) shows the hGPR35b mutants for arrestin-3 recruitment and $G\alpha_{13}$ activation.

Mutants for arrestin-3 interaction in Cys27Ser backbone	Mutants for $G\alpha_{13}$ activation in Cys27Ser backbone
S5C tagged with eYFP	S5C in GPR35- $G\alpha_{13}$ SPASM
T10C tagged with eYFP	T10C in GPR35- $G\alpha_{13}$ SPASM
G14C tagged with eYFP	G14C in GPR35- $G\alpha_{13}$ SPASM
S15C tagged with eYFP	S15C in GPR35- $G\alpha_{13}$ SPASM
M22C tagged with eYFP	M22C in GPR35- $G\alpha_{13}$ SPASM
S25C tagged with eYFP	S25C in GPR35- $G\alpha_{13}$ SPASM
S29C tagged with eYFP	S29C in GPR35- $G\alpha_{13}$ SPASM
M32C tagged with eYFP	M32C in GPR35- $G\alpha_{13}$ SPASM
G34C tagged with eYFP	G34C in GPR35- $G\alpha_{13}$ SPASM

Table 2.1 Name of mutants in the Cys27Ser backbone of hGPR35b

For creating these mutants, the following primers were designed, synthesised, and used. They are displayed in (Table 2.2).

Primer sequence (5´ to 3´)	Template	Mutation	For/Rev
CAAGGATGACGACGATAAGCTGAGTGGTTGTCGGGCTGTC	hGPR35b C27S	S5C	For
TATCGTCGTCATCCTTGTAATCCATGGTGGCAAGCTTAAG	hGPR35b C27S	S5C	Rev
GCTGTCCCCTGTCCACACCGTGGCAGTGAAGAGCTGCTG	hGPR35b C27S	T10C	For
CGGTGTGGACAGGGGACAGCCCGGGAACCACTCAGC	hGPR35b C27S	T10C	Rev
CACACCGTTGCAGTGAAGAGCTGCTGAAGTACATGC	hGPR35b C27S	G14C	For
CTTCACTGCAACGGTGTGGAGTGGGGACAGCCCGGGAAC	hGPR35b C27S	G14C	Rev
CACCGTGGCTGTGAAGAGCTGCTGAAGTACATGCTTC	hGPR35b C27S	S15C	For
CAGCTCTTCACAGCCACGGTGTGGAGTGGGGACAGCCCG	hGPR35b C27S	S15C	Rev
GAAGTACTGCCTTCATAGTCCTAGCGTCTCTCTGACCATG	hGPR35b C27S	M22C	For
CTATGAAGGCAGTACTTCAGCAGCTCTTCACTGCCACGG	hGPR35b C27S	M22C	Rev
GCTTCATTGTCCTAGCGTCTCTCTGACCATGAATGG	hGPR35b C27S	S25C	For
GACGCTAGGACAATGAAGCATGTACTTCAGCAGCTCTTC	hGPR35b C27S	S25C	Rev
GTCCTAGCGTCTGTCTGACCATGAATGGCACCTACAAC	hGPR35b C27S	S29C	For
CATGGTCAGACAGACGCTAGGACTATGAAGCATGTAC	hGPR35b C27S	S29C	Rev
CTGACCTGCAATGGCACCTACAACACCTGTGGCTCCAGC	hGPR35b C27S	M32C	For
GTTGTAGGTGCCATTGCAGGTCAGAGAGACGCTAGGAC	hGPR35b C27S	M32C	Rev
CCATGAATTGCACCTACAACACCTGTGGCTCCAGCGAC	hGPR35b C27S	G34C	For
GGTGTTGTAGGTGCAATTCATGGTCAGAGAGACGCTAGG	hGPR35b C27S	G34C	Rev

Table 2.2 List of primers for creating mutants in various positions of Cys27Ser backbone of hGPR35b

Later, I generated some additional mutants in wild type (WT) and C27S backbone of the hGPR35b. I mutated arginine (R) at position 13 to proline (P), histidine (H) and cysteine (C) in both Wild type and C27S backbone hGPR35b and they are shown in (Table 2.3).

R13 'SPASM' Mutants for $G\alpha_{13}$ activation	R13 mutants for arrestin interaction
R13P in WT GPR35b	**R13P in WT GPR35b**
R13P in C27S GPR35b	**R13P in C27S GPR35b**
R13H in WT GPR35b	**R13H in WT GPR35b**
R13H in C27S GPR35b	**R13H in C27S GPR35b**
R13C in WT GPR35b	**R13C in WT GPR35b**
R13C in C27S GPR35b	**R13C in C27S GPR35b**

Table 2.3 Name of arginine (at position 13) mutants in the wild type and Cys27Ser backbone of hGPR35b

The following primers were created, produced, and utilised to make these mutants and are displayed in (Table 2.4).

Primer sequence (5´ to 3´)	For/Rev
TGGCAGTGAAGAGCTGCTGAAGTACATGCTTCATAGTCC	**GPR35 forward primer**
TTCAGCAGCTCTTCACTGCCAGGGTGTGGAGTGGGGACAG	**R13P reverse primer**
TTCAGCAGCTCTTCACTGCCATGGTGTGGAGTGGGGACAG	**R13H reverse primer**
TTCAGCAGCTCTTCACTGCCACAGTGTGGAGTGGGGACAG	**R13C reverse primer**

Table 2.4 List of primers for arginine (at position 13) mutagenesis experiments

In nanoluciferase based complementation assay, where interactions between GPR35 and different GRKs were investigated, I produced several GPR35 constructs with SmBiT tag so that they can recombine with GRKs that are tagged with LgBiT. The name of the SmBiT tagged constructs are mentioned here.

1. hGPR35a, 2 hGPR35b, 3. hGPR35 PDM, 4. mGPR35, 5. mGPR35 PDM.

The primers were designed, created, and successfully utilised for generating the receptor constructs with SmBiT and they are displayed in (Table 2.5).

Sequence of primer (5´ to 3´)	For/Rev
TATAGGGCTAGCGCCACCATGAATGGCACCTACAACACC	**hGPR35a forward**
TATAGGGCTAGCGCCACCATGCTGAGTGGTTCCCGGGCTG	**hGPR35b forward**
CCACCGCTCGAGCCGGCGAGGGTCACGCACAGAG	**hGPR35 reverse**
TATAGGGCTAGCGCCACCATGAATAGTACAACCTG	**mGPR35 forward**
CCACCGCTCGAGCCGGTGAGGCTCAGGATCTGGG	**mGPR35 reverse**
CCACCGCTCGAGCCGGCGAGGGCCAGGATCTGGGC	**mGPR35 PDM reverse**

Table 2.5 List of primers for generating GPR35 (human and mouse orthologues) construct with SmBiT tag to utilise them in GPR35-GRK profiling

In the GPR35-GRK5 interaction assay, I also used truncated and mutated versions of GRK5 along with the full-length form of GRK5 to properly investigate the reason for concentration dependent signal reduction. The necessary primers for truncation and mutation of GRK5 are displayed in (Table 2.6).

Primer sequence (5´ to 3´)	For/Rev
ATATATAAGCTTGCCACCATGGTCTTCACACTCGAAG	**Forward primer for truncated GRK5**
GGGCCCTCTAGATCATCCGGAGGGTGGTTTC	**Reverse primer for truncated GRK5**
GAACCGCCCGCGGCAGGGCTGCTCCAGAGACTCTTCGCGGCGCAGCATCAGAACAATTCC	**Forward primer for mutated GRK5**
CTGATGCTGCGCCGCGAAGAGTCTCTGGAGCAGCCCTGCCGCGGGCGGTTCCGGAG	**Reverse primer for mutated GRK5**

Table 2.6 List of primers for truncated and mutated forms of GRK5

2.6 Cloning and molecular biology

2.6.1 LB (Luria-Bertani) medium and LB agar plates preparation

800 ml of deionised, distilled water was added to the dry reagents, which contained 10 g of tryptone, 5 g of yeast extracts, and 10 g of NaCl. The pH of the solution was then adjusted to 7.0 using NaOH. The solution was then increased to a volume of 1 L. Following that, the solution was autoclaved on the liquid cycle for 20 min at 15 psi. After making LB medium as described above, 15 g of bacto-agar was added per 1L of LB, and the mixture was autoclaved at 126°C to create LB agar plates. The bottles were autoclaved, allowed to cool to 55°C, and then the correct quantity of filter-sterilised ampicillin was added with a final concentration of 50–100 µg/ml. After properly blending the ampicillin and LB agar in the bottle with a swirl, about 20 ml of agar was placed into a 10 cm petri dish. After that, the plates were left at room temperature for 20 min so that the agar could solidify. The plates were inverted and kept at 4°C in the dark once they had dried and solidified.

2.6.2 Competent bacteria preparation

A supply of XL1-blue cells from Agilent Technologies was taken out, thawed on ice, streaked out on an LB agar plate without antibiotics, and cultivated overnight at 37ºC to create competent bacteria for chemical transformation. The next day, a single colony was selected and cultivated in 5 ml of LB media (without antibiotics) at 37°C and 220 rpm for the whole night. This 100 ml of LB media was then used to subculture the 5 ml culture, which was subsequently cultivated at 37 ºC in a shaking incubator until the optical density at 600 nm reached 0.48. By freezing on ice for 5 min, the growth of bacteria was stopped and then centrifuging at 1811 x g for 10 min at 4ºC in 50 ml sterile falcon tubes was conducted. Bacterial cell pellets from each of the 50 ml falcon tubes were carefully pipetted into 20 ml of solution 1 (30 mM CH_3COOK, 10 mM RbCl, 10 mM $CaCl_2$, 50 mM $MnCl_2$, and 15% (v/v) glycerol; pH 5.8; filter sterilised and refrigerated at 4ºC) and then cooled on ice for 5 min. Further centrifugation of the cold pellets took place at 1811 x g for 10 min at 4 ºC. The pellets from this second centrifugation were then carefully re-suspended in 2 ml of solution 2 (10 mM 3-morpholinopropane-1-sulfonic acid (MOPS), 10 mM RbCl, 75 mM $CaCl_2$, 15% (v/v) glycerol, pH 6.5 with HCl; filter

sterilised and stored at 4ºC) by gentle pipetting and chilled on ice for an additional 15 min. Bacterial cells were then divided into 220 µl quantities and placed in sterile, 1.5 ml microcentrifuge tubes that had already been cooled.

2.6.3 Chemical transformation of plasmid cDNA with competent cells

XL1-blue cells that were chemically competent were removed from -80°C and allowed to thaw on ice for 20 min. For each transformation, 50 µl of defrosted competent cells were aliquoted into a 1.5 ml microcentrifuge tube that had been precooled, along with 1 µl of DNA (10–100 ng), and the tube was gently mixed by flicking the bottom. After 15 min on ice, the competent cell/DNA mixture underwent a heat shock treatment at 42°C for 90 sec by being placed in tubes on a rack submerged in water. The tubes were then put on ice right away for 2 min. Each tube received 500 µl of LB media devoid of antibiotics, and bacteria were allowed to express antibiotic resistance genes by growing at 37°C for 45 min to 1 h in a shaking incubator (220 rpm). A 10 cm LB agar plate that was pre-warmed and included 100 µg/ml ampicillin was then plated with 50 to 200 µl of transformation using a sterile spreader. Overnight, the plates were incubated at 37°C while being held upside down. Colonies on the LB agar ampicillin plate can only be generated by cells with the transformed plasmid. The next day, a single colony was selected and cultivated overnight at 37°C in a shaking incubator in 5 ml of LB media containing 100 µg/µl ampicillin.

2.6.4 Plasmid DNA purification

2.6.4.1 Miniprep purification

Microgram quantities of plasmid DNA were purified using the QIAprep® Spin Miniprep Kit. Here,1-5 ml bacterial overnight culture was centrifuged at 13,000 rpm for 3 min at room temperature. Pelleted bacterial cells were resuspended in 250 µl buffer P1 and then transferred to a microcentrifuge tube. 250 µl buffer P2 was added and mixed thoroughly by inverting the tube 4-6 times until the solution became clear. The lysis reaction was not allowed to proceed for more than 5 min. The solution turned blue because LyseBlue reagent was used. After that 300 µl buffer N3 was added and mixed immediately and thoroughly by inverting the tube 4-6 times. The solution now turned colourless as LyseBlue was added previously.

It was then centrifuged for 10 min at 13,000 rpm in a table-top microcentrifuge. After spinning, 800 µl of supernatant was applied to QIAprep 2.0 spin column with the help of a pipette. This was centrifuged for 30-60 sec and the flow-through was discarded. Then the QIAprep 2.0 spin column was washed by adding 0.75 ml buffer PE. This was then centrifuged for 30-60 sec and the flow-through was discarded. The QIAprep 2.0 spin column was transferred to the collection tube. This was again centrifuged for 1 min to remove residual wash buffer. Finally, the QIAprep 2.0 spin column was placed in a clean 1.5 ml microcentrifuge tube. For eluting DNA, 100 µl water was added to the centre of the spin column. It was allowed to stand for at least 1 min and then centrifuged for 1 min. The resulting DNA was stored at -20°C.

2.6.4.2 Maxiprep purification

Following the manufacturer's instructions, plasmid DNA in milligram quantities was purified using the QIAGEN® Plasmid Maxi Kit. In brief, centrifugation was carried out on a 200–500 mL overnight culture at 3000 x g for 30 min at 4°C. Re-suspending the bacterial pellet in pre-chilled resuspension buffer and lysing it with the addition of lysis buffer was conducted. After being incubated for 5 min at room temperature, the lysate was neutralised by adding neutralisation buffer that had already been refrigerated, and it was then incubated for 20 min on ice. Centrifugation at the speed of 3000 x g was performed on the resultant solution for 15 min at 4°C. A 15 mL equilibration buffer was used to acclimatise a QIAGEN-tip 100 column before the lysate supernatant was added and allowed to pass through the column by gravity flow. The column was cleaned twice with wash buffer after the flow-through was discarded. After precipitating the DNA with 10.5 mL of isopropanol and eluting it in 15 mL of elution buffer, the DNA was centrifuged at 3000 x g for 30 min. After being air-dried and desalted with 2 mL of 70% (v/v) ethanol, the pellet was placed in a sterile microcentrifuge tube and centrifuged at 16,000 x g for 15 min. The pure DNA pellet was air dried before being dissolved in 0.5–1 mL of nuclease-free water.

2.6.4.3 Measurement of DNA concentration

Using a UV spectrophotometer, the absorbance of diluted samples (1:200) at 260 nm and 280 nm was measured to determine the amount of plasmid DNA present and its purity. The absorbance reveals the amount of DNA at 260 nm (A260), while the purity of the sample is indicated by the ratio of A260/A280, with a ratio between 1.8 and 2.0 being regarded as very pure DNA.

2.6.5 Polymerase chain reaction (PCR)

Certain DNA segments were amplified, and restriction sites were added using PCR. In sterile 500 µL PCR tubes, 50 µl reactions containing the following elements were set up:

1 × GoTaq® Colorless Buffer

Deoxyribonucleotides (dNTPs): 0.8 mM (deoxyadenosine triphosphate, deoxycytidine triphosphate, deoxyguanosine triphosphate, and deoxythymidine triphosphate are all 0.2 mM concentrations)

Forward and reverse primers, each 0.5 µM

Template DNA (100 ng)

GoTaq® DNA Polymerase, 5 units

Nuclease-Free water to 50 µl

The following conditions were used to thermally cycle reaction mixtures:

Preheating 95°C 2 min

Denaturation 95°C 30 sec

Annealing 50–60°C* 30 sec

Extension 72°C 2 min

Repeat actions 2-4. (x 29)

Last extension: 10 min at 72°C

Hold 4°C ∞

*Depends on primer's melting temperature (Tm)

2.6.6 PCR Purification

According to the manufacturer's recommendations, PCR products were purified using the QIAquick® PCR Purification Kit (QIAGEN). Briefly, PCR product was put to a QIAquick spin column after being diluted in five volumes of binding solution and centrifuged at 13,000 rpm for 1 min. The flow-through was thrown out and the column washed once, centrifuging as before. The flow-through was discarded, and the column was centrifuged once more to get rid of any leftover ethanol. 50 µL of nuclease-free water was used to elute the DNA, and it was then centrifuged after standing on the column for 1 min.

2.6.7 Restriction endonuclease digestion

Sticky-end DNA fragments for ligation were produced using restriction endonuclease enzyme digestion. The necessary insert segments and the plasmid vectors of pcDNA3.1(+), pcDNA3.1/Hygro (+), or pcDNA5/FRT/TO were digested overnight at 37°C in digests of 50–100 µl that comprise the following components:

1 x CutSmart® Buffer

50 µL PCR product or 10–50 µg vector DNA

According to the manufacturer's recommendations for supercoiled plasmid DNA, 1–10 units restrictions endonucleases with high fidelity (HF®) from New England Biolabs

Sterile, deionised water

2.6.8 Agarose gel electrophoresis

Agarose gel electrophoresis was used to separate the DNA insert and vector fragments. In TAE buffer, 1% (w/v) agarose and 1 x SYBR® Safe DNA dye (Life Technologies) were dissolved to create gels. Gels were immersed in TAE buffer after they had set, samples had been prepared by adding 1 x DNA loading buffer, and then 5- 50 µl/well of sample had been placed onto the gel. The electrophoresis of the samples was carried out at 125 V for 20–30 min. Using a 5 µl HyperladderTM 1kb (Bioline) alongside the samples allowed me to determine the size and concentration of the DNA fragments.

2.6.9 Gel extraction

After gel electrophoresis, DNA insert, and vector fragments were extracted from the gel using the QIAquick Gel Extraction Kit (QIAGEN) in accordance with the manufacturer's guidelines. In a nutshell, razor blades were used to cut the bands out of the gel after they had been seen under UV light. After being placed in sterile microcentrifuge tubes, gel fragments were weighed. The solubilisation buffer was added in 3 gel volumes, and the gel pieces were then broken down by incubation at 50°C for 10 min while vortexing every 2-3 min. Isopropanol was dissolved in 1 gel volume, and the mixture was then put to a QIAquick spin column and centrifuged at 13,000 rpm for 1 min. The centrifugation process was repeated after the flow-through was discarded and the column rinsed once. The column was centrifuged once more to remove any remaining ethanol after discarding the flow-through. 30–50 µl of nuclease-free water was used to elute the DNA, and it was then centrifuged after standing on the column for 1 min.

2.6.10 DNA dephosphorylation

In order to eliminate the 5' phosphate groups from digested vector fragments and lessen the possibility of re-ligating empty vector, vector fragments were treated with calf intestinal alkaline phosphatase (Quick CIP, New England Biolabs). Per µg of vector, 1 unit of Quick CIP and 0.1 volume of 10 x rCutSmartTM Buffer were added. The Quick CIP was totally and permanently inactivated by heating the samples for 2 min at 80°C after samples had been incubated for 30 min at 37°C.

2.6.11 DNA ligation

Recombinant plasmid DNA was created through the ligation of DNA sticky ends. 20 µl ligation reactions using the following elements were used as the starting point for the addition of pieces of the insert and the vector at molar ratios of 1:3, 1:1, and 3:1

T4 DNA Ligase Reaction Buffer, 1 x

vector DNA at 100 ng

Insert DNA X ng

400 units of T4 DNA Ligase (1 µL)

Ligation processes were kept at room temperature for 3 h, or at 4°C overnight, or at 15°C for 4–18 hr.

According to section (2.6.3), 5 µL of the ligated product was transformed into XL1-Blue competent bacteria.

2.6.12 In vitro site-directed mutagenesis

A QuickChange II Site-Directed Mutagenesis procedure was used to carry out the point mutation of interest on the DNA sequence (Stratagene, Cheshire, UK). In this technique, a double-stranded mutant plasmid with the required mutation was amplified by PCR using two synthetic oligonucleotide primers, each of which used a double-stranded plasmid vector as the template and each of which contained the desired mutation. Using a piece of software like Agilent Quick-change (https://www.genomics.agilent.com/primerDesignProgram.jsp), two mutagenic oligonucleotide primers were created that are complementary to one another and include the desired mutation in the middle of the primer. When creating primers, it was made sure that the length would be between 25 and 45 bases, the GC content would be higher (40 to 60%), and the melting temperature (Tm) would be around 78ºC. For the purpose of amplifying the mutant plasmid, a PCR amplification reaction (sample reaction) with a final volume of 50 µl was set up on ice in a sterile PCR tube with the following ingredients:

5 µl of 10x Pfu DNA polymerase buffer with $MgSO_4$/Q5 High fidelity DNA polymerase buffer

200 µM of each dNTP in 1 µl of 10 mM dNTP mix

Forward oligonucleotide primer, 1.25 µl (125 ng)

Reverse oligonucleotide primer, 1.25 µl (125 ng)

dsDNA template ranging from 50 to 100 ng

1 µl of (2.5 units/µl) Pfu DNA Polymerase/Q5 High fidelity DNA Polymerase enzyme

Sufficient nuclease-free water to fill 50 µl

With the exception of the two primers, a second PCR reaction (the control reaction) was set up on ice in a different PCR tube. The following conditions were used to thermally cycle reaction mixtures of both (sample reaction and control reaction) using an Eppendorf Mastercycler.

Preheating 95°C 30 sec

Denaturation 95°C 30 sec

Annealing 55° 1 min

Extension 72°C 10 min

Repeat steps 2–4 (x 17)

Hold 4°C ∞

Following the end of heat cycling, 1 µl of (10 units/l) DpnI restriction endonuclease was added to the reaction mixtures for the sample and the control, which was then gently mixed and spun down in a microcentrifuge for 1 min. The parental methylated dsDNA was subsequently digested by the reaction mixes over a 2 h

period at 37ºC while leaving the synthesised mutant plasmid intact. Following the procedure outlined in the transformation section (2.6.3), 3 µl of the DpnI-treated DNA from each control and sample reaction was then transformed into separate 50 µl of XL1-blue capable bacteria.

2.6.13 DNA sequencing

Products from cloning and mutagenesis were sequenced to ensure that the right alterations had been made. DNA sequencing was carried out by DNA Sequencing & Services (MRC I PPU, College of Biological Sciences, University of Dundee, Scotland; www.dnaseq.co.uk) on an Applied Biosystems model 3730 automated capillary DNA sequencer using Applied Biosystems Big-Dye Ver 3.1 chemistry. The NCBI Basic Local Alignment Search Tool (BLAST) (www.blast.ncbi.nlm.nih.gov) were used to analyse DNA sequences.

2.7 Culture of mammalian cell

2.7.1 Mammalian cell lines maintenance

2.7.1.1 Parental HEK293T cells

Human embryonic kidney (HEK) 293T cells or any parental cell lines genome edited for lacking expression of either G protein, GRKs or arrestins were maintained in Dulbecco's modified Eagle's medium supplemented with 0.292 g/l L-glutamine, 1% penicillin/streptomycin mixture, and 10% heat-inactivated fetal bovine serum at 37˚C in a 5% CO_2 humidified atmosphere.

2.7.1.2 Flp-In T-REx-293 cells

Flp-In TREx 293 cells (Thermo Fisher) were maintained in Dulbecco's modified Eagle's medium without sodium pyruvate, supplemented with 10% fetal bovine serum, 1% penicillin/streptomycin mixture, and 10 µg/ml blasticidin at 37˚C in a 5% CO_2 humidified atmosphere.

2.7.1.3 Cell line cryopreservation

For long-term liquid nitrogen storage, cell lines were cryopreserved. Trypsin-EDTA was used to detach confluent cells, which were then centrifuged at 500 x g for 5

min. Before being moved to liquid nitrogen storage, the pellet was redissolved in 2-3 mL FCS + 10% (v/v) DMSO and divided into 1 mL aliquots that were frozen at -80°C. Cryopreserved cells were brought back to life by rapidly defrosting in a 37°C water bath and transferring to 10 mL of pre-warmed culture medium in a flask. After 8 to 16 h, the medium was changed to eliminate the DMSO.

2.7.1.4 Passaging of cells

Medium was withdrawn using a pipette within a laminar flow cabinet under sterile circumstances once it had reached the necessary confluence. The T75 cell culture flask was rinsed with 1X PBS to remove the residual medium. Then pre-warmed 2 mL (approx.) 0.5% trypsin-EDTA was added and evenly distributed to ensure coverage. The flask was then kept at 37°C in a 5% CO_2 incubator for 2-3 min. After that flask was tapped gently to ensure complete cell dissociation from the plasticware. Cells were re-suspended by addition of a pre-warmed medium containing serum by a sterile 10 mL pipette, before transferring (1-2 mL) to a sterile T75 cell culture flask having 10 mL medium.

2.7.2 Transient transfection of cell lines

The standard technique for transient transfection was PEI-mediated transient transfection. 5 µg of DNA was diluted in 250 µl of 150 mM NaCl for a 10 cm culture dish, and then it was combined 1:1 with 250 µl of 150 mM NaCl that also contained 30 µg of PEI. Before adding dropwise to the dish, the mixture was vortexed for 10 sec and allowed to sit for 10 min at room temperature. At 37°C, cells were treated with PEI overnight. Following the overnight incubation, fresh culture media was added to the transfection medium. Before being used in tests, the cells underwent a further 24–48 h of incubation.

2.7.3 Production of stable transfection of cell lines

Several hGPR35a and mGPR35-based constructs were transfected into doxycycline-inducible Flp-In TREx 293 cells in a stable manner. Using the FRT stable integration site, the relevant cDNA-containing pcDNA5/FRT/TO vector was transfected into cells. The appropriate cDNA/pcDNA5/FRT/TO construct and a pOG44 Flp recombinase vector were co-transfected into cells using PEI in a 1:8 ratio. To choose stable transfectants, cells were subcultured 1:10 and 1:30 after

48 h. The medium was then changed to maintenance medium with 200 µg/ml hygromycin and 10 µg/ml blasticidin after 24 h. Until individual colonies were visible to the naked eye (10–14 days), the medium was changed every three days. Following trypsin-EDTA incubation, cells were detached into polyclonal cell lines that were maintained in hygromycin selection media. When necessary, 100 ng/ml doxycycline was added to the mixture for 18 to 24 h to activate the expression of integrated gene.

2.7.4 Mycoplasma testing of cell lines

As mycoplasma contamination is a significant problem for mammalian cell culture, cell lines were regularly inspected for possible contamination with mycoplasma. For this, elimination of mycoplasmas was ensured by using a mycoplasma detection kit MycoStrip™ (https://www.invivogen.com/plasmocin).

2.8 Biochemical assays and procedures

2.8.1 Immunoblotting

2.8.1.1 Harvesting of cell

Initially, cells were harvested by removing the growing medium and washing in a PBS buffer that was extremely cold. In case of drug treatment to cells, cells were stimulated with agonist/antagonist or inhibitor and then washed with ice cold PBS. The cells were removed from the 10 cm dish's bottom using a disposable cell scraper and 10 ml of PBS buffer. A 15 mL falcon tube was used to hold the cell suspension. The tubes are centrifuged at 3,000 rpm at 4ºC for 5 min. The cell pellets were then kept at -80˚C until they were needed for a subsequent experiment.

2.8.1.2 Cell lysate preparation

HEK293 cells that had been transfected to express eYFP and HA-fusion receptor constructs produced cell lysates. Cells were initially stimulated using a vehicle or a variety of suitable ligands. Then cells were harvested in ice-cold PBS and lysed in lysis buffer (150 mM NaCl, 50 mM Tris-HCl, 5 mM EDTA, 1% Nonidet P-40, 0.5% Na-deoxycholate, and 0.1% SDS), supplemented with cOmplete™ EDTA-free Protease Inhibitor Cocktail (Roche) and PhosSTOP™ Phosphatase Inhibitor Cocktail

(Roche) (if immunoblotting for phosphoproteins). The lysates were rotated at 4°C for 30 min. After that, samples were centrifuged at 14200 rpm for 15 min at 4°C.

2.8.1.3 Production of crude plasma membrane

The frozen cell pellets were thawed and suspended in 5 volumes of ice-cold TE Membrane buffer. The cells were then ruptured by homogenising the mixture with 30 strokes of a ground glass on Teflon. Unbroken cells and nuclei were eliminated by centrifugation in a chilled microcentrifuge at a low speed (1200 rpm). The supernatant fraction was next centrifuged in a Beckman Optima TLX Ultracentrifuge (Palo Alto, CA) using a TLA100.2 rotor at 50,000 rpm for 20–30 min. The pellets were reconstituted in ice-cold TE Membrane buffer and injected into a 25-gauge needle-equipped syringe. The membranes were kept at -80°C until needed after being diluted to a good working concentration, typically 1µg/µl.

2.8.1.4 Membrane and cytosolic fractions

In 10 cm dishes, cells were seeded, and they were then cultivated until confluent. Cells were scraped into 2-3 mL of ice-cold PBS, washed once with ice-cold PBS, and then centrifuged at 1200 rpm for 5 min at 4°C. For at least 30 min, cell pellets were incubated at -80°C. The thawed pellets were resuspended in 1 ml of TE buffer with Roche's cOmpleteTM EDTA-free Protease Inhibitor Cocktail, and then they were homogenised by being passed through 5 x in a 25-gauge needle and 50 x in a Dounce homogenizer. To remove cell debris, homogenate was centrifuged at 500 x g for 5 min at 4°C. Supernatants were carefully collected and centrifuged at 100,000 x g for 60 min at 4°C. For cytosolic fractions, supernatant was gathered. To get membrane fractions, membrane pellets were reconstituted in 400 µl of protease inhibitor-containing TE buffer and subjected to 5 x through a 25-gauge needle.

2.8.1.5 Protein concentration determination

Using a reference curve of 0.2-2 mg/ml BSA, the protein concentrations of samples used for immunoblotting were assessed by the bicinchoninic assay (BCA). A transparent 96-well plate was filled with 10 µl of sample or standard. 200 µl/well of Pierce BCA Reagent B was applied to the samples after being diluted 1:50 in Pierce BCA Reagent A. The plate was incubated at 37°C for 15 min before being

measured using a POLARStar Omega (BMG Labtech) for absorbance at 562 nm. The standard curve was interpolated to determine sample concentrations. The samples were aliquoted, diluted to 1 µg/µl, and stored at -20°C.

2.8.1.6 SDS-PAGE and protein transfer

HA-tagged and eYFP linked receptor constructs were immunoprecipitated from 200 µl cell lysate using a monoclonal anti-HA antibody linked to agarose and GFP-trap kit (Chromotek) respectively. Immunocomplexes were resuspended in 100 µl Laemmli buffer after being washed 3 × in wash buffer and incubated at 60°C for 5 min. 20 ml of immunoprecipitated proteins were resolved by SDS-PAGE on NuPAGE Novex 4 to 12% Bis-Tris Gels (Thermo Fisher) after centrifugation at 2500g for 5 min. Using a wet transfer mechanism, proteins were moved from the gel onto nitrocellulose membrane at 30 V for 90 min after gels were run in NuPAGE MOPS SDS Running Buffer (Thermo Fisher) at 200 V for around 1 h and 10 min.

2.8.1.7 Blocking and antibody treatment (Western blot)

Following transfer, the nitrocellulose membrane was blocked for 1 h at room temperature on an orbital shaker with 5% bovine serum albumin (BSA) in Tris-buffered saline (TBS, 50 mM Tris-Cl, 150 mM NaCl, pH 7.6). The membrane was next exposed to the appropriate primary antibody for an overnight incubation at 4°C in 5% BSA TBS mixed with 0.1% Tween (TBS-T). Anti-HA and anti-GFP were diluted 1:1000, $pSer^{298}$/$pSer^{301}$-mGPR35 and anti-$pSer^{300}$/$pSer^{303}$-hGPR35a were diluted 1:10,000. IRDye 800CW anti-rabbit, anti-rat, or anti-goat secondary antibody was diluted 1:10,000 in 5% BSA TBST and incubated for 2 h at room temperature on the membrane after washing it for 3 × 5 min with TBS-T. Proteins were found using a LI-COR Odyssey imaging system in accordance with the manufacturer's recommendations after washing for 3 × 5 min with TBS-T.

For GRK isoform-directed antisera and the anti-LgBiT monoclonal antibody, the following dilutions were used: Anti- LgBiT monoclonal antibody: 1:500, anti-GRK 2- 1:500, anti-GRK 3- 1:250, anti-GRK 5-1:250 and anti-GRK 6- 1:1000. IRDye 800CW anti-rabbit or horseradish peroxidase anti-mouse secondary antibody diluted 1:10,000 in 5% dried Skimmed Milk Powder In TBS-T.

2.8.1.8 Treatment with Lambda Protein Phosphatase

Immunocomplexes were exposed to λ-PPase for 90 min at 30°C at a final concentration of 10 unit/µL to remove phosphate groups from phosphorylated serine and threonine residues before being eluted with 2× Laemmli buffer.

2.8.1.9 N-glycosylation status analysis

At a final concentration of 1 unit/µL, peptide N-glycosidase F (NGaseF) was used to carry out the endoglycosidase treatment experiment overnight at 37°C.

2.8.2 Immunocytochemistry

To evaluate receptor expression and subcellular localisation, immunocytochemistry study was employed. Cells were maintained at 37°C in a 5% CO_2 humidified environment after being seeded at 7.5 × 10^4 cells/well on poly-D-lysine-coated 13 mm round coverslips in 24-well plates. As previously mentioned, cells were treated, and after that, they were fixed with 4% (w/v) paraformaldehyde in PBS for 10 min at room temperature. Fixed cells were permeabilised for 10 min at room temperature using TBS + 0.1% saponin after being rinsed in TBS for 3 × 5 min. Before being incubated with primary antibodies (anti-pSer^{300}/pSer^{303}-hGPR35a, pSer^{298}/pSer^{301}-mGPR35, GPR35 C-terminal (non-phospho) and anti-HA were diluted 1:400 in blocking buffer) overnight at 4ºC, cells were first blocked for 1 h at room temperature in blocking buffer (TBS, 10% goat serum, and 1% BSA). Following a 3 × 5 min TBS wash, the cells were treated for 1 h at room temperature with secondary antibodies (Alexa Fluor 488-goat anti-rabbit IgG and Alexa Fluor 488-donkey anti-rat IgG diluted to 1:400 in blocking buffer). Using VECTASHIELD Mounting Media with DAPI (Vector laboratories), coverslips were mounted onto glass slides after cells were washed for 3 × 5 min in TBS. The photos were taken using a Zeiss LSM 880 confocal with a 63x/1.4 NA Plan Apochromat oil-immersion objective. MetaMorph software was then used to analyse the images obtained from confocal microscopy.

2.9 Cell based assays

2.9.1 Bioluminescence resonance energy transfer (BRET) studies using SPASM sensors

The GPR35a- $G\alpha_{13}$ sensor was described fully by (Mackenzie et al., 2019) and an equivalent GPR35b-$G\alpha_{13}$ sensor was generated (Marti-Solano et al., 2020) by replacement of GPR35a with GPR35b which contains an additional 31 amino acids at the N-terminus but is otherwise identical in sequence to GPR35a (Milligan, 2011). These were transfected transiently into parental HEK293T cells 2 days prior to experiments using polyethyleneimine linear MW-25000. 30 min before the assay, cells were washed with Hanks Buffered Saline Solution containing 10 mM HEPES and incubated in the same buffer at 37°C. Results are expected to be independent of expression levels because bioluminescence resonance energy transfer (BRET) generates a ratiometric signal and each sensor is a single polypeptide, however this was verified experimentally by measuring levels of substrate-induced luciferase activity (Figure 2.2).

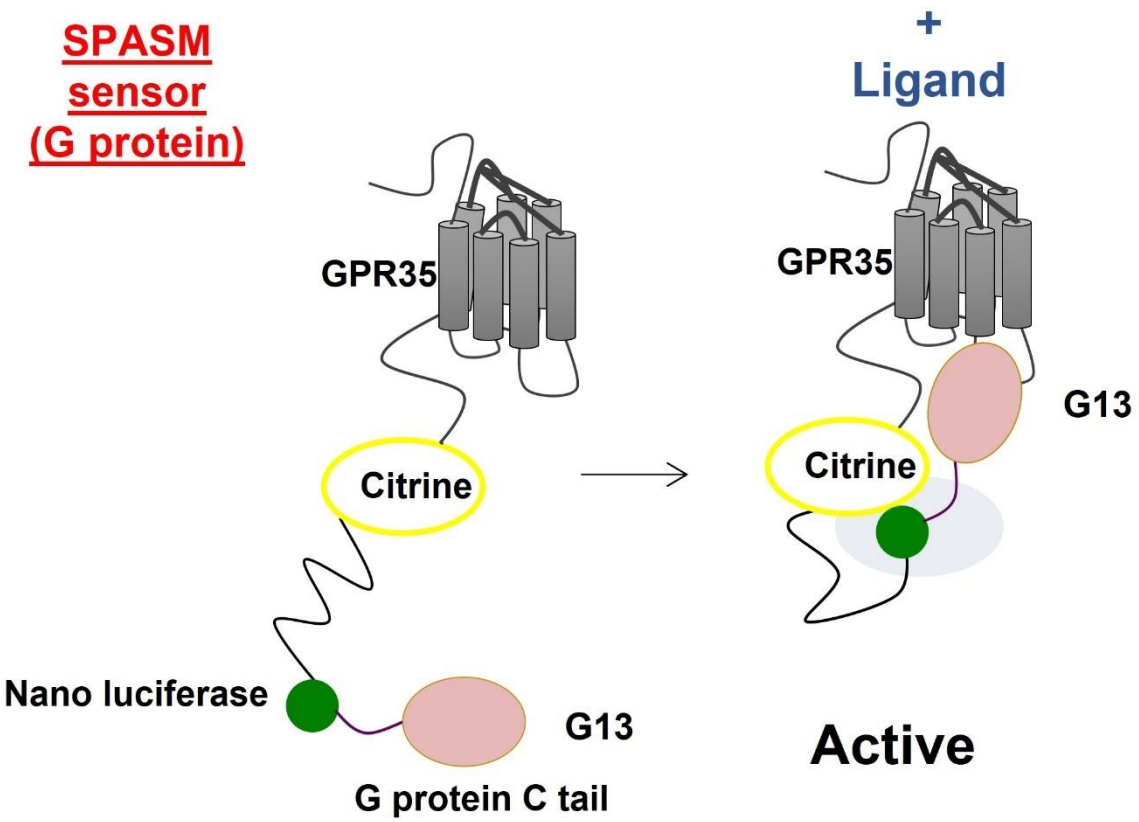

Figure 2.2 GPR35- $G\alpha_{13}$ sensor
With the binding of agonist ligand, GPR35 interacts with $G\alpha_{13}$ resulting in enhanced BRET signal as the Nanoluc and Citrine components move close together.

'SPASM': Systematic protein affinity strength modulation sensors. This sensor is made up of a single receptor construct linked to mCitrine at its C terminus, an ER/K α helical linker, nanoluciferase, a bioluminescent protein, and a peptide matching to the last 27 amino acids of $G\alpha_{13}$.

2.9.2 Arrestin recruitment BRET assays

HEK293T cells were seeded in 10 cm dishes and transiently co-transfected with GPR35-eYFP with a FLAG epitope tag engineered into the N-terminal domain, and with arrestin-3 fused to *Renilla* luciferase (arrestin-3- RLuc) in a 4:1 ratio using PEI. Arrestin-3-RLuc alone was transfected into control cells. After 24 h, cells were separated by trypsin-EDTA incubation, seeded at 6×10^4 cells/well on white 96-well plates coated with poly-D-lysine, and then incubated overnight at 37°C. Hanks' buffered saline solution (HBSS) was prewarmed (37°C) once to wash the cells, and they were then incubated in HBSS for 30 to 60 min. To determine the relative receptor expression during incubation, the eYFP signal (excitation 485 nm, emission 520 nm) was read on a PHERAstar FS (BMG Labtech). The RLuc substrate coelenterazine-h (Promega) was added, and the plate was incubated for 10 min at 37°C in a light-protected environment. Agonists were added in triplicate at the appropriate quantities, the plate was incubated for a further 5 min. at 37°C, and the emissions at 475 nm and 535 nm were read with a PHERAstar FS. Net BRET values were obtained by dividing the emission at 535 nm by the emission at 475 nm and subtracting the 535 nm/475 nm ratio for cells expressing only the arrestin-3-RLuc donor (the basal BRET): Net BRET = (em535 nm/em475 nm) – (em535 nm/em475 nm [RLuc only]). Similar studies were carried out with arrestin-2-RLuc (Figure 2.3).

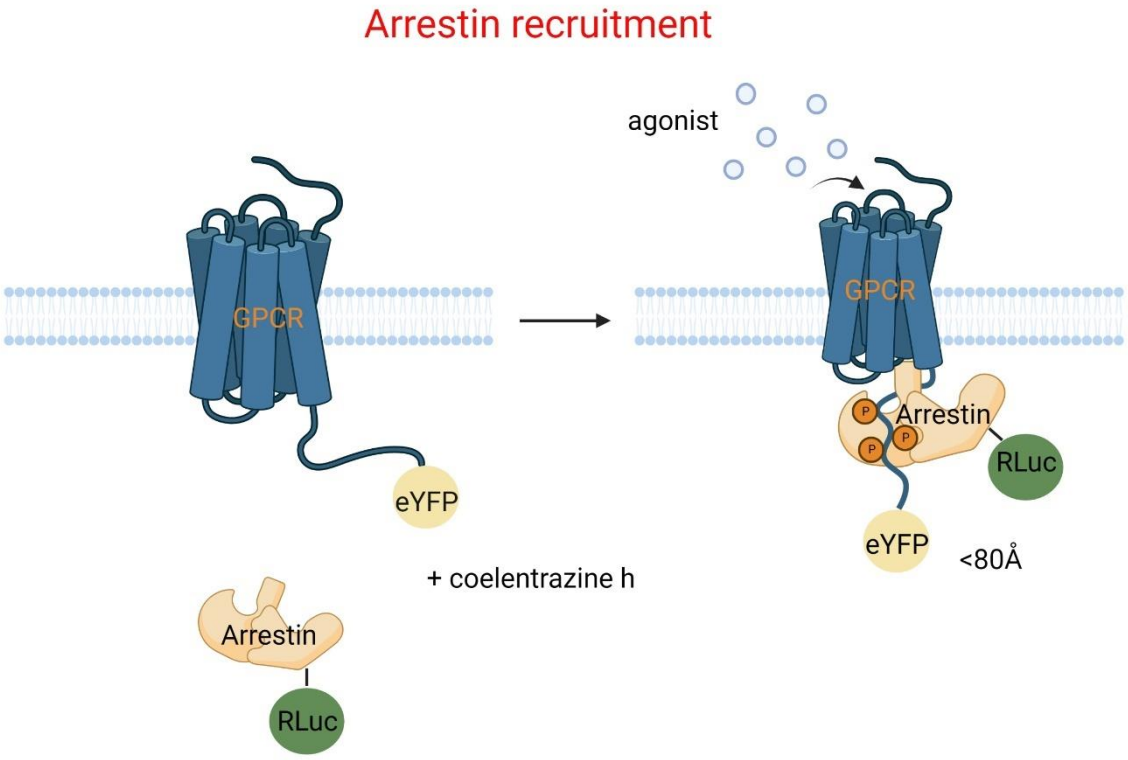

Figure 2.3 BRET-based GPR35-arrestin-3 interaction assay
Enhanced yellow fluorescent protein (eYFP)-tagged GPR35 and an arrestin-3 variant that was tagged with Renilla luciferase (RLuc) were cotransfected into cells. After the addition of a GPR35 agonist, arrestin-3-RLuc and GPR35-eYFP interacted. If GPR35 and arrestin-3 brought eYFP and RLuc near a BRET-compliant distance (<80 Å), light released upon substrate oxidation by the luciferase was transferred to eYFP and then subsequently re-emitted at a longer wavelength. If eYFP and RLuc were not close together, no such impact would happen. This figure was created with BioRender.com.

2.9.3 Nanoluciferase based complementation assay for GRKs-GPR35 interaction

Nanoluciferase based complementation assay is basically a protein-protein interaction assay where nanoluciferase (Nluc) recombine quickly and produce a strong luminescent signal upon supplemented with the corresponding substrate (Dixon et al., 2016). The fundamental design of this split nanoluciferase technique is that, GRK is N-terminally or C-terminally tagged with a fragment of the Nanoluciferase (NLuc) enzyme, coined the LgBiT fragment (18 kDa), while the GPCR of interest is C-terminally tagged with the complementary 11-residue fragment, namely the SmBiT tag (Palmer et al., 2022). Here, the GRK of interest, N/C-terminally tagged with LgBiT was co-transfected with GPR35 C-terminally tagged with the complementary SmBiT fragment at 1:10 ratio in HEK-293 derived cell lines. Following 24 h, cells were separated by incubation with trypsin-EDTA and seeded in white 96-well plates covered with poly-D-lysine. They were then

incubated overnight at 37°C. Hanks' buffered saline solution (HBSS) was prewarmed (37°C) to wash the cells, and they were then incubated in HBSS for 30 to 60 min. Upon ligand binding and G protein dissociation, the active conformation of the receptor is able to accommodate specific GRKs allowing NLuc complementation. Cells supplemented with the NLuc substrate produce strong bioluminescence (Figure 2.4) which can then easily be measured with a definite protocol by plate reader PHERAstar FS.

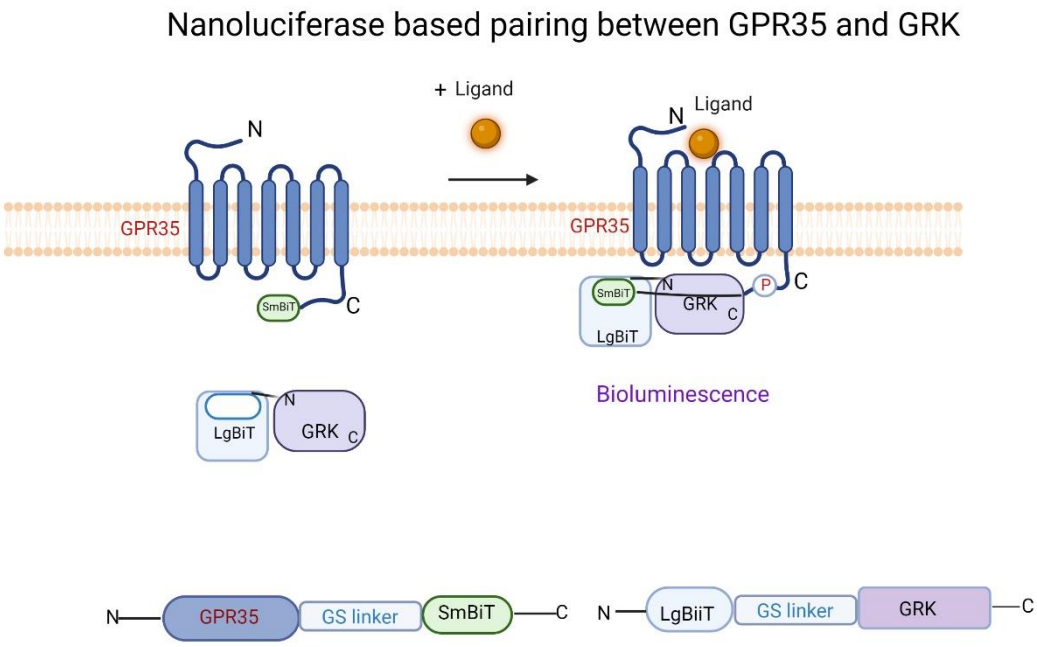

Figure 2.4 Nanoluciferase based complementation assay between GPR35 and GRKs
Demonstration of the GPR35 and GRK constructs and associated SmBiT and LgBiT tag. Representation of the nanoBiT system for pairing between GPR35 and GRKs. This figure was created with BioRender.com.

2.9.4 Modelling with Alphafold

GRK proteins in multimer mode and the human GPR35a sequence were used to make AlphaFold predictions (Jumper et al., 2021, Mirdita et al., 2022, Evans et al., 2022) using the Colabfold Notebook (https://colab.research.google.com/github/sokrypton/ColabFold/blob/main/AlphaFold2.ipynb).

2.10 Statistical analysis

Data are reported as the mean ± SEM of three independent experiments, and when necessary, a bar diagram is used to represent the data. Utilising the GraphPad Prism software package, version 9.4.0 (GraphPad), data analysis and curve fitting were performed.

Chapter 3 Mutagenesis studies in the isoforms of human GPR35

3.1 Introduction

G protein-coupled receptors are historically the most successful group of drug targets. About 30–40% of currently available authorised medicines target GPCRs (Drews, 2000, Hopkins and Groom, 2002). In fact, several GPCR ligands have been among the top 100 pharmaceutical products sold worldwide (Zambrowicz and Sands, 2003). GPCRs are effective therapeutic targets due to their dual functions as modulators of intracellular signalling and transducers of extracellular signals across the cell membrane, eliminating the requirement for membrane-permeable ligands. Many GPCRs also directly contribute to the disease's pathophysiology, making them excellent therapeutic targets. However, despite their success, it is estimated that only 59 of the 370 non-olfactory GPCRs have been successfully used as drug targets. This indicates that the remaining ones may have largely modulatory functions that make them unsuitable for this purpose or that there is still much room for improvement in the field of GPCR drug development (Sams-Dodd, 2005, Garland, 2013, Gashaw et al., 2011).

GPCRs can modify physiology in various human tissues in response to external signals. When comparing various physiological systems, GPCR-mediated signalling can differ due to differences in the sequence (Hauser et al., 2018, Thompson et al., 2014) or expression (Kenakin, 2019) of a receptor potentially resulting in signalling bias. Creating functionally varied GPCR isoforms with various expression patterns in various tissues is an underappreciated source of such bias. An individual GPCR gene, which contains introns, can be spliced into different isoforms with various signalling characteristics and different signalling states can be produced by certain isoform combinations expressed in various organs (Marti-Solano et al., 2020). Several of the isoforms that have been discovered can impact cellular responses to medications and serve as new targets for the creation of medications with greater tissue selectivity based on structural alterations and expression patterns (Marti-Solano et al., 2020).

The family of GPCRs consists of around 800 genes encoded in the human genome. In addition to the numerous unique genes that code for GPCRs, different promoter usage, pre-mRNA splicing, and alternative translation initiation all increase the number of functionally unique proteins. Almost 40% of the examined GPCRs contain more than one isoform, according to a thorough examination of transcript-

level mRNA databases (Marti-Solano et al., 2020). These isoforms differ in essential functional properties and frequently display tissue-specific expression patterns (Minneman, 2001, Markovic and Challiss, 2009, Cong et al., 2021)

The orphan class A (rhodopsin-like) GPCR GPR35 is such a type of receptor with multiple isoforms. In humans, the GPR35 gene is found on chromosome 2q37.3 and can be alternatively spliced to produce the variants GPR35a or GPR35b (Quon et al., 2020, Kaya et al., 2021). Whereas GPR35b results in a larger N-terminal domain by 31 amino acids, GPR35a only encodes for 309 amino acids (Okumura et al., 2004). Among all the transcripts, only two mRNAs encode GPR35b (also referred to as "GPR35 long"), while all other known/annotated transcripts encode the reference isoform GPR35a (also known as "GPR35 short") (Schihada et al., 2022). Although the location of hGPR35a and hGPR35b mRNA expression in human tissues has been identified, their putative unique roles are unknown because of their remarkably comparable pharmacology (Quon et al., 2020, Milligan, 2023). The tissue-specificity and activity of the short and long GPR35 variants are also poorly understood because of the complex expression pattern of the GPR35 gene and the potential for alternate translation initiation (Marti-Solano et al., 2020). GPR35a and GPR35b are situated in comparable cellular compartments but GPR35b is more frequently connected with carcinogenesis because of its expression in gastric and colon cancer cells. However, the functional distinctions between the two isoforms are unclear and require further research.

3.1.1 Aims

GPR35 is a poorly characterised receptor that has attracted increased attention as a therapeutic target through its potential involvement in a spectrum of inflammatory and cardiovascular diseases, however, many of its biological functions remain largely undefined (Divorty et al., 2015). There are GPR35 orthologues in mouse and rat that have 73 and 72% identity with human GPR35a (hGPR35a), respectively, and in less-studied non-mammalian species like the amphibian Xenopus tropicalis that has 33% homology with hGPCR35a (Quon et al., 2020, Taniguchi et al., 2006). Recently, the zebrafish homolog of human GPR35, *Danio rerio*, was cloned, resulting in the discovery of two paralogs, gpr35a and gpr35b, with 26% and 24% of the same sequence as human GPR35, respectively (Kaya et al., 2020). Human GPR35 has two isoforms. The shorter isoform is known

as GPR35a (309 amino acids) while the longer isoform is coined as GPR35b (340 amino acids). There are 31 extra amino acids in the N-terminal domain of the longer form (Quon et al., 2020). Despite having very similar pharmacology, the longer isoform's agonist effectiveness is significantly lower than the shorter one (Marti-Solano et al., 2020). Sequence comparisons also predict that hGPR35b can generate an additional extracellular disulphide bond in comparison to hGPR35a, although this possibility—or any potential consequences—has not yet been properly investigated (Quon et al., 2020). To fully investigate the pharmacology and function of these two isoforms of human GPR35, a site directed mutagenesis strategy was developed and then G protein and arrestin interactions with these isoforms were determined. The aims of this chapter were to

Study and compare the protein alignment of hGPR35a and hGPR35b

Prediction of disulphide bonds in hGPR35 isoforms and determination of the importance of these by mutagenesis and functional studies

Assessment of the arrestin recruitment and G protein activation of additional mutants of hGPR35b

Mutation of the amino acid residue Arginine (R13) of hGPR35b in both wild type and Cys27Ser backbone of hGPR35b and pharmacological characterisation of the mutants by both arrestin and G protein-based assay.

3.2 Results

3.2.1 Comparison of protein alignment of human GPR35 isoforms

3.2.1.1 Alternative splicing of the human GPR35 gene produces two isoforms that differ by only 31 amino acids

In case of GPCRs, alternative promoter usage, pre-mRNA splicing along with alternative translation can generate functional proteins that are distinct from each other. GPR35 is such a GPCR that has an alternative receptor isoform originating from the same gene. The existence of a second GPR35 isoform was first noted in 2004 (Okumura et al., 2004). The shorter human GPR35 isoform is denoted as hGPR35a, while the longer counterpart is known as hGPR35b.

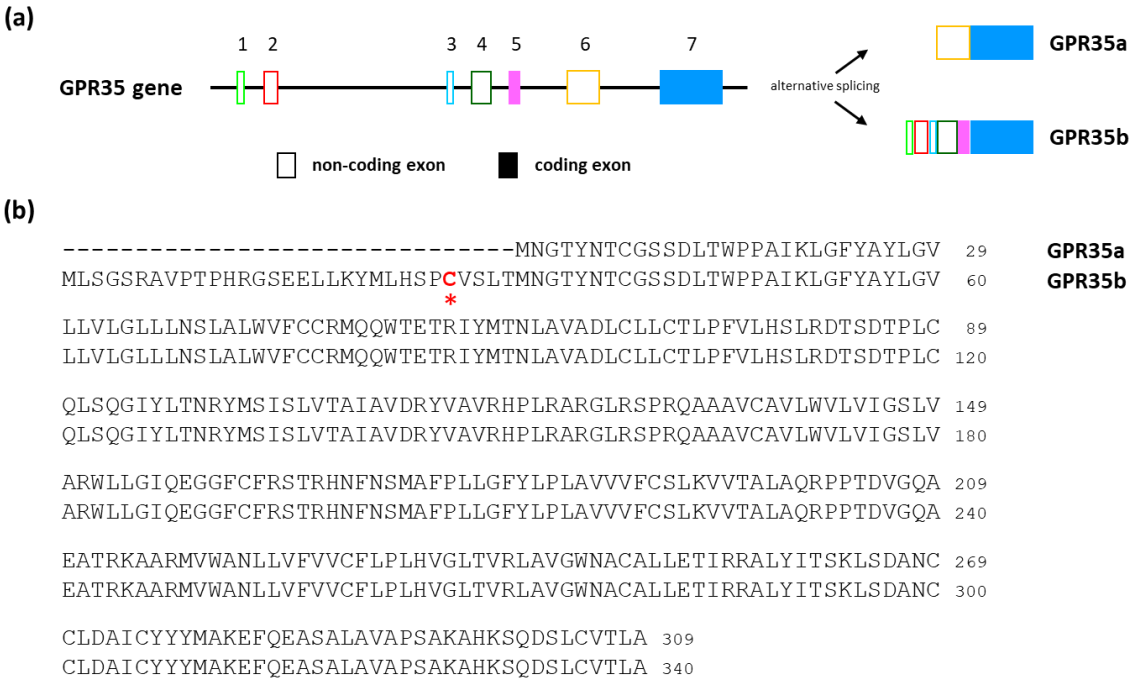

Figure 3.1 The human GPR35 gene generates the GPR35a and GPR35b isoforms by alternative splicing
(a) The human GPR35 gene is located at chromosome 2q.37.3. Both GPR35a and GPR35b mRNA contain exon 7, whereas GPR35b mRNA also contains exon 5. **(b)** GPR35b has a 31 amino acid N-terminal extension that includes a cysteine residue which may be able to create a disulphide bond (indicated with a red *) (Quon et al., 2020).

3.2.1.2 Possible disulphide bonds in hGPR35 and the contribution of these bonds to function

In hGPR35a cysteine at position 8 in the N-terminus and cysteine 248 in extracellular loop 3 most likely are linked by a disulphide bond. To investigate the function of this proposed disulphide bond and the pharmacology of hGPR35a in general, I mutated these amino acids to serine. The generated mutants, along with the wild type version of hGPR35a were employed to assess arrestin recruitment potential and G protein activation using bioluminescence resonance energy transfer (BRET) assays (Figure 3.2).

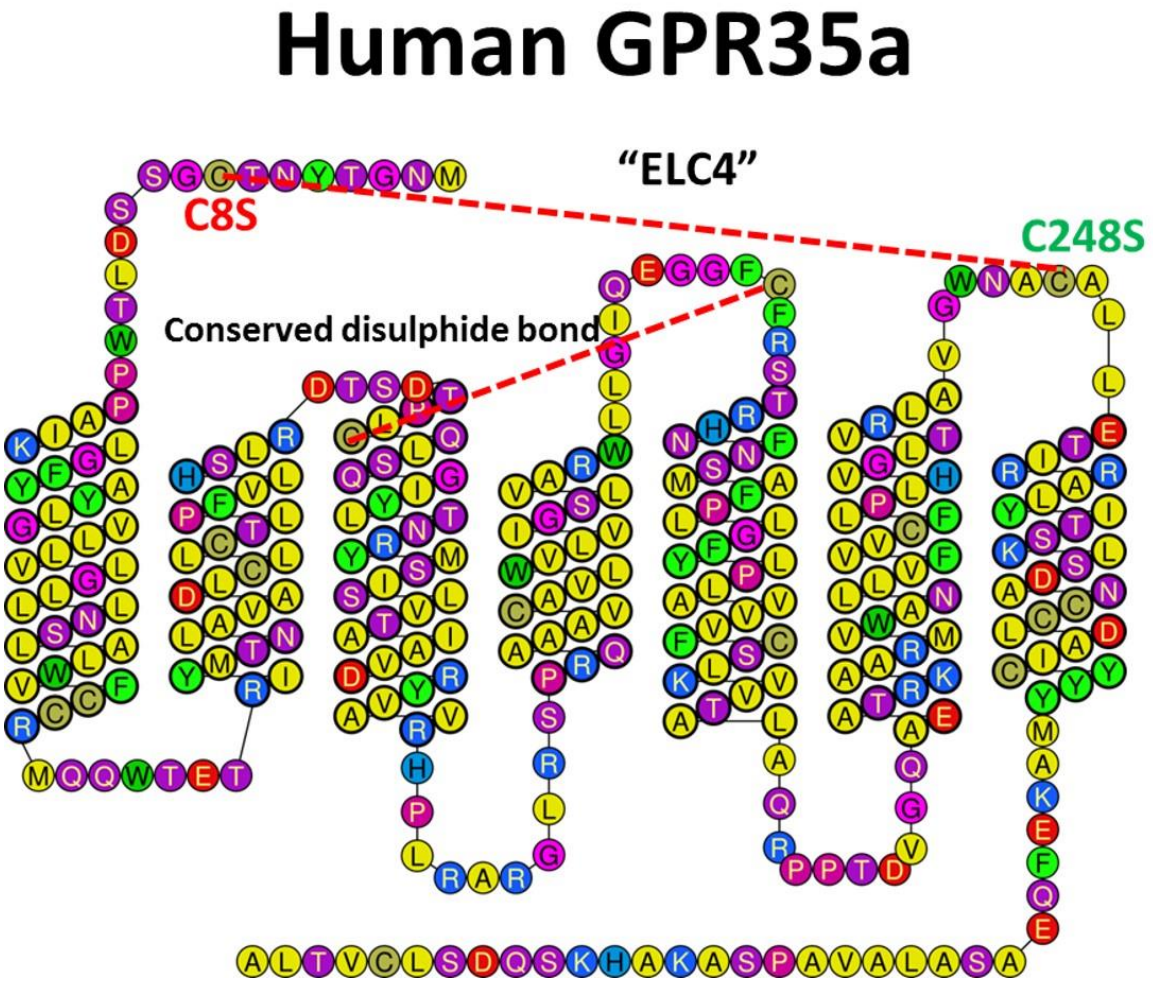

Figure 3.2 Primary structure of human GPR35a
Snake plot of human GPR35a. Here, the protein single-chain spans the cytoplasmic membrane via seven transmembrane helices (TM1-7), and it is characterised by three ECLs (ECL1-3) and three ICLs (ICL1-3), as well as a helical intracellular C terminus. There is also a prediction that hGPR35a may generate a '4th extracellular loop' via a disulphide bridge from the N-terminus to ECL3

In the case of hGPR35b, addition to the equivalent disulphide bond between the cysteines at position 39 and 279, there is the potential for an additional disulphide bond between cysteine at position 27 and 279. For hGPR35a equivalent disulphide bond in hGPR35b, I altered the cysteines at position 39 and 279 to serine in order to better understand the role played by this putative disulphide bond and the pharmacology of hGPR35b. For the potential additional disulphide bond between cysteine at position 27 and 279, I altered the cysteine (position 27 of long isoform) to serine. The generated mutants hGPR35b (C27S, C39S and C279S) along with wild type hGPR35b were examined to measure their arrestin interaction capacity and G protein activation in response to ligands using BRET assays (Figure 3.3).

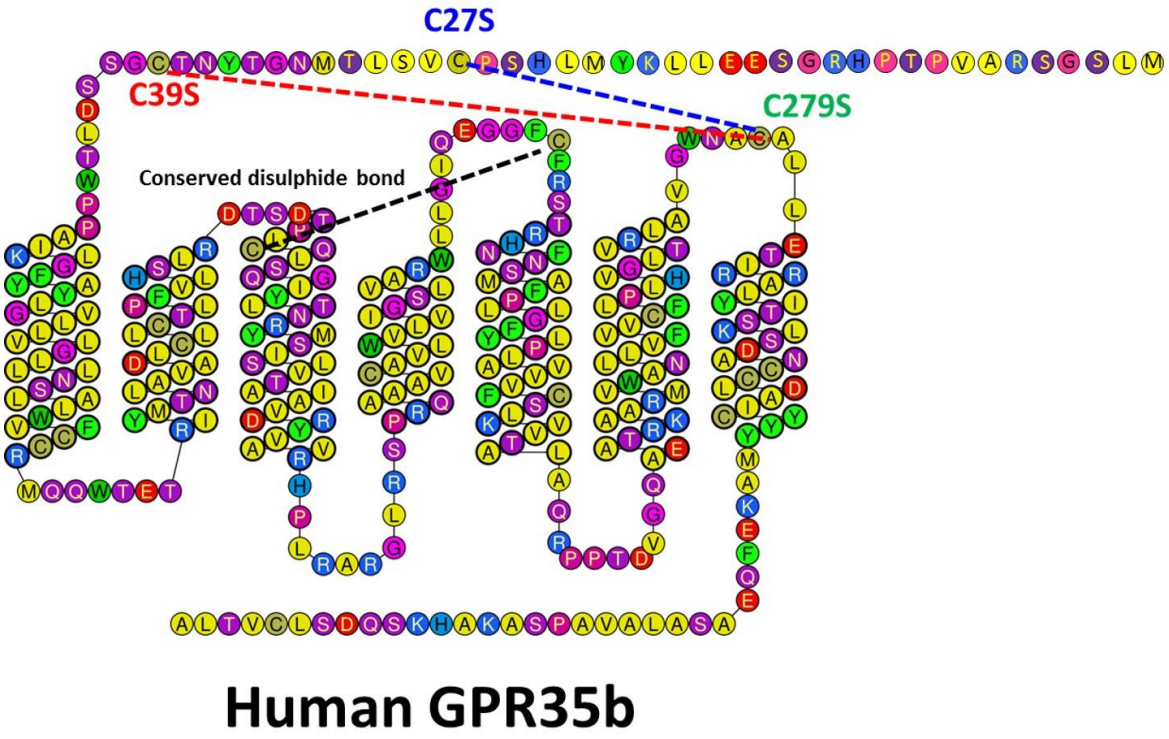

Figure 3.3 Primary structure of human GPR35b
Snake plot of human GPR35b. Here, in addition to the similar structure of hGPR35a, there is an N-terminal extension of 31 amino acids. The N-terminal splice addition of hGPR35b offers an additional or alternate disulphide bond partner.

3.2.2 Human GPR35 (wild type and mutants): interactions with arrestin and activation of G protein

3.2.2.1 Comparison of two isoforms of hGPR35 in arrestin-3 recruitment and $G\alpha_{13}$ activation

Parental 293 cells were transfected transiently to co-express either (hGPR35a WT, hGPR35a C8S, hGPR35a C248S) each tagged with eYFP and arrestin-3-RLuc. The GPR35 agonist lodoxamide, which exhibits high potency at human GPR35 (MacKenzie et al., 2014), is added in the presence of a luciferase substrate and resulted in a concentration-dependent increase in measured BRET (Figure 3.4A) with pEC_{50} 7.99± 0.03 (mean± SEM, n=3 for wild type). The cysteine at position 8 in the N-terminus presumably forms a disulphide bond with the cysteine 248 of extracellular loop 3 and changing either of these residues to serine almost completely eliminated the agonist effect in arrestin-3 recruitment assays (Figure 3.4A). When 293 cells were transfected to co-express either (hGPR35b WT, hGPR35b C27S, hGPR35b C39S, hGPR35b C279S), each tagged with eYFP and arrestin-3-RLuc, there was a concentration-dependent moderate increase in

measured BRET upon addition of luciferase substrate and lodoxamide with pEC_{50} 8.16± 0.05 (mean± SEM, n=3 for wild type) (Figure 3.4B). The measured BRET generated by hGPR35b WT was significantly less than for hGPR35a WT. Mutation of the hGPR35a equivalent cysteine residues in hGPR35b (hGPR35b C39S, hGPR35b C279S) also greatly reduced agonist function. A second cysteine is found in hGPR35b at position 27. Mutation of this residue significantly enhanced agonist-mediated BRET suggesting that hGPR35b activation by agonists may be constrained by the presence of another disulphide bond (Figure 3.4B).

For $G\alpha_{13}$ activation, (hGPR35a WT, hGPR35a C8S, hGPR35a C248S) were transiently expressed in parental HEK293 cells in the context of $G\alpha_{13}$ SPASM sensors. Following addition of a luciferase substrate and lodoxamide, a concentration-dependent increase in BRET was observed with pEC_{50} 8.55± 0.04 (mean± SEM, n=3 for wild type) (Figure 3.4C). These other two mutants (hGPR35a C8S, hGPR35a C248S) could not activate $G\alpha_{13}$ like hGPR35a WT and almost eliminated response to lodoxamide (Figure 3.4C). When each of hGPR35b WT, hGPR35b C27S, hGPR35b C39S, hGPR35b C279S were transiently expressed in parental HEK293 cells as $G\alpha_{13}$ SPASM sensors, I detected a concentration-dependent increase in BRET with pEC_{50} 8.77± 0.08 (mean± SEM, n=3 for wild type) after addition of luciferase substrate and lodoxamide (Figure 3.4D). Again, the measured BRET ($G\alpha_{13}$ activation) generated by hGPR35b WT was remarkably lower than for hGPR35a WT. Mutation of the GPR35a equivalent cysteine residues in hGPR35b (hGPR35b C39S, hGPR35b C279S) also greatly reduced agonist function with low BRET signals generated. But mutation of the hGPR35b specific cysteine at position 27 to serine generated high BRET signals in response to lodoxamide in such $G\alpha_{13}$ activation studies suggesting that an extra disulphide bond limits agonist-induced activation of the long isoform of hGPR35 (Figure 3.4D).

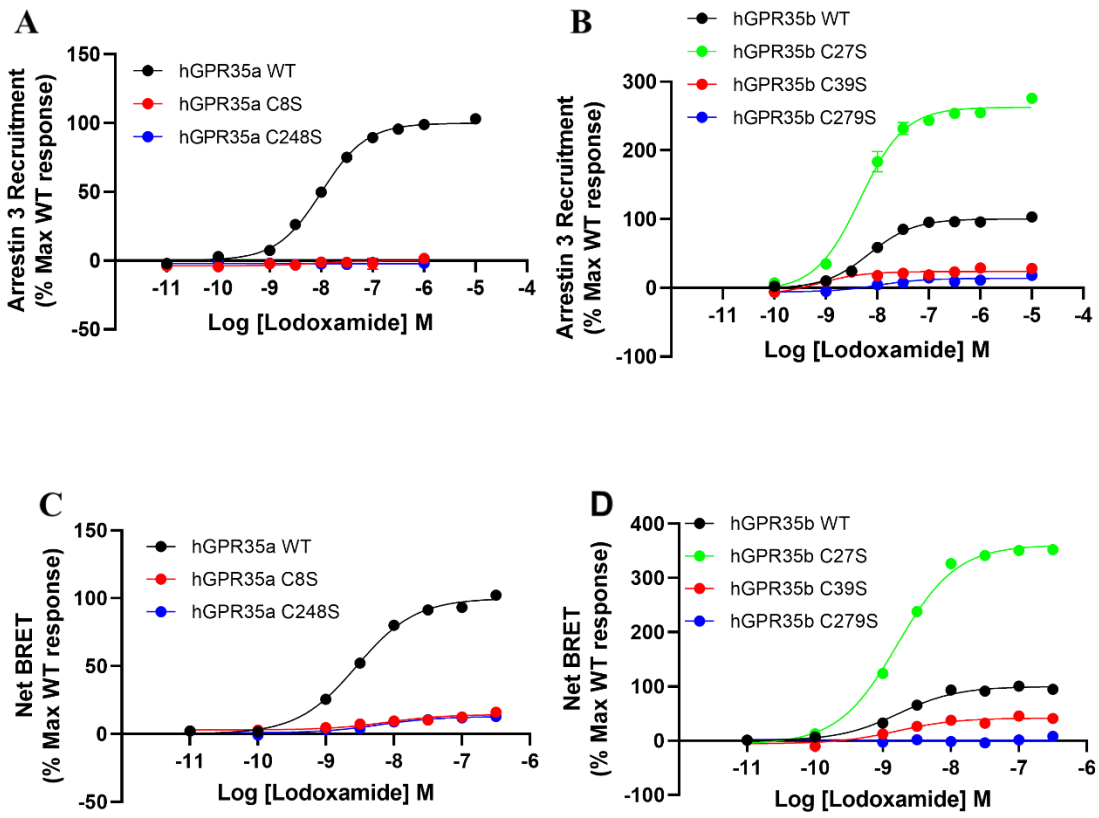

Figure 3.4 Demonstration and comparison of hGPR35 (wild type and mutants) interaction with arrestin-3 and validation of the effectiveness of hGPR35-Gα_{13} SPASM sensors
(A) Parental HEK293 cells were transfected transiently to co-express either hGPR35a WT (black circles), hGPR35a C8S (red circles) and hGPR35a C248S (blue circles) each tagged with eYFP and arrestin-3-RLuc. **(B)** Parental 293 cells were again transfected transiently to co-express either hGPR35b WT (black circles), hGPR35b C27S (green circles), hGPR35b C39S (red circles) and hGPR35b C279S (blue circles) each tagged with eYFP and arrestin-3-RLuc. **(C)** Comparison of effect of hGPR35a WT (black circles), hGPR35a C8S (red circles) and hGPR35a C248S (blue circles) transiently expressed in parental HEK293 cells as Gα_{13} SPASM sensors. **(D)** Demonstration of the effects of hGPR35b WT (black circles), hGPR35b C27S (green circles), hGPR35b C39S (red circles) and hGPR35b C279S (blue circles) transiently expressed in parental HEK293 cells as Gα_{13} SPASM sensors. BRET signals were observed after stimulating with indicated concentrations of lodoxamide for 5 min. Data are the mean± SEM of outcomes from three independent experiments.

3.2.2.2 Direct comparison among short/long isoforms of hGPR35 and hGPR35b C27S in arrestin-3 recruitment and Gα_{13} activation

HEK 293 cells were transfected transiently to co-express either hGPR35a WT, hGPR35b WT, or hGPR35b C27S, each tagged with eYFP, and arrestin-3-RLuc. In the presence of a luciferase substrate and after the addition of the potent hGPR35 agonist lodoxamide, there was a concentration-dependent increase in measured BRET (Figure 3.5A) with pEC_{50} 8.07± 0.05 (mean± SEM, n=3 for hGPR35a wild type). Compared to hGPR35a WT, the measured BRET produced by hGPR35b WT was 71.3% lower with pEC_{50} 8.08± 0.06 (mean± SEM, n=3 for hGPR35b wild type). But when hGPR35b C27S was employed, there was a sharp increase in signal that

signified greater efficacy in response to agonist than wild type version of hGPR35b (Figure 3.5A).

When hGPR35a WT, hGPR35b WT, or hGPR35b C27S were transiently expressed in parental HEK293 cells as $G\alpha_{13}$ SPASM sensors for G protein activation measurement, there was again a concentration-dependent increase in measured BRET (Figure 3.5B) with pEC_{50} 8.55± 0.04 (mean± SEM, n=3 for hGPR35a wild type). Here, hGPR35b produced a 72.49% lower BRET signal with pEC_{50} 8.78± 0.08 (mean± SEM, n=3 for hGPR35b wild type) in comparison to hGPR35a. However, hGPR35b C27S mutant generated BRET signal in response to lodoxamide that was similar in extent to hGPR35a wild type in $G\alpha_{13}$ activation (Figure 3.5B).

From the experiments shown in Figure 3.5 it can be stated that cysteine 27 in the long isoform of GPR35 acted as a dampener of ligand induced hGPR35b efficacy. Mutation of this cysteine to serine resulted in the efficacy of hGPR35b now being equivalent to hGPR35a.

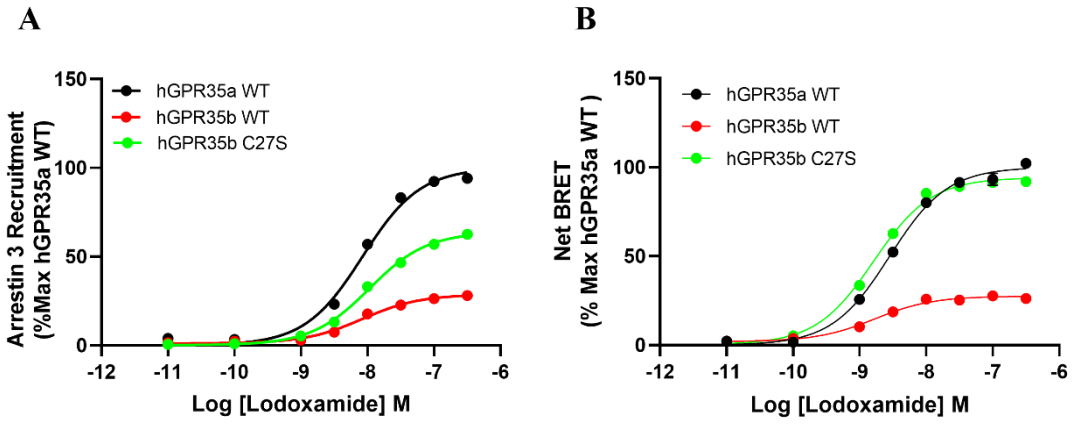

Figure 3.5 Direct comparison of the effects of the two isoforms of hGPR35 and hGPR35b C27S in arrestin-3 recruitment and hGPR35-$G\alpha_{13}$ SPASM sensors
(A) Experiments akin to **Figure 3.4** were performed. Parental 293 cells were transfected transiently to co-express either hGPR35a WT-eYFP (black circles), hGPR35b WT-eYFP (red circles) or hGPR35b C27S-eYFP (green circles) along with arrestin-3-RLuc. (**B**) Comparison of effect of hGPR35a WT (black circles), hGPR35b WT (red circles) and hGPR35b C27S (green circles) transiently expressed in parental HEK293 cells as $G\alpha_{13}$ SPASM sensors. BRET signals were measured after stimulating with the indicated concentrations of lodoxamide for 5 min. Data are the mean± SEM of outcomes from three independent experiments.

From the above experiments of section (3.2.2), it was clear that hGPR35a generates substantially greater efficacy in response to lodoxamide than hGPR35b in both arrestin and G protein-based assays. In hGPR35a, cysteine at position 8 in

the N terminal region likely creates a disulphide bond with cysteine at 248 of extracellular loop 3. Alteration of either of these residues nearly eliminated lodoxamide function in both types of experiments. In hGPR35b, there may be hGPR35a equivalent disulphide bond formation between the amino acid cysteine at positions 39 and 279. Alterations of either of these amino acids to serine also greatly reduced signal in response to lodoxamide in arrestin-3 recruitment and $G\alpha_{13}$ activation. In hGPR35b there is an extra cysteine at position 27. Alteration of this residue resulted in significantly increased efficacy of lodoxamide in both arrestin and G protein-based assays, suggesting an additional disulphide bond limits agonist-induced activation of hGPR35b.

3.2.3 Generation of additional mutants to further investigate the role of the N-terminal extension of hGPR35b

In the previous sections, I found that although the pharmacology of human GPR35 splice variants is highly similar, the long isoform (hGPR35b) generates lower efficacy in response to lodoxamide than the short form (hGPR35a). After predicting the possible disulphide bonds in both isoforms and results from the mutagenesis experiments, it was clear that the additional cysteine at position 27 of the N-terminal extension of hGPR35b greatly limits the agonist-induced hGPR35b activation. Cysteine 27 position is a dampener of hGPR35b efficacy because mutation of this residue to serine results in the efficacy of the long isoform being equivalent to that of the short isoform. To learn more about the function of the hGPR35b N-terminal extension, nine more mutants in which cysteine replaced various residues in the setting of the Cys27Ser hGPR35b backbone were created. Mutants were generated with a C-terminal enhanced yellow fluorescent protein (eYFP) tag so that they could be utilised in arrestin-3 interaction assays. The same mutants were also made in GPR35-$G\alpha_{13}$ SPASM sensors for G protein activation measurement. The mutants of hGPR35b for arrestin-3 recruitment and $G\alpha_{13}$ activation are displayed in (Table 3.1).

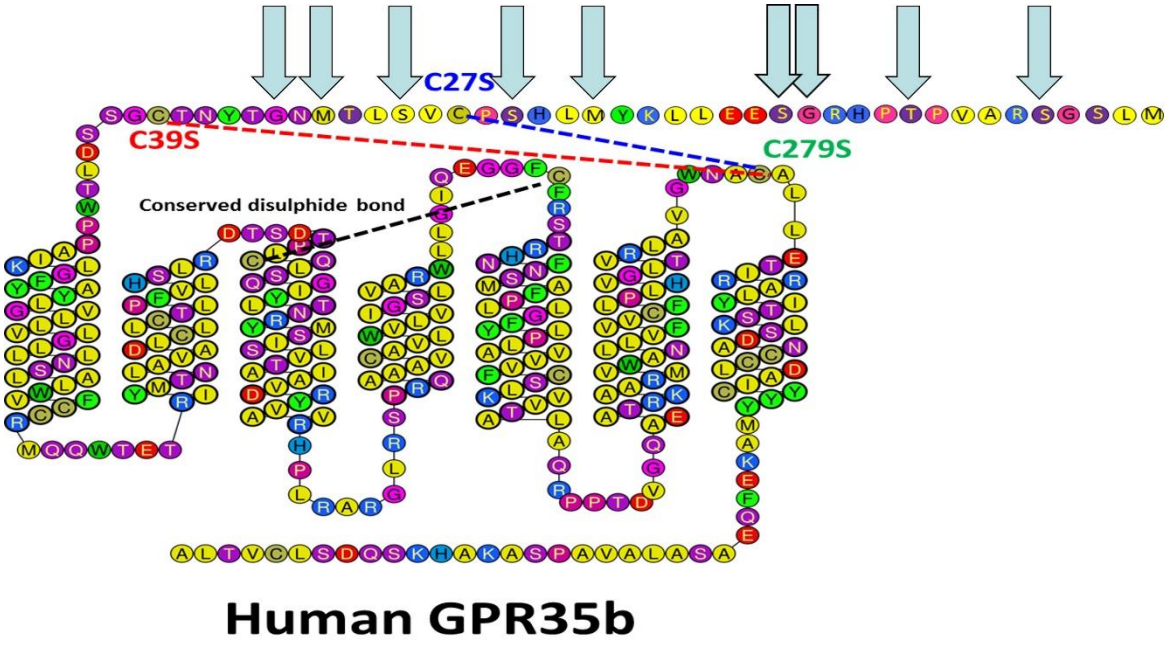

Figure 3.6 Additional mutagenic sites in the N-terminal domain of hGPR35b
9 extra mutants were created in Cys27Ser backbone of hGPR35b where cysteine was introduced at different positions instead of (serine at 5, threonine at 10, glycine at 14, serine at 15, methionine at 22, serine at 25, serine at 29, methionine at 32 and glycine at 34) across the N-terminal extension of hGPR35b.

Position of the mutants in Cys27Ser backbone	Mutants for arrestin-3 interaction	Mutants for $G\alpha_{13}$ activation
Amino acid 5	S5C tagged with eYFP	S5C in GPR35- $G\alpha_{13}$ SPASM
Amino acid 10	T10C tagged with eYFP	T10C in GPR35- $G\alpha_{13}$ SPASM
Amino acid 14	G14C tagged with eYFP	G14C in GPR35- $G\alpha_{13}$ SPASM
Amino acid 15	S15C tagged with eYFP	S15C in GPR35- $G\alpha_{13}$ SPASM
Amino acid 22	M22C tagged with eYFP	M22C in GPR35- $G\alpha_{13}$ SPASM
Amino acid 25	S25C tagged with eYFP	S25C in GPR35- $G\alpha_{13}$ SPASM
Amino acid 29	S29C tagged with eYFP	S29C in GPR35- $G\alpha_{13}$ SPASM
Amino acid 32	M32C tagged with eYFP	M32C in GPR35- $G\alpha_{13}$ SPASM
Amino acid 34	G34C tagged with eYFP	G34C in GPR35- $G\alpha_{13}$ SPASM

Table 3.1 List of additional mutants in the Cys27Ser backbone of hGPR35b
9 mutants were generated in Cys27Ser backbone of hGPR35b for both arrestin-3 interaction and $G\alpha_{13}$ activation measurements.

After the generation of the additional nine mutants in different locations of the N-terminal extension of hGPR35b, I employed a series of ligands that are agonists or partial agonists of human GPR35 for measuring arrestin-3 interaction with the receptor and also activating G protein $G\alpha_{13}$ (Table 3.2).

hGPR35 ligand	Chemical name
Bufrolin	**6-butyl-4,10-dioxo-1,7-dihydro-1,7-phenanthroline-2,8-dicarboxylic acid**
Lodoxamide	**2-[2-chloro-5-cyano-3-(oxaloamino) anilino]-2-oxoacetic acid**
Pamoic Acid	**4-[(3-carboxy-2-hydroxynaphthalen-1-yl) methyl]-3-hydroxynaphthalene-2-carboxylic acid**
Cromolyn	**5-[3-(2-carboxy-4-oxochromen-5-yl) oxy-2-hydroxypropoxy]-4-oxochromene-2-carboxylic acid**
Doxantrazole	**10,10-dioxo-3-(2H-tetrazol-5-yl) thioxanthen-9-one**
Zaprinast	**5-(2-propoxyphenyl)-2,6-dihydrotriazolo[4,5-d] pyrimidin-7-one**
PSB-13253	**6-bromo-8-[(4-methoxybenzoyl) amino]-4-oxochromene-2-carboxylic acid**
Amlexanox	**2-amino-5-oxo-7-propan-2-ylchromeno[2,3-b] pyridine-3-carboxylic acid**

Table 3.2 Commonly used names and chemical names of human GPR35 ligands used
In total 8 ligands (full and partial agonists) were used to measure arrestin-3 recruitment and $G\alpha_{13}$ activation for hGPR35.

3.2.3.1 Comparison among different hGPR35b mutants in arrestin recruitment and G protein activation using bufrolin as an agonist

Parental 293 cells were transfected transiently to co-express either hGPR35b C27S (S5C, T10C, G14C, S15C, M22C, S25C, S29C, M32C and G34C), each tagged with eYFP, and with arrestin-3-RLuc. hGPR35a WT, hGPR35b WT and hGPR35b C27S tagged with eYFP were used as controls. After the addition of luciferase substrate and bufrolin, there was a concentration-dependent increase in measured BRET (Figure 3.7A) with pEC_{50} 7.69± 0.01 (mean± SEM, n=3 for hGPR35a WT) (Table 3.3).

Compared to hGPR35a WT, the measured BRET produced by hGPR35b WT was significantly (67.68%) lower with pEC_{50} 7.61± 0.01 (mean± SEM, n=3 for hGPR35b WT). However, using hGPR35b C27S resulted in a dramatic rise in signal, indicating better efficacy in response to bufrolin than the hGPR35b wild type version. Among the new mutants in the backbone of hGPR35b C27S (S5C, T10C, M22C, S25C, S29C, and M32C) mutants displayed statistically similar arrestin-3 recruitment activities to hGPR35b WT and they were all significantly different from hGPR35a WT (Emax, $P < 0.001$). The rest of the mutants in the backbone of hGPR35b C27S (G14C, S15C, and G34C) demonstrated moderate enhancement of BRET signals compared to signals generated by hGPR35b WT (Figure 3.7A) (Table 3.3).

For $G\alpha_{13}$ activation, hGPR35b C27S (S5C, T10C, G14C, S15C, M22C, S25C, S29C, M32C and G34C) were transiently expressed in parental HEK293 cells as $G\alpha_{13}$ SPASM sensors. hGPR35a WT, hGPR35b WT and hGPR35b C27S were also expressed as $G\alpha_{13}$ SPASM sensors. Following addition of luciferase substrate and bufrolin, a concentration-dependent increase in BRET (Figure 3.7B) was found with pEC_{50} 8.05± 0.05 (mean± SEM, n=3 for hGPR35a WT). Here, hGPR35b generated a 78.79% lower BRET signal with pEC_{50} 6.97± 0.01 (mean± SEM, n=3 for hGPR35b WT). However, in response to bufrolin, the hGPR35b C27S mutant generated BRET signal that was not statistically different from signals produced by the hGPR35a WT. In the backbone of hGPR35b C27S, each of the nine new mutants showed $G\alpha_{13}$ activation that was very similar to hGPR35b WT and significantly different from hGPR35a WT (Emax, $p < 0.001$) (Figure 3.7B) (Table 3.3).

From this series of experiments, it was found that when cysteine was introduced into various positions of the N-terminal domain of hGPR35b, all of the positions demonstrated arrestin-3 recruitment potential and $G\alpha_{13}$ activation that was similar in extent to that of hGPR35b WT. The most probable reason for this is the creation of new disulphide bonds from various sites of N-terminal domain to extracellular loop 3 of hGPR35b.

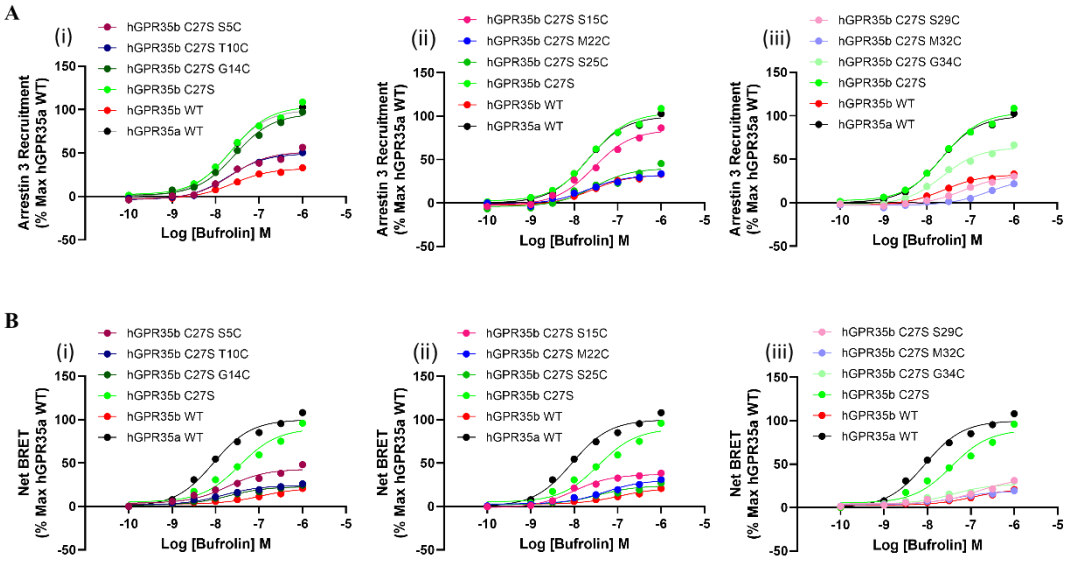

Figure 3.7 Measurement and comparison of interaction among various mutants of hGPR35b and arrestin-3 and demonstration of the effectiveness of different mutants of hGPR35b-$G\alpha_{13}$ SPASM sensors using bufrolin

(A) Parental HEK293 cells were transfected transiently to co-express either **(i)** hGPR35b C27S S5C (maroon circles), hGPR35b C27S T10C (deep blue circles), hGPR35b C27S G14C (bottle green circles), **(ii)** hGPR35b C27S S15C (pink circles), hGPR35b C27S M22C (blue circles), hGPR35b C27S S25C (light green circles), **(iii)** hGPR35b C27S S29C (light pink circles), hGPR35b C27S M32C (light blue circles) and hGPR35b C27S G34C (paste circles) each tagged with eYFP and

arrestin-3-RLuc. **(B)** Comparison of the effects of **(i)** hGPR35b C27S S5C (maroon circles), hGPR35b C27S T10C (deep blue circles), hGPR35b C27S G14C (bottle green circles), **(ii)** hGPR35b C27S S15C (pink circles), hGPR35b C27S M22C (blue circles), hGPR35b C27S S25C (light green circles), **(iii)** hGPR35b C27S S29C (light pink circles), hGPR35b C27S M32C (light blue circles) and hGPR35b C27S G34C (paste circles) transiently expressed in parental HEK293 cells as $G\alpha_{13}$ SPASM sensors. In both assays **(A**) and **(B**) hGPR35a WT (black circles), hGPR35b WT (red circles) and hGPR35b C27S (green circles) were used as control. BRET signals were recorded after treating with indicated concentrations of bufrolin for 5 min. Each dataset represents the mean ± SEM of three independent experiments. Data were analysed by one-way ANOVA followed by Dunnett's multiple comparisons test and statistical results are shown in the following tables.

	hGPR35b C27S S5C	**hGPR35b C27S T10C**	**hGPR35b C27S G14C**	**hGPR35b C27S S15C**	**hGPR35b C27S M22C**	**hGPR35b C27S S25C**	**hGPR35b C27S S29C**	**hGPR35b C27S M32C**	**hGPR35b C27S G34C**	**hGPR35b C27S**	**hGPR35b WT**	**hGPR35a WT**
pEC$_{50}$	7.65± 0.01 P= 0.09 (ns)	7.71± 0.01 P= 0.55 (ns)	7.55± 0.01 P<0.001 (***)	7.55± 0.01 P<0.001 (***)	7.69± 0.03 P>0.99 (ns)	7.57± 0.01 P<0.001 (***)	7.15± 0.01 P<0.001 (***)	6.60± 0.01 P<0.001 (***)	7.64± 0.01 P<0.01 (**)	7.63± 0.01 P<0.01 (**)	7.61± 0.01 P<0.001 (***)	7.69± 0.01
%E$_{max}$	51.63 ± 0.13 P<0.001 (***)	49.56 ± 0.01 P<0.001 (***)	95.36 ± 0.37 P<0.001 (***)	84.24 ± 0.32 P<0.001 (***)	32.18 ± 0.21 P<0.001 (***)	40.00 ± 0.13 P<0.001 (***)	31.64 ± 0.18 P<0.001 (***)	27.80 ± 0.17 P<0.001 (***)	63.69 ± 0.28 P<0.001 (***)	103.9 ± 0.07 P<0.001 (***)	32.32 ± 0.25 P<0.001 (***)	100

Table 3.3 Comparison of pEC$_{50}$ and %Emax among GPR35 wild type and various mutants in arrestin recruitment assays using bufrolin

hGPR35a, hGPR35b and various mutants of hGPR35b were compared in terms of pEC$_{50}$ and %Emax using BRET based arrestin recruitment assays. Results are expressed as mean ± SEM of three individual experiments. Data were analysed by one-way ANOVA followed by Dunnett's multiple comparisons test where the value for hGPR35a was used as control. ns = non-significant, * p<0.05, ** p<0.01, ***p<0.001.

	hGPR35b C27S S5C	**hGPR35b C27S T10C**	**hGPR35b C27S G14C**	**hGPR35b C27S S15C**	**hGPR35b C27S M22C**	**hGPR35b C27S S25C**	**hGPR35b C27S S29C**	**hGPR35b C27S M32C**	**hGPR35b C27S G34C**	**hGPR35b C27S**	**hGPR35b WT**	**hGPR35a WT**
pEC$_{50}$	7.70± 0.01 P<0.001 (***)	7.82± 0.03 P<0.001 (***)	7.70± 0.01 P<0.001 (***)	8.01± 0.01 P= 0.84 (ns)	7.29± 0.01 P<0.001 (***)	7.46± 0.02 P<0.001 (***)	6.84± 0.02 P<0.001 (***)	7.36± 0.03 P<0.001 (***)	7.39± 0.05 P<0.01 (**)	7.44± 0.01 P<0.01 (**)	6.97± 0.01 P<0.001 (***)	8.05± 0.01
%E$_{max}$	43.10 ± 0.34 P<0.001 (***)	24.23 ± 0.05 P<0.001 (***)	22.78 ± 0.36 P<0.001 (***)	37.03 ± 0.19 P<0.001 (***)	30.58 ± 0.27 P<0.001 (***)	23.98 ± 0.35 P<0.001 (***)	33.09 ± 0.45 P<0.001 (***)	18.79 ± 0.23 P<0.001 (***)	27.12 ± 0.38 P<0.001 (***)	89.73 ± 0.66 P<0.001 (***)	21.21 ± 0.41 P<0.001 (***)	100

Table 3.4 Comparison of pEC$_{50}$ and %E$_{max}$ among GPR35 wild type and various mutants in G protein activation assays using bufrolin

hGPR35a, hGPR35b and various mutants of hGPR35b were compared in terms of pEC$_{50}$ and %E$_{max}$ by BRET based G protein assays using GPR35-$G\alpha_{13}$ SPASM sensors . Results are expressed as mean ± SEM of three separate experiments. Data were analysed by one-way ANOVA followed by Dunnett's multiple comparisons test where the value for hGPR35a was used as control. ns = non-significant, * p<0.05, ** p<0.01, ***p<0.001.

3.2.3.2 Comparison of arrestin recruitment and G protein activation in various hGPR35b mutants with reference agonist lodoxamide

A transient transfection was performed on parental 293 cells to co-express either hGPR35b C27S (S5C, T10C, G14C, S15C, M22C, S25C, S29C, M32C and G34C) tagged with eYFP and arrestin-3-RLuc. As controls, hGPR35a WT, hGPR35b WT, and hGPR35b C27S were tagged with eYFP and used. There was a concentration-dependent rise in the amount of measured BRET following the addition of luciferase substrate and lodoxamide (Figure 3.8A) with pEC_{50} 7.82± 0.01 (mean± SEM, n=3 for hGPR35a WT) (Table 3.5). The measured BRET generated by hGPR35b WT was substantially (61.17%) lower than that of hGPR35a WT with pEC_{50} 7.82± 0.01 (mean± SEM, n=3 for hGPR35b WT). However, the signal increased when hGPR35b C27S was used, showing that this variant responded to lodoxamide more effectively than hGPR35b wild type. Among the new mutants in the backbone of hGPR35b C27S (M22C, S25C, S29C, and M32C) mutants displayed statistically similar arrestin-3 recruitment activities to hGPR35b WT and they were all significantly different from hGPR35a WT (Emax, $p < 0.001$) (Figure 3.8A). The rest of the mutants in the backbone of hGPR35b C27S (S5C, T10C, G14C, S15C and G34C) demonstrated moderate enhancement of BRET signals compared to signals generated by hGPR35b WT (Figure 3.8A) (Table 3.5).

In order to activate $G\alpha_{13}$ in parental HEK293 cells, hGPR35b C27S (S5C, T10C, G14C, S15C, M22C, S25C, S29C, M32C and G34C) were transiently expressed as $G\alpha_{13}$ SPASM sensors. hGPR35a WT, hGPR35b WT and hGPR35b C27S were also expressed as $G\alpha_{13}$ SPASM sensors as controls. A gradual rise in BRET (Figure 3.8B) was discovered with the application of luciferase substrate and lodoxamide with pEC_{50} 8.22± 0.01 (mean± SEM, n=3 for hGPR35a WT) (Table 3.6). In this instance, $G\alpha_{13}$ activation was triggered by a (79.46%) lower BRET signal produced by hGPR35b with pEC_{50} 8.07± 0.07 (mean± SEM, n=3 for hGPR35b WT). However, in response to lodoxamide, the hGPR35b C27S mutant generated BRET signal that was not statistically different from signals produced by the hGPR35a wild type. The nine newly introduced mutants in the backbone of hGPR35b C27S produced $G\alpha_{13}$ activation signals that were nearly comparable to that of hGPR35b WT and significantly different from hGPR35a WT (Emax, $p < 0.001$) (Figure 3.8B) (Table 3.6).

These tests revealed that cysteine had been inserted at varied positions of the N-terminal domain of hGPR35b. All the positions showed lower arrestin-3 recruitment signals than that of hGPR35a WT and hGPR35b C27S. $G\alpha_{13}$ activation by these new mutants were similar to the effects generated by hGPR35b WT.

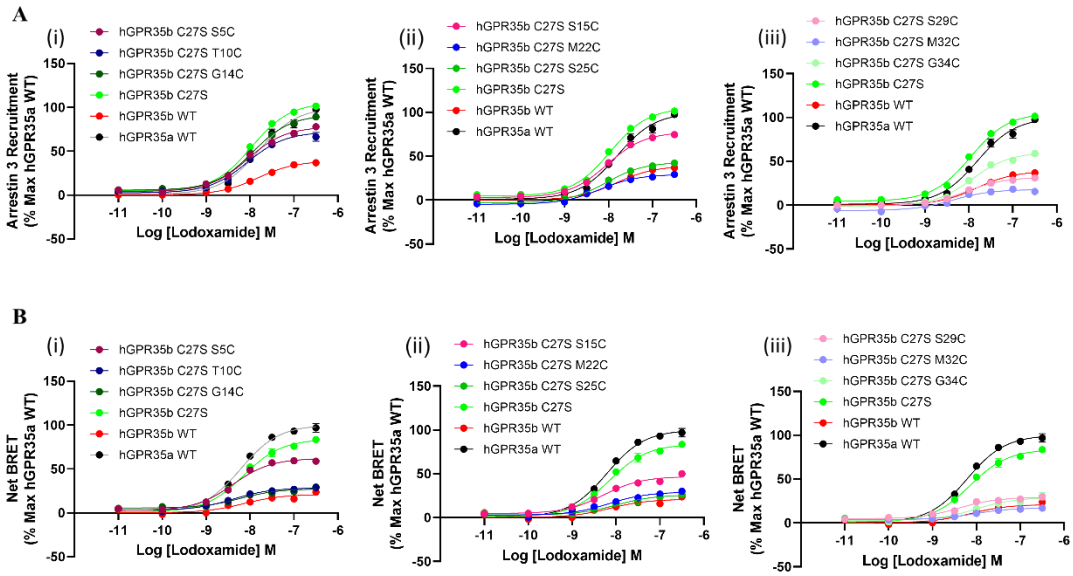

Figure 3.8 Comparison of interaction among various mutants of hGPR35b and arrestin-3 and validation of the effectiveness of different mutants of hGPR35b-$G\alpha_{13}$ SPASM sensors using reference agonist lodoxamide

(A) Parental HEK293 cells were transfected transiently to co-express either **(i)** hGPR35b C27S S5C (maroon circles), hGPR35b C27S T10C (deep blue circles), hGPR35b C27S G14C (bottle green circles), **(ii)** hGPR35b C27S S15C (pink circles), hGPR35b C27S M22C (blue circles), hGPR35b C27S S25C (light green circles), **(iii)** hGPR35b C27S S29C (light pink circles), hGPR35b C27S M32C (light blue circles) and hGPR35b C27S G34C (paste circles) each tagged with eYFP and arrestin-3-RLuc. **(B)** Comparison of the effects of **(i)** hGPR35b C27S S5C (maroon circles), hGPR35b C27S T10C (deep blue circles), hGPR35b C27S G14C (bottle green circles), **(ii)** hGPR35b C27S S15C (pink circles), hGPR35b C27S M22C (blue circles), hGPR35b C27S S25C (light green circles), **(iii)** hGPR35b C27S S29C (light pink circles), hGPR35b C27S M32C (light blue circles) and hGPR35b C27S G34C (paste circles) transiently expressed in parental HEK293 cells as $G\alpha_{13}$ SPASM sensors. In both assays **(A)** and **(B)** hGPR35a WT (black circles), hGPR35b WT (red circles) and hGPR35b C27S (green circles) were used as control. BRET signals were observed after treating with indicated concentrations of lodoxamide for 5 min. Each dataset represents the mean ± SEM of three independent experiments. Data were analysed by one-way ANOVA followed by Dunnett's multiple comparisons test and statistical results are shown in the following tables.

	hGPR35b C27S S5C	hGPR35b C27S T10C	hGPR35b C27S G14C	hGPR35b C27S S15C	hGPR35b C27S M22C	hGPR35b C27S S25C	hGPR35b C27S S29C	hGPR35b C27S M32C	hGPR35b C27S G34C	hGPR35b C27S	hGPR35b WT	hGPR35a WT
pE C_{50}	8.06± 0.01 P<0.01 (**)	8.07± 0.01 P<0.01 (**)	7.95± 0.01 P<0.05 (*)	8.05± 0.01 P<0.01 (**)	8.16± 0.04 P<0.001 (***)	8.03± 0.02 P<0.01 (**)	8.04± 0.02 P<0.01 (**)	8.29± 0.08 P<0.001 (***)	7.94± 0.01 P= 0.06 (ns)	7.97± 0.01 P<0.05 (*)	7.82± 0.01 P>0.99 (ns)	7.82± 0.01
%E max	78.35 ± 0.38 P<0.001 (***)	71.70 ± 0.31 P<0.001 (***)	91.39 ± 0.15 P<0.001 (***)	77.86 ± 0.16 P<0.001 (***)	29.54 ± 0.26 P<0.001 (***)	43.78 ± 0.49 P<0.001 (***)	32.03 ± 0.27 P<0.001 (***)	17.96 ± 0.12 P<0.001 (***)	60.47 ± 0.16 P<0.001 (***)	105.0 ± 0.40 P<0.001 (***)	38.72 ± 0.21 P<0.001 (***)	99.89 ± 0.12

Table 3.5 Comparison of pEC_{50} and %Emax among GPR35 wild type and various mutants in arrestin recruitment assays using lodoxamide

hGPR35a, hGPR35b and various mutants of hGPR35b were compared in terms of pEC_{50} and $\%E_{max}$ using BRET based arrestin recruitment assays. Results are expressed as mean ± SEM of three individual experiments. Data were analysed by one-way ANOVA followed by Dunnett's multiple comparisons test where the value for hGPR35a was used as control. ns = non-significant, * p<0.05, ** p<0.01, ***p<0.001.

	hGPR35b C27S S5C	hGPR35b C27S T10C	hGPR35b C27S G14C	hGPR35b C27S S15C	hGPR35b C27S M22C	hGPR35b C27S S25C	hGPR35b C27S S29C	hGPR35b C27S M32C	hGPR35b C27S G34C	hGPR35b C27S	hGPR35b WT	hGPR35a WT
pE C_{50}	8.40± 0.02 P<0.05 (*)	8.38± 0.01 P<0.05 (*)	8.19± 0.03 P= 0.99 (ns)	8.28± 0.01 P= 0.57 (ns)	8.12± 0.04 P= 0.15 (ns)	7.96± 0.02 P<0.001 (***)	8.37± 0.03 P<0.05 (*)	8.07± 0.02 P<0.05 (*)	7.97± 0.03 P<0.001 (***)	8.13± 0.01 P= 0.37 (ns)	8.07± 0.07 P<0.05 (*)	8.22± 0.01
%E max	62.02 ± 0.14 P<0.001 (***)	28.92 ± 0.42 P<0.001 (***)	27.81 ± 0.44 P<0.001 (***)	47.07 ± 0.21 P<0.001 (***)	29.14 ± 0.07 P<0.001 (***)	26.48 ± 0.54 P<0.001 (***)	29.38 ± 0.27 P<0.001 (***)	17.04 ± 0.16 P<0.001 (***)	29.07 ± 0.26 P<0.001 (***)	83.81 ± 0.14 P<0.001 (***)	21.54 ± 0.54 P<0.001 (***)	100.1 ± 0.05

Table 3.6 Comparison of pEC_{50} and $\%E_{max}$ among GPR35 wild type and various mutants in G protein activation assays using lodoxamide

hGPR35a, hGPR35b and various mutants of hGPR35b were compared in terms of pEC_{50} and $\%E_{max}$ by BRET based G protein assays using GPR35-$G\alpha_{13}$ SPASM sensors . Results are expressed as mean ± SEM of three separate experiments. Data were analysed by one-way ANOVA followed by Dunnett's multiple comparisons test where the value for hGPR35a was used as control. ns = non-significant, * p<0.05, ** p<0.01, ***p<0.001.

3.2.3.3 Measurement of arrestin recruitment and G protein activation in various hGPR35b mutants with partial agonist pamoic acid

After using two full agonists of hGPR35, I decided to switch to pamoic acid in these experiments which is a potent partial agonist of hGPR35. Parental 293 cells were transfected transiently to co-express either hGPR35b C27S (S5C, T10C, G14C, S15C, M22C, S25C, S29C, M32C and G34C) each tagged with eYFP and arrestin-3-RLuc. hGPR35a WT, hGPR35b WT and hGPR35b C27S tagged with eYFP were used as controls. After addition of luciferase substrate and pamoic acid, there was a

concentration-dependent increase in measured BRET (Figure 3.9A) with pEC_{50} 7.18± 0.02 (mean± SEM, n=3 for hGPR35a WT) (Table 3.7). Similar outcomes to previous experiments were achieved upon using hGPR35b WT and hGPR35b C27S mutant. Among the new mutants in the backbone of hGPR35b C27S (M22C, S25C, S29C, and M32C) mutants displayed statistically similar arrestin-3 recruitment activities to hGPR35b WT and they were all significantly different from hGPR35a WT (Emax, $p < 0.001$) (Figure 3.9A). The rest of the mutants in the backbone of hGPR35b C27S (S5C, T10C, G14C, S15C and G34C) demonstrated moderate enhancement of BRET signals compared to signals generated by hGPR35b WT (Figure 3.9A) (Table 3.7). As pamoic acid shows partial agonism to hGPR35, the raw signal intensity was significantly lower than the signals produced by full agonist lodoxamide.

For $G\alpha_{13}$ activation, hGPR35b C27S (S5C, T10C, G14C, S15C, M22C, S25C, S29C, M32C and G34C) were transiently expressed in parental HEK293 cells as $G\alpha_{13}$ SPASM sensors. hGPR35a WT, hGPR35b WT and hGPR35b C27S were also expressed as $G\alpha_{13}$ SPASM sensors. Following addition of luciferase substrate and pamoic acid, a concentration-dependent increase in BRET (Figure 3.9B) was found with pEC_{50} 7.02± 0.04 (mean± SEM, n=3 for hGPR35a WT) (Table 3.8). Comparable results to earlier studies were obtained with the hGPR35b WT and hGPR35b C27S mutant in $G\alpha_{13}$ activation. In the backbone of hGPR35b C27S, the nine newly generated mutants showed $G\alpha_{13}$ activation that were not statistically different from those of hGPR35b WT (Figure 3.9B) (Table 3.8). Again, the raw $G\alpha_{13}$ activation signals were lower compared to the signals generated by full agonist.

These tests revealed that the hGPR35b's N-terminal domain had the cysteine inserted at varied positions. All the new mutants showed arrestin-3 recruitment potential and $G\alpha_{13}$ activation to a statistically similar level to that shown by hGPR35b WT. The creation of additional disulphide bonds from various sites of the hGPR35b N-terminal domain to extracellular loop 3 is the most likely cause of this.

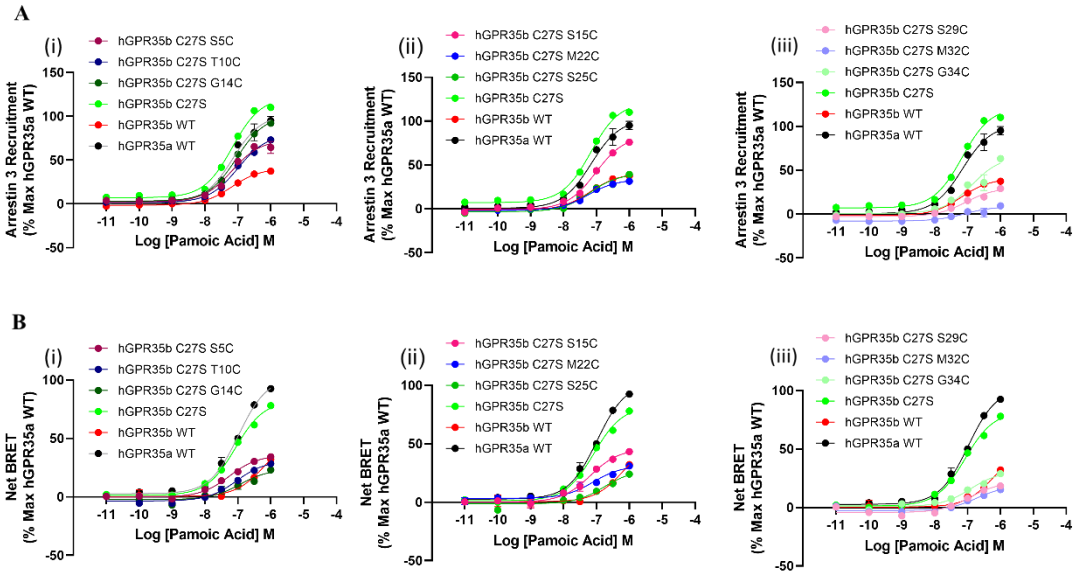

Figure 3.9 Measurement of interaction among various mutants of hGPR35b and arrestin-3 and demonstration of the effectiveness of different mutants of hGPR35b-Gα_{13} SPASM sensors using partial agonist pamoic acid

(A) Parental HEK293 cells were transfected transiently to co-express either **(i)** hGPR35b C27S S5C (maroon circles), hGPR35b C27S T10C (deep blue circles), hGPR35b C27S G14C (bottle green circles), **(ii)** hGPR35b C27S S15C (pink circles), hGPR35b C27S M22C (blue circles), hGPR35b C27S S25C (light green circles), **(iii)** hGPR35b C27S S29C (light pink circles), hGPR35b C27S M32C (light blue circles) and hGPR35b C27S G34C (paste circles) each tagged with eYFP and arrestin-3-RLuc. **(B)** Comparison of the effects of **(i)** hGPR35b C27S S5C (maroon circles), hGPR35b C27S T10C (deep blue circles), hGPR35b C27S G14C (bottle green circles), **(ii)** hGPR35b C27S S15C (pink circles), hGPR35b C27S M22C (blue circles), hGPR35b C27S S25C (light green circles), **(iii)** hGPR35b C27S S29C (light pink circles), hGPR35b C27S M32C (light blue circles) and hGPR35b C27S G34C (paste circles) transiently expressed in parental HEK293 cells as Gα_{13} SPASM sensors. In both assays **(A)** and **(B)** hGPR35a WT (black circles), hGPR35b WT (red circles) and hGPR35b C27S (green circles) were used as control. BRET signals were monitored after treating with indicated concentrations of pamoic acid for 5 min. Each dataset represents the mean ± SEM of three independent experiments. Data were analysed by one-way ANOVA followed by Dunnett's multiple comparisons test and statistical results are shown in the following tables.

	hGPR 35b C27S S5C	**hGPR 35b C27S T10C**	**hGPR 35b C27S G14C**	**hGPR 35b C27S S15C**	**hGPR 35b C27S M22C**	**hGPR 35b C27S S25C**	**hGPR 35b C27S S29C**	**hGPR 35b C27S M32C**	**hGPR 35b C27S G34C**	**hGPR 35b C27S**	**hGPR 35b WT**	**hGPR 35a WT**
pE C_{50}	7.16± 0.02 P>0.999 (ns)	7.00± 0.01 P<0.05 (*)	7.04± 0.01 P=0.111 (ns)	7.03± 0.02 P=0.079 (ns)	7.20± 0.05 P=0.999 (ns)	7.11± 0.08 P=0.731 (ns)	7.05± 0.01 P=0.134 (ns)	7.03± 0.06 P=0.619 (ns)	6.86± 0.01 P<0.001 (***)	7.16± 0.01 P>0.999 (ns)	7.18± 0.01 P>0.999 (ns)	7.18± 0.02
%E max	74.15 ± 0.89 P<0.001 (***)	80.49 ± 1.06 P<0.001 (***)	101.4 ± 0.05 P>0.999 (ns)	83.43 ± 0.04 P<0.001 (***)	34.42 ± 0.92 P<0.001 (***)	41.82 ± 1.64 P<0.001 (***)	30.04 ± 0.17 P<0.001 (***)	7.75 ± 0.90 P<0.001 (***)	65.34 ± 0.53 P<0.001 (***)	122.6 ± 0.90 P<0.001 (***)	41.47 ± 0.92 P<0.001 (***)	101.1 ± 1.10

Table 3.7 Comparison of pEC_{50} and %Emax among GPR35 wild type and various mutants in arrestin recruitment assays using pamoic acid

hGPR35a, hGPR35b and various mutants of hGPR35b were compared in terms of pEC_{50} and $\%E_{max}$ using BRET based arrestin recruitment assays. Results are expressed as mean ± SEM of three individual experiments. Data were analysed by one-way ANOVA followed by Dunnett's multiple comparisons test where the value for hGPR35a was used as control. ns = non-significant, * p<0.05, ** p<0.01, ***p<0.001.

	hGPR 35b C27S S5C	hGPR 35b C27S T10C	hGPR 35b C27S G14C	hGPR 35b C27S S15C	hGPR 35b C27S M22C	hGPR 35b C27S S25C	hGPR 35b C27S S29C	hGPR 35b C27S M32C	hGPR 35b C27S G34C	hGPR 35b C27S	hGPR 35b WT	hGPR 35a WT
pEC$_{50}$	7.21± 0.05 P= 0.54 (ns)	7.02± 0.02 P>0.999 (ns)	6.74± 0.20 P= 0.18 (ns)	7.15± 0.02 P= 0.83 (ns)	7.02± 0.07 P>0.999 (ns)	6.74± 0.02 P= 0.19 (ns)	6.89± 0.04 P= 0.82 (ns)	6.70± 0.03 P= 0.09 (ns)	6.88± 0.03 P= 0.84 (ns)	7.09± 0.02 P= 0.99 (ns)	6.33± 0.15 P<0.001 (***)	7.02± 0.04
%E$_{max}$	36.99 ± 1.29 P<0.001 (***)	30.69 ± 0.28 P<0.001 (***)	26.98 ± 3.43 P<0.001 (***)	46.26 ± 0.61 P<0.001 (***)	32.64 ± 1.30 P<0.001 (***)	28.65 ± 1.14 P<0.001 (***)	22.11 ± 0.43 P<0.001 (***)	19.16 ± 0.54 P<0.001 (***)	31.92 ± 1.03 P<0.001 (***)	81.84 ± 0.46 P<0.001 (***)	48.41 ± 4.44 P<0.001 (***)	101.2 ± 1.20

Table 3.8 Comparison of pEC$_{50}$ and %E$_{max}$ among GPR35 wild type and various mutants in G protein activation assays using pamoic acid
hGPR35a, hGPR35b and various mutants of hGPR35b were compared in terms of pEC$_{50}$ and %E$_{max}$ by BRET based G protein assays using GPR35-Gα_{13} SPASM sensors . Results are expressed as mean ± SEM of three separate experiments. Data were analysed by one-way ANOVA followed by Dunnett's multiple comparisons test where the value for hGPR35a was used as control. ns = non-significant, * p<0.05, ** p<0.01, ***p<0.001.

3.2.3.4 Determination of arrestin recruitment and G protein activation in various hGPR35b mutants with anti-asthma drug cromolyn

In this section, studies were carried out with cromolyn, an agonist ligand for GPR35. This ligand is used to treat allergic rhinitis, vernal conjunctivitis, keratitis, and keratoconjunctivitis, as well as bronchial asthma (Minutello and Gupta, 2020). A transient transfection was performed in parental 293 cells to co-express either hGPR35b C27S (S5C, T10C, G14C, S15C, M22C, S25C, S29C, M32C and G34C) tagged with eYFP and arrestin-3-RLuc. As controls, hGPR35a WT, hGPR35b WT, and hGPR35b C27S were tagged with eYFP and used. There was a concentration-dependent rise in the amount of measured BRET (Figure 3.10A) following the addition of luciferase substrate and cromolyn with pEC$_{50}$ 5.67± 0.01 (mean± SEM, n=3 for hGPR35a WT) (Table 3.9). Comparable results to earlier studies were obtained with the hGPR35b WT and hGPR35b C27S mutant. Among the new mutants in the backbone of hGPR35b C27S (M22C, S29C, and M32C) mutants displayed statistically similar arrestin-3 recruitment activities to hGPR35b WT and they were all significantly different from hGPR35a WT (Emax, $p < 0.001$) (Figure 3.10A). The rest of the mutants in the backbone of hGPR35b C27S (S5C, T10C, G14C, S15C, S25C and G34C) demonstrated moderate enhancement of BRET signals compared to signals generated by hGPR35b WT (Figure 3.10A) (Table 3.9).

In order to activate $G\alpha_{13}$ in parental HEK293 cells, hGPR35b C27S (S5C, T10C, G14C, S15C, M22C, S25C, S29C, M32C and G34C) were transiently expressed as $G\alpha_{13}$ SPASM sensors. hGPR35a WT, hGPR35b WT and hGPR35b C27S were also expressed as $G\alpha_{13}$ SPASM sensors as controls. A concentration-dependent rise in BRET (Figure 3.10B) was discovered with the application of luciferase substrate and cromolyn with pEC_{50} 5.31± 0.01 (mean± SEM, n=3 for hGPR35a WT) (Table 3.10). Comparable outcomes to previous research were achieved in $G\alpha_{13}$ activation with the hGPR35b WT and hGPR35b C27S mutants. The nine mutants at various positions in the backbone of hGPR35b C27S demonstrated $G\alpha_{13}$ activation that was not statistically different from those of hGPR35b WT (Figure 3.10B) (Table 3.10).

These tests revealed that cysteine had been inserted at varied positions of the N-terminal domain of hGPR35b. All nine of the novel mutants showed arrestin-3 recruitment potential and $G\alpha_{13}$ activation to a substantially same level as that shown by hGPR35b WT. The creation of additional disulphide bonds from various sites of the hGPR35b N-terminal domain to extracellular loop 3 is the most likely cause of this.

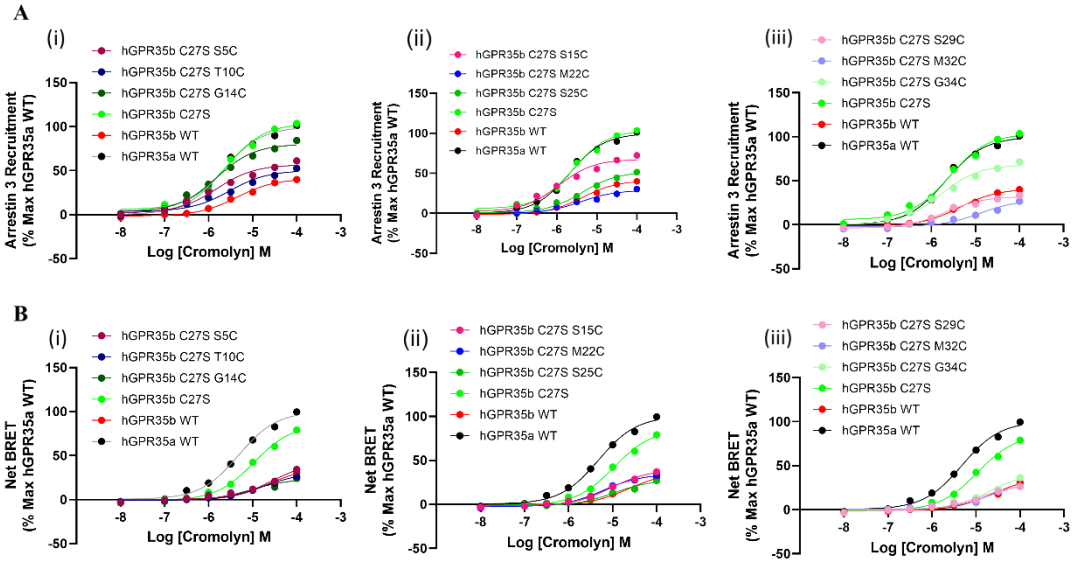

Figure 3.10 Comparison of interaction among various mutants of hGPR35b and arrestin-3 and validation of the effectiveness of different mutants of hGPR35b-$G\alpha_{13}$ SPASM sensors using GPR35 agonist cromolyn

(A) Parental HEK293 cells were transfected transiently to co-express either **(i)** hGPR35b C27S S5C (maroon circles), hGPR35b C27S T10C (deep blue circles), hGPR35b C27S G14C (bottle green circles), **(ii)** hGPR35b C27S S15C (pink circles), hGPR35b C27S M22C (blue circles), hGPR35b C27S S25C (light green circles), **(iii)** hGPR35b C27S S29C (light pink circles), hGPR35b C27S M32C (light blue circles) and hGPR35b C27S G34C (paste circles) each tagged with eYFP and arrestin-3-RLuc. **(B)** Comparison of the effects of **(i)** hGPR35b C27S S5C (maroon circles), hGPR35b C27S T10C (deep blue circles), hGPR35b C27S G14C (bottle green circles), **(ii)** hGPR35b C27S S15C (pink circles), hGPR35b C27S M22C (blue circles), hGPR35b C27S S25C (light green

circles), **(iii)** hGPR35b C27S S29C (light pink circles), hGPR35b C27S M32C (light blue circles) and hGPR35b C27S G34C (paste circles) transiently expressed in parental HEK293 cells as $G\alpha_{13}$ SPASM sensors. In both assays **(A)** and **(B)** hGPR35a WT (black circles), hGPR35b WT (red circles) and hGPR35b C27S (green circles) were used as control. BRET signals were recorded after treating with indicated concentrations of cromolyn for 5 min. Each dataset represents the mean ± SEM of three independent experiments. Data were analysed by one-way ANOVA followed by Dunnett's multiple comparisons test and statistical results are shown in the following tables.

	hGPR 35b C27S S5C	**hGPR 35b C27S T10C**	**hGPR 35b C27S G14C**	**hGPR 35b C27S S15C**	**hGPR 35b C27S M22C**	**hGPR 35b C27S S25C**	**hGPR 35b C27S S29C**	**hGPR 35b C27S M32C**	**hGPR 35b C27S G34C**	**hGPR 35b C27S**	**hGPR 35b WT**	**hGPR 35a WT**
pEC$_{50}$	5.84± 0.02 P<0.001 (***)	5.53± 0.01 P<0.01 (**)	5.82± 0.01 P<0.01 (**)	5.94± 0.01 P<0.001 (***)	5.38± 0.02 P<0.001 (***)	5.35± 0.01 P<0.001 (***)	5.67± 0.02 P>0.999 (ns)	4.85± 0.04 P<0.001 (***)	5.83± 0.03 P<0.01 (**)	5.60± 0.01 P=0.11 (ns)	5.36± 0.01 P<0.001 (***)	5.67± 0.01
%E$_{max}$	57.07 ± 0.24 P<0.001 (***)	50.54 ± 0.24 P<0.001 (***)	80.78 ± 0.53 P<0.001 (***)	67.34 ± 0.13 P<0.001 (***)	28.77 ± 0.01 P<0.001 (***)	52.10 ± 0.35 P<0.001 (***)	32.38 ± 0.18 P<0.001 (***)	29.53 ± 1.14 P<0.001 (***)	67.79 ± 0.34 P<0.001 (***)	103.3 ± 0.50 P<0.01 (**)	40.74 ± 0.21 P<0.001 (***)	99.88 ± 0.12

Table 3.9 Comparison of pEC$_{50}$ and %Emax among GPR35 wild type and various mutants in arrestin recruitment assays using cromolyn

hGPR35a, hGPR35b and various mutants of hGPR35b were compared in terms of pEC$_{50}$ and %E$_{max}$ using BRET based arrestin recruitment assays. Results are expressed as mean ± SEM of three individual experiments. Data were analysed by one-way ANOVA followed by Dunnett's multiple comparisons test where the value for hGPR35a was used as control. ns = non-significant, * p<0.05, ** p<0.01, ***p<0.001.

	hGPR 35b C27S S5C	**hGPR 35b C27S T10C**	**hGPR 35b C27S G14C**	**hGPR 35b C27S S15C**	**hGPR 35b C27S M22C**	**hGPR 35b C27S S25C**	**hGPR 35b C27S S29C**	**hGPR 35b C27S M32C**	**hGPR 35b C27S G34C**	**hGPR 35b C27S**	**hGPR 35b WT**	**hGPR 35a WT**
pEC$_{50}$	4.49± 0.06 P<0.001 (***)	4.70± 0.06 P<0.001 (***)	4.91± 0.11 P<0.01 (**)	5.01± 0.02 P<0.01 (**)	5.18± 0.04 P=0.38 (ns)	4.95± 0.02 P<0.01 (**)	4.87± 0.04 P<0.001 (***)	4.68± 0.01 P<0.001 (***)	4.66± 0.01 P<0.001 (***)	4.97± 0.01 P<0.01 (**)	4.58± 0.06 P<0.001 (***)	5.31± 0.01
%E$_{max}$	45.35 ± 2.44 P<0.001 (***)	32.14 ± 1.56 P<0.001 (***)	25.18 ± 1.59 P<0.001 (***)	40.27 ± 0.72 P<0.001 (***)	34.86 ± 0.38 P<0.001 (***)	28.44 ± 0.38 P<0.001 (***)	29.89 ± 0.62 P<0.001 (***)	32.69 ± 0.54 P<0.001 (***)	43.71 ± 0.91 P<0.001 (***)	86.24 ± 0.29 P<0.001 (***)	38.15 ± 1.70 P<0.001 (***)	100.2 ± 0.20

Table 3.10 Comparison of pEC$_{50}$ and %E$_{max}$ among GPR35 wild type and various mutants in G protein activation assays using cromolyn

hGPR35a, hGPR35b and various mutants of hGPR35b were compared in terms of pEC$_{50}$ and %E$_{max}$ by BRET based G protein assays using GPR35-$G\alpha_{13}$ SPASM sensors . Results are expressed as mean ± SEM of three separate experiments. Data were analysed by one-way ANOVA followed by Dunnett's multiple comparisons test where the value for hGPR35a was used as control. ns = non-significant, * p<0.05, ** p<0.01, ***p<0.001.

3.2.3.5 Measurement of arrestin recruitment and G protein activation in various hGPR35b mutants with partial agonist doxantrazole

Parental 293 cells were transfected transiently to co-express either hGPR35b C27S (S5C, T10C, G14C, S15C, M22C, S25C, S29C, M32C and G34C) each tagged with eYFP and arrestin-3-RLuc. hGPR35a WT, hGPR35b WT and hGPR35b C27S tagged with eYFP were used as controls. After addition of luciferase substrate and doxantrazole, there was a concentration-dependent increase in measured BRET (Figure 3.11A) with pEC_{50} 4.98± 0.01 (mean± SEM, n=3 for hGPR35a WT) (Table 3.11). Similar outcomes to previous experiments were achieved using the hGPR35b WT and hGPR35b C27S mutants. Among the new mutants in the backbone of hGPR35b C27S (M22C, S29C, and M32C) mutants displayed statistically similar arrestin-3 recruitment activities to hGPR35b WT and they were all significantly different from hGPR35a WT (Emax, $p < 0.001$). The rest of the mutants in the backbone of hGPR35b C27S (S5C, T10C, G14C, S15C, S25C and G34C) demonstrated moderate enhancement of BRET signals compared to signals generated by hGPR35b WT (Figure 3.11A) (Table 3.11). As doxantrazole shows partial agonism to hGPR35, the raw signal intensity was significantly lower than full agonist.

For $G\alpha_{13}$ activation, hGPR35b C27S (S5C, T10C, G14C, S15C, M22C, S25C, S29C, M32C and G34C) were transiently expressed in parental HEK293 cells as $G\alpha_{13}$ SPASM sensors. hGPR35a WT, hGPR35b WT and hGPR35b C27S were also expressed as $G\alpha_{13}$ SPASM sensors. Following the addition of luciferase substrate and doxantrazole, a concentration-dependent increase in BRET (Figure 3.11B) was found with pEC_{50} 4.90± 0.01 (mean± SEM, n=3 for hGPR35a WT) (Table 3.12). Similar results to earlier studies were obtained when $G\alpha_{13}$ activation was carried out using the hGPR35b WT and hGPR35b C27S mutants. The nine mutants at various positions in the backbone of hGPR35b C27S demonstrated $G\alpha_{13}$ activation that were not statistically different from those of hGPR35b WT (Figure 3.10B) (Table 3.12). Here, the raw $G\alpha_{13}$ activation signals were lower than those generated by any full agonist of hGPR35.

These assays showed that cysteine was introduced into the hGPR35b N-terminal domain at several locations. The $G\alpha_{13}$ activation and arrestin-3 recruitment potential of the new mutants were comparable to those of hGPR35b WT in almost all cases. The most plausible reason for this is the formation of additional

disulphide bonds between extracellular loop 3 and various places of the hGPR35b N-terminal domain.

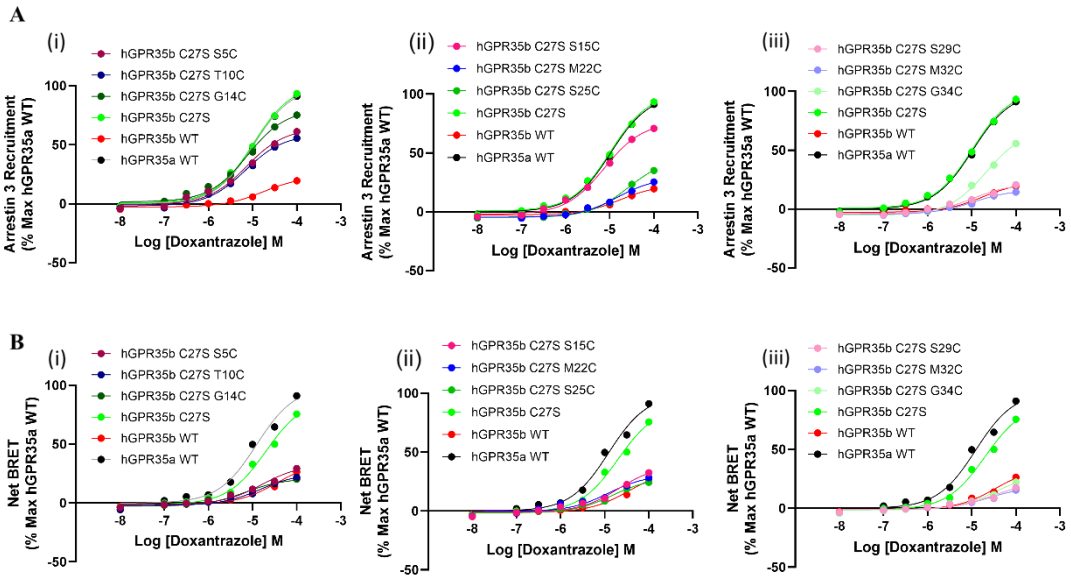

Figure 3.11 Measurement of interaction among various mutants of hGPR35b and arrestin-3 and demonstration of the effectiveness of different mutants of hGPR35b-Gα_{13} SPASM sensors using partial agonist doxantrazole

(A) Parental HEK293 cells were transfected transiently to co-express either **(i)** hGPR35b C27S S5C (maroon circles), hGPR35b C27S T10C (deep blue circles), hGPR35b C27S G14C (bottle green circles), **(ii)** hGPR35b C27S S15C (pink circles), hGPR35b C27S M22C (blue circles), hGPR35b C27S S25C (light green circles), **(iii)** hGPR35b C27S S29C (light pink circles), hGPR35b C27S M32C (light blue circles) and hGPR35b C27S G34C (paste circles) each tagged with eYFP and arrestin-3-RLuc. **(B)** Comparison of the effects of **(i)** hGPR35b C27S S5C (maroon circles), hGPR35b C27S T10C (deep blue circles), hGPR35b C27S G14C (bottle green circles), **(ii)** hGPR35b C27S S15C (pink circles), hGPR35b C27S M22C (blue circles), hGPR35b C27S S25C (light green circles), **(iii)** hGPR35b C27S S29C (light pink circles), hGPR35b C27S M32C (light blue circles) and hGPR35b C27S G34C (paste circles) transiently expressed in parental HEK293 cells as Gα_{13} SPASM sensors. In both assays **(A)** and **(B)** hGPR35a WT (black circles), hGPR35b WT (red circles) and hGPR35b C27S (green circles) were used as control. BRET signals were recorded after treating with various concentrations of doxantrazole for 5 min. Each dataset represents the mean ± SEM of three independent experiments. Data were analysed by one-way ANOVA followed by Dunnett's multiple comparisons test and statistical results are shown in the following tables.

	hGPR35b C27S S5C	**hGPR35b C27S T10C**	**hGPR35b C27S G14C**	**hGPR35b C27S S15C**	**hGPR35b C27S M22C**	**hGPR35b C27S S25C**	**hGPR35b C27S S29C**	**hGPR35b C27S M32C**	**hGPR35b C27S G34C**	**hGPR35b C27S**	**hGPR35b WT**	**hGPR35a WT**
pEC_{50}	5.14± 0.01 P<0.001 (***)	5.15± 0.01 P<0.001 (***)	5.12± 0.01 P<0.001 (***)	5.11± 0.02 P<0.001 (***)	4.81± 0.02 P<0.001 (***)	4.60± 0.01 P<0.001 (***)	4.99± 0.01 P=0.96 (ns)	4.92± 0.05 P=0.15 (ns)	4.66± 0.01 P<0.001 (***)	4.98± 0.01 P=0.99 (ns)	4.76± 0.01 P<0.001 (***)	4.98± 0.01
%E max	63.90 ± 0.19 P<0.001 (***)	59.20 ± 0.28 P<0.001 (***)	80.38 ± 0.24 P<0.001 (***)	76.17 ± 0.14 P<0.001 (***)	29.58 ± 0.47 P<0.001 (***)	45.55 ± 0.01 P<0.001 (***)	21.30 ± 0.12 P<0.001 (***)	16.83 ± 0.48 P<0.001 (***)	69.17 ± 0.77 P<0.001 (***)	101.6 ± 0.30 P<0.05 (*)	23.25 ± 0.17 P<0.001 (***)	99.84 ± 0.16

Table 3.11 Comparison of pEC_{50} and %Emax among GPR35 wild type and various mutants in arrestin recruitment assays using doxantrazole

hGPR35a, hGPR35b and various mutants of hGPR35b were compared in terms of pEC_{50} and $\%E_{max}$ using BRET based arrestin recruitment assays. Results are expressed as mean ± SEM of three individual experiments. Data were analysed by one-way ANOVA followed by Dunnett's multiple comparisons test where the value for hGPR35a was used as control. ns = non-significant, * p<0.05, ** p<0.01, ***p<0.001.

	hGPR 35b C27S S5C	**hGPR 35b C27S T10C**	**hGPR 35b C27S G14C**	**hGPR 35b C27S S15C**	**hGPR 35b C27S M22C**	**hGPR 35b C27S S25C**	**hGPR 35b C27S S29C**	**hGPR 35b C27S M32C**	**hGPR 35b C27S G34C**	**hGPR 35b C27S**	**hGPR 35b WT**	**hGPR 35a WT**
pEC_{50}	4.79± 0.01 P<0.05 (*)	4.81± 0.02 P<0.05 (*)	5.17± 0.01 P<0.001 (***)	4.68± 0.01 P<0.001 (***)	4.88± 0.03 P=0.99 (ns)	4.81± 0.01 P<0.05 (*)	4.57± 0.02 P<0.001 (***)	4.59± 0.05 P<0.001 (***)	4.47± 0.01 P<0.001 (***)	4.70± 0.01 P<0.001 (***)	4.45± 0.01 P<0.001 (***)	4.90± 0.01
$\%E_{max}$	32.71 ± 0.08 P<0.001 (***)	25.56 ± 0.37 P<0.001 (***)	20.81 ± 0.07 P<0.001 (***)	39.49 ± 0.60 P<0.001 (***)	31.58 ± 0.76 P<0.001 (***)	28.80 ± 0.49 P<0.001 (***)	21.73 ± 0.19 P<0.001 (***)	19.26 ± 0.86 P<0.001 (***)	29.36 ± 0.18 P<0.001 (***)	89.08 ± 0.02 P<0.001 (***)	35.61 ± 0.67 P<0.001 (***)	99.55 ± 0.45

Table 3.12 Comparison of pEC_{50} and $\%E_{max}$ among GPR35 wild type and various mutants in G protein activation assays using doxantrazole
hGPR35a, hGPR35b and various mutants of hGPR35b were compared in terms of pEC_{50} and $\%E_{max}$ by BRET based G protein assays using GPR35-$G\alpha_{13}$ SPASM sensors. Results are expressed as mean ± SEM of three separate experiments. Data were analysed by one-way ANOVA followed by Dunnett's multiple comparisons test where the value for hGPR35a was used as control. ns = non-significant, * p<0.05, ** p<0.01, ***p<0.001.

3.2.3.6 Investigation of arrestin recruitment and G protein activation in various hGPR35b mutants with phosphodiesterase inhibitor zaprinast

In this section, zaprinast was employed to pharmacologically characterise the different mutants of long isoform of human GPR35. Zaprinast is a well-known cGMP specific-phosphodiesterase (cGMP-PDEs) inhibitor (Taniguchi et al., 2006). A transient transfection was performed on parental 293 cells to co-express either hGPR35b C27S (S5C, T10C, G14C, S15C, M22C, S25C, S29C, M32C and G34C) tagged with eYFP and arrestin-3-RLuc. As controls, hGPR35a WT, hGPR35b WT, and hGPR35b C27S were tagged with eYFP and used. There was a concentration-dependent rise in the amount of measured BRET (Figure 3.12A) following the addition of luciferase substrate and zaprinast with pEC_{50} 5.73± 0.01 (mean± SEM, n=3 for hGPR35a WT) (Table 3.13). Similar outcomes to previous investigations were achieved using the hGPR35b WT and hGPR35b C27S mutants. Among the new mutants in the backbone of hGPR35b C27S (M22C, S25C, S29C, and M32C) mutants displayed statistically similar arrestin-3 recruitment activities to hGPR35b WT and they were all significantly different from hGPR35a WT (Emax, $p < 0.001$). The rest of the mutants in the backbone of hGPR35b C27S (S5C, T10C, G14C, S15C and

G34C) demonstrated moderate enhancement of BRET signals compared to signals generated by hGPR35b WT (Figure 3.12A) (Table 3.13).

In order to activate $G\alpha_{13}$ in parental HEK293 cells, hGPR35b C27S (S5C, T10C, G14C, S15C, M22C, S25C, S29C, M32C and G34C) were transiently expressed as $G\alpha_{13}$ SPASM sensors. hGPR35a WT, hGPR35b WT and hGPR35b C27S were also expressed as $G\alpha_{13}$ SPASM sensors as controls. A concentration-dependent rise in BRET (Figure 3.12B) was discovered with the application of luciferase substrate and zaprinast with pEC_{50} 5.78± 0.01 (mean± SEM, n=3 for hGPR35a WT) (Table 3.14). Similar results to earlier studies were obtained when $G\alpha_{13}$ activation was carried out using the hGPR35b WT and hGPR35b C27S mutants. The nine newly generated mutants in the backbone of hGPR35b C27S demonstrated $G\alpha_{13}$ activation that was statistically comparable to that of hGPR35b WT (Figure 3.12B) (Table 3.14).

These tests revealed that cysteine was inserted at varied positions of the N-terminal domain of hGPR35b. All the novel mutants showed arrestin-3 recruitment potential and $G\alpha_{13}$ activation to a substantially same degree as that shown by hGPR35b WT. The creation of additional disulphide bonds from various sites of the hGPR35b N-terminal domain to extracellular loop 3 is the most probable cause of this.

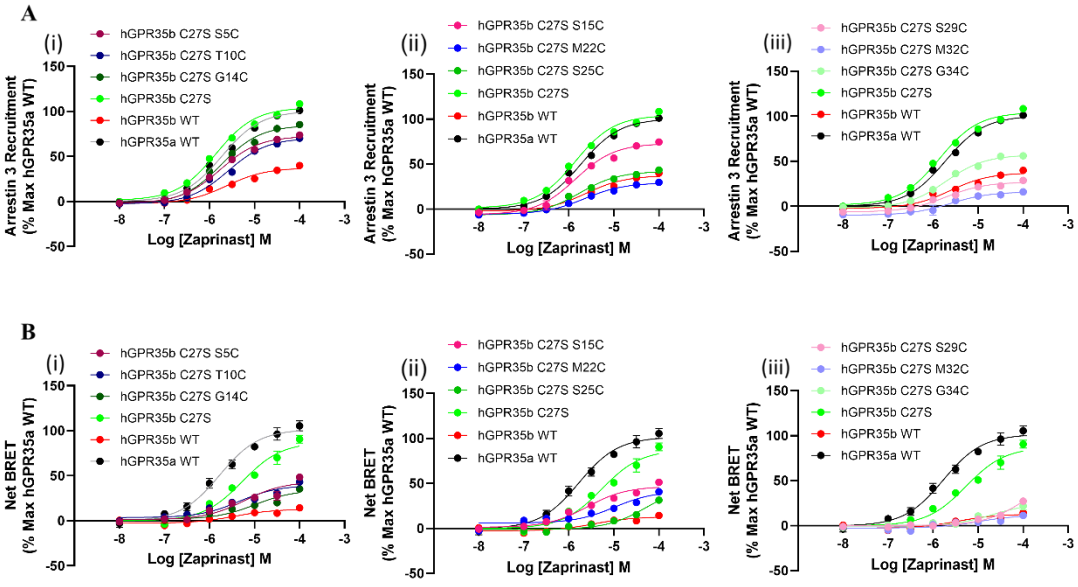

Figure 3.12 Comparison of interaction among various mutants of hGPR35b and arrestin-3 and validation of the effectiveness of different mutants of hGPR35b-$G\alpha_{13}$ SPASM sensors using GPR35 agonist zaprinast

(A) Parental HEK293 cells were transfected transiently to co-express either **(i)** hGPR35b C27S S5C (maroon circles), hGPR35b C27S T10C (deep blue circles), hGPR35b C27S G14C (bottle green circles), **(ii)** hGPR35b C27S S15C (pink circles), hGPR35b C27S M22C (blue circles), hGPR35b C27S S25C (light green circles), **(iii)** hGPR35b C27S S29C (light pink circles), hGPR35b C27S M32C (light blue circles) and hGPR35b C27S G34C (paste circles) each tagged with eYFP and arrestin-3-RLuc. **(B)** Comparison of the effects of **(i)** hGPR35b C27S S5C (maroon circles), hGPR35b C27S T10C (deep blue circles), hGPR35b C27S G14C (bottle green circles), **(ii)** hGPR35b C27S S15C (pink circles), hGPR35b C27S M22C (blue circles), hGPR35b C27S S25C (light green circles), **(iii)** hGPR35b C27S S29C (light pink circles), hGPR35b C27S M32C (light blue circles) and hGPR35b C27S G34C (paste circles) transiently expressed in parental HEK293 cells as $G\alpha_{13}$ SPASM sensors. In both assays **(A)** and **(B)** hGPR35a WT (black circles), hGPR35b WT (red circles) and hGPR35b C27S (green circles) were used as control. BRET signals were observed after treating with indicated concentrations of zaprinast for 5 min. Each dataset represents the mean ± SEM of three independent experiments. Data were analysed by one-way ANOVA followed by Dunnett's multiple comparisons test and statistical results are shown in the following tables.

	hGPR35b C27S S5C	**hGPR35b C27S T10C**	**hGPR35b C27S G14C**	**hGPR35b C27S S15C**	**hGPR35b C27S M22C**	**hGPR35b C27S S25C**	**hGPR35b C27S S29C**	**hGPR35b C27S M32C**	**hGPR35b C27S G34C**	**hGPR35b C27S**	**hGPR35b WT**	**hGPR35a WT**
pEC$_{50}$	5.76± 0.01 P=0.12 (ns)	5.58± 0.01 P<0.001 (***)	5.74± 0.01 P=0.94 (ns)	5.85± 0.01 P<0.001 (***)	5.64± 0.01 P<0.001 (***)	5.78± 0.02 P<0.05 (*)	5.72± 0.01 P=0.96 (ns)	5.59± 0.02 P<0.001 (***)	5.73± 0.01 P>0.99 (ns)	5.86± 0.01 P<0.001 (***)	5.62± 0.01 P<0.001 (***)	5.73± 0.01
%E$_{max}$	72.71 ± 0.11 P<0.001 (***)	70.96 ± 0.51 P<0.001 (***)	84.86 ± 0.27 P<0.001 (***)	73.12 ± 0.15 P<0.001 (***)	29.55 ± 0.39 P<0.001 (***)	41.91 ± 0.1 P<0.001 (***)	27.03 ± 0.14 P<0.001 (***)	16.09 ± 0.01 P<0.001 (***)	57.26 ± 0.14 P<0.001 (***)	104.8 ± 0.50 P<0.001 (***)	37.89 ± 0.64 P<0.001 (***)	100.2 ± 0.20

Table 3.13 Comparison of pEC$_{50}$ and %Emax among GPR35 wild type and various mutants in arrestin recruitment assays using zaprinast

hGPR35a, hGPR35b and various mutants of hGPR35b were compared in terms of pEC$_{50}$ and %E$_{max}$ using BRET based arrestin recruitment assays. Results are expressed as mean ± SEM of three individual experiments. Data were analysed by one-way ANOVA followed by Dunnett's multiple comparisons test where the value for hGPR35a was used as control. ns = non-significant, * p<0.05, ** p<0.01, ***p<0.001.

	hGPR35b C27S S5C	**hGPR35b C27S T10C**	**hGPR35b C27S G14C**	**hGPR35b C27S S15C**	**hGPR35b C27S M22C**	**hGPR35b C27S S25C**	**hGPR35b C27S S29C**	**hGPR35b C27S M32C**	**hGPR35b C27S G34C**	**hGPR35b C27S**	**hGPR35b WT**	**hGPR35a WT**
pEC$_{50}$	5.23± 0.01 P<0.001 (***)	5.33± 0.02 P<0.001 (***)	5.03± 0.05 P<0.001 (***)	5.59± 0.01 P=0.09 (ns)	4.98± 0.01 P<0.001 (***)	4.27± 0.02 P<0.001 (***)	3.98± 0.02 P<0.001 (***)	4.89± 0.11 P<0.001 (***)	4.58± 0.09 P<0.001 (***)	5.27± 0.01 P<0.001 (***)	5.47± 0.03 P<0.01 (**)	5.78± 0.01
%E$_{max}$	43.52 ± 0.04 P<0.001 (***)	39.58 ± 0.13 P<0.001 (***)	33.91 ± 0.47 P<0.001 (***)	46.90 ± 0.22 P<0.001 (***)	41.53 ± 0.20 P<0.001 (***)	48.98 ± 1.65 P<0.001 (***)	56.18 ± 2.19 P<0.001 (***)	12.63 ± 1.02 P<0.001 (***)	26.53 ± 1.44 P<0.001 (***)	87.59 ± 0.24 P<0.001 (***)	12.72 ± 0.14 P<0.001 (***)	100.8 ± 0.75

Table 3.14 Comparison of pEC$_{50}$ and %E$_{max}$ among GPR35 wild type and various mutants in G protein activation assays using zaprinast

hGPR35a, hGPR35b and various mutants of hGPR35b were compared in terms of pEC_{50} and $\%E_{max}$ by BRET based G protein assays using GPR35-$G\alpha_{13}$ SPASM sensors . Results are expressed as mean ± SEM of three separate experiments. Data were analysed by one-way ANOVA followed by Dunnett's multiple comparisons test where the value for hGPR35a was used as control. ns = non-significant, * p<0.05, ** p<0.01, ***p<0.001.

3.2.3.7 Measurement of arrestin recruitment and G protein activation in various hGPR35b mutants with GPR35 agonist PSB-13253

Parental 293 cells were transfected transiently to co-express either hGPR35b C27S (S5C, T10C, G14C, S15C, M22C, S25C, S29C, M32C and G34C) each tagged with eYFP and arrestin-3-RLuc. hGPR35a WT, hGPR35b WT and hGPR35b C27S tagged with eYFP were used as controls. After addition of luciferase substrate and PSB-13253, there was a concentration-dependent increase in measured BRET (Figure 3.13A) with pEC_{50} 7.31± 0.01 (mean± SEM, n=3 for hGPR35a WT) (Table 3.15). Similar outcomes to previous investigations were achieved using the hGPR35b WT and hGPR35b C27S mutants. Among the new mutants in the backbone of hGPR35b C27S (M22C, S25C, S29C, and M32C) mutants displayed statistically similar arrestin-3 recruitment activities to hGPR35b WT and they were all significantly different from hGPR35a WT (Emax, $p < 0.001$). The remaining hGPR35b C27S backbone mutants (S5C, T10C, G14C, S15C, and G34C) showed a moderate increase in BRET signals as compared to signals generated by hGPR35b WT (Figure 3.13A) (Table 3.15).

For $G\alpha_{13}$ activation, hGPR35b C27S (S5C, T10C, G14C, S15C, M22C, S25C, S29C, M32C and G34C) were transiently expressed in parental HEK293 cells as $G\alpha_{13}$ SPASM sensors. hGPR35a WT, hGPR35b WT and hGPR35b C27S were also expressed as $G\alpha_{13}$ SPASM sensors. Following addition of luciferase substrate and PSB-13253, a concentration-dependent increase in BRET (Figure 3.13B) was found with pEC_{50} 7.38± 0.01 (mean± SEM, n=3 for hGPR35a WT) (Table 3.16). Similar results to earlier studies were obtained when $G\alpha_{13}$ activation was carried out using the hGPR35b WT and hGPR35b C27S mutants. The nine newly generated mutants in the backbone of hGPR35b C27S demonstrated $G\alpha_{13}$ activation that was statistically comparable to that of hGPR35b WT (Figure 3.13B) (Table 3.16).

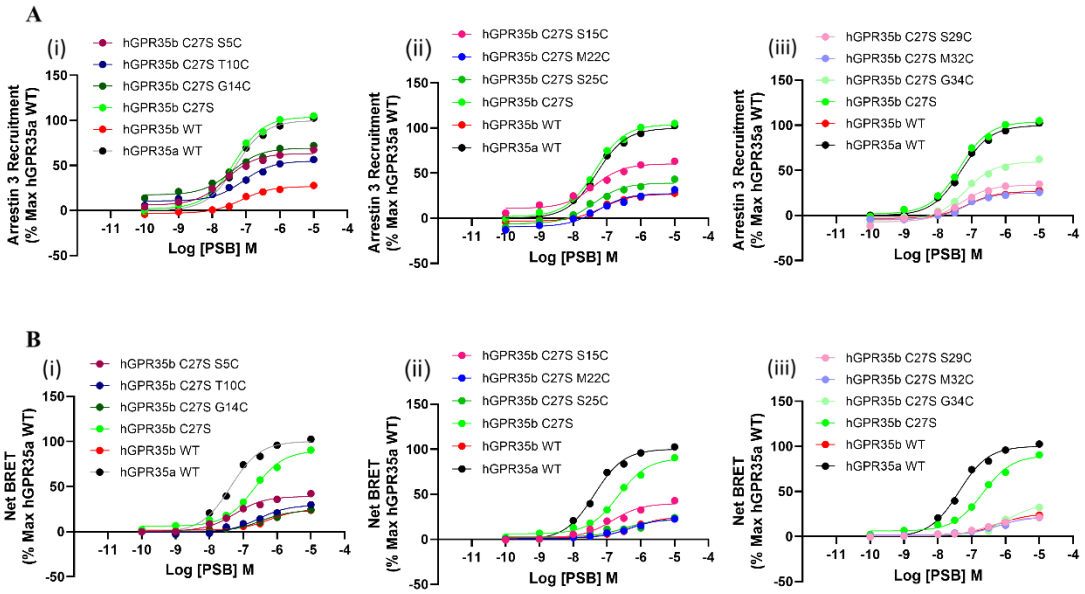

Figure 3.13 Measurement of interaction among various mutants of hGPR35b and arrestin-3 and demonstration of the effectiveness of different mutants of hGPR35b-Gα$_{13}$ SPASM sensors using GPR35 agonist PSB-13253

(A) Parental HEK293 cells were transfected transiently to co-express either **(i)** hGPR35b C27S S5C (maroon circles), hGPR35b C27S T10C (deep blue circles), hGPR35b C27S G14C (bottle green circles), **(ii)** hGPR35b C27S S15C (pink circles), hGPR35b C27S M22C (blue circles), hGPR35b C27S S25C (light green circles), **(iii)** hGPR35b C27S S29C (light pink circles), hGPR35b C27S M32C (light blue circles) and hGPR35b C27S G34C (paste circles) each tagged with eYFP and arrestin-3-RLuc. **(B)** Comparison of the effects of **(i)** hGPR35b C27S S5C (maroon circles), hGPR35b C27S T10C (deep blue circles), hGPR35b C27S G14C (bottle green circles), **(ii)** hGPR35b C27S S15C (pink circles), hGPR35b C27S M22C (blue circles), hGPR35b C27S S25C (light green circles), **(iii)** hGPR35b C27S S29C (light pink circles), hGPR35b C27S M32C (light blue circles) and hGPR35b C27S G34C (paste circles) transiently expressed in parental HEK293 cells as Gα$_{13}$ SPASM sensors. In both assays **(A)** and **(B)** hGPR35a WT (black circles), hGPR35b WT (red circles) and hGPR35b C27S (green circles) were used as control. BRET signals were recorded after treating with various concentrations of PSB-13253 for 5 min. Each dataset represents the mean ± SEM of three independent experiments. Data were analysed by one-way ANOVA followed by Dunnett's multiple comparisons test and statistical results are shown in the following tables.

	hGPR 35b C27S S5C	**hGPR 35b C27S T10C**	**hGPR 35b C27S G14C**	**hGPR 35b C27S S15C**	**hGPR 35b C27S M22C**	**hGPR 35b C27S S25C**	**hGPR 35b C27S S29C**	**hGPR 35b C27S M32C**	**hGPR 35b C27S G34C**	**hGPR 35b C27S**	**hGPR 35b WT**	**hGPR 35a WT**
pEC$_{50}$	7.61± 0.01 P<0.001 (***)	7.05± 0.04 P<0.001 (***)	7.41± 0.02 P<0.05 (*)	7.37± 0.02 P=0.26 (ns)	7.30± 0.04 P>0.99 (ns)	7.39± 0.01 P=0.07 (ns)	7.34± 0.01 P=0.93 (ns)	7.17± 0.02 P<0.01 (**)	7.20± 0.02 P<0.05 (*)	7.36± 0.01 P=0.41 (ns)	7.13± 0.01 P<0.001 (***)	7.31± 0.01
%E$_{max}$	63.54 ± 0.36 P<0.001 (***)	55.24 ± 0.26 P<0.001 (***)	69.59 ± 0.34 P<0.001 (***)	60.79 ± 0.43 P<0.001 (***)	27.23 ± 0.22 P<0.001 (***)	39.31 ± 0.29 P<0.001 (***)	34.29 ± 0.44 P<0.001 (***)	25.82 ± 0.55 P<0.001 (***)	59.79 ± 0.05 P<0.001 (***)	103.8 ± 0.25 P<0.001 (***)	26.78 ± 0.01 P<0.001 (***)	99.93 ± 0.07

Table 3.15 Comparison of pEC$_{50}$ and %Emax among GPR35 wild type and various mutants in arrestin recruitment assays using PSB-13253

hGPR35a, hGPR35b and various mutants of hGPR35b were compared in terms of pEC$_{50}$ and %E$_{max}$ using BRET based arrestin recruitment assays. Results are expressed as mean ± SEM of three individual experiments. Data were analysed by one-way ANOVA followed by Dunnett's multiple comparisons test where the value for hGPR35a was used as control. ns = non-significant, * p<0.05, ** p<0.01, ***p<0.001.

	hGPR 35b C27S S5C	hGPR 35b C27S T10C	hGPR 35b C27S G14C	hGPR 35b C27S S15C	hGPR 35b C27S M22C	hGPR 35b C27S S25C	hGPR 35b C27S S29C	hGPR 35b C27S M32C	hGPR 35b C27S G34C	hGPR 35b C27S	hGPR 35b WT	hGPR 35a WT
pE C_{50}	7.22± 0.02 P=0.58 (ns)	6.52± 0.02 P<0.001 (***)	6.49± 0.01 P<0.001 (***)	6.84± 0.01 P<0.01 (**)	6.26± 0.07 P<0.001 (***)	6.7±0.21 P<0.01 (**)	6.45± 0.06 P<0.001 (***)	6.18± 0.04 P<0.001 (***)	5.96± 0.01 P<0.001 (***)	6.68± 0.01 P<0.001 (***)	6.19± 0.02 P<0.001 (***)	7.38± 0.01
%E $_{max}$	39.69 ± 0.48 P<0.001 (***)	29.72 ± 0.24 P<0.001 (***)	24.07 ± 0.21 P<0.001 (***)	40.06 ± 0.21 P<0.001 (***)	23.68 ± 0.64 P<0.001 (***)	21.23 ± 0.79 P<0.001 (***)	21.78 ± 0.21 P<0.001 (***)	21.98 ± 0.31 P<0.001 (***)	35.37 ± 0.92 P<0.001 (***)	90.34 ± 0.34 P<0.001 (***)	25.28 ± 0.09 P<0.001 (***)	100.1 ± 0.10

Table 3.16 Comparison of pEC_{50} and $\%E_{max}$ among GPR35 wild type and various mutants in G protein activation assays using PSB-13253
hGPR35a, hGPR35b and various mutants of hGPR35b were compared in terms of pEC_{50} and $\%E_{max}$ by BRET based G protein assays using GPR35-$G\alpha_{13}$ SPASM sensors . Results are expressed as mean ± SEM of three separate experiments. Data were analysed by one-way ANOVA followed by Dunnett's multiple comparisons test where the value for hGPR35a was used as control. ns = non-significant, * p<0.05, ** p<0.01, ***p<0.001.

3.2.3.8 Investigation of arrestin recruitment and G protein activation in various hGPR35b mutants with GPR35 agonist amlexanox

A transient transfection was performed on parental 293 cells to co-express either hGPR35b C27S (S5C, T10C, G14C, S15C, M22C, S25C, S29C, M32C and G34C) tagged with eYFP and arrestin-3-RLuc. As controls, hGPR35a WT, hGPR35b WT, and hGPR35b C27S were also tagged with eYFP and used. There was a concentration-dependent rise in the amount of measured BRET (Figure 3.14A) following the addition of luciferase substrate and amlexanox with pEC_{50} 5.39± 0.01 (mean± SEM, n=3 for hGPR35a WT) (Table 3.17). Similar outcomes to previous investigations were achieved using the hGPR35b WT and hGPR35b C27S mutants. Among the new mutants in the backbone of hGPR35b C27S (M22C, S25C, S29C, and M32C) mutants displayed statistically similar arrestin-3 recruitment activities to hGPR35b WT and they were all significantly different from hGPR35a WT (Emax, $p < 0.001$). The remaining hGPR35b C27S backbone mutants (S5C, T10C, G14C, S15C, and G34C) showed a moderate increase in BRET signals as compared to signals generated by hGPR35b WT (Figure 3.14A) (Table 3.17).

In order to activate $G\alpha_{13}$ in parental HEK293 cells, hGPR35b C27S (S5C, T10C, G14C, S15C, M22C, S25C, S29C, M32C and G34C) were transiently expressed as $G\alpha_{13}$ SPASM sensors. hGPR35a WT, hGPR35b WT and hGPR35b C27S were also expressed as $G\alpha_{13}$ SPASM sensors as controls. A gradual increase in BRET with

increasing concentration (Figure 3.14B) was discovered with the application of luciferase substrate and amlexanox with pEC_{50} 5.22± 0.01 (mean± SEM, n=3 for hGPR35a WT) (Table 3.18). Similar results to earlier studies were obtained when $G\alpha_{13}$ activation was carried out using the hGPR35b WT and hGPR35b C27S mutants. The nine newly generated mutants in the backbone of hGPR35b C27S demonstrated $G\alpha_{13}$ activation that was statistically comparable to that of hGPR35b WT (Figure 3.14B) (Table 3.18).

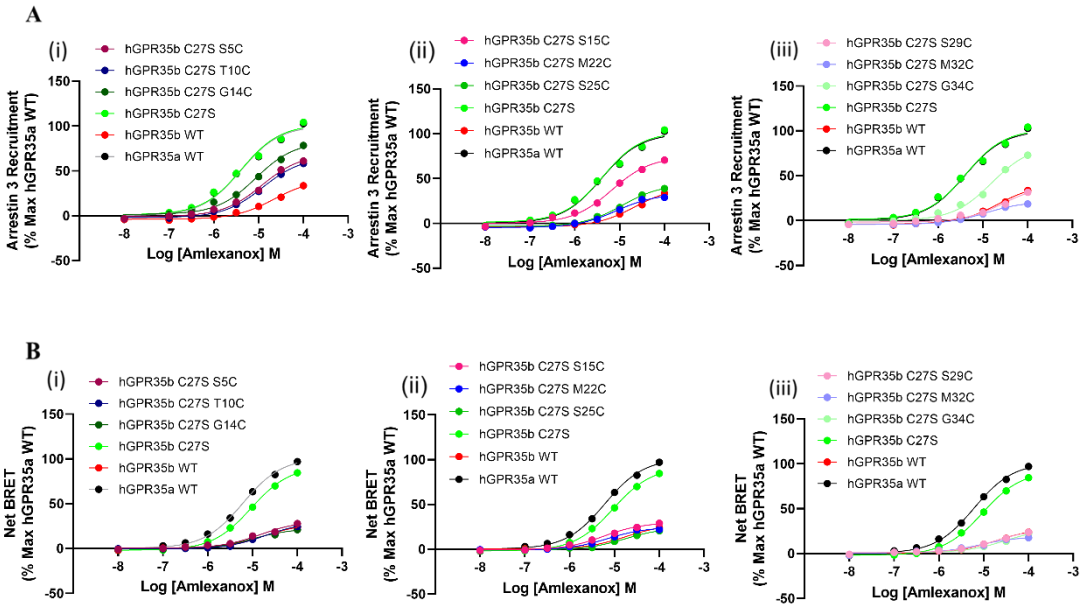

Figure 3.14 Comparison of interaction among various mutants of hGPR35b and arrestin-3 and validation of the effectiveness of different mutants of hGPR35b-$G\alpha_{13}$ SPASM sensors using GPR35 agonist amlexanox

(A) Parental HEK293 cells were transfected transiently to co-express either (i) hGPR35b C27S S5C (maroon circles), hGPR35b C27S T10C (deep blue circles), hGPR35b C27S G14C (bottle green circles), (ii) hGPR35b C27S S15C (pink circles), hGPR35b C27S M22C (blue circles), hGPR35b C27S S25C (light green circles), (iii) hGPR35b C27S S29C (light pink circles), hGPR35b C27S M32C (light blue circles) and hGPR35b C27S G34C (paste circles) each tagged with eYFP and arrestin-3-RLuc. (B) Comparison of the effects of (i) hGPR35b C27S S5C (maroon circles), hGPR35b C27S T10C (deep blue circles), hGPR35b C27S G14C (bottle green circles), (ii) hGPR35b C27S S15C (pink circles), hGPR35b C27S M22C (blue circles), hGPR35b C27S S25C (light green circles), (iii) hGPR35b C27S S29C (light pink circles), hGPR35b C27S M32C (light blue circles) and hGPR35b C27S G34C (paste circles) transiently expressed in parental HEK293 cells as $G\alpha_{13}$ SPASM sensors. In both assays (A) and (B) hGPR35a WT (black circles), hGPR35b WT (red circles) and hGPR35b C27S (green circles) were used as control. BRET signals were observed after treating with indicated concentrations of amlexanox for 5 min. Each dataset represents the mean ± SEM of three independent experiments. Data were analysed by one-way ANOVA followed by Dunnett's multiple comparisons test and statistical results are shown in the following tables.

	hGPR35b C27S S5C	hGPR35b C27S T10C	hGPR35b C27S G14C	hGPR35b C27S S15C	hGPR35b C27S M22C	hGPR35b C27S S25C	hGPR35b C27S S29C	hGPR35b C27S M32C	hGPR35b C27S G34C	hGPR35b C27S	hGPR35b WT	hGPR35a WT
pEC_{50}	4.93± 0.01	4.91± 0.01	5.06± 0.01	5.18± 0.01	5.08± 0.01	4.94± 0.01	4.55± 0.01	4.93± 0.01	4.81± 0.01	5.39± 0.01	4.63± 0.03	5.39± 0.01

	P<0.001 (***)	P<0.001 (***)	P<0.001 (***)	P<0.001 (***)	P<0.001 (***)	P<0.001 (***)	P<0.001 (***)	P<0.001 (***)	P<0.001 (***)	P>0.99 (ns)	P<0.001 (***)	
%E max	68.94 ± 0.11 P<0.001 (***)	65.47 ± 0.14 P<0.001 (***)	82.86 ± 0.13 P<0.001 (***)	74.44 ± 0.07 P<0.001 (***)	32.52 ± 0.34 P<0.001 (***)	43.92 ± 0.09 P<0.001 (***)	39.53 ± 0.35 P<0.001 (***)	21.41 ± 0.13 P<0.001 (***)	84.17 ± 0.01 P<0.001 (***)	102.0 ± 0.05 P<0.05 (*)	41.75 ± 0.93 P<0.001 (***)	100.2 ± 0.20

Table 3.17 Comparison of pEC_{50} and %Emax among GPR35 wild type and various mutants in arrestin recruitment assays using amlexanox

hGPR35a, hGPR35b and various mutants of hGPR35b were compared in terms of pEC_{50} and $\%E_{max}$ using BRET based arrestin recruitment assays. Results are expressed as mean ± SEM of three individual experiments. Data were analysed by one-way ANOVA followed by Dunnett's multiple comparisons test where the value for hGPR35a was used as control. ns = non-significant, * p<0.05, ** p<0.01, ***p<0.001.

	hGPR35b C27S S5C	**hGPR35b C27S T10C**	**hGPR35b C27S G14C**	**hGPR35b C27S S15C**	**hGPR35b C27S M22C**	**hGPR35b C27S S25C**	**hGPR35b C27S S29C**	**hGPR35b C27S M32C**	**hGPR35b C27S G34C**	**hGPR35b C27S**	**hGPR35b WT**	**hGPR35a WT**
pEC_{50}	4.81± 0.02 P<0.001 (***)	4.71± 0.01 P<0.001 (***)	4.98± 0.01 P<0.001 (***)	5.22± 0.02 P>0.99 (ns)	5.13± 0.02 P<0.05 (*)	4.75± 0.01 P<0.001 (***)	4.73± 0.01 P<0.001 (***)	5.04± 0.04 P<0.01 (**)	4.54± 0.02 P<0.001 (***)	5.03± 0.01 P<0.001 (***)	4.73± 0.03 P<0.001 (***)	5.22± 0.01
%E max	31.17 ± 0.44 P<0.001 (***)	29.97 ± 0.48 P<0.001 (***)	22.53 ± 0.02 P<0.001 (***)	30.34 ± 0.45 P<0.001 (***)	25.31 ± 0.53 P<0.001 (***)	24.38 ± 0.02 P<0.001 (***)	27.63 ± 0.24 P<0.001 (***)	19.41 ± 0.37 P<0.001 (***)	27.49 ± 0.29 P<0.001 (***)	92.05 ± 0.03 P<0.001 (***)	28.48 ± 0.80 P<0.001 (***)	100.7 ± 0.65

Table 3.18 Comparison of pEC_{50} and $\%E_{max}$ among GPR35 wild type and various mutants in G protein activation assays using amlexanox

hGPR35a, hGPR35b and various mutants of hGPR35b were compared in terms of pEC_{50} and $\%E_{max}$ by BRET based G protein assays using GPR35-$G\alpha_{13}$ SPASM sensors . Results are expressed as mean ± SEM of three separate experiments. Data were analysed by one-way ANOVA followed by Dunnett's multiple comparisons test where the value for hGPR35a was used as control. ns = non-significant, * p<0.05, ** p<0.01, ***p<0.001.

To summarise the key results obtained after using different agonists and partial agonists in arrestin and G protein based assays, comparisons of all the ligands were made, keeping lodoxamide value as control. This would make the outcomes clearer and key results of arrestin recruitment and G protein activation assays are shown in the following tables (Table 3.19) (Table 3.20).

	Lodoxamide	Bufrolin	Pamoic Acid	Cromolyn	Doxantrazole	Zaprinast	PSB-13253	Amlexanox
pEC_{50}	7.82±0.02	7.69±0.01 P<0.001 (***)	7.12±0.02 P<0.001 (***)	5.67±0.01 P<0.001 (***)	4.98±0.01 P<0.001 (***)	5.73±0.01 P<0.001 (***)	7.31±0.01 P<0.001 (***)	5.40±0.01 P<0.001 (***)
$\%E_{max}$	100± 0.34	67.94± 1.22 P<0.001 (***)	65.36± 5.77 P<0.001 (***)	89.68± 2.00 P<0.05 (*)	34.11± 0.37 P<0.001 (***)	103.3± 3.04 P=0.78 (ns)	126.1± 0.01 P<0.01 (**)	45.75 ± 0.17 P<0.001 (***)

Table 3.19 Comparison of pEC_{50} and %Emax among different GPR35 ligands using hGPR35a wild type in arrestin recruitment assay
pEC_{50} and %Emax were compared among different ligands in hGPR35a wild type using BRET based arrestin recruitment assays. Results are expressed as mean ± SEM of three individual experiments. Data were analysed by one-way ANOVA followed by Dunnett's multiple comparisons test where the value for lodoxamide was used as control. ns = non-significant, * p<0.05, ** p<0.01, ***p<0.001.

	Lodoxamide	Bufrolin	Pamoic Acid	Cromolyn	Doxantrazole	Zaprinast	PSB-13253	Amlexanox
pEC_{50}	8.22±0.01	8.05±0.01 P<0.01 (**)	7.02±0.04 P<0.001 (***)	5.31±0.01 P<0.001 (***)	4.90±0.01 P<0.001 (***)	5.78±0.01 P<0.001 (***)	7.37±0.01 P<0.001 (***)	5.22±0.01 P<0.001 (***)
$\%E_{max}$	100.1± 1.69	82.95± 0.94 P<0.01 (**)	81.25± 1.80 P<0.001 (***)	88.58± 1.53 P<0.01 (**)	41.94± 0.58 P<0.001 (***)	81.98± 0.01 P<0.01 (**)	104.5± 0.01 P=0.55 (ns)	66.86 ± 1.70 P<0.001 (***)

Table 3.20 Comparison of pEC_{50} and %Emax among different GPR35 ligands using hGPR35a wild type in G protein activation assay
pEC_{50} and %Emax were compared among different ligands in hGPR35a wild type using BRET based G protein activation assays. Results are expressed as mean ± SEM of three individual experiments. Data were analysed by one-way ANOVA followed by Dunnett's multiple comparisons test where the value for lodoxamide was used as control. ns = non-significant, * p<0.05, ** p<0.01, ***p<0.001.

3.2.4 Investigation of the potential role of arginine (R) 13 polymorphisms on the function of human GPR35b

As there are some correlation reports on arginine13 polymorphisms with better survival from cancer, I generated some additional mutants in both wild type and the C27S backbone of hGPR35b. From the UK Biobank database, I have come to know that patients with R13H or R13P polymorphisms had better survival for GI-associated cancers, including pancreatic cancer and liver cancer, compared to patients that have arginine (R) at position 13. I mutated arginine (R) at position 13 to each of proline (P), histidine (H) and cysteine (C). After confirming the alterations by sequencing, I assessed the effects of these changes on both activation of the G protein $G\alpha_{13}$ and arrestin-3 recruitment by utilising a series of

agonists of GPR35. Ligands used in this section were: pamoic acid, GSK 938, zaprinast, lodoxamide, PSB-13253, cromolyn, amlexanox and doxantrazole.

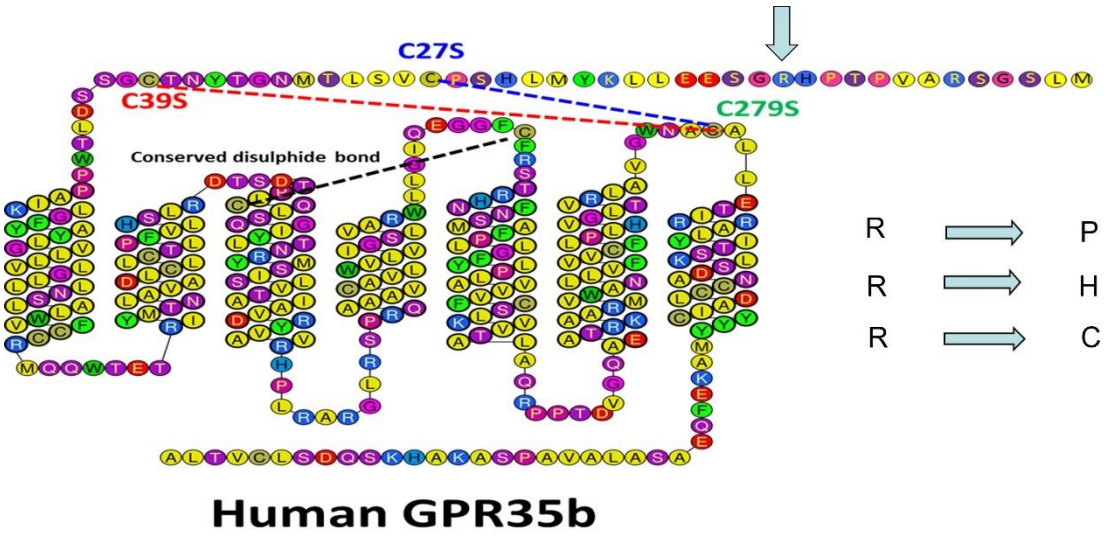

Figure 3.15 Primary structure of human GPR35b with the indication of amino acid arginine at position 13
Snake plot of human GPR35b. Arginine at position 13 of hGPR35b was mutated to proline, histidine, or cysteine

R13 'SPASM' Mutants for $G\alpha_{13}$ activation	R13 mutants for arrestin interaction
R13P in WT GPR35b	R13P in WT GPR35b
R13P in C27S GPR35b	R13P in C27S GPR35b
R13H in WT GPR35b	R13H in WT GPR35b
R13H in C27S GPR35b	R13H in C27S GPR35b
R13C in WT GPR35b	R13C in WT GPR35b
R13C in C27S GPR35b	R13C in C27S GPR35b

Table 3.21 List of arginine (R) (at position 13) mutants in the wild type and Cys27Ser backbone of hGPR35b
Arginine (at position 13) was mutated to proline, histidine, or cysteine in both wild type and the Cys27Ser backbone of hGPR35b for both arrestin-3 interaction and $G\alpha_{13}$ activation measurement.

3.2.4.1 Investigation of arrestin recruitment and G protein activation in various hGPR35b R13 mutants with human GPR35 partial agonist pamoic acid

Parental 293 cells were transfected transiently to co-express either hGPR35b (R13P C27S, R13H C27S and R13C C27S) (Figure 3.16A(i)) and hGPR35b (R13P WT, R13H WT and R13C WT) (Figure 3.16A(ii)) each tagged with eYFP and arrestin-3-RLuc. hGPR35a WT, hGPR35b WT and hGPR35b C27S tagged with eYFP were used as controls. After adding luciferase substrate and pamoic acid, there was a

concentration-dependent increase in measured BRET with pEC_{50} 7.15± 0.02 (mean± SEM, n=3 for hGPR35a WT) (Table 3.22). The measured BRET produced by hGPR35b WT was significantly (55.30%) lower with pEC_{50} 7.21± 0.01 (mean± SEM, n=3 for hGPR35b WT). However, using hGPR35b C27S resulted in a dramatic rise in signal, indicating better efficacy in response to pamoic acid than hGPR35b wild type version.

Among the new R13 mutants, R13P and R13H mutants at C27S backbone generated statistically comparable BRET signals to hGPR35a WT and hGPR35b C27S but R13C at C27S backbone generated lower BRET which was similar to hGPR35b WT but significantly different from hGPR35a WT (Emax, $p < 0.001$) (Figure 3.16A(i)) (Table 3.22). Among the new R13 mutants, R13P at wild type backbone demonstrated arrestin-3 recruitment activities that were comparable to signals produced by hGPR35a WT and hGPR35b C27S. However, other mutants R13H and R13C at wild type backbone generated lower BRET and can be compared to hGPR35b WT (Figure 3.16A(ii)) (Table 3.22).

For $G\alpha_{13}$ activation, hGPR35b (R13P C27S, R13H C27S and R13C C27S) (Figure 3.16B (i)) and hGPR35b (R13P WT, R13H WT and R13C WT) (Figure 3.16B(ii)) were transiently expressed in parental HEK293 cells as $G\alpha_{13}$ SPASM sensors. hGPR35a WT, hGPR35b WT and hGPR35b C27S were also expressed as $G\alpha_{13}$ SPASM sensors as controls. Following the addition of luciferase substrate and pamoic acid, a concentration-dependent increase in BRET was found with pEC_{50} 7.24± 0.01 (mean± SEM, n=3 for hGPR35a WT) (Table 3.23). Similar results to earlier studies were obtained when $G\alpha_{13}$ activation was carried out using the hGPR35b WT and hGPR35b C27S mutants.

Among the new R13 mutants, R13H mutant at C27S backbone generated statistically comparable BRET signals of $G\alpha_{13}$ activation to hGPR35a WT and hGPR35b C27S (Figure 3.16B(i)) (Table 3.23). While R13P at C27S backbone generated moderate signal R13C at C27S was without any significant effects and can be compared to hGPR35b WT (Figure 3.16B(i)) (Table 3.23). Upon consideration of the R13 mutants in wild type backbone, none of them were able to produce statistically significant signals upon stimulation with pamoic acid (Figure 3.16B(ii)) (Table 3.23).

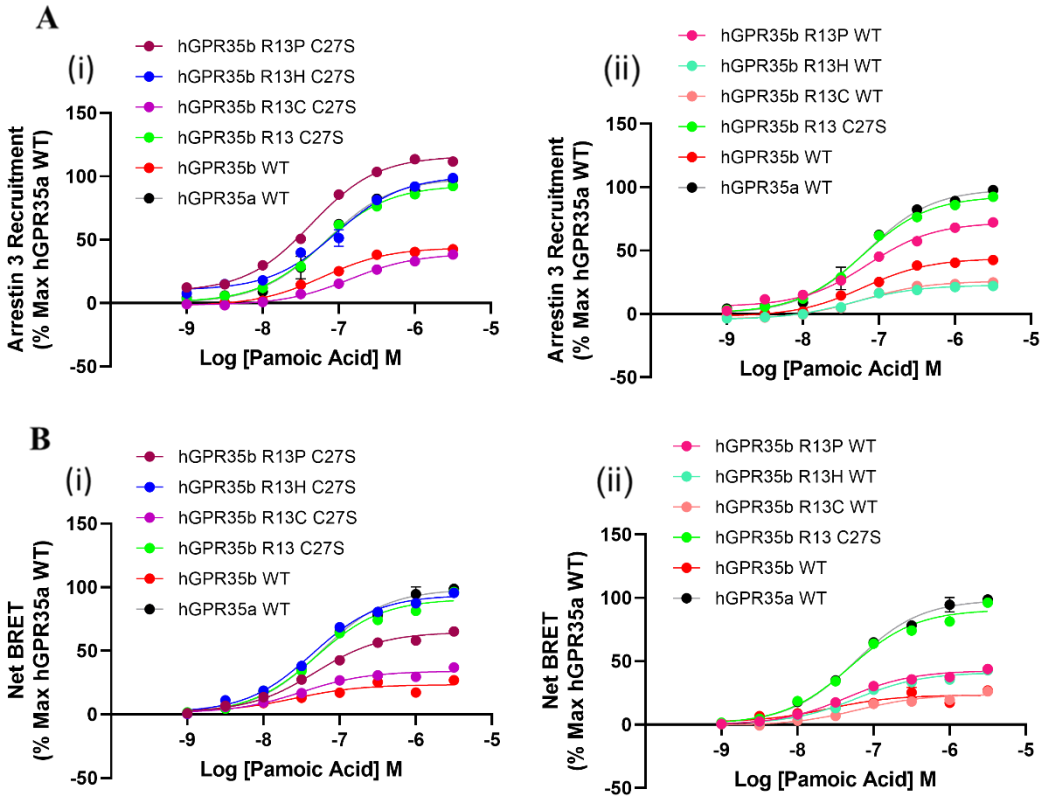

Figure 3.16 Demonstration and comparison of the arrestin-3 recruitment of hGPR35b R13 mutants (C27S and wild type backbone) and validation of the effectiveness of hGPR35b R13-Gα_{13} SPASM sensors (C27S and wild type backbone) using pamoic acid
(A) Parental HEK293 cells were transfected transiently to co-express either **(i)** hGPR35b R13P C27S (marron circles), hGPR35b R13H C27S (blue circles), hGPR35b R13C C27S (purple circles), **(ii)** hGPR35b R13P WT (pink circles), hGPR35b R13H WT (paste circles) and hGPR35b R13C WT (light red circles) each tagged with eYFP and arrestin-3-RLuc. **(B)** Comparison of the effects of **(i)** hGPR35b R13P C27S (marron circles), hGPR35b R13H C27S (blue circles), hGPR35b R13C C27S (purple circles), **(ii)** hGPR35b R13P WT (pink circles), hGPR35b R13H WT (paste circles) and hGPR35b R13C WT (light red circles) transiently expressed in parental HEK293 cells as Gα_{13} SPASM sensors. In both assays **(A)** and **(B)** hGPR35a WT (black circles), hGPR35b WT (red circles) and hGPR35b C27S (green circles) were used as control. BRET signals were monitored after treating with indicated concentrations of pamoic acid for 5 min. Each dataset represents the mean ± SEM of three independent experiments. Data were analysed by one-way ANOVA followed by Dunnett's multiple comparisons test and statistical results are shown in the following tables.

	hGPR 35b R13P C27S	**hGPR 35b R13H C27S**	**hGPR 35b R13C C27S**	**hGPR 35b R13P WT**	**hGPR 35b R13H WT**	**hGPR 35b R13C WT**	**hGPR 35b R13 C27S**	**hGPR 35b WT**	**hGPR 35a WT**
pEC_{50}	7.35±0.01 P<0.001 (***)	7.04±0.01 P<0.01 (**)	6.86±0.01 P<0.001 (***)	7.16±0.01 P=0.91 (ns)	7.33±0.02 P<0.001 (***)	7.21±0.02 P<0.05 (*)	7.21±0.01 P<0.05 (*)	7.21±0.01 P<0.05 (*)	7.15±0.02
$\%E_{max}$	116±0.15 P<0.001 (***)	100.3±0.10 P=0.039 (ns)	39.18±0.01 P<0.001 (***)	71.92±0.34 P<0.001 (***)	23.47±0.76 P<0.001 (***)	26.19±0.23 P<0.001 (***)	93.10±0.10 P<0.001 (***)	44.03 ±0.15 P<0.001 (***)	99.33±0.68

Table 3.22 Comparison of pEC_{50} and %Emax among hGPR35b R13 mutants (C27S and wild type backbone) in arrestin recruitment assays using pamoic acid
hGPR35a, hGPR35b and various hGPR35b R13 mutants (C27S and wild type backbone) were compared in terms of pEC_{50} and $\%E_{max}$ using BRET based arrestin recruitment assays. Results are expressed as mean ± SEM of three individual experiments. Data were analysed by one-way ANOVA followed by Dunnett's multiple comparisons test where the value for hGPR35a was used as control. ns = non-significant, * p<0.05, ** p<0.01, ***p<0.001.

	hGPR 35b R13P C27S	hGPR 35b R13H C27S	hGPR 35b R13C C27S	hGPR 35b R13P WT	hGPR 35b R13H WT	hGPR 35b R13C WT	hGPR 35b R13 C27S	hGPR 35b WT	hGPR 35a WT
pEC_{50}	7.34±0.02 P<0.01 (**)	7.35±0.01 P<0.01 (**)	7.51±0.01 P<0.001 (***)	7.37±0.01 P<0.001 (***)	7.23±0.01 P=0.94 (ns)	7.20±0.01 P=0.22 (ns)	7.30±0.01 P=0.08 (ns)	7.58±0.01 P<0.001 (***)	7.24±0.01
$\%E_{max}$	64.22± 0.52 P<0.001 (***)	94.17± 0.26 P<0.01 (**)	34.13± 0.09 P<0.001 (***)	42.63± 0.08 P<0.001 (***)	41.25± 0.03 P<0.001 (***)	24.42± 0.63 P<0.001 (***)	91.23± 0.47 P<0.001 (***)	23.85 ± 0.47 P<0.001 (***)	99.26± 0.74

Table 3.23 Comparison of pEC_{50} and %Emax among hGPR35b R13 mutants (C27S and wild type backbone) in G protein activation assays using pamoic acid
hGPR35a, hGPR35b and various hGPR35b R13 mutants (C27S and wild type backbone) were compared in terms of pEC_{50} and $\%E_{max}$ by BRET based G protein assays using GPR35-$G\alpha_{13}$ SPASM sensors. Results are expressed as mean ± SEM of three individual experiments. Data were analysed by one-way ANOVA followed by Dunnett's multiple comparisons test where the value for hGPR35a was used as control. ns = non-significant, * p<0.05, ** p<0.01, ***p<0.001.

3.2.4.2 Measurement of arrestin recruitment and G protein activation in various hGPR35b R13 mutants with GPR35 potent agonist GSK 938

Parental 293 cells were transfected transiently to co-express either hGPR35b (R13P C27S, R13H C27S and R13C C27S) (Figure 3.17A(i)) and hGPR35b (R13P WT, R13H WT and R13C WT) (Figure 3.17A(ii)) each tagged with eYFP and arrestin-3-RLuc. hGPR35a WT, hGPR35b WT and hGPR35b C27S tagged with eYFP were used as controls. There was a concentration-dependent increase in measured BRET with pEC_{50} 7.80± 0.01 (mean ± SEM, n=3 for hGPR35a WT) after stimulation with luciferase substrate and GPR35 agonist GSK 938 (Table 3.24). Comparable results to earlier studies were obtained with the hGPR35b WT and hGPR35b C27S mutant.

Among the new R13 mutants, R13P and R13H mutants at C27S backbone generated statistically comparable BRET signals to hGPR35a WT and hGPR35b C27S but R13C at C27S backbone generated lower BRET which was similar to hGPR35b WT but significantly different from hGPR35a WT (Emax, $p < 0.001$) (Figure 3.17A(i))

(Table 3.24). Among the new R13 mutants, R13P at wild type backbone, demonstrated arrestin-3 recruitment activities that were comparable to signals produced by hGPR35a WT and hGPR35b C27S. However, other mutants R13H and R13C at wild type backbone generated lower BRET and can be compared to hGPR35b WT (Figure 3.17A(ii)) (Table 3.24).

For $G\alpha_{13}$ activation, hGPR35b (R13P C27S, R13H C27S and R13C C27S) (Figure 3.17B(i)) and hGPR35b (R13P WT, R13H WT and R13C WT) (Figure 3.17B(ii) were transiently expressed in parental HEK293 cells as $G\alpha_{13}$ SPASM sensors. hGPR35a WT, hGPR35b WT and hGPR35b C27S were also expressed as $G\alpha_{13}$ SPASM sensors as controls. Following the addition of luciferase substrate and GSK 938, a concentration-dependent increase in BRET was found with pEC_{50} 8.19± 0.02 (mean± SEM, n=3 for hGPR35a WT) (Table 3.25). Similar results to earlier studies were obtained when $G\alpha_{13}$ activation was carried out using the hGPR35b WT and hGPR35b C27S mutants.

Among the new R13 mutants, R13H mutant at C27S backbone generated statistically comparable BRET signals of $G\alpha_{13}$ activation to hGPR35a WT and hGPR35b C27S (Figure 3.17B(i)) (Table 3.25). While R13P at C27S backbone generated moderate signal R13C at C27S was without any significant effects and can be compared to hGPR35b WT (Figure 3.17B(i)) (Table 3.25). None of the R13 mutants in the wild type backbone were able to produce remarkable signals in response to GSK 938 stimulation (Figure 3.17B(ii)) (Table 3.25).

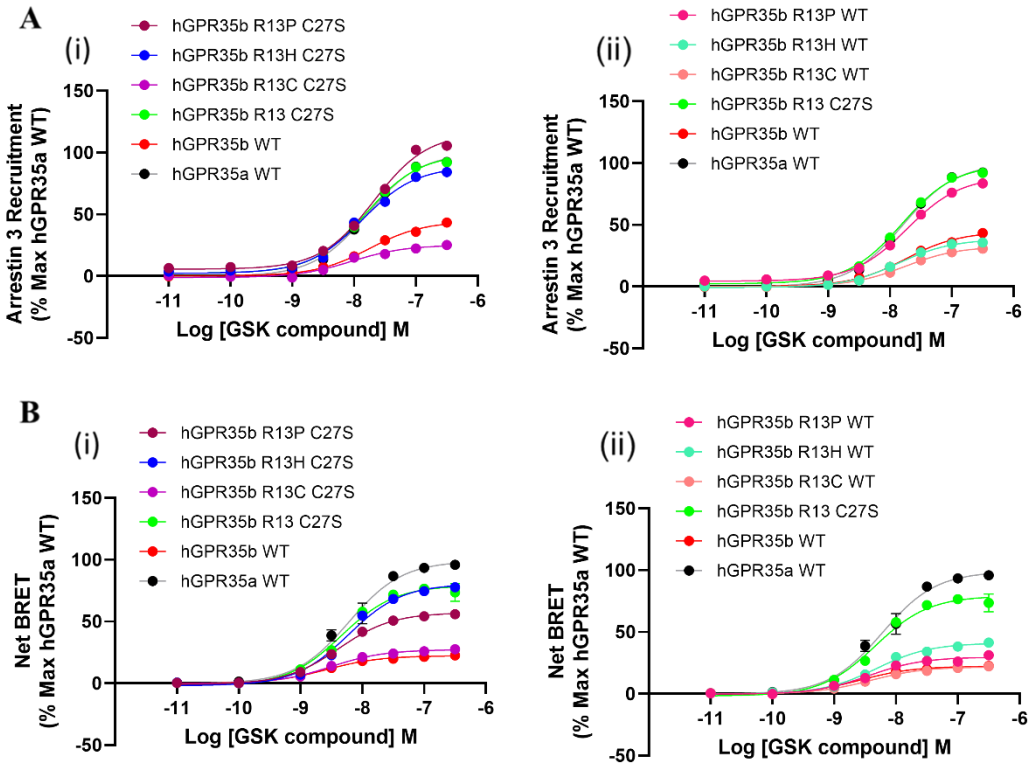

Figure 3.17 Demonstration and comparison of the arrestin-3 recruitment of hGPR35b R13 mutants (C27S and wild type backbone) and validation of the effectiveness of hGPR35b R13-Gα$_{13}$ SPASM sensors (C27S and wild type backbone) using GSK 938

(A) Parental HEK293 cells were transfected transiently to co-express either **(i)** hGPR35b R13P C27S (marron circles), hGPR35b R13H C27S (blue circles), hGPR35b R13C C27S (purple circles), **(ii)** hGPR35b R13P WT (pink circles), hGPR35b R13H WT (paste circles) and hGPR35b R13C WT (light red circles) each tagged with eYFP and arrestin-3-RLuc. **(B)** Comparison of the effects of **(i)** hGPR35b R13P C27S (marron circles), hGPR35b R13H C27S (blue circles), hGPR35b R13C C27S (purple circles), **(ii)** hGPR35b R13P WT (pink circles), hGPR35b R13H WT (paste circles) and hGPR35b R13C WT (light red circles) transiently expressed in parental HEK293 cells as Gα$_{13}$ SPASM sensors. In both assays **(A)** and **(B)** hGPR35a WT (black circles), hGPR35b WT (red circles) and hGPR35b C27S (green circles) were used as control. BRET signals were recorded after treating with indicated concentrations of GSK 938 for 5 min. Each dataset represents the mean ± SEM of three independent experiments. Data were analysed by one-way ANOVA followed by Dunnett's multiple comparisons test and statistical results are shown in the following tables.

	hGPR 35b R13P C27S	**hGPR 35b R13H C27S**	**hGPR 35b R13C C27S**	**hGPR 35b R13P WT**	**hGPR 35b R13H WT**	**hGPR 35b R13C WT**	**hGPR 35b R13 C27S**	**hGPR 35b WT**	**hGPR 35a WT**
pEC$_{50}$	7.68±0.01 P<0.001 (***)	7.86±0.01 P<0.05 (*)	8.03±0.01 P<0.001 (***)	7.72±0.01 P<0.01 (**)	7.87±0.01 P<0.01 (**)	7.77±0.01 P=0.09 (ns)	7.82±0.02 P=0.37 (ns)	7.76±0.01 P<0.05 (*)	7.80±0.01
%E$_{max}$	115.7±0.10 P<0.001 (***)	89.01±0.30 P<0.001 (***)	25.88±0.74 P<0.001 (***)	89.53±0.43 P<0.001 (***)	38.70±0.23 P<0.001 (***)	32.60±0.03 P<0.001 (***)	98.81±0.16 P=0.17 (ns)	44.67 ± 0.21 P<0.001 (***)	99.93±0.07

Table 3.24 Comparison of pEC$_{50}$ and %Emax among hGPR35b R13 mutants (C27S and wild type backbone) in arrestin recruitment assays using GSK 938

hGPR35a, hGPR35b and various hGPR35b R13 mutants (C27S and wild type backbone) were compared in terms of pEC_{50} and $\%E_{max}$ using BRET based arrestin recruitment assays. Results are expressed as mean ± SEM of three individual experiments. Data were analysed by one-way ANOVA followed by Dunnett's multiple comparisons test where the value for hGPR35a was used as control. ns = non-significant, * p<0.05, ** p<0.01, ***p<0.001.

	hGPR 35b R13P C27S	**hGPR 35b R13H C27S**	**hGPR 35b R13C C27S**	**hGPR 35b R13P WT**	**hGPR 35b R13H WT**	**hGPR 35b R13C WT**	**hGPR 35b R13 C27S**	**hGPR 35b WT**	**hGPR 35a WT**
pEC_{50}	8.38±0.01 P<0.01 (**)	8.23±0.01 P=0.75 (ns)	8.49±0.02 P<0.001 (***)	8.43±0.01 P<0.001 (***)	8.31±0.01 P<0.05 (*)	8.39±0.02 P<0.001 (***)	8.35±0.02 P<0.01 (**)	8.55±0.04 P<0.001 (***)	8.19±0.03
$\%E_{max}$	57.24± 0.09 P<0.001 (***)	80.55± 0.15 P<0.001 (***)	27.53± 0.29 P<0.001 (***)	29.86± 0.14 P<0.001 (***)	41.13± 0.09 P<0.001 (***)	21.93± 0.09 P<0.001 (***)	78.42± 0.78 P<0.001 (***)	22.59 ± 0.32 P<0.001 (***)	99.49± 0.52

Table 3.25 Comparison of pEC_{50} and %Emax among hGPR35b R13 mutants (C27S and wild type backbone) in G protein activation assays using GSK 938
hGPR35a, hGPR35b and various hGPR35b R13 mutants (C27S and wild type backbone) were compared in terms of pEC_{50} and $\%E_{max}$ by BRET based G protein assays using GPR35-$G\alpha_{13}$ SPASM sensors. Results are expressed as mean ± SEM of three individual experiments. Data were analysed by one-way ANOVA followed by Dunnett's multiple comparisons test where the value for hGPR35a was used as control. ns = non-significant, * p<0.05, ** p<0.01, ***p<0.001.

3.2.4.3 Investigation of arrestin recruitment and G protein activation in various hGPR35b R13 mutants with GPR35 agonist zaprinast

HEK 293 cells were transfected transiently to co-express either hGPR35b (R13P C27S, R13H C27S and R13C C27S) (Figure 3.18A(i)) and hGPR35b (R13P WT, R13H WT and R13C WT) (Figure 3.18A(ii)) each tagged with eYFP and arrestin-3-RLuc. hGPR35a WT, hGPR35b WT and hGPR35b C27S tagged with eYFP were used as controls. There was a concentration-dependent increase in measured BRET with pEC_{50} 5.26± 0.02 (mean± SEM, n=3 for hGPR35a WT) after stimulation with luciferase substrate and zaprinast (Table 3.26). There were similar outcomes to previous research when using the hGPR35b WT and hGPR35b C27S mutants.

Among the new R13 mutants, R13P and R13H mutants at C27S backbone generated statistically comparable BRET signals to hGPR35a WT and hGPR35b C27S but R13C at C27S backbone generated lower BRET which was similar to hGPR35b WT but significantly different from hGPR35a WT (Emax, $p < 0.001$) (Figure 3.18A(i)) (Table 3.26). Among the new R13 mutants, R13P at wild type backbone, demonstrated arrestin-3 recruitment activities that were comparable to signals produced by

hGPR35a WT and hGPR35b C27S. However, other mutants R13H and R13C at wild type backbone generated lower BRET and can be compared to hGPR35b WT (Figure 3.18A(ii)) (Table 3.26).

For $G\alpha_{13}$ activation, hGPR35b (R13P C27S, R13H C27S and R13C C27S) (Figure 3.18B(i)) and hGPR35b (R13P WT, R13H WT and R13C WT) (Figure 3.18B(ii)) were transiently expressed in parental HEK293 cells as $G\alpha_{13}$ SPASM sensors. hGPR35a WT, hGPR35b WT and hGPR35b C27S were also expressed as $G\alpha_{13}$ SPASM sensors as controls. Following the addition of luciferase substrate and zaprinast, a concentration-dependent increase in BRET was found with pEC_{50} 5.43± 0.01 (mean± SEM, n=3 for hGPR35a WT) (Table 3.27). Similar results to earlier studies were obtained when $G\alpha_{13}$ activation was carried out using the hGPR35b WT and hGPR35b C27S mutants.

Among the new R13 mutants, R13H mutant at C27S backbone generated statistically comparable BRET signals of $G\alpha_{13}$ activation to hGPR35a WT and hGPR35b C27S (Figure 3.18B(i)) (Table 3.27). While R13P at C27S backbone generated moderate signal R13C at C27S was without any significant effects and can be compared to hGPR35b WT (Figure 3.18B(i)) (Table 3.27). None of the R13 mutants in the wild type backbone were able to produce any discernible signals when stimulated with zaprinast (Figure 3.18B(ii)) (Table 3.27).

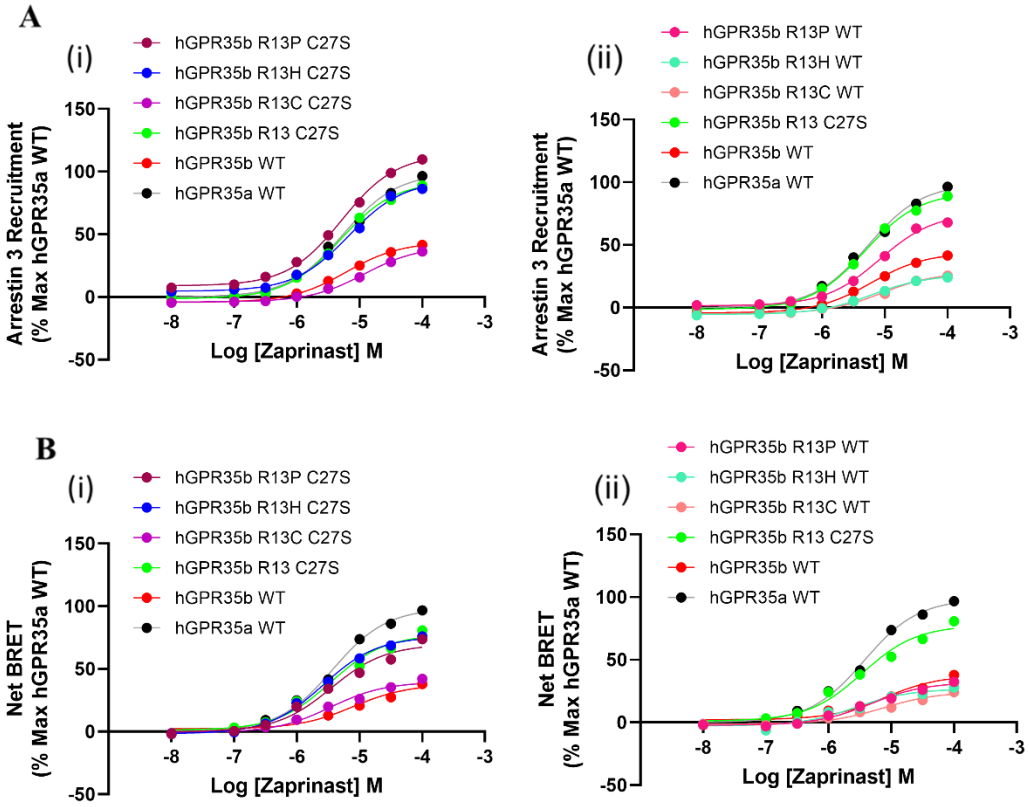

Figure 3.18 Demonstration and comparison of the arrestin-3 recruitment of hGPR35b R13 mutants (C27S and wild type backbone) and validation of the effectiveness of hGPR35b R13-Gα_{13} SPASM sensors (C27S and wild type backbone) using zaprinast
(A) Parental HEK293 cells were transfected transiently to co-express either **(i)** hGPR35b R13P C27S (marron circles), hGPR35b R13H C27S (blue circles), hGPR35b R13C C27S (purple circles), **(ii)** hGPR35b R13P WT (pink circles), hGPR35b R13H WT (paste circles) and hGPR35b R13C WT (light red circles) each tagged with eYFP and arrestin-3-RLuc. **(B)** Comparison of the effects of **(i)** hGPR35b R13P C27S (marron circles), hGPR35b R13H C27S (blue circles), hGPR35b R13C C27S (purple circles), **(ii)** hGPR35b R13P WT (pink circles), hGPR35b R13H WT (paste circles) and hGPR35b R13C WT (light red circles) transiently expressed in parental HEK293 cells as Gα_{13} SPASM sensors. In both assays **(A)** and **(B)** hGPR35a WT (black circles), hGPR35b WT (red circles) and hGPR35b C27S (green circles) were used as control. BRET signals were measured after treating with indicated concentrations of zaprinast for 5 min. Each dataset represents the mean ± SEM of three independent experiments. Data were analysed by one-way ANOVA followed by Dunnett's multiple comparisons test and statistical results are shown in the following tables.

	hGPR 35b R13P C27S	**hGPR 35b R13H C27S**	**hGPR 35b R13C C27S**	**hGPR 35b R13P WT**	**hGPR 35b R13H WT**	**hGPR 35b R13C WT**	**hGPR 35b R13 C27S**	**hGPR 35b WT**	**hGPR 35a WT**
pEC$_{50}$	5.30±0.01 P=0.37 (ns)	5.17±0.01 P<0.05 (*)	4.94±0.01 P<0.001 (***)	5.09±0.01 P<0.001 (***)	5.20±0.01 P=0.14 (ns)	5.01±0.04 P<0.001 (***)	5.32±0.01 P=0.10 (ns)	5.21±0.01 P=0.22 (ns)	5.26±0.02

%E_{max}	113.1± 0.80 P<0.001 (***)	93.05± 0.02 P<0.001 (***)	40.30± 0.28 P<0.001 (***)	75.58± 0.16 P<0.001 (***)	26.03± 0.06 P<0.001 (***)	28.91± 0.69 P<0.001 (***)	92.56± 0.39 P<0.001 (***)	44.08 ± 0.20 P<0.001 (***)	99.42± 0.59

Table 3.26 Comparison of pEC_{50} and %Emax among hGPR35b R13 mutants (C27S and wild type backbone) in arrestin recruitment assays using zaprinast
hGPR35a, hGPR35b and various hGPR35b R13 mutants (C27S and wild type backbone) were compared in terms of pEC_{50} and $\%E_{max}$ using BRET based arrestin recruitment assays. Results are expressed as mean ± SEM of three individual experiments. Data were analysed by one-way ANOVA followed by Dunnett's multiple comparisons test where the value for hGPR35a was used as control. ns = non-significant, * p<0.05, ** p<0.01, ***p<0.001.

	hGPR 35b R13P C27S	**hGPR 35b R13H C27S**	**hGPR 35b R13C C27S**	**hGPR 35b R13P WT**	**hGPR 35b R13H WT**	**hGPR 35b R13C WT**	**hGPR 35b R13 C27S**	**hGPR 35b WT**	**hGPR 35a WT**
pEC_{50}	5.46±0.01 P=0.12 (ns)	5.58±0.01 P<0.001 (***)	5.45±0.02 P=0.43 (ns)	5.32±0.01 P<0.001 (***)	5.56±0.01 P<0.001 (***)	5.12±0.01 P<0.001 (***)	5.46±0.01 P=0.12 (ns)	5.10±0.04 P<0.001 (***)	5.43±0.01
%E_{max}	69.81± 0.17 P<0.001 (***)	75.86± 0.03 P<0.001 (***)	40.24± 0.54 P<0.001 (***)	32.02± 0.01 P<0.001 (***)	26.91± 0.15 P<0.001 (***)	24.52± 0.14 P<0.001 (***)	78.11± 0.60 P<0.001 (***)	37.91 ± 0.24 P<0.001 (***)	99.34± 0.67

Table 3.27 Comparison of pEC_{50} and %Emax among hGPR35b R13 mutants (C27S and wild type backbone) in G protein activation assays using zaprinast
hGPR35a, hGPR35b and various hGPR35b R13 mutants (C27S and wild type backbone) were compared in terms of pEC_{50} and $\%E_{max}$ by BRET based G protein assays using GPR35-$G\alpha_{13}$ SPASM sensors. Results are expressed as mean ± SEM of three individual experiments. Data were analysed by one-way ANOVA followed by Dunnett's multiple comparisons test where the value for hGPR35a was used as control. ns = non-significant, * p<0.05, ** p<0.01, ***p<0.001.

3.2.4.4 Investigation of G protein activation in various hGPR35b R13 mutants with human GPR35 potent agonist lodoxamide

For $G\alpha_{13}$ activation, hGPR35b (R13P C27S, R13H C27S and R13C C27S) (Figure 3.19(i)) and hGPR35b (R13P WT, R13H WT and R13C WT) (Figure 3.19(ii)) were transiently expressed in parental HEK293 cells as $G\alpha_{13}$ SPASM sensors. hGPR35a WT, hGPR35b WT and hGPR35b C27S were also expressed as $G\alpha_{13}$ SPASM sensors as controls. Following the addition of luciferase substrate and lodoxamide, a concentration-dependent increase in BRET was found with pEC_{50} 8.43± 0.01 (mean± SEM, n=3 for hGPR35a WT) (Table 3.28). Similar outcomes to previous experiments were achieved when $G\alpha_{13}$ activation was carried out using the hGPR35b WT and hGPR35b C27S mutants.

Among the new R13 mutants, R13H mutant at C27S backbone generated statistically comparable BRET signals of $G\alpha_{13}$ activation to hGPR35a WT and hGPR35b C27S (Figure 3.19(i)) (Table 3.28). While R13P at C27S backbone generated moderate signal but R13C at C27S was without any significant effects and can be compared to hGPR35b WT (Figure 3.19(i)) (Table 3.28). None of the R13 mutants in the wild type backbone were able to generate any recognisable signals when stimulated with lodoxamide (Figure 3.19(ii)) (Table 3.28).

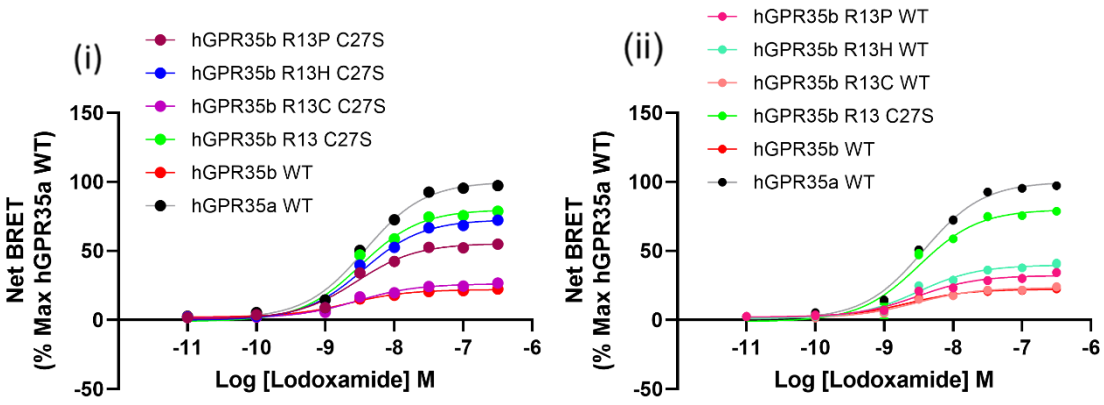

Figure 3.19 Demonstration of the effectiveness of hGPR35b R13-$G\alpha_{13}$ SPASM sensors (C27S and wild type backbone) using GPR35 reference ligand lodoxamide
Comparison of the effects of **(i)** hGPR35b R13P C27S (marron circles), hGPR35b R13H C27S (blue circles), hGPR35b R13C C27S (purple circles), **(ii)** hGPR35b R13P WT (pink circles), hGPR35b R13H WT (paste circles) and hGPR35b R13C WT (light red circles) transiently expressed in parental HEK293 cells as $G\alpha_{13}$ SPASM sensors. In both **(i)** and **(ii)** hGPR35a WT (black circles), hGPR35b WT (red circles) and hGPR35b C27S (green circles) were used as control. BRET signals were measured after treating with indicated concentrations of lodoxamide for 5 min. Each dataset represents the mean ± SEM of three independent experiments. Data were analysed by one-way ANOVA followed by Dunnett's multiple comparisons test and statistical results are shown in the following table.

	hGPR 35b R13P C27S	**hGPR 35b R13H C27S**	**hGPR 35b R13C C27S**	**hGPR 35b R13P WT**	**hGPR 35b R13H WT**	**hGPR 35b R13C WT**	**hGPR 35b R13 C27S**	**hGPR 35b WT**	**hGPR 35a WT**
pEC_{50}	8.55±0.01 P<0.001 (***)	8.45±0.01 P=0.06 (ns)	8.54±0.01 P<0.001 (***)	8.52±0.01 P<0.001 (***)	8.50±0.01 P<0.001 (***)	8.54±0.01 P<0.001 (***)	8.50±0.01 P<0.001 (***)	8.66±0.01 P<0.001 (***)	8.43±0.01
$\%E_{max}$	55.68± 0.23 P<0.001 (***)	72.89± 0.21 P<0.001 (***)	26.41± 0.25 P<0.001 (***)	32.28± 0.03 P<0.001 (***)	39.94± 0.12 P<0.001 (***)	23.41± 0.12 P<0.001 (***)	80.11± 0.05 P<0.001 (***)	22.45 ± 0.19 P<0.001 (***)	100.2± 0.65

Table 3.28 Comparison of pEC_{50} and %Emax among hGPR35b R13 mutants (C27S and wild type backbone) in G protein activation assays using lodoxamide
hGPR35a, hGPR35b and various hGPR35b R13 mutants (C27S and wild type backbone) were compared in terms of pEC_{50} and $\%E_{max}$ by BRET based G protein assays using GPR35-$G\alpha_{13}$ SPASM

sensors. Results are expressed as mean ± SEM of three individual experiments. Data were analysed by one-way ANOVA followed by Dunnett's multiple comparisons test where the value for hGPR35a was used as control. ns = non-significant, * p<0.05, ** p<0.01, ***p<0.001.

3.2.4.5 Investigation of G protein activation in various hGPR35b R13 mutants with GPR35 agonist PSB-13253 and cromolyn

For $G\alpha_{13}$ activation, hGPR35b (R13P C27S, R13H C27S and R13C C27S) (Figure 3.20A, B(i)) and hGPR35b (R13P WT, R13H WT and R13C WT) (Figure 3.20A, B(ii)) were transiently expressed in parental HEK293 cells as $G\alpha_{13}$ SPASM sensors. hGPR35a WT, hGPR35b WT and hGPR35b C27S were also expressed as $G\alpha_{13}$ SPASM sensors as controls. After addition of luciferase substrate and PSB-13253 and cromolyn, a concentration-dependent increase in BRET was found with PSB-13253, pEC_{50} 8.06± 0.01 (mean± SEM, n=3 for hGPR35a WT) (Table 3.29) and with cromolyn, pEC_{50} 5.52± 0.01 (mean± SEM, n=3 for hGPR35a WT) (Table 3.30). Similar results to earlier studies were obtained when $G\alpha_{13}$ activation was carried out using the hGPR35b WT and hGPR35b C27S mutants.

Among the new R13 mutants, R13H mutant at C27S backbone generated statistically comparable BRET signals of $G\alpha_{13}$ activation to hGPR35a WT and hGPR35b C27S (Figure 3.20A, B(i)) (Table 3.29) (Table 3.30). While R13P at C27S backbone generated moderate signal but R13C at C27S was without any significant effects and can be compared to hGPR35b WT (Figure 3.20A, B(i)) (Table 3.29) (Table 3.30). None of the R13 mutants in the wild type backbone were able to generate any discernible signals when stimulated with PSB-13253 and cromolyn (Figure 3.20A, B(ii)) (Table 3.29) (Table 3.30).

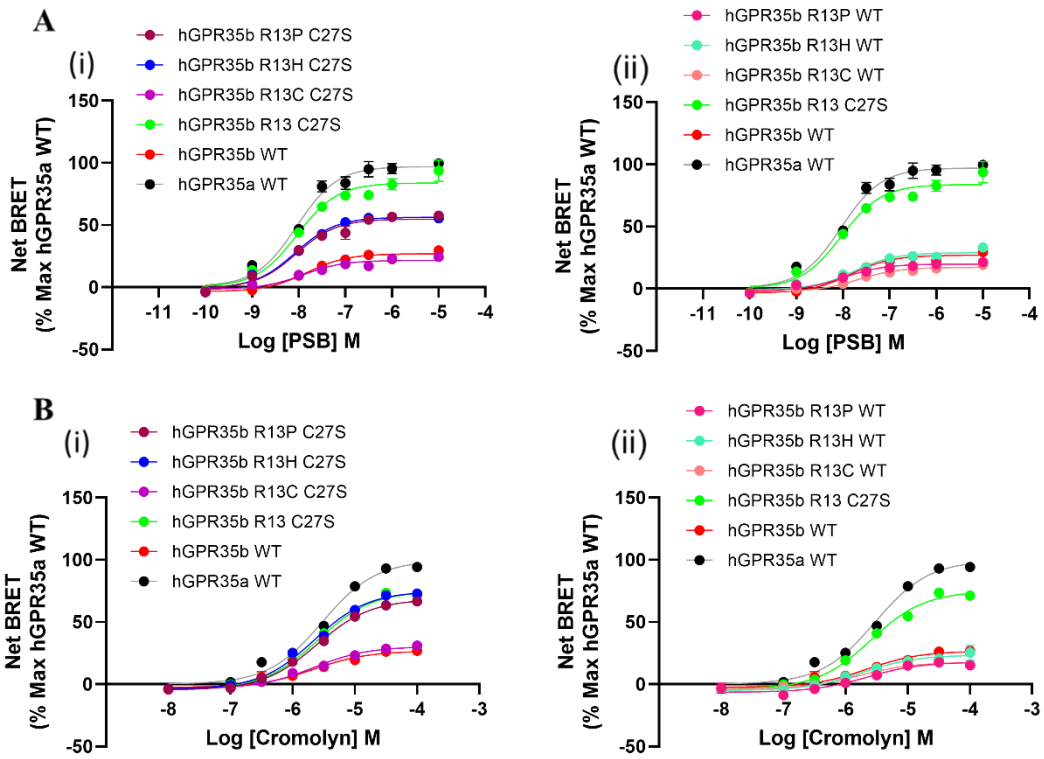

Figure 3.20 Validation of the effectiveness of hGPR35b R13-Gα$_{13}$ SPASM sensors (C27S and wild type backbone) using PSB-13253 and cromolyn
Comparison of the effects of **(i)** hGPR35b R13P C27S (marron circles), hGPR35b R13H C27S (blue circles), hGPR35b R13C C27S (purple circles), **(ii)** hGPR35b R13P WT (pink circles), hGPR35b R13H WT (paste circles) and hGPR35b R13C WT (light red circles) transiently expressed in parental HEK293 cells as Gα$_{13}$ SPASM sensors. In both **(i)** and **(ii)** hGPR35a WT (black circles), hGPR35b WT (red circles) and hGPR35b C27S (green circles) were used as control. BRET signals were monitored after treating with indicated concentrations of **(A)** PSB-13253 and **(B)** cromolyn for 5 min. Each dataset represents the mean ± SEM of three separate studies. Data were analysed by one-way ANOVA followed by Dunnett's multiple comparisons test and statistical results are shown in the following tables.

	hGPR 35b R13P C27S	**hGPR 35b R13H C27S**	**hGPR 35b R13C C27S**	**hGPR 35b R13P WT**	**hGPR 35b R13H WT**	**hGPR 35b R13C WT**	**hGPR 35b R13 C27S**	**hGPR 35b WT**	**hGPR 35a WT**
pEC$_{50}$	8.06±0.01 P>0.99 (ns)	8.07±0.01 P>0.99 (ns)	7.91±0.01 P=0.49 (ns)	7.99±0.01 P=0.96 (ns)	7.78±0.01 P=0.05 (ns)	7.68±0.01 P<0.05 (*)	8.02±0.02 P=0.99 (ns)	8.01±0.18 P=0.99 (ns)	8.06±0.01
%E$_{max}$	54.91± 0.02 P<0.001 (***)	56.33± 0.05 P<0.001 (***)	21.82± 0.14 P<0.001 (***)	19.96± 0.09 P<0.001 (***)	29.18± 0.21 P<0.001 (***)	17.00± 0.23 P<0.001 (***)	84.31± 0.42 P<0.001 (***)	24.61 ± 2.36 P<0.001 (***)	98.54± 1.47

Table 3.29 Comparison of pEC$_{50}$ and %Emax among hGPR35b R13 mutants (C27S and wild type backbone) in G protein activation assays using PSB 13253
hGPR35a, hGPR35b and various hGPR35b R13 mutants (C27S and wild type backbone) were compared in terms of pEC$_{50}$ and %E$_{max}$ by BRET based G protein assays using GPR35-Gα$_{13}$ SPASM sensors. Results are expressed as mean ± SEM of three individual experiments. Data were analysed by one-way ANOVA followed by Dunnett's multiple comparisons test where the value for hGPR35a was used as control. ns = non-significant, * p<0.05, ** p<0.01, ***p<0.001.

	hGPR 35b R13P C27S	hGPR 35b R13H C27S	hGPR 35b R13C C27S	hGPR 35b R13P WT	hGPR 35b R13H WT	hGPR 35b R13C WT	hGPR 35b R13 C27S	hGPR 35b WT	hGPR 35a WT
pEC_{50}	5.62±0.01 P=0.17 (ns)	5.66±0.01 P<0.05 (*)	5.65±0.01 P<0.05 (*)	5.65±0.01 P<0.05 (*)	5.69±0.05 P<0.01 (**)	5.74±0.04 P<0.01 (**)	5.60±0.01 P=0.26 (ns)	5.60±0.01 P=0.26 (ns)	5.52±0.01
$\%E_{max}$	68.64± 0.22 P<0.001 (***)	74.90± 0.01 P<0.001 (***)	30.42± 0.08 P<0.001 (***)	18.22± 0.35 P<0.001 (***)	23.78± 0.25 P<0.001 (***)	18.06± 0.35 P<0.001 (***)	75.39± 0.43 P<0.001 (***)	27.42 ± 0.65 P<0.001 (***)	99.86± 0.14

Table 3.30 Comparison of pEC_{50} and %Emax among hGPR35b R13 mutants (C27S and wild type backbone) in G protein activation assays using cromolyn
hGPR35a, hGPR35b and various hGPR35b R13 mutants (C27S and wild type backbone) were compared in terms of pEC_{50} and $\%E_{max}$ by BRET based G protein assays using GPR35-$G\alpha_{13}$ SPASM sensors. Results are expressed as mean ± SEM of three individual experiments. Data were analysed by one-way ANOVA followed by Dunnett's multiple comparisons test where the value for hGPR35a was used as control. ns = non-significant, * p<0.05, ** p<0.01, ***p<0.001.

3.2.4.6 Measurement of G protein activation in various hGPR35b R13 mutants with GPR35 agonist amlexanox and doxantrazole

For $G\alpha_{13}$ activation, hGPR35b (R13P C27S, R13H C27S and R13C C27S) (Figure 3.21A, B(i)) and hGPR35b (R13P WT, R13H WT and R13C WT) (Figure 3.21A, B(ii)) were transiently expressed in parental HEK293 cells as $G\alpha_{13}$ SPASM sensors. hGPR35a WT, hGPR35b WT and hGPR35b C27S were also expressed as $G\alpha_{13}$ SPASM sensors as controls. Following addition of luciferase substrate and amlexanox and doxantrazole, a concentration-dependent increase in BRET was found with amlexanox, pEC_{50} 5.28± 0.03 (mean± SEM, n=3 for hGPR35a WT) (Table 3.31) and with doxantrazole, pEC_{50} 5.23± 0.01 (mean± SEM, n=3 for hGPR35a WT) (Table 3.32). Similar results to earlier studies were obtained when $G\alpha_{13}$ activation was carried out using the hGPR35b WT and hGPR35b C27S mutants.

Among the new R13 mutants, R13H mutant at C27S backbone generated statistically comparable BRET signals of $G\alpha_{13}$ activation to hGPR35a WT and hGPR35b C27S (Figure 3.21A, B(i)) (Table 3.31) (Table 3.32). While R13P at C27S backbone generated moderate signal but R13C at C27S was without any significant effects and can be compared to hGPR35b WT (Figure 3.21A, B(i)) (Table 3.31) (Table 3.32). None of the R13 mutants in the wild type backbone were able to

generate any discernible signals when stimulated with amlexanox and doxantrazole (Figure 3.21A, B(ii)) (Table 3.31) (Table 3.32).

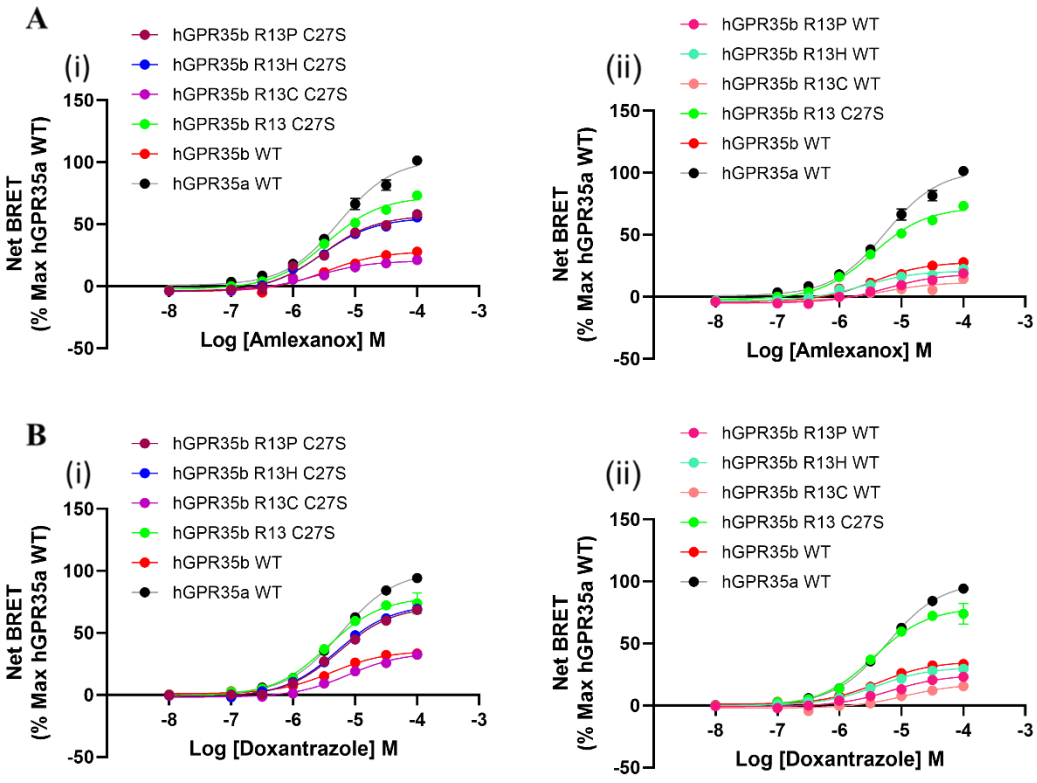

Figure 3.21 Demonstration of the effectiveness of hGPR35b R13-Gα_{13} SPASM sensors (C27S and wild type backbone) using amlexanox and doxantrazole
Comparison of the effects of **(i)** hGPR35b R13P C27S (marron circles), hGPR35b R13H C27S (blue circles), hGPR35b R13C C27S (purple circles), **(ii)** hGPR35b R13P WT (pink circles), hGPR35b R13H WT (paste circles) and hGPR35b R13C WT (light red circles) transiently expressed in parental HEK293 cells as Gα_{13} SPASM sensors. In both **(i)** and **(ii)** hGPR35a WT (black circles), hGPR35b WT (red circles) and hGPR35b C27S (green circles) were used as control. BRET signals were recorded after treating with indicated concentrations of **(A)** amlexanox and **(B)** doxantrazole for 5 min. Each dataset represents the mean ± SEM of three independent experiments. Data were analysed by one-way ANOVA followed by Dunnett's multiple comparisons test and statistical results are shown in the following tables.

	hGPR 35b R13P C27S	**hGPR 35b R13H C27S**	**hGPR 35b R13C C27S**	**hGPR 35b R13P WT**	**hGPR 35b R13H WT**	**hGPR 35b R13C WT**	**hGPR 35b R13 C27S**	**hGPR 35b WT**	**hGPR 35a WT**
pEC_{50}	5.52±0.01 P<0.01 (**)	5.54±0.01 P<0.001 (***)	5.60±0.02 P<0.001 (***)	5.22±0.01 P=0.46 (ns)	5.66±0.05 P<0.001 (***)	5.26±0.04 P=0.97 (ns)	5.46±0.01 P<0.05 (*)	5.44±0.03 P<0.05 (*)	5.28±0.03
$\%E_{max}$	57.89± 0.57 P<0.001 (***)	55.31± 0.02 P<0.001 (***)	20.62± 0.01 P<0.001 (***)	18.90± 0.19 P<0.001 (***)	20.97± 0.08 P<0.001 (***)	12.06± 0.26 P<0.001 (***)	71.99± 0.29 P<0.001 (***)	28.66 ± 0.52 P<0.001 (***)	101.2± 1.2

Table 3.31 Comparison of pEC_{50} and %Emax among hGPR35b R13 mutants (C27S and wild type backbone) in G protein activation assays using amlexanox
hGPR35a, hGPR35b and various hGPR35b R13 mutants (C27S and wild type backbone) were compared in terms of pEC_{50} and $\%E_{max}$ by BRET based G protein assays using GPR35-$G\alpha_{13}$ SPASM sensors. Results are expressed as mean ± SEM of three individual experiments. Data were analysed by one-way ANOVA followed by Dunnett's multiple comparisons test where the value for hGPR35a was used as control. ns = non-significant, * p<0.05, ** p<0.01, ***p<0.001.

	hGPR 35b R13P C27S	hGPR 35b R13H C27S	hGPR 35b R13C C27S	hGPR 35b R13P WT	hGPR 35b R13H WT	hGPR 35b R13C WT	hGPR 35b R13 C27S	hGPR 35b WT	hGPR 35a WT
pEC_{50}	5.26±0.01 P=0.84 (ns)	5.28±0.01 P=0.34 (ns)	5.08±0.03 P<0.01 (**)	5.14±0.04 P<0.05 (*)	5.39±0.01 P<0.001 (***)	4.96±0.01 P<0.001 (***)	5.47±0.02 P<0.001 (***)	5.37±0.01 P<0.01 (**)	5.23±0.01
$\%E_{max}$	72.03± 0.52 P<0.001 (***)	72.51± 0.39 P<0.001 (***)	34.62± 0.34 P<0.001 (***)	25.33± 0.66 P<0.001 (***)	31.63± 0.66 P<0.001 (***)	17.47± 0.07 P<0.001 (***)	77.26± 1.71 P<0.001 (***)	35.88 ± 0.32 P<0.001 (***)	99.92± 0.09

Table 3.32 Comparison of pEC_{50} and %Emax among hGPR35b R13 mutants (C27S and wild type backbone) in G protein activation assays using doxantrazole
hGPR35a, hGPR35b and various hGPR35b R13 mutants (C27S and wild type backbone) were compared in terms of pEC_{50} and $\%E_{max}$ by BRET based G protein assays using GPR35-$G\alpha_{13}$ SPASM sensors. Results are expressed as mean ± SEM of three individual experiments. Data were analysed by one-way ANOVA followed by Dunnett's multiple comparisons test where the value for hGPR35a was used as control. ns = non-significant, * p<0.05, ** p<0.01, ***p<0.001.

3.2.5 Expression pattern of hGPR35 (wild type and mutants) and fluorescent protein expression

From the results reported in section 3.2.2, it was clear that hGPR35a generates substantially greater efficacy in response to agonists than hGPR35b in both G protein activation and arrestin recruitment. To investigate whether these differences were due to variation in expression after transient transfection into parental 293 cells, I measured the total expression of both isoforms of hGPR35 along with several mutants of the receptor. The experimental results demonstrated that there were no significant variations ($p>0.05$, one way ANOVA followed by Dunnett's multiple comparison test) in total mCitrine expression across the various forms of the mCitrine tagged SPASM receptor constructs in G protein-based study (Figure 3.22A) except for the hGPR35b C27S S15C mutant which displayed significantly ($p=0.048$) higher expression levels compared to hGPR35a wild type version. In the case of arrestin interaction assays with the receptor (with mutants), the total enhanced yellow fluorescent protein (eYFP) was measured. Once again, analysis showed that the expression levels of various

eYFP tagged receptor mutants were not statistically different from that of eYFP tagged hGPR35a wild type version ($p>0.05$, one way ANOVA followed by Dunnett's multiple comparison test)(Figure 3.22B).

When the expression of fluorescent proteins was visualised with fluorescent microscopy, I noticed that both hGPR35a (Figure 3.23A) and hGPR35b (Figure 3.23B) were expressed after transient transfection in parental 293 cells, although at this moment, I did not quantify this.

From the results of the section 3.2.5, it was proven that there were statistically similar amounts of total mCitrine expression and total (eYFP) expression for both isoforms of the receptor along with various mutants. These findings eliminated the possibility that the low efficacy of agonist responses at the hGPR35b compared to hGPR35a reflected differences in expression. Rather, the potential additional disulphide bond might be key in this issue. Molecular modelling and, possibly, data from atomic level structures are absolutely necessary for thoroughly understanding this matter.

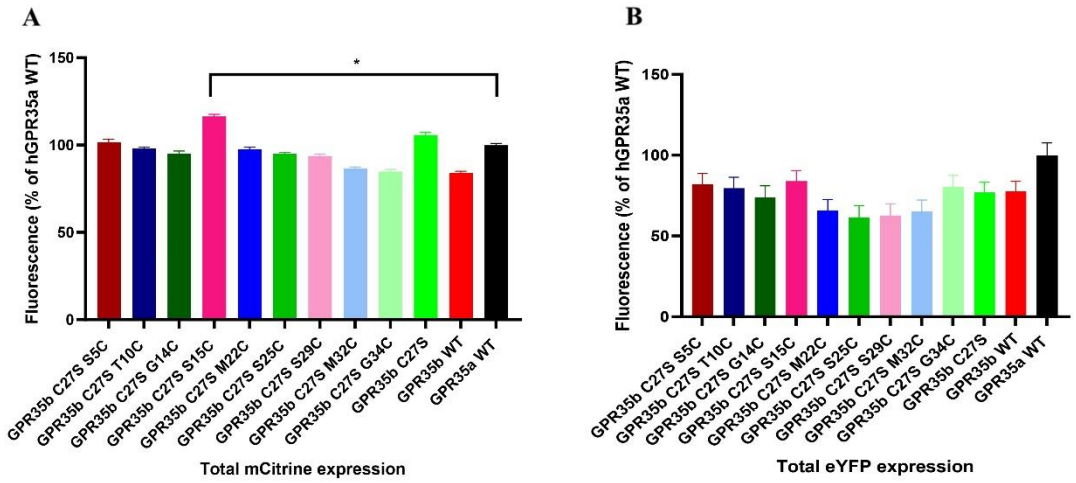

Figure 3.22 Comparison of the expression levels of different mutants of hGPR35b compared to wild type isoforms of hGPR35
(A) Total mCitrine expression of all the mutants as well as comparison with the wild type controls (SPASM sensors), **(B)** Relative expression levels of eYFP -tagged mutants and wild type receptor.

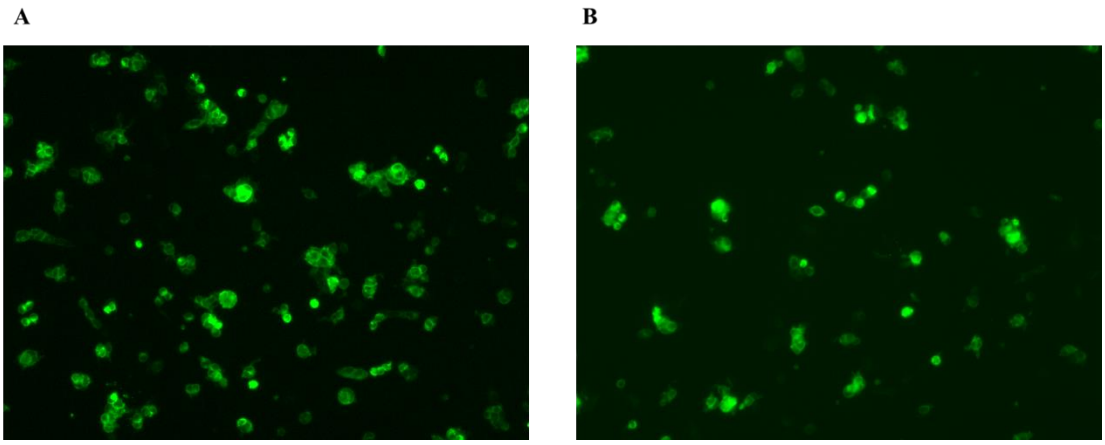

Figure 3.23 Detection of GPR35-eYFP form of hGPR35, expression with fluorescent microscope
eYFP tagged form of **(A)** hGPR35a and **(B)** hGPR35b after transient transfection in parental 293 cells.

3.3 Discussion

GPCRs are the largest and most studied group of transmembrane polypeptides which are also the most tractable group of proteins for the development of small molecule therapeutics (Grigoriadis et al., 2009, Lundstrom, 2009). GPR35 is still classified as an 'orphan receptor' despite being discovered more than 20 years ago and nominally characterised in 2006 as a receptor for the tryptophan metabolite kynurenic acid (Milligan, 2023). Research on the type of endogenous ligand(s) that activate GPR35 is still quite active. GPR35, an open reading frame corresponding to a 309 amino acid polypeptide on chromosome 2, was originally discovered in human genomic DNA (O'Dowd et al., 1998). There seems to be a different variant of GPR35 with an extended N-terminal sequence, and it has been reported that GPR35 expression in NIH3T3 cells exhibits transforming activity, which is consistent with suggestions that GPR35 may be involved in gastric malignancies (Okumura et al., 2004). The original 309 amino acid containing polypeptide is commonly known as hGPR35a or ("GPR35 short") while the 31 amino acid extended form is familiar as hGPR35b or ("GPR35 long"). The two isoforms were similar in $G\alpha_{13}$ activation and arrestin-3 signalling, although the maximal signal intensity generated by the longer isoform was markedly lower. However, the potency of the agonist ligand remained comparable along the two isoforms (Marti-Solano et al., 2020). However, a recent report claimed the differences in the ability of the long and short isoforms to mediate interactions with G proteins versus arrestin-3 (Schihada et al., 2022). As a result, despite the fact that the

hGPR35b isoform has received relatively less attention, there are obvious discrepancies in descriptions of their functions that need to be resolved.

Upon considering the sequences of the two isoforms of hGPR35, it was found that compared to hGPR35a, hGPR35b has the capacity to produce one additional extracellular disulphide bond. However, a thorough investigation of this possibility—or any potential consequences—has not yet been made. In order to completely examine the pharmacology and function of two human GPR35 isoforms, site-directed mutagenesis was used and the interactions of these isoforms with G proteins and arrestins were then discovered.

In my studies, I found that there was a considerable difference in agonist efficacy between the longer form to shorter counterparts (longer isoform is about 70% less efficient), although their pharmacology is almost similar. As the amino acid cysteine is responsible for disulphide bond formation, initially mutagenesis was done on specific cysteine residues of both isoforms to understand the putative role played by the disulphide bonds in hGPR35. Cysteine at position 8 in the N-terminus of hGPR35a presumably forms a disulphide bond with cysteine 248 of extracellular loop 3, as changing either of these residues to serine almost completely removed the agonist role in arrestin-3 recruitment and $G\alpha_{13}$ activation. In hGPR35b, along with hGPR35a equivalent disulphide bond between the cysteine at position 39 and 279, there is an additional disulphide bond between cysteine at position 27 and 279. It was evident from my results that, mutation of the hGPR35a equivalent cysteine residues in hGPR35b (hGPR35b C39S, hGPR35b C279S) also greatly reduced agonist function in arrestin-3 recruitment and $G\alpha_{13}$ activation. However, mutation of the hGPR35b specific cysteine residue at position 27 resulted in significantly increased agonist function (arrestin recruitment and G protein activity), indicating that hGPR35b agonist-induced activation is constrained by a second disulphide bond. From the whole set of experiments, it was clear and straightforward that cysteine at position 27 of N-terminal domain of hGPR35b acted as a dampener of hGPR35b efficacy. Mutation of this cysteine to serine resulted in the efficacy of hGPR35b now being equivalent to hGPR35a.

To learn more about the function of the hGPR35b N-terminal extension, nine more mutants with cysteine in place of different residues in the Cys27Ser hGPR35b backbone were created. After generation of the additional nine mutants in

different positions of N-terminal extension of hGPR35b, I employed a series of ligands that are agonists or partial agonists of human GPR35 for measuring arrestin-3 interaction with the receptor and also activating G protein $G\alpha_{13}$. After conducting both arrestin and G protein-based experiments with different ligands (in total 8), it was evident that all the new mutants demonstrated arrestin-3 recruitment potential and $G\alpha_{13}$ activation almost similar in extent that was demonstrated by hGPR35b WT. None of the new mutants were able to produce a higher response (arrestin-3 or $G\alpha_{13}$) than hGPR35a WT or hGPR35b C27S. The creation of additional disulphide bonds from various sites of the hGPR35b N-terminal domain to extracellular loop 3 might be the most likely cause of this. To completely comprehend the significance of the organisation of the N-terminal domain of hGPR35b, molecular modelling and maybe knowledge from atomic level structures are very necessary.

Very recently, several studies have linked arginine polymorphisms in hGPR35b to improved cancer survival. According to data from the UK Biobank, people with R13H or R13P polymorphisms had better survival for GI-associated diseases such as pancreatic cancer and liver cancer than those who have arginine (R) at position 13. So, I generated some additional mutants in wild type (WT) and C27S backbone of the hGPR35b. Therefore, in the first case, I changed the arginine (R) at position 13 in both the wild type and C27S backbone of hGPR35b to proline (P), histidine (H), and cysteine (C). Following the confirmation of the mutants through sequencing, I evaluated the impact of the mutants on the activation of the G protein $G\alpha_{13}$ and the recruitment of arrestin-3 by using a number of GPR35 agonists. After carrying out arrestin and G protein-based experimental studies, it was found that R13P and R13H mutants at C27S backbone generated statistically comparable BRET signals (arrestin-3 recruitment) like hGPR35a WT and hGPR35b C27S, but R13C at C27S backbone generated lower BRET that was similar to hGPR35b WT. Among the R13 mutants, R13P at wild type backbone showed a moderate increase in BRET (arrestin-3 recruitment) in comparison to signals produced by hGPR35a WT and hGPR35b C27S. However, other mutants R13H and R13C at wild type backbone generated lower BRET signals and can be compared to hGPR35b WT. In the G protein activation assay with GPR35- $G\alpha_{13}$ SPASM sensors, R13H mutant at C27S backbone generated statistically comparable BRET signals ($G\alpha_{13}$ activation) to hGPR35a WT and hGPR35b C27S. While R13P at C27S backbone generated moderate signal R13C at C27S was without any significant effects and

can be compared to hGPR35b WT. None of the R13 mutations in the wild type backbone were able to generate any discernible signals of $G\alpha_{13}$ activation.

The entire series of results clearly demonstrate that R13P and R13H polymorphic mutants (C27S and wild type backbone) generated comparable signal intensity (BRET) like hGPR35a WT and hGPR35b C27S mutants in arrestin recruitment assays. This finding may support the hypothesis (although not fully clear) of better survival of patients with GI-associated diseases with R13P and R13H polymorphic variants. The other mutant R13C acted like hGPR35b WT in arrestin-3 recruitment. The formation of additional disulphide bonds from the R13 site of hGPR35b N-terminal domain to extracellular loop 3 might be the most likely reason for this.

In the case of G protein activation, the R13H mutant at the C27S backbone produced a similar signal to hGPR35a WT and hGPR35b C27S mutants. R13P (C27S backbone) also generated moderate intensity of signal while R13C (C27S backbone) was without any effects and acted like hGPR35b WT. In the wild type of backbone, none of the R13 mutants were able to produce any observable signs of $G\alpha_{13}$ activation.

From the whole series of experiments (arrestin based assay and G protein activation) with R13P, R13H and R13P, it can be stated that R13P and R13H polymorphic mutants may help pancreatic cancer and liver cancer patients with extended life span. However, further in-depth study of these polymorphic variants is warranted before concluding a remark.

I also investigated the expression pattern of human GPR35 (wild type and mutants). It was found that total mCitrine and total eYFP expression of both isoforms of hGPR35 along with several mutants at various positions of the receptor were statistically comparable. Fluorescent protein visualisation of both isoforms of hGPR35 was also conducted by microscopy and expression was noticed. Overall, these findings suggest that the difference between the two isoforms in agonist response efficacy is not due to differences in the expression of the receptor. Instead, the disulphide bond may be important in this situation. It is crucial to use molecular modelling and, possibly, data from atomic level structures to completely understand this issue.

Chapter 4 Agonist induced phosphorylation of orthologues of the orphan receptor GPR35

4.1 Introduction

GPCRs, the largest class of cell surface receptors, are essential for regulating a variety of physiological processes (Drube et al., 2022). Numerous ligands such as neurotransmitters, hormones, light, lipids, and odorants activate these receptors (Matthees et al., 2021). GPCRs modulate a variety of intracellular signalling pathways after activation. For this reason, GPCRs have been successfully targeted for many therapeutic indications (Sharmin et al., 2020) and have been studied in detail with respect to structure and function. However, a substantial number of members of GPCRs remain in the orphan status because they have not been matched with suitable endogenous activators. As a result, the true therapeutic potential of such orphan GPCRs is challenging to reveal. GPR35 is such an orphan receptor that was originally discovered as an open reading frame (ORF), situated on chromosome 2q37.3 in human (O'Dowd et al., 1998).

Since G proteins, GPCR kinases (GRKs), and arrestins are the most common interaction partners of GPCRs, they contact active receptors in a manner that is identical to their opened intracellular cavity (Flock et al., 2017). Small loop structures or alpha-helical domains are typically inserted through this process into the GPCR cavity (Matthees et al., 2021). For the main signalling transducers, the trimeric G proteins, this interaction leads to a guanosine diphosphate (GDP)—guanosine triphosphate (GTP) exchange followed by dissociation of Gα and Gβγ subunits (Flock et al., 2015). In order to cause a physiological response, the activated G protein subunits can individually control the amounts of second messengers like calcium, diacylglycerol (DAG), and cyclic adenosine monophosphate (cAMP). GRKs then phosphorylate intracellular peptide stretches of activated GPCRs. Subsequently, this build-up of negative charges enables arrestins to attach with high affinity, starting the desensitisation and internalisation of receptors (Gurevich and Gurevich, 2019). Arrestins and G proteins at least share binding surfaces, therefore arrestin-bound receptors are canonically unable to enhance their primary signalling further (DeWire et al., 2007). In addition, arrestins have been demonstrated to operate as scaffolds for over 100 intracellular proteins (Crépieux et al., 2017), allowing the development of particular effector-hubs that control intracellular trafficking and signalling of active GPCRs (Matthees et al., 2021).

An essential part of GPCR signalling is the agonist-dependent phosphorylation of the receptor's intracellular domains, which has significant effects on the desensitisation of G protein signalling, the internalisation and recycling of the receptor, and the receptor's ability to promote G protein independent signalling (Nobles et al., 2011, Ren et al., 2005). GPCRs can be phosphorylated at serine and threonine residues on any area of the intracellular domain, but this occurs most frequently on the third intracellular loop and/or the C-terminal tail (Tobin, 2008). Moreover, the specific positions of the phosphorylated residues can affect receptor function and subsequent signalling (Prihandoko et al., 2016, Nobles et al., 2011). As the signalling of most GPCRs via G proteins is terminated by the phosphorylation of active receptor by specific kinases (GRKs) and subsequent binding of arrestin proteins, the in-depth analysis of the sites and mechanism of agonist regulated phosphorylation of GPCR is of paramount importance. GPR35 is a poorly characterised orphan GPCR and has garnered increased attention as a therapeutic target through its potential contributions to a spectrum of conditions ranging from non-alcoholic steatohepatitis to lower intestinal inflammation (Quon et al., 2020, Milligan, 2023). As GPR35 is a therapeutically important GPCR and there is marked variation between human and rodent orthologues of this receptor, a clear understanding of the regulation of this receptor is of utmost importance. The development of novel reagents and tools such as site-directed mutagenesis and phosphorylation site specific antisera (Figure 4.1) will significantly improve the analysis of the roles of GPR35 in health and illness.

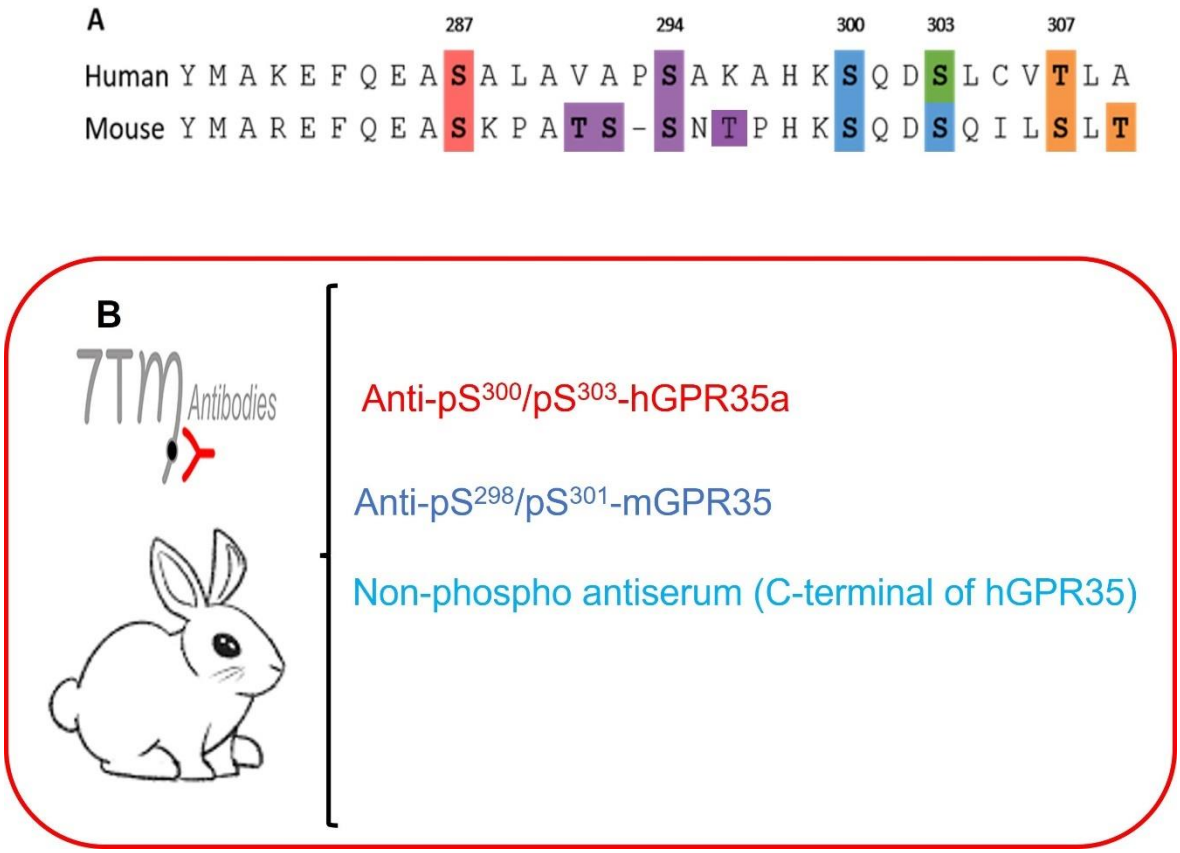

Figure 4.1 Generation and characterisation of GPR35 phospho-site specific antisera
(A) Potential phosphorylation sites in the C-terminal tail of hGPR35a and mGPR35, **(B)** Development of phosphorylation site specific antisera and C-terminal tail antisera to detect the post activation status of receptor GPR35.

4.1.1 Aims

Agonist mediated phosphorylation of GPCRs is a key step in engaging GRKs and subsequent interaction with the isoforms of arrestin (Gurevich and Gurevich, 2019). Even though this phenomenon is well known for many GPCRs, a complete map of identifying the precise sites of such posttranslational regulation and the degree to which each changed amino acid may contribute to the action is still rare. In this chapter, I have discussed both of these issues concerning GPR35 and make use of this knowledge to produce phospho-site-specific antibodies that serve as activation state-specific biosensors. The aims of this chapter were to

Investigate whether both orthologues (human and mouse) of GPR35 undergo agonist-dependent phosphorylation

Determination of the species and agonist specific differences in receptor phosphorylation

Assessment of the species selective antagonism characteristics of GPR35

Investigation of the location and specific sites at which phosphorylation takes place

Characterisation of phosphorylation site specific antisera

Immunocytochemical detection of the post activation status of GPR35.

4.2 Results

4.2.1 Production and characterisation of cell line stably express GPR35

4.2.1.1 Characterisation of cell lines that demonstrate stable expression of human GPR35 and mouse GPR35 with Hemagglutinin (HA) tag at its C-terminus

For most of the GPCRs, agonist-mediated phosphorylation of hydroxy-amino acids in the C- terminal tail of the receptor, the third intracellular loop, or both are regulated by G protein-coupled receptors kinase (GRKs), which was followed by receptor-arrestin interactions. To apply this for mouse GPR35 and its human equivalent splice variant hGPR35a, I stably expressed C-terminally HA epitope tagged forms of either human GPR35a (hGPR35a-HA) (Figure 4.2A) or mouse GPR35 (mGPR35-HA) (Figure 4.2B) in Flp-ln-TREx 293 cells. After that. I probed cells with an anti-HA antibody to make sure that expression was, in fact, induced for each orthologue after treating such cells with doxycycline, which is expected to induce expression of the receptor constructs.

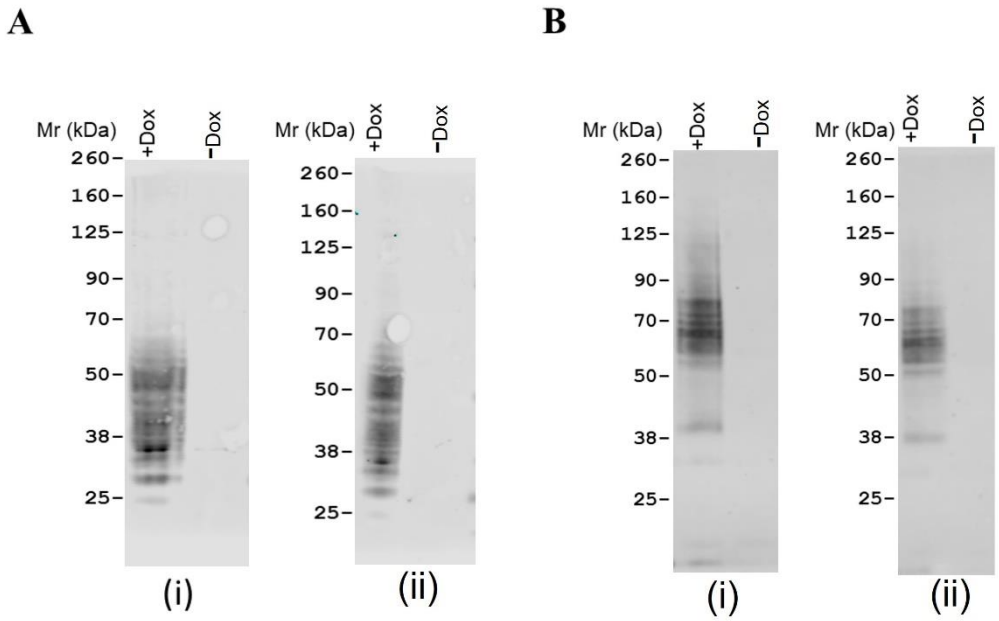

Figure 4.2 Characterisation of Human GPR35-HA and Mouse GPR35-HA stable cell lines
Cells were harvested, membranes were prepared and subsequently resolved by SDS-PAGE to separate the protein by mass and eventually detected by the HA epitope tag antibody in western blot. **(A)** Human GPR35-HA stable cell line and **(B)** Mouse GPR35-HA stable cell line. **(i)** 10 µg and **(ii)** 5µg of protein.

4.2.1.2 Characterisation of cell lines that show stable expression of human GPR35 PDM and mouse GPR35 PDM with Hemagglutinin (HA) tag at its C-terminus

As GPCRs are usually phosphorylated at serine and threonine residues mostly on the third intracellular loop and/or the C-terminal tail, I wished to confirm that phosphorylation is dependent entirely on phospho serine and phospho threonine residues in the C- terminal tail of the receptor GPR35. For this, I created cell lines that stably express C-terminally HA epitope tagged forms of either human GPR35a phosphodeficient (hGPR35a-PDM-HA) (Figure 4.3A) or mouse GPR35 phosphodeficient (mGPR35-PDM-HA) (Figure 4.3B) as controls. I first probed cells with an anti-HA antibody to make sure that expression was, in fact, induced for each orthologue after treating such cells with doxycycline, which is predicted to promote receptor construct expression.

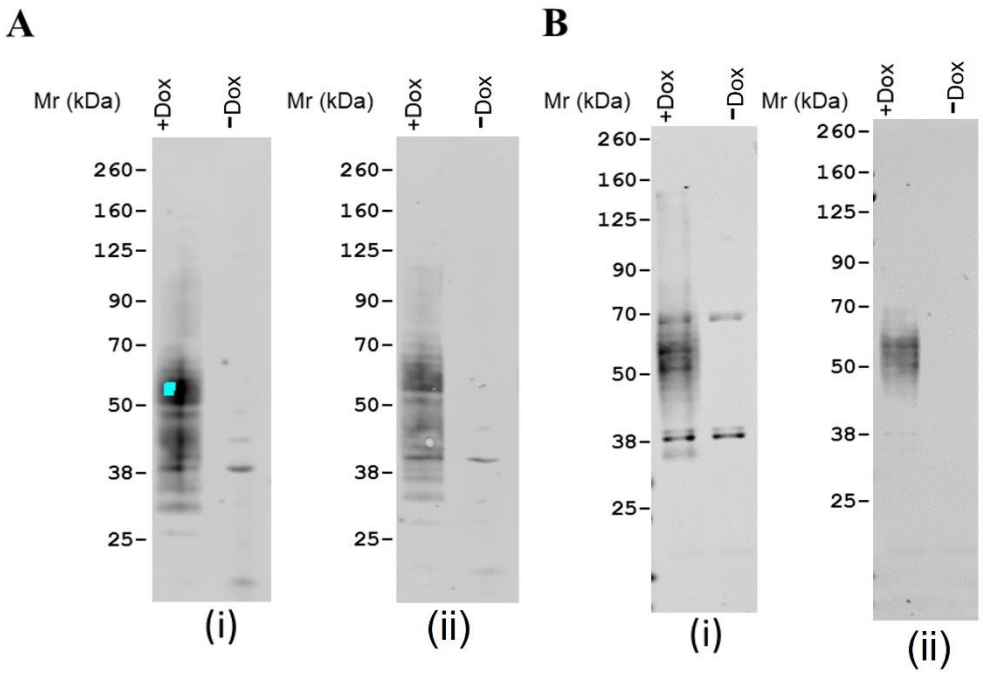

Figure 4.3 Characterisation of Human GPR35-PDM-HA and Mouse GPR35-PDM-HA stable cell lines

Cells were harvested, membranes were prepared and subsequently resolved by SDS-PAGE to separate the protein by mass and eventually detected by the HA epitope tag antibody in western blot. **(A)** Human GPR35-PDM-HA stable cell line and **(B)** Mouse GPR35-PDM stable cell line. **(i)** 10 µg and **(ii)** 5µg of protein. PDM, phosphorylation-deficient mutant.

4.2.1.3 Characterisation of cell lines that demonstrate stable expression of human GPR35, mouse GPR35, human GPR35 PDM and mouse GPR35 PDM with (eYFP) tag at its C-terminus

Phosphorylation of the active receptor is closely related to the binding of arrestin protein. In order to investigate the role of agonist-regulated phosphorylation sites in possible connections between agonist-induced interactions of the receptor and arrestins proteins, I prepared cells that stably express (eYFP) tagged forms of both hGPR35a (Figure 4.4A) and mGPR35 (Figure 4.4B). Phosphorylation deficient versions of human and mouse GPR35 cell lines with (eYFP) tag were also generated as controls (Figure 4.4C, D). I first probed cells with an anti-GFP antibody to check that each orthologue's expression was actually elevated after treating such cells with doxycycline, which is expected to promote the expression of the receptor constructs.

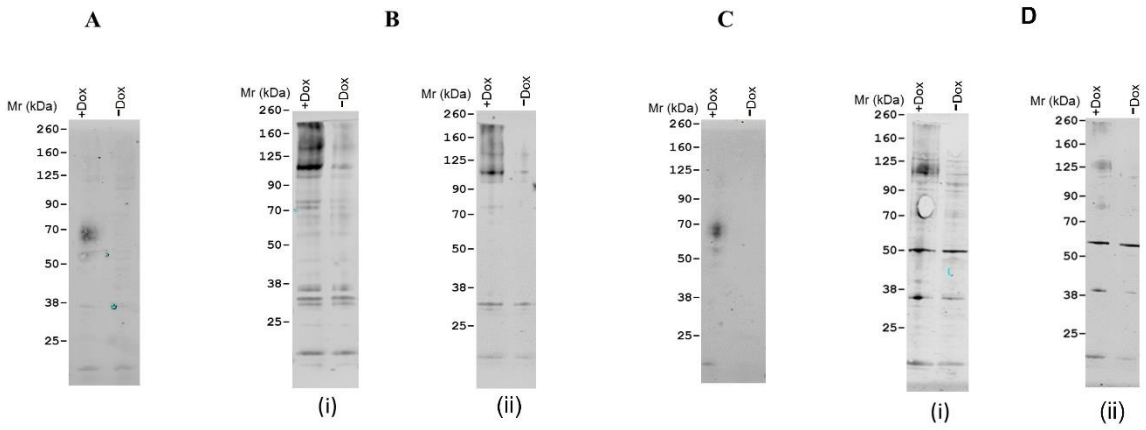

Figure 4.4 Characterisation of Human GPR35-eYFP, Mouse GPR35-eYFP, Human GPR35- PDM -eYFP PDM and Mouse GPR35-PDM-eYFP stable cell lines
Cells were harvested, membranes were prepared and subsequently resolved by SDS-PAGE to separate the protein by mass and eventually detected by the GFP epitope tag antibody in western blot. **(A)** Human GPR35-eYFP stable cell line and **(B)** Mouse GPR35-eYFP stable cell line, **(C)** Human GPR35- PDM-eYFP stable cell line and **(D)** Mouse GPR35- PDM -eYFP stable cell line. **(i)** 10 µg and **(ii)** 5µg of protein. PDM, phosphorylation-deficient mutant.

4.2.2 Validation of GPR35 phospho-site–specific antisera in cell lines expressing mouse orthologue of GPR35

4.2.2.1 Characterisation of mGPR35-pSer^{298}/pSer^{301} in cell lines expressing both wild type and phosphorylation deficient forms of GPR35

I have known from previous studies that except Ser^{294}, each of the five hydroxy-amino acids in the C-terminal tail of human GPR35a were phosphorylated in response to agonist occupancy of the receptor and played roles to attach with arretin-3, which inhibits additional G protein-coupled receptor signalling (Divorty et al., 2022). It was found that Ser^{303} was key to such interactions. the serine corresponding to human GPR35a residue 303 (301 for mouse) also played a dominant role in arrestin-3 interactions for mouse GPR35. For this reason, I employed the peptide sequence from mGPR35 (TPHKpSQDpSQILSLT) to generate mGPR35-pSer^{298}/ pSer^{301}-directed antibodies.

Following the capture of the receptor construct *via* anti-HA agarose beads, immunoblotting with an anti-HA antiserum in a cell line stably expressing mouse GPR35 with an HA epitope tag at the C-terminus showed the presence of a number of polypeptides except one without doxycycline induced. A smear of HA-immunoreactivity in the vicinity of 50 kDa was notable among these. Parallel immunoblotting of such samples with mGPR35pSer^{298}/pSer^{301} detected the

polypeptides in the approximate size of just over 50 kDa and did so in a manner that was dependent on pre-treatment of the cells with a number of agonists, as the antiserum did not identify this polypeptide in vehicle treated cells (Figure 4.5A). A similar experiment was conducted in cells that stably expressed the mouse GPR35 (PDM) version with an HA epitope tag at the C-terminus. After immunoblotting with anti-HA antiserum, again, all the polypeptides were visible with smears of HA-immunoreactivity in the region of 50 kDa. One polypeptide was again invisible in immunoblot because it was uninduced with doxycycline. When parallel immunoblotting of such samples with mGPR35pSer^{298}/pSer^{301} was conducted, the antiserum could not detect anything (Figure 4.5B) because all of the potential phosphorylation sites of mouse GPR35 are mutated in this cell line. This finding again validates that phosphorylation depends entirely on phospho serine and phospho threonine residues in the C-terminal tail of the mouse GPR35.

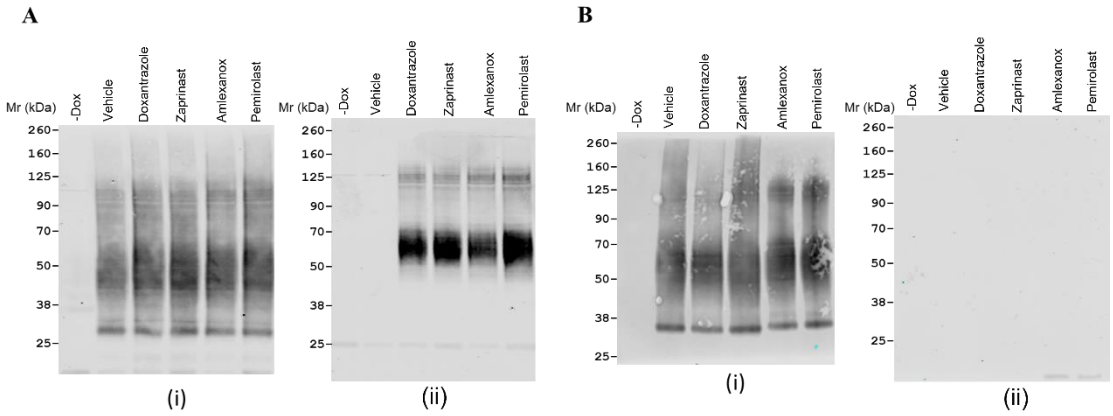

Figure 4.5 Characterisation of GPR35 phospho-site–specific antisera in cell lines stably expressing Mouse GPR35-HA and Mouse GPR35-PDM-HA
Experiments were performed using a Flp-In TREx 293 cell line induced to express **(A)** mouse GPR35-HA and **(B)** mouse GPR35- PDM-HA. These cell lines were treated with vehicle and different GPR35 agonists; Doxantrazole, zaprinast, amlexanox and pemirolast (each at 10 μM). Following capture of the receptor construct *via* anti-HA agarose beads, samples were resolved by SDS-PAGE and immunoblotted to detect **(i)** the HA epitope tag and **(ii)** mGPR35-pSer^{298}/pSer^{301}. Results are representative of three independent experiments.

4.2.2.2 Comparison of extent of phosphorylation of mouse GPR35 by endogenous *vs* synthetic agonist

As GPR35 can be activated by the endogenously produced tryptophan metabolite kynurenic acid (Wang et al., 2006, Kaya et al., 2021) and by a synthetic ligand zaprinast (Taniguchi et al., 2006, Kaya et al., 2021), I compared the phosphorylation potential of these two ligands directly. I used a cell line that

stably express mouse GPR35 with a HA epitope tag at C-terminus. After the capture of the mouse GPR35 by anti-HA agarose beads, several doxycycline-induced polypeptides were found during immunoblotting using an anti-HA antiserum (Figure 4.6A). All of these demonstrated smears of HA-immunoreactivity in the region of 50 kDa. When parallel immunoblotting of the same samples was detected with either hGPR35pSer^{300}/pSer^{303} (Figure 4.6B) or mGPR35pSer^{298}/pSer^{301} (Figure 4.6C), there was the presence of polypeptides above 50 kDa. There were also more rapidly migrating forms of polypeptide(s) identified by these phospho-site-specific antisera upon treatment with agonists. These may be glycosylated forms of the receptor mGPR35-HA. The most important outcome from this experiment is that synthetic agonist zaprinast showed better potency than endogenous agonist kynurenic acid in mouse GPR35 phosphorylation after applying both phospho-site specific antisera. Another significant issue is that hGPR35pSer^{300}/pSer^{303} antisera was also active at mouse GPR35 as the sequence of amino acids between the two orthologues is similar. To be more precise, there are 309 amino acids in hGPR35a, while mGPR35 contains 307 amino acids.

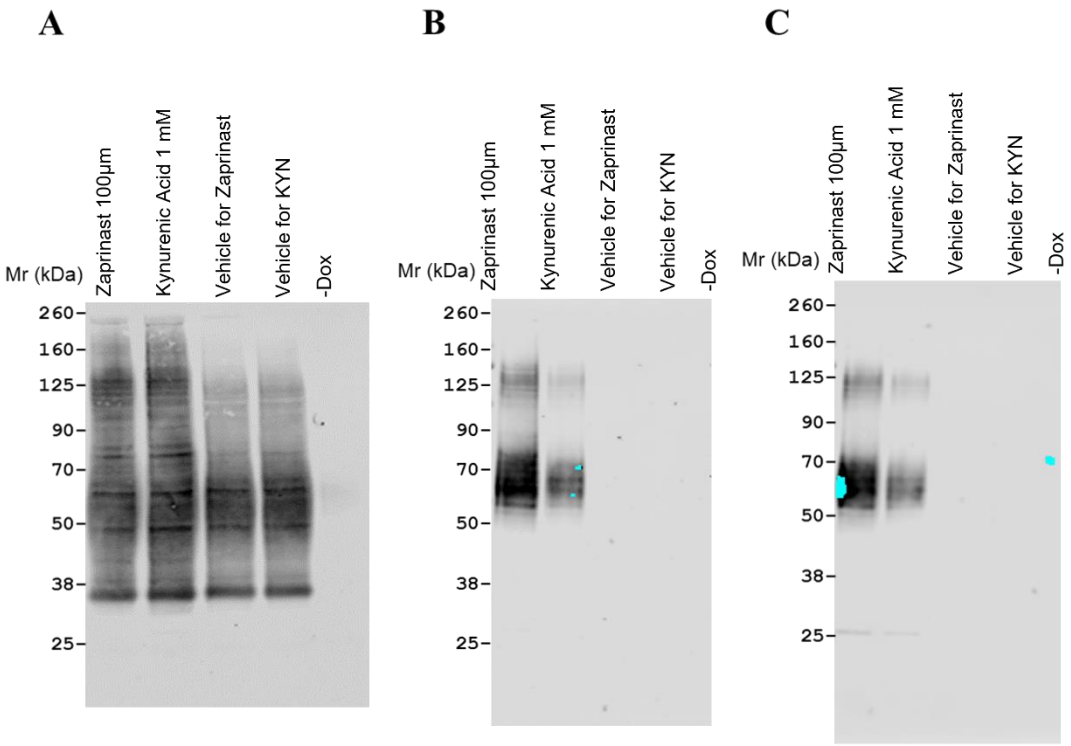

Figure 4.6 Comparison of phosphorylation activity between Kynurenic acid and Zaprinast in cell line stably expressing Mouse GPR35-HA

Experiments similar to **Figure 4.5** were conducted using a Flp-In TREx 293 cell line induced to stably express mouse GPR35-HA. Zaprinast, a potent synthetic agonist (100 µM) and kynurenic acid, a proposed but weak endogenous ligand (1 mM) were used. These cells were also treated with vehicles at different concentrations corresponding to ligand concentration. Following capture of the

receptor construct *via* anti-HA agarose beads, samples were resolved by SDS-PAGE and immunoblotted to detect **(A)** the HA epitope tag and **(B)** hGPR35-pSer^{300}-pSer^{303} and **(C)** mGPR35-pSer^{298}/pSer^{301} Results are representative of three independent experiments.

4.2.2.3 Arrestin interaction pattern of mouse GPR35 with kynurenic acid and zaprinast

As phosphorylation of the receptor is closely related to interaction with arrestin adapter protein, I investigated the arrestin-3 recruitment potential of kynurenic acid and zaprinast with mouse GPR35. For this assay, mGPR35-eYFP and arrestin-3-RLuc were transiently co-transfected into parental 293 cells. In the presence of a luciferase substrate, the addition of the GPR35 endogenous agonist kynurenic acid (Figure 4.7A) resulted in a concentration-dependent increase in measured BRET with pEC_{50} 3.23. In equivalent studies, after adding luciferase substrate, the addition of synthetic agonist zaprinast (Figure 4.7B) also caused concentration-dependent increase in BRET with pEC_{50} 6.32. Data from these experiments clearly demonstrated that zaprinast was more potent than kynurenic acid in arrestin-3 recruitment potential with mouse GPR35. The important finding from this study is that results obtained from phosphorylation experiment are consistent with arrestin interaction by the endogenous and synthetic ligands of mouse GPR35.

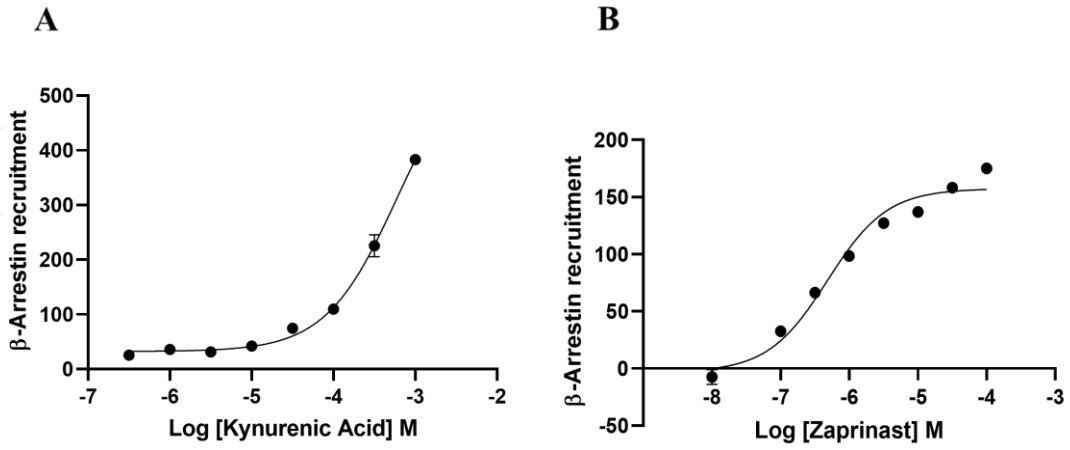

Figure 4.7 Comparison of arrestin-3 recruitment activity between Kynurenic acid and Zaprinast

Parental HEK293 cells were transfected transiently to express mGPR35-eYFP and arrestin-3-RLuc. Cells were exposed to the indicated concentrations of **(A)** kynurenic acid and **(B)** zaprinast for 5 min and BRET was measured following substrate addition. This experiment was performed once only (n=1).

4.2.3 GPR35 phosphorylation is almost entirely agonist mediated

To investigate if GPR35 phosphorylation is agonist regulated or not, I performed a series of immunoblots with different cell lines that stably express human GPR35a-HA, human GPR35a-PDM-HA, mouse GPR35-HA and mouse GPR35-PDM-HA. Following the capture of the receptor construct *via* anti-HA agarose beads, immunoblotting with an anti-HA antiserum detected two separate bands of approximate molecular mass (M_r) 55 and 43 KDa for both hGPR35a-HA (Figure 4.8A), hGPR35a-PDM-HA (Figure 4.8B). Parallel immunoblot with hGPR35apSer^{300}/pSer^{303} detected hGPR35a-HA in two bands: approx. 55 and 43 KDa after treatment with agonist zaprinast (Figure 4.8A). But hGPR35apSer^{300}/pSer^{303} was unable to detect any receptor when the experiment was conducted with phosphorylation deficient version of the human orthologue of the receptor (Figure 4.8B). The observed multiple forms of hGPR35a-HA in this study might be due to differential N-glycosylation of the receptor protein. When the similar study was replicated for the mouse form of GPR35, again the anti-HA antiserum detected smear of HA-immunoreactivity in the region of 50 kDa for mGPR35-HA (Figure 4.8C) and mGPR35-PDM-HA (Figure 4.8D). Parallel immunoblotting of such samples with mGPR35pSer^{298}/pSer^{301} detected approximately just over 50 kDa (single species of apparent molecular mass M_r) and did so in a way that was dependent on the cells first being pre-treated with the agonist zaprinast, as the antiserum failed to recognise this polypeptide in cells that had been treated with a vehicle (Figure 4.8C). Similar to the human orthologue of GPR35, antiserum mGPR35pSer^{298}/pSer^{301} failed to detect receptor when immunoblotting was done with phosphorylation deficient version of mouse GPR35 (Figure 4.8D).

From this set of experiments, it is clear that phosphorylation is completely agonist dependent, especially for mouse orthologues of GPR35. This experiment also proved that GPR35 phosphorylation is dependent mainly on phospho serine and phospho threonine residues in the C- terminal tail of the GPR35 as phospho-site specific antisera could not detect any receptor in phospho-deficient from of both orthologues of the receptor.

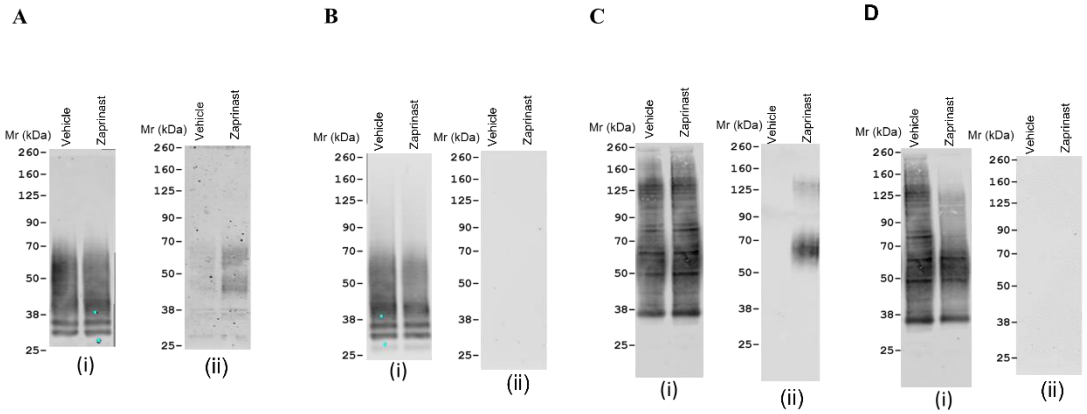

Figure 4.8 Comparison of phosphorylation among Human GPR35-HA, Human GPR35-PDM-HA, Mouse GPR35-HA and Mouse GPR35-PDM-HA stable cell lines
Experiments were performed using Flp-In TREx 293 cell lines induced to express **(A)** human GPR35-HA, **(B)** human GPR35- PDM-HA, **(C)** mouse GPR35-HA and **(D)** mouse GPR35- PDM-HA. These cell lines were treated with vehicle and a synthetic agonist for GPR35, zaprinast (100 µM for hGPR35a and 10 µM for mGPR35). Following capture of the receptor construct *via* anti-HA agarose beads, samples were resolved by SDS-PAGE and immunoblotted to detect **(i)** the HA epitope tag and **(ii)** hGPR35-pSer^{300}-pSer^{303}/mGPR35-pSer^{298}/pSer^{301}. Results are representative of three independent experiments.

4.2.4 Validation of GPR35 phospho-site–specific antisera in cell lines expressing human orthologue of GPR35

Previous research has shown that with the exception of Ser^{294}, human GPR35a's five hydroxy-amino acids were completely phosphorylated in response to agonist occupancy of the receptor and played a role in interactions with arretin-3, which inhibits the G protein mediated signalling (Divorty et al., 2022). It is also found that alteration of both Ser^{300} and Ser^{303} to Ala greatly reduced the ability of receptor agonists to facilitate connections with arrestin adapter proteins (Divorty et al., 2022). To determine the level of activation of the receptor, antisera that could specifically recognise phosphorylated versions of GPR35 were produced. Based on the aforementioned findings, I immunised rabbits with a peptide from hGPR35a known as (KAHKpSQDpSLCVTL) that contained both pSer^{300} and pSer^{303}.

Immunoblotting with an anti-HA antiserum in cell lines stably expressing human GPR35a with a HA epitope tag at the C-terminus revealed the presence of a number of polypeptides with the exception of one that was not doxycycline-induced after the receptor construct was captured using anti-HA agarose beads. Two separate bands of apparent molecular mass (M_r) 55 and 43 KDa stood out

among these. After treatment with a series of agonist and antagonist ligands, a parallel immunoblot using hGPR35pSer^{300}/pSer^{303} could identify hGPR35a-HA in two bands at approximately 55 and 43 KDa (Figure 4.9A). The antiserum failed to recognise the receptor polypeptide(s) in cells treated with the vehicle. Here, lodoxamide and zaprinast, two agonists of hGPR35, promoted phosphorylation of the receptor and were detected by hGPR35apSer^{300}/pSer^{303} (Figure 4.9A). In addition, pamoic acid proved itself once more a hGPR35a partial agonist, in comparison to lodoxamide and zaprinast at this endpoint, despite being able to facilitate hGPR35a-HA identification by hGPR35a-pSer^{300}/pSer^{303} antibodies. As expected from the direct phosphorylation assays, the human-specific GPR35 antagonist did not increase the phosphorylation of pSer^{300}/pSer^{303} inside hGPR35a-HA. This was shown by the absence of immunodetection with the hGPR35a-pSer^{300}/pSer^{303} antibodies. However, the impact of lodoxamide was countered by the addition of CID-2745687 before using an agonist (Figure 4.9A). In this way, the interactions depicted in (Figure 4.9A), genuinely reflected agonist regulated phosphorylation of human GPR35.

In cells that stably express the human GPR35 (PDM) variant with a HA epitope tag at the C-terminus, a similar experiment was carried out. After the receptor construct was captured using anti-HA beads, immunoblotting with an anti-HA antiserum in such cell lines revealed the presence of several polypeptides, except for one that was not doxycycline induced. Two separate bands of approximate molecular mass (M_r) 55 and 43 KDa for hGPR35a-PDM-HA were detected (Figure 4.9B). However, when an experiment was carried out using a phosphorylation-deficient version of the human orthologue of the receptor, hGPR35pSer^{300}/pSer^{303} was unable to identify any receptor (Figure 4.9B).

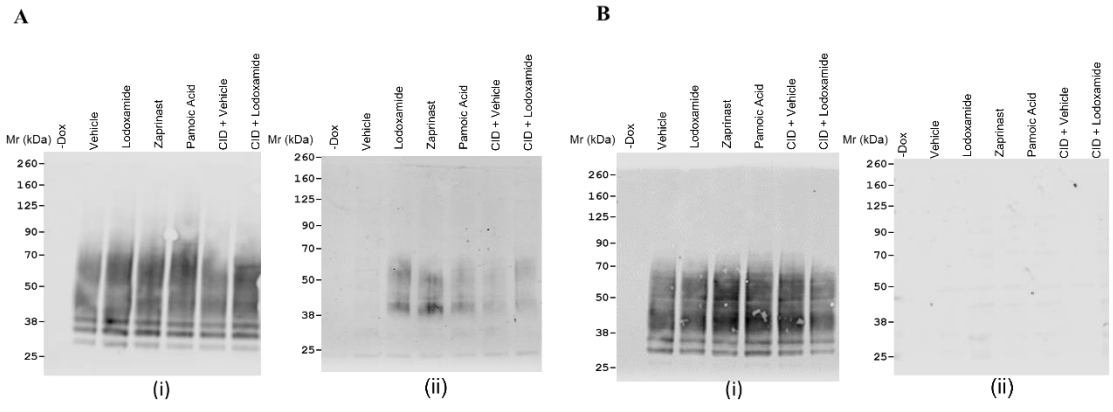

Figure 4.9 Characterisation of GPR35 phospho-site–specific antisera in Human GPR35-HA and Human GPR35- PDM-HA stable cell lines using multiple agonists and antagonist
Experiments were performed using a Flp-In TREx 293 cell line induced to express **(A)** human GPR35-HA and **(B)** human GPR35-PDM-HA. These cell lines were treated with vehicle and different GPR35 agonists; lodoxamide (100 nM), zaprinast (10 μM), pamoic acid (100 nM) each for 5 min and GPR35 antagonist, CID-2745687 (10 μM) for 15 min. Pre-treatment with CID-2745687 at 10 μM was also done for 15 min before adding lodoxamide for 5 min. Immunoblots of anti-HA immunoprecipitated samples were shown. **(i)** the HA epitope tag and **(ii)** hGPR35-pSer^{300}-pSer^{303}. Results are representative of three independent experiments.

4.2.5 Demonstration and proof of species selectivity of agonist and antagonist of GPR35

GPR35 is a unique receptor in several aspects that make translation difficult. Rodents only express one version of a protein, whereas humans express two different protein isoform sequences. The pharmacology of the GPR35 orthologues in humans and rodents are significantly different from each other, with differences between rat and mouse GPR35 being just as noticeable as those between either of these species and human versions. There are also agonist and antagonist ligands of GPR35 that show activity in a species selective way.

In our previous section, pamoic acid acted as a partial agonist in the phosphorylation of hGPR35a and antagonist CID-2745687 prevented lodoxamide induced hGPR35a phosphorylation. As there are some reports about these two ligands on their potential species selectivity issues, I utilised them along with reference ligand zaprinast in a cell line that stably expresses mouse GPR35 with an HA tag at the C-terminal. After capture of the mouse GPR35 by anti-HA-agarose beads, several doxycycline-induced polypeptides were found during immunoblotting using an anti-HA antiserum. All of these showed a smear of HA-immunoreactivity at the 50 kDa mark (Figure 4.10A). Parallel immunoblotting of these samples with mGPR35pSer^{298}/pSer^{301} detected the polypeptides with an approximate size of just over 50 kDa, and it did so in a way that required pre-treating the cells with a number of agonists, antagonist, and partial agonist, as the antiserum failed to find this polypeptide in cells that had been exposed to a vehicle (Figure 4.10B). As zaprinast is a well characterised agonist for mouse GPR35, it promoted phosphorylation of the receptor and was detected by mGPR35pSer^{298}/pSer^{301}. This phospho-site-specific antiserum was also able to detect polypeptide(s) that were moving more quickly after being exposed to agonists. They could represent receptor mGPR35-HA glycosylated variants. As predicted by CID-2745687's known pharmacology and species selectivity, pre-

treatment of this antagonist compound did not fully inhibit the effect of zaprinast at mGPR35. Pamoic acid, although a partial agonist at hGPR35, failed to promote the phosphorylation of mGPR35 and there was no detection of the phosphorylation signal by the mGPR35pSer^{298}/pSer^{301} (Figure 4.10B). This study once again validated the species selective characteristics of some agonist and antagonist of GPR35.

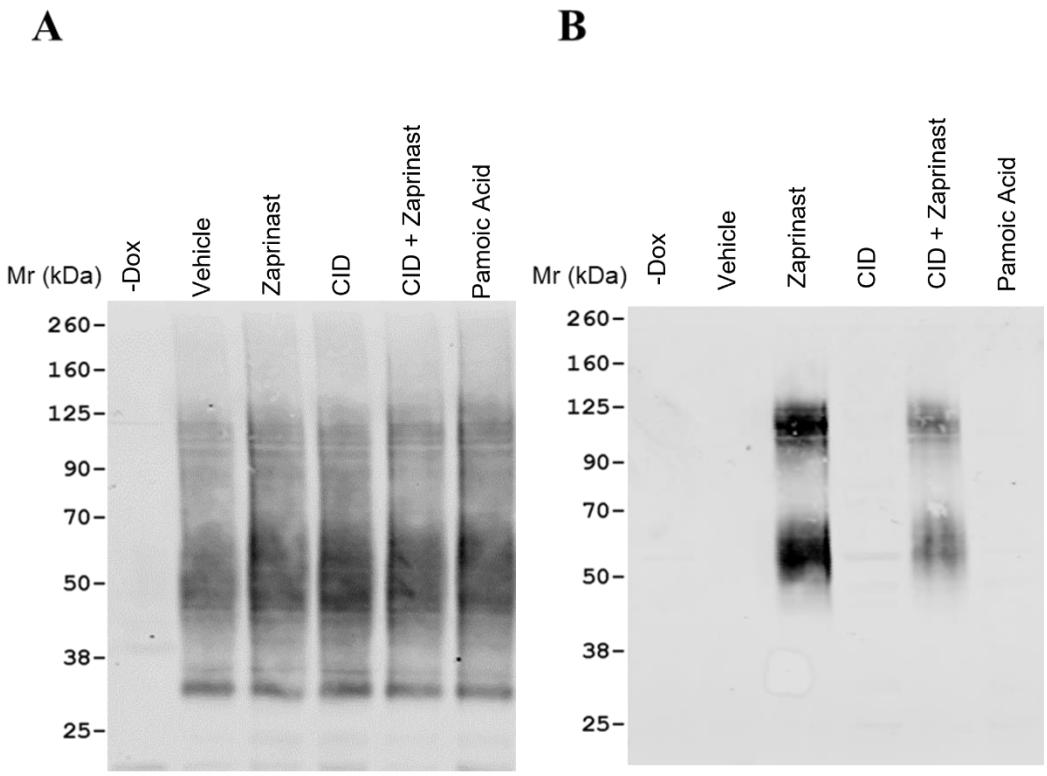

Figure 4.10 Validation of species selectivity of GPR35 agonist Pamoic acid and GPR35 antagonist CID-2745687

Experiments were performed using a Flp-In TREx 293 cell line induced to express mouse GPR35-HA. This cell line is treated with vehicle and two synthetic GPR35 agonists, zaprinast and pamoic acid (each at 10 μM) for 5 min as well as GPR35 anatagonist, CID-2745687 (10 μM) for 15 min. Pre-treatment with CID-2745687 at 10 μM was also done for 15 min before the addition of zaprinast for 5 min. Immunoblots of anti-HA immunoprecipitated samples were shown. **(A)** the HA epitope tag and **(B)** mGPR35-pSer^{298}/pSer^{301}. Results are representative of three independent experiments.

4.2.6 GPR35 phospho-site–specific antisera function as biosensors of human and mouse orthologues of GPR35 in immunocytochemistry-based experiments

4.2.6.1 Human GPR35 phospho-site–specific antisera detect the post activation status of hGPR35

As hGPR35a-pSer^{300}-pSer^{303}antisera was effective in detecting the post-activation status of human GPR35 in an immunoblot based phosphorylation assay, an attempt was made to reproduce the similar outcomes in immunocytochemical experiment using this antibody.

In Flp-In TREx 293 cells induced to express human GPR35-HA, immunocytochemical investigations using hGPR35a-pSer^{300}-pSer^{303}antisera identified the relevant receptors in a way that was agonist (zaprinast)-dependent (Figure 4.11, left panels). Specific signal was observed largely both at the cell surface and in punctate intracellular vesicles upon expression of the human GPR35a construct and treatment with zaprinast. In cells induced to express human GPR35-HA, hGPR35a-pSer^{300}-pSer^{303} antisera indicated a level of detection in the absence of zaprinast that would suggest a certain amount of constitutive phosphorylation of the receptor in this assay (Figure 4.11, left panels). DAPI, a nuclear stain, was used to counterstain the samples (Figure 4.11, centre panels). Brightfield images were also demonstrated Figure 4.11, right panels).

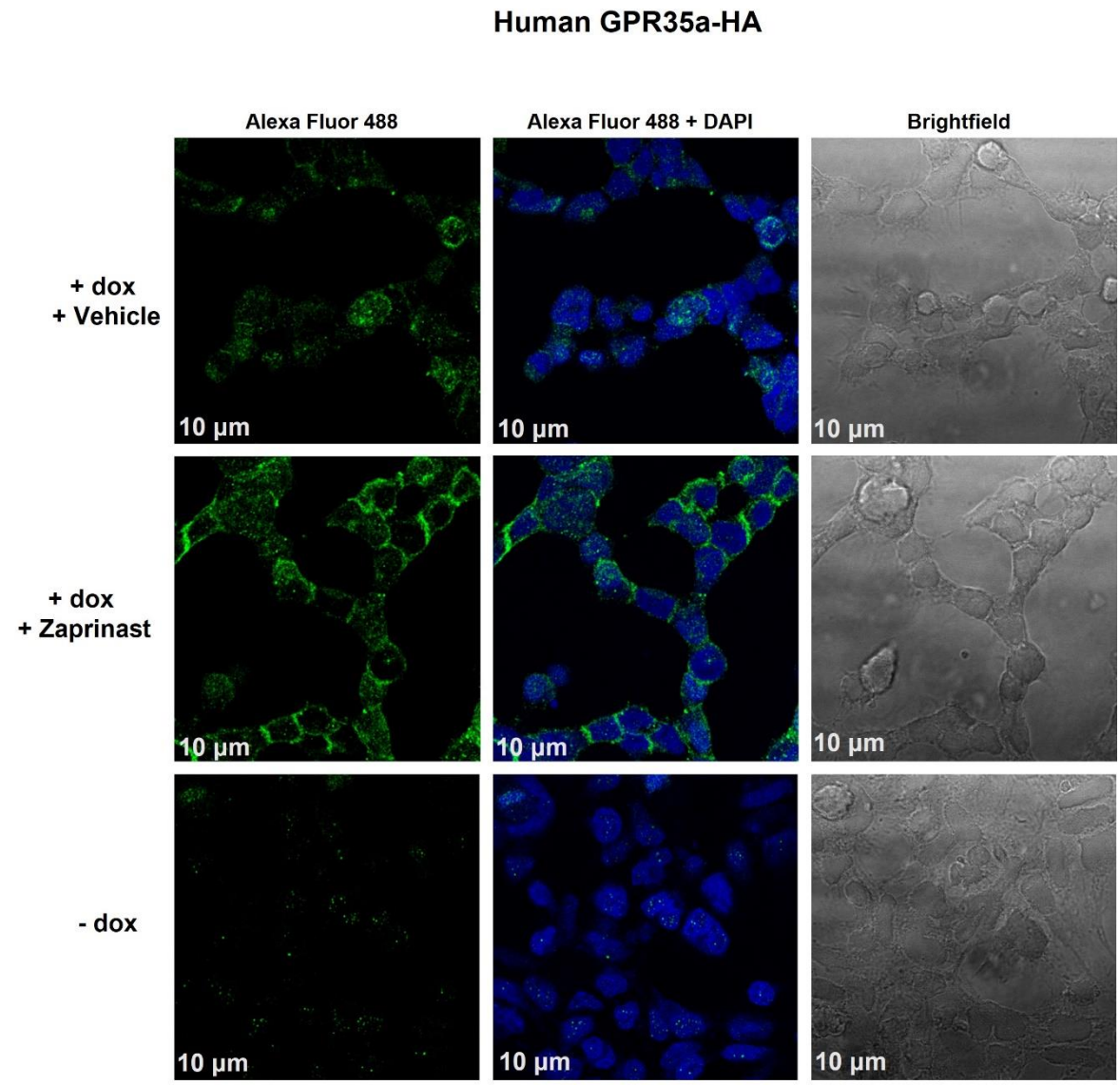

Figure 4.11 Human GPR35a phospho-site–specific antisera pSer^{300}-pSer^{303} can act as a biosensor of agonist activated, fully matured hGPR35 in immunocytochemical studies
Cells in **Figure 4.11** able to express hGPR35-HA was either uninduced (−dox) or induced by treatment with doxycycline (+dox) and then treated with either vehicle or zaprinast. Such cells were then used in immunocytochemical studies employing hGPR35-pSer^{300}/pSer^{303} (*left panels*) (Alexa Fluor 488). Samples were counterstained with the nuclear dye DAPI (*centre panels*). Brightfield images (*right panels*) are also shown. Scale bar = 10 µm. Representative images are shown**.** hGPR35, human GPR35.

4.2.6.2 Mouse GPR35 phospho-site–specific antisera detect the post activation status of mGPR35

As the pharmacology of the GPR35 orthologues in humans and mouse are significantly different from each other (Quon et al., 2020) and there are some reported species selectivity issues of agonists and antagonists of this receptor, I decided to utilise the mGPR35-pSer^{298}-pSer^{301}antisera for immunocytochemical detection of mouse GPR35.

In Flp-In TREx 293 cells, murine GPR35-HA expression is induced and immunocytochemical investigations using mGPR35-pSer^{298}-pSer^{301}antisera detected the relevant receptors in an entirely agonist (zaprinast)-dependent way (Figure 4.12, left panels). When the mouse GPR35 construct was expressed and zaprinast was administered, a distinct signal was mostly seen at the cell surface and in punctate intracellular vesicles. The nuclear stain DAPI was used to counterstain the samples (Figure 4.12, centre panels). Moreover, brightfield photos were shown (Figure 4.12, right panels).

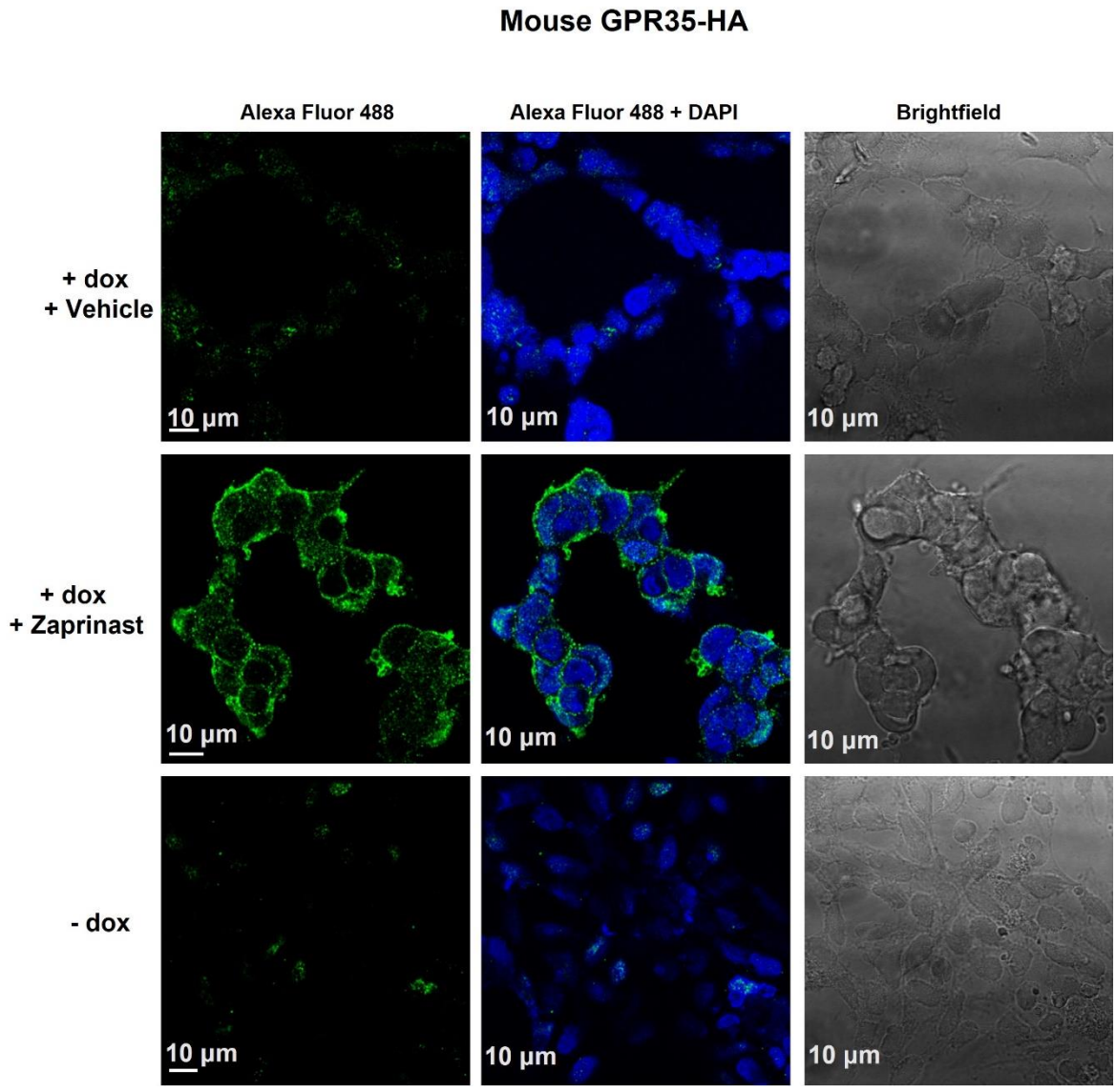

Figure 4.12 Mouse GPR35 phospho-site–specific antisera pSer^{298}-pSer^{301} can act as a biosensor of agonist activated, fully matured mGPR35 in immunocytochemical studies
Cells in **Figure 4.12** able to express mGPR35-HA was either uninduced (−dox) or induced by treatment with doxycycline (+dox) and then treated with either vehicle or zaprinast. Such cells were then used in immunocytochemical studies employing mGPR35-pSer^{298}/pSer^{301} (*left panels*) (Alexa Fluor 488). Samples were counterstained with the nuclear dye DAPI (*centre panels*). Brightfield images (*right panels*) are also shown. Scale bar = 10 µm. Representative images are shown**.** mGPR35, mouse GPR35.

4.2.7 GPR35 phospho-site–specific antisera cannot detect phosphodeficient form of human and mouse orthologues of GPR35 in immunocytochemistry-based investigations

4.2.7.1 Human GPR35 phospho-site–specific antisera were unable to detect hGPR35-PDM-HA

As hGPR35a-pSer^{300}-pSer^{303}antisera was proven as an effective biosensor to detect the post activation status of human GPR35 in immunocytochemical study (Divorty et al., 2022), an attempt was made to confirm the genuineness of this identification.

In Flp-In TREx 293 cells induced to express human GPR35-PDM-HA, immunocytochemical investigations using hGPR35a-pSer^{300}-pSer^{303}antisera failed to recognise hGPR35-PDM-HA (Figure 4.13, left panels). Simultaneous detection of each orthologue by anti-HA verified the continuous presence of receptor protein (PDM) irrespective of treatment with vehicle or agonist (Figure 4.13, centre panels). The samples were counterstained with the nuclear stain DAPI and merged images of DAPI with receptor protein (Figure 4.13, right panels).

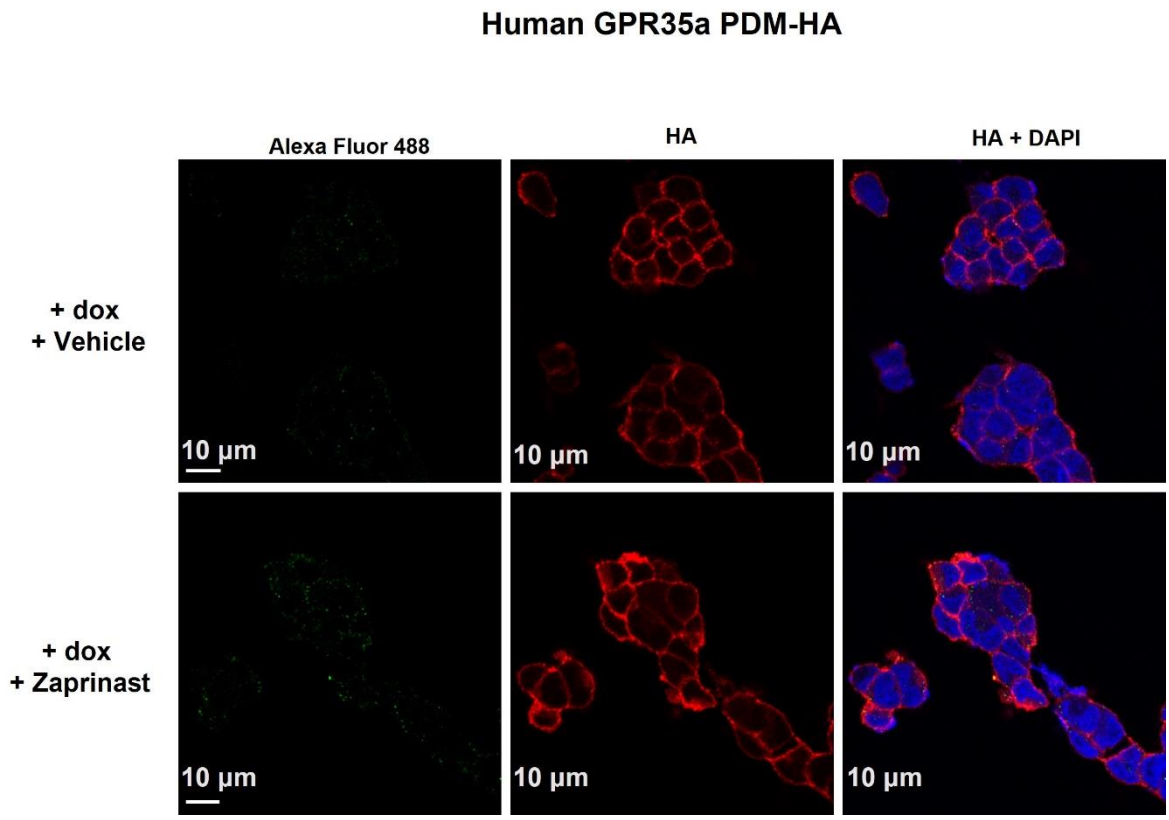

Figure 4.13 Phospho-site–specific antisera fail to identify hGPR35a-PDM-HA in immunocytochemical studies
In experiments akin to those of **Figure 4.11**, Flp-In-TREx 293 cells harboring hGPR35-PDM-HA was induced to express the receptor by pre-treatment with doxycycline (+dox) and then with either zaprinast or vehicle. Immunocytochemical studies employed hGPR35-pSer^{300}/pSer^{303} (Alexa Fluor 488). Samples were counterstained with the nuclear dye DAPI. Scale bar = 10 µm. Representative images are shown. PDM, phosphorylation-deficient mutant.

4.2.7.2 Mouse GPR35 phospho-site–specific antisera were unable to detect mGPR35-PDM-HA

To establish the authenticity of mGPR35-pSer^{298}-pSer^{301}antisera in detecting real phosphorylation state of the receptor, a cell line was generated to express mouse GPR35-PDM-HA in Flp-In TREx system.

Upon doxycycline induction and mouse GPR35-PDM-HA expression, immunocytochemical experiment using mGPR35-pSer^{298}-pSer^{301}antisera could not detect mGPR35-PDM-HA (Figure 4.14, left panels). Independent of treatment with a vehicle or an agonist, parallel identification of each orthologue by anti-HA verified the persistent presence of the receptor protein (PDM) (Figure 4.14, centre panel). The samples were counterstained with the nuclear dye DAPI, and DAPI and receptor protein pictures were combined (Figure 4.14, right panels).

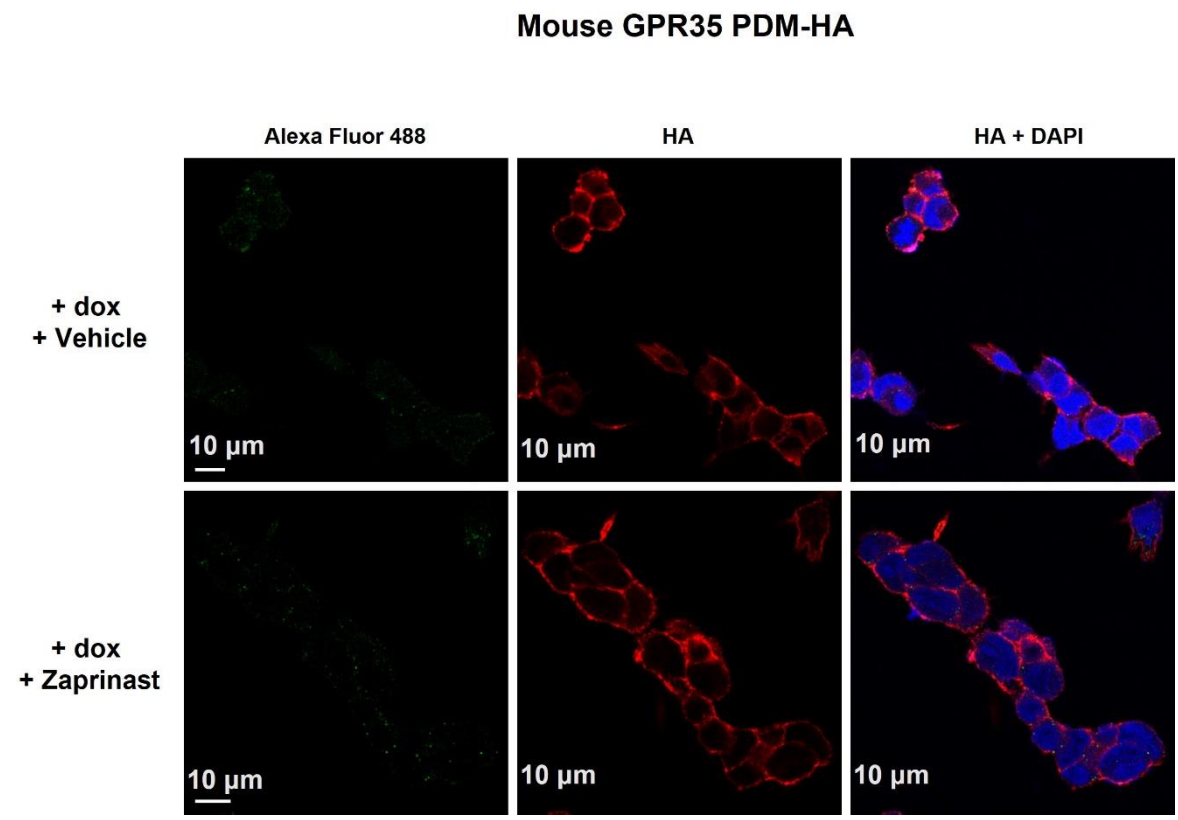

Figure 4.14 Phospho-site–specific antisera fail to identify mGPR35-PDM-HA in immunocytochemical studies
In experiments akin to those of **Figure 4.12**, Flp-In-TREx 293 cells harboring mGPR35-PDM-HA was induced to express the receptor by pre-treatment with doxycycline (+dox) and then with either zaprinast or vehicle. Immunocytochemical studies employed mGPR35-pSer^{298}/pSer^{301} (Alexa Fluor 488). Samples were counterstained with the nuclear dye DAPI. Scale bar = 10 µm. Representative images are shown. PDM, phosphorylation-deficient mutant.

4.2.8 Effects of Lambda protein phosphatase (λ-PPase) in GPR35 phosphorylation

Lambda Protein Phosphatase is a Mn^{2+}-dependent protein phosphatase with activity towards phosphorylated serine, threonine, and tyrosine residues. The primary function of this enzyme is to liberate phosphate groups from phosphorylated serine, threonine, and tyrosine residues of proteins (Zhuo et al., 1993).

As I have used the phosphorylation site specific antibody to identify the post activation status of human and mouse orthologues of GPR35, an appropriate control is required to ensure that the antibodies indeed are identifying the pSer^{300}, pSer^{303}, or both sites. For this reason, a cell line stably expressing human GPR35-eYFP was stimulated with vehicle and agonist zaprinast, followed by treatment with Lambda protein phosphatase, and then separated by SDS-PAGE. As λ-PPase

chops or releases phosphate groups from phosphorylated serine or threonine, there remains no scope of phosphorylation. As a result, hGPR35a-pSer^{300}-pSer^{303}antisera failed to detect the receptor (Figure 4.15, right panels). Human GPR35-eYFP expressing stable cell line untreated with λ-PPase was used as a control (Figure 4.15, left panels). They were, as usual, treated with vehicle and agonist zaprinast, and then separated by SDS-PAGE and detected clearly by hGPR35a-pSer^{300}-pSer^{303}antisera.

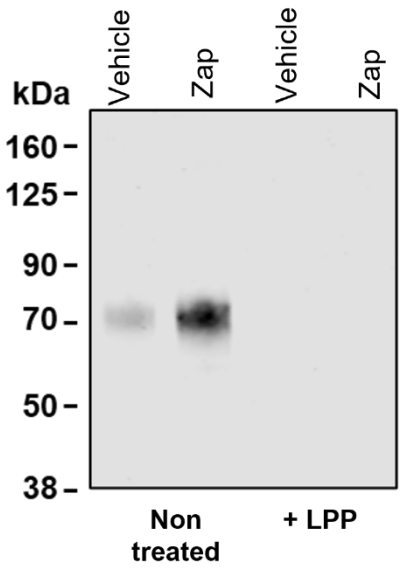

Figure 4.15 Demonstration of the effects of Lambda protein phosphatase in reversing phosphorylation
Cell line stably expressing human GPR35-eYFP was stimulated with vehicle and agonist zaprinast and then was subsequently treated with Lambda protein phosphatase prior to separation by SDS-PAGE (*right panels*). Cells non treated with Lambda protein phosphatase, stimulated by vehicle and zaprinast were used as a control (*left panels*). The samples were immunoblotted to detect hGPR35-pSer^{300}/pSer^{303}.

4.2.9 GPR35 are N-glycosylated

In this chapter, I have observed multiple forms of both mGPR35-HA and hGPR3a-HA in various experimental studies. GPR35 has also been reported to have different glycosylation states (Jenkins et al., 2011). Differential N-glycosylation of the receptor protein may be the cause of these various types of receptor proteins. After treatment with the enzyme N-glycosidase F, samples were resolved by SDS-PAGE and carbohydrates were removed and a single anti-HA

immunoreactive band of some (apparent M_r) 32 KDa was seen (Figure 4.16). Each time, this apparent Mr is in agreement with the orthologues' primary amino acid sequence; (mGPR35 =307 amino acids, hGPR35a = 309 amino acids).

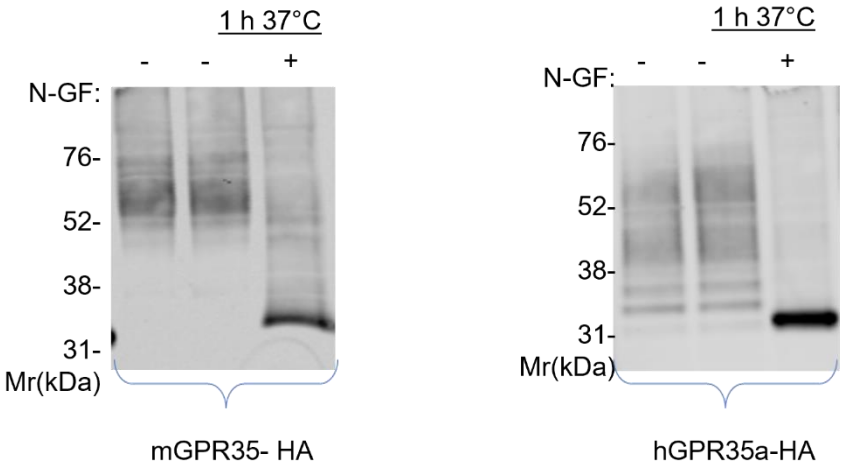

Figure 4.16 Mouse and human GPR35-HA are N-glycosylated
Representative anti-HA immunoblots of mGPR35-HA and hGPR35a-HA-expressing HEK293 cell lysates in their native states or following treatment with N-glycosidase F (N-GF = *N*-glycosidase F).

4.2.10 Generation and characterisation of a stable cell line that expresses human GPR35b-HA

Although it is known that hGPR35 is produced in two different isoforms, which differ only by 31 amino acids in the length of their extracellular N-termini, nothing is known about how these isoforms operate. With the help of gene expression analysis in immune and gastrointestinal cells, it is found that these isoforms emerge from distinct promoter usage and alternative splicing. Among all the transcripts, only two mRNAs encode GPR35b (also referred to as "GPR35 long"), while all known/annotated transcripts encode the reference isoform GPR35a (also known as "GPR35 short") (Schihada et al., 2022). Although the location of hGPR35a and hGPR35b mRNA expression in human tissues has been identified, their putative unique roles are unknown because of their remarkably comparable pharmacology (Quon et al., 2020). In both G protein and arrestin interaction assays, agonist efficacy was found to be almost 70% lower in the longer isoform compared to the shorter one (Marti-Solano et al., 2020) even though both isoforms display highly similar pharmacology. However, in a recent study, it was observed that the extended N-terminus of the long isoform limits G protein activation but elevates receptor–arrestin interaction (Schihada et al., 2022). Although the G protein based

experimental outcomes were similar between the two groups, there was a marked difference in arrestin interaction with both isoforms of hGPR35. As all the G protein and arrestin recruitment assays were conducted on a transient transfection setting into parental 293 cells, I decided to generate and characterise a Flp-In TREx 293 based cell line that would stably express hGPR35b with a HA tag at the C-terminal of the receptor and the receptor will be integrated into the genome of the cells. I first examined cells with anti-HA antibodies to confirm that expression was, in fact, induced for each orthologue after treating such cells with doxycycline, which is supposed to promote the expression of the receptor constructs (Figure 4.17A). After initial characterisation, I decided to use different hGPR35 specific agonist, partial agonist, and antagonist to fully decipher the pharmacology of the new cell line and use the hGPR35a-HA receptor construct as a control. Following capturing the receptor with anti-HA agarose beads, immunoblotting was conducted with an anti-HA antiserum, and this showed the presence of a number of polypeptides (each having two separate bands of approximate molecular mass (M_r) 55 and 43 KDa) for hGPR35a-HA but not for hGPR35b-HA (Figure 4.17B). To further diagnose this unusual finding of hGPR35b-HA, I decided to use phosphorylation site specific antibody and GPR35-C-terminal antisera in this setting. Immunoblotting with a hGPR35-pSer^{300}/pSer^{303} antibody detected the signal generated by lodoxamide after phosphorylation of hGPR35a-HA but not any signal upon treatment with vehicle justifying again the agonist regulated phosphorylation of hGPR35a-HA. Pamoic acid, a partial agonist, once again showed a very mild phosphorylation signal compared to lodoxamide while the hGPR35a antagonist CID-2745687 completely wiped out the phosphorylation signals generated by lodoxamide. When the same hGPR35-pSer^{300}/pSer^{303} antibody was employed to detect the phosphorylation outcomes of hGPR35b-HA with different ligands, unfortunately, no signals were found (Figure 4.17D). I then opted to employ GPR35-C-terminal antisera to detect the receptor independent of phosphorylation state. Here, as expected and opposite to the result obtained from phospho antibody, the non-phospho C-terminal antisera detected signal well for samples that were treated with partial agonist pamoic acid and antagonist CID-2745687 before lodoxamide for hGPR35a-HA. This C-terminal antisera also detected the vehicle treated sample, but it poorly detected the samples that were stimulated with potent hGPR35a agonist lodoxamide. Lodoxamide might generate negative charges upon phosphorylation and thereby reducing the epitope

recognition ability by this C-terminal antisera. The above-mentioned scenario was for hGPR35a-HA but when similar experiment was conducted with hGPR35-HA in a stable cell line, no signals in immunoblots were produced (Figure 4.17E). As receptor phosphorylation is closely related to arrestin protein interaction, I did an arrestin-3 bystander BRET assay with both hGPR35a-HA and hGPR35b-HA employing lodoxamide as a reference agonist for hGPR35. Here, after doxycycline induction, I observed a lodoxamide mediated sharp BRET signal of arrestin-3 recruitment by hGPR35a-HA (Figure 4.17C) but not hGPR35b-HA. The results from all of these experiments in section (4.2.10) clearly demonstrated that hGPR35b is expressed at a very low level in the Flp-In TREx 293 based stable cell line system. Although hGPR35b recruits arrestin-3 (although lower efficacy than hGPR35a) (Marti-Solano et al., 2020), the experiment was conducted in a transient setting. Here, in the Flp-In TREx 293 based system, hGPR35b could not generate any response.

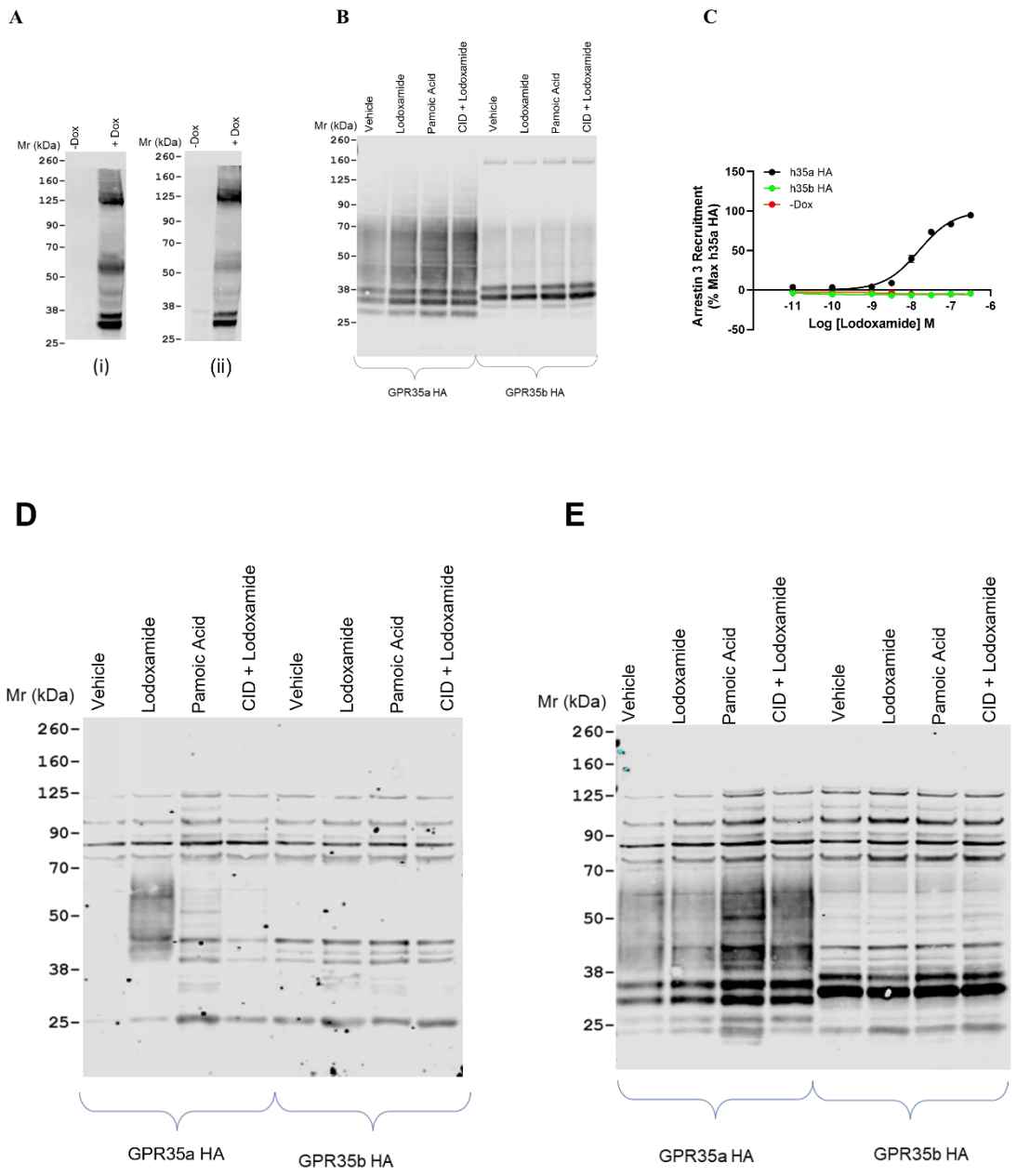

Figure 4.17 Characterisation of Human GPR35b-HA stable cell line
(A) Human GPR35b-HA stable cells were harvested, cell lysates were produced and subsequently resolved by SDS-PAGE to separate the protein by mass and eventually detected by the HA epitope tag antibody in western blot; **(i)** 10 µg and **(ii)** 5µg of protein. **(B)**, **(D)** and **(E)** Both human GPR35a-HA (left panels) and human GPR35b-HA (right panels) were treated with vehicle and different GPR35 agonists lodoxamide (100 nM), pamoic acid (100 nM) each for 5 min and GPR35 antagonist, CID2745687 (10 µM) for 15 min. Pre-treatment with CID-2745687 at 10 µM was also done for 15 min before the addition of lodoxamide for 5 min. Immunoblots of anti-HA immunoprecipitated samples were shown with the **(B)** HA epitope tag, **(D)** hGPR35-pSer^{300}/pSer^{303} and **(E)** Non-phospho-site GPR35 C-terminal tail antiserum for both isoforms of hGPR35. **(C)** GPR35a-HA and GPR35b-HA were expressed transiently and used in arrestin-3 bystander BRET assays.

4.2.11 Deorphanisation of GPR35 by suggested endogenous ligand 5-HIAA

Officially, GPR35 is still classified as an orphan receptor, even though it is currently a highly popular therapeutic target for several illnesses, such as non-

alcoholic steatohepatitis and lower intestine inflammation (Quon et al., 2020, Milligan, 2023). Very recently, two publications claim that serotonin metabolite 5-hydroxyindoleacetic acid (5-HIAA) can act as an endogenous GPR35 ligand (De Giovanni et al., 2022, De Giovanni et al., 2023a). This group stated that GPR35 is upregulated on activated neutrophils, and it helps in inflammatory recruitment. They also claimed that 5-HIAA produced by mast cells and platelets encourages neutrophil transendothelial migration. It is also mentioned that serotonin reuptake and metabolism inhibitors can reduce GPR35 performance (De Giovanni et al., 2022, De Giovanni et al., 2023a). After observing their interesting findings, I used 5-HIAA in a cell-based assay to measue its potential to activate G protein $G\alpha_{13}$, recruit arrestin with GPR35 and finally determine the phosphorylation ability for GPR35.

In a BRET based arrestin-3 interaction assay, hGPR35a-eYFP and arrestin-3-RLuc were simultaneously expressed in HEK 293 cells by transfection. After luciferase substrate addition, cells were treated with lodoxamide and 5-HIAA for 5 min and BRET was measured. Lodoxamide was used as a control in this experiment. From the experiment, it was found that hGPR35a reference ligand lodoxamide could recruit arrestin-3 with hGPR35a with a pEC_{50} of 8.29, but the new proposed endogenous ligand 5-HIAA was without any effects (Figure 4.18A).

Next, I utilised this new ligand in the G protein activation assay for hGPR35a. For this, hGPR35a was transfected into parental 293 cells as $G\alpha_{13}$ SPASM sensor. Following the addition of luciferase substrate, cells were stimulated with lodoxamide and 5-HIAA for 5 min and BRET was measured. The obtained results suggested that lodoxamide could recruit $G\alpha_{13}$ with a pEC_{50} of 8.29 but 5-HIAA was unsuccessful (Figure 4.18B).

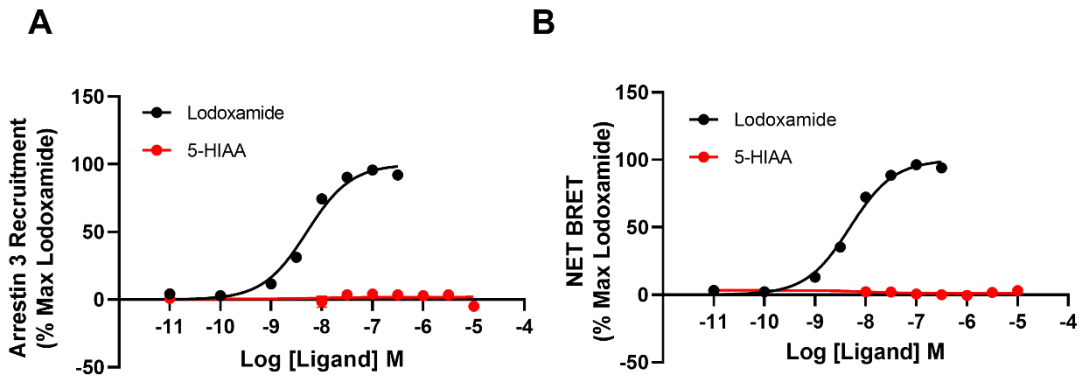

Figure 4.18 Validation of the potential of 5-HIAA as an endogenous agonist of GPR35
(A) Parental HEK293 cells were transfected transiently to express either hGPR35a-eYFP and arrestin-3-RLuc. Cells were exposed to the indicated concentrations of lodoxamide (black circles) and 5-HIAA (red circles) for 5 min and after substrate addition BRET was measured. **(B)** Comparison of the effect of hGPR35a transiently expressed in parental HEK293 cells as $G\alpha_{13}$ SPASM sensors; BRET signals were monitored after treating with indicated concentrations of lodoxamide (black circles) and 5-HIAA (red circles) for 5 min. In both **(A)** and **(B)**, lodoxamide, the reference ligand was used as a control. This experiment was performed once only (n=1).

After conducting the BRET based assay for arrestin and G protein activation potential of 5-HIAA, I decided to investigate the phosphorylation potential of this new GPR35 ligand in immunoblot. For this, I developed a stable transfected Flp-In TREx 293 cell line that expresses mGPR35 with an enhanced yellow fluorescent protein (eYFP) tag at its C-terminus using doxycycline as an inducer (mGPR35-eYFP). When the receptor was caught using GFP-trap, immunoblot with an anti-GFP antibody demonstrated equal loading of proteins onto the gels (Figure 4.19A). After stimulating the receptor with zaprinast (10 µM, 5 min) and GSK 938 (100 nM, 5 min) and claimed endogenous ligand of GPR35, 5-HIAA (De Giovanni et al., 2023a, De Giovanni et al., 2022) (10 µM, 5 min), the phosphorylated receptor was visible upon treatment with zaprinast and GSK 938 using anti mGPR35-pSer^{298}/pSer^{301} antiserum (Figure 4.19B). Although 5-HIAA is advertised as a powerful endogenous ligand of GPR35, even at a concentration of 10 µM, a serotonin metabolite failed to phosphorylate mGPR35. Zaprinast and GSK 938 were used as reference agonists for mouse GPR35 in this study.

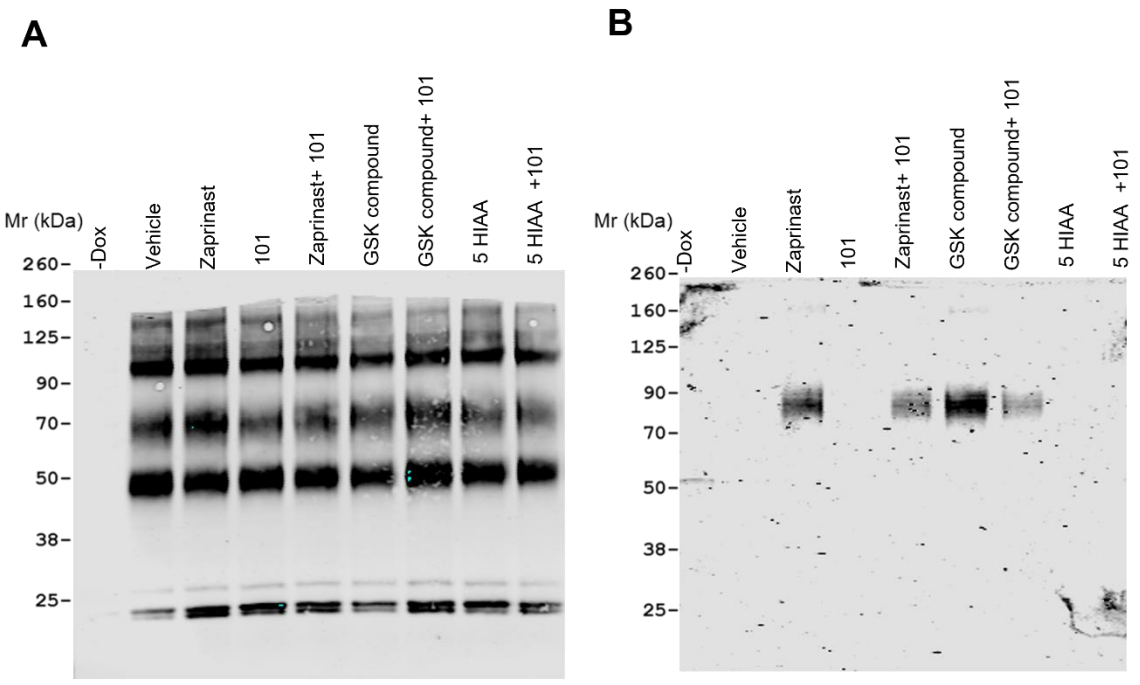

Figure 4.19 Investigation of the potential of 5-HIAA in phosphorylation of GPR35
A Flp-In TREx 293 cell line induced to express mouse GPR35-eYFP was treated with vehicle, zaprinast (10 μM), GSK 938 (100 nM), 5HIAA (10 μM), compound 101 (10 μM) or above mentioned 3 ligands plus compound 101. Following capture of the receptor construct *via* a GFP-trap, samples were resolved by SDS-PAGE and immunoblotted to detect **(A)** the GFP epitope tag and **(B)** mGPR35-pSer^{298}/pSer^{301}. Results are representative of three independent experiments.

From the above-mentioned experiments, it is clear that serotonin metabolite 5-hydroxyindoleacetic acid (5-HIAA) was not successful in demonstrating its potential as an activator of GPR35. The discrepancy between my result to the single report published by (De Giovanni et al., 2022) maybe because of the difference in the assay system. This group provided evidence of 5-hydroxyindoleacetic acid (5-HIAA) as an endogenous activator of GPR35 in the context of neutrophil function by using murine WEHI-231 B lymphoma cell model while I conducted all the experiments (arrestin recruitment, phosphorylation, and G protein activation) for GPR35 with 5-HIAA in cell based in-vitro system. So further studies are warranted to establish the claim for being an endogenous ligand for GPR35.

4.2.12 Investigation of the potential of cinnabarinic acid to activate GPR35 endogenously

As kynurenic acid was first proposed as an endogenous agonist for GPR35 (O'Dowd et al., 1998), scientists were interested to screen other compounds of kynurenine metabolism pathway to assess their potential as a probable endogenous ligand for orphan receptor GPR35. Later, cinnabarinic acid was identified as an endogenous metabolite of the kynurenine pathway (Fazio et al., 2012). I then decided to employ this compound in BRET based arrestin-3 recruitment assay and G protein activation assay.

Transfected HEK 293 cells were used to co-express hGPR35a-eYFP and arrestin-3-RLuc in a BRET-based arrestin-3 interaction experiment. Cells were exposed to lodoxamide and cinnabarinic acid for 5 min after adding the luciferase substrate, and BRET was then evaluated. In this experiment, lodoxamide served as a control. The experiment revealed that the reference ligand for hGPR35a, lodoxamide, has a pEC_{50} of 7.76 for recruiting arrestin-3 with hGPR35a while cinnabarinic acid showed pEC_{50} of 3.80 for hGPR35a interaction with arrestin-3 (Figure 4.20A).

I then used this new ligand in the G protein activation experiment with hGPR35a. To do this, hGPR35a was transfected into parental 293 cells as $G\alpha_{13}$ SPASM sensor. After luciferase substrate addition, cells were stimulated for 5 min with lodoxamide and cinnabarinic acid, and BRET was assessed. The results showed that lodoxamide had a pEC_{50} of 8.22 and could recruit $G\alpha_{13}$. On the other hand, cinnabarinic acid showed pEC_{50} of 4.08 in recruiting $G\alpha_{13}$ with hGPR35a (Figure 4.20B).

From the two experiments stated above, it can be claimed that the potency of cinnabarinic acid was very low (arrestin-3 recruitment and G protein activation) compared to the reference ligand lodoxamide for hGPR35a. One important aspect worth mentioning is the physical appearance of cinnabarinic acid. As the colour of cinnabarinic acid is red to very dark red, there was a very high signal observed in graph. This high signal point does not really interpret actual interactions with hGPR35a rather than an artefact of this assay due to its very bright colour. The low potency of cinnabarinic acid (arrestin recruitment and G protein activation)

for GPR35 will not probably attract the scientists to utilise this for future study and this will fail to stand up to further scrutiny.

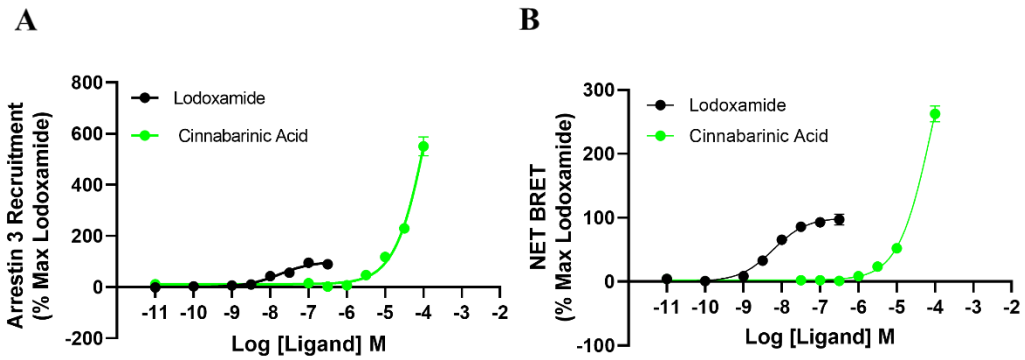

Figure 4.20 Validation of the potential of cinnabarinic acid as an endogenous agonist of GPR35
(A) Parental HEK293 cells were transfected transiently to express either hGPR35a-eYFP and arrestin-3-RLuc. Cells were exposed to the indicated concentrations of lodoxamide (black circles) and cinnabarinic acid (green circles) for 5 min and after substrate addition BRET was measured. **(B)** Comparison of effect of hGPR35a transiently expressed in parental HEK293 cells in $G\alpha_{13}$ SPASM sensors; BRET signals were monitored after treating with indicated concentrations of lodoxamide (black circles) and cinnabarinic acid (green circles) for 5 min. In both **(A)** and **(B)**, lodoxamide, the reference ligand was used as a control. This experiment was performed once only (n=1).

4.2.13 Contribution of some individual phosphorylation sites in GPR35 phosphorylation

A set of five phospho-acceptor amino acids near the C-terminal tail of the human GPR35 are phosphorylated in an agonist-mediated way to regulate the receptor (Divorty et al., 2022). Among these, I chose 2 important sites (Ser^{303} and Thr^{307}) and determined the contribution of these sites in the phosphorylation of hGPR35a by a BRET based arrestin-3 interaction assay. In this assay, I used the Ser^{303}Ala and Thr ^{307}Ala mutants along with hGPR35 (WT) and hGPR35 (PDM) as controls.

Here, parental 293 cells were transiently transfected to co-express (hGPR35a-eYFP WT), (hGPR35a-PDM-eYFP), (hGPR35a-eYFP Ser^{303}Ala), (hGPR35a-eYFP Thr ^{307}Ala), and arrestin-3 tagged with Renilla luciferase (arrestin-3-RLuc) (Figure 4.21). After luciferase substrate addition, cells were treated with lodoxamide for 5 min and BRET was measured. From this experiment, it was observed that hGPR35a-eYFP WT recruited arrestin-3 in response to lodoxamide in a concentration dependent way (pEC_{50} of 7.75). The full phospho deficient form of this receptor could not recruit arrestin-3 at all. There was also a significant

reduction of arrestin-3 recruitment when hGPR35a-eYFP Ser^{303}Ala and hGPR35a-eYFP Thr ^{307}Ala were used suggesting the potential contribution of these sites in arrestin-3 recruitment and, thereby, hGPR35a phosphorylation (Figure 4.21).

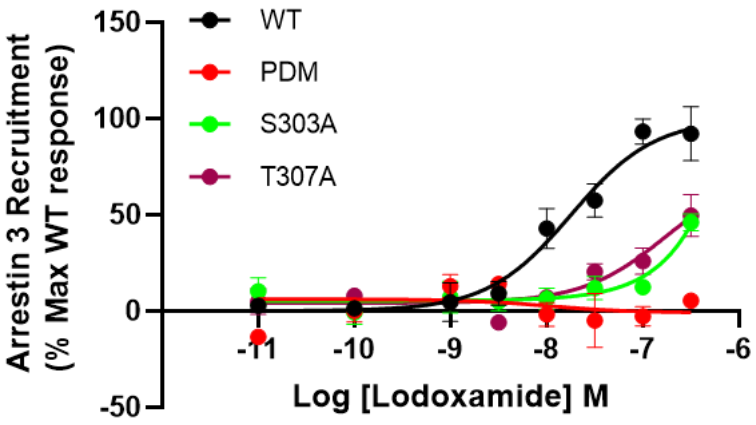

Figure 4.21 Role of some important phosphorylation site mutants in arrestin-3 recruitment Lodoxamide concentration–response curves for hGPR35a-eYFP WT (black circles), the phosphorylation-deficient mutant (*red circles*), Ser^{303}Ala (*green circles*) and Thr^{307}Ala (*maroon circles*) in arrestin-3 interaction assay. This experiment was performed once only (n=1).

4.3 Discussion

Agonist mediated phosphorylation of GPCRs is a key step in engaging GRKs and subsequent interaction with the isoforms of arrestin (Gurevich and Gurevich, 2019). Despite the fact that this phenomenon is well known for many GPCRs, a complete map of the identification of the precise sites of such posttranslational regulation and the degree to which each altered amino acid may contribute to the action is still rare. In this chapter, by utilising the knowledge of complete scenario of GPR35 phosphorylation and the contribution of individual amino acids for arrestin recruitment and phosphorylation (Divorty et al., 2022), novel phospho-site-specific antibodies were produced that eventually served as activation state-specific biosensors.

It was observed that Ser^{303} (and also Ser^{300}) were significant in arrestin recruitment to hGPR35a, along with the equivalent amino acids in mouse orthologues of GPR35. By developing phospho-specific antibodies to these amino acid pairs in the human receptor sequence and their equivalents in the mouse orthologue, it can be

certainly claimed that GPR35 may be differentially phosphorylated on these residues in physiologically relevant settings (Divorty et al., 2022). Very recently, the non-phospho-site GPR35 C-terminal tail antiserum was developed, and with this antiserum, it is possible to detect the total GPR35 receptors, particularly the non-phosphorylated portions, thereby playing its role as a promising biosensor.

Agonists caused the hydroxy-amino acids in the C-terminal tail of the receptor, the third intracellular loop, or both to be phosphorylated by G protein-coupled receptor kinases (GRKs), which was followed by interactions between the receptor and the arrestin protein. I stably expressed C-terminally HA epitope tagged versions of either human GPR35a (hGPR35a-HA) or mouse GPR35 (mGPR35-HA) in Flp-ln-TREx 293 cells to apply this to human GPR35a and its mouse counterpart mouse GPR35. I first probed cells with an anti-HA antibody to make sure that expression was, in fact, induced for each orthologue after treating such cells with doxycycline, which is expected to induce the expression of the receptor construct. Similarly, phosphorylation deficient versions of these cell lines were also generated and characterised to use those cell lines as control.

For characterising mGPR35-pSer^{298}/pSer^{301} antisera, a number of agonists were utilised to stimulate the Flp-In TREx 293 cells stably expressing mGPR35-HA. The phospho specific antisera clearly detected the phosphorylation signals mediated by different agonists. When a similar study was conducted in phosphorylation deficient versions of mouse receptor, mGPR35-pSer^{298}/pSer^{301} could not detect anything thereby validating that phosphorylation is dependent entirely on phospho serine and phospho threonine residues in the C-terminal tail of the mouse GPR35.

Given that GPR35 is highly expressed in colon crypts and because there is still evidence linking inflammatory disorders of the lower gastrointestinal tract to a single nucleotide polymorphism (T108M variant) in the protein's transmembrane III (Quon et al., 2020) deorphanisation and characterisation of the receptor is crucial. Although a significant number of synthetic ligands and the naturally occurring tryptophan metabolite kynurenic acid (Wang et al., 2006) can both activate this receptor, it is nevertheless classified as an orphan GPCR (Quon et al., 2020). To tackle this issue, I directly compared the phosphorylation potential of endogenous ligand kynurenic acid (Kaya et al., 2021) with a well-known synthetic ligand zaprinast (Taniguchi et al., 2006) using a cell line that stably

expresses mouse GPR35 with a HA epitope tag at C-terminus. The outcomes of the immunoblot based phosphorylation study demonstrated that in phosphorylation of mouse GPR35, the synthetic ligand zaprinast was more effective than the endogenous agonist kynurenic acid. An equivalent result was obtained when an arrestin recruitment experiment was conducted with mouse GPR35 using the endogenous ligand kynurenic acid and synthetic agonist zaprinast.

Studies were also undertaken to investigate whether GPR35 phosphorylation is agonist regulated or not. Flp-In TREx 293 cell lines were used to stably express both human and mouse orthologues of GPR35. After immunoblotting with GPR35 phosphorylation site specific antisera, both human and mouse GPR35 were phosphorylated upon stimulation with receptor specific agonists. When the receptors were stimulated with only vehicles, no detectable phosphorylation signals were noticed. Outcomes from the above experiments clearly revealed that phosphorylation of GPR35 is entirely agonist mediated.

For characterising hGPR35a-pSer^{300}/pSer^{303} antisera, a number of agonists, partial agonist and antagonist were employed in the Flp-In TREx 293 cells stably expressing hGPR35a-HA. Again, the phosphorylation site specific antisera could not identify the receptor polypeptide(s) in vehicle treated cells but the same phospho- specific antisera clearly detected the phosphorylation signals mediated by two full agonists lodoxamide and zaprinast. Upon stimulation with pamoic acid, which is a partial agonist of hGPR35a, faint signal of receptor phosphorylation was detected by the hGPR35a-pSer^{300}/pSer^{303} antisera thereby again justifying its partial agonism to the receptor. After addition of the human specific GPR35a antagonist, CID-2745687, there was no significant phosphorylation noticed by the phospho-specific antisera. It was also anticipated because of its antagonistic features to the receptor. In addition, the antagonist CID-2745687 successfully reversed the phosphorylation effects mediated by lodoxamide and this was evident by the lack of immunodetection with the hGPR35a-pSer^{300}/pSer^{303} antibody. When a similar study was carried out on human receptors lacking phosphorylation, hGPR35a-pSer^{300}/pSer^{303} was unable to detect anything, proving that phosphorylation is fully dependent on phospho serine and phospho threonine residues in the C-terminal tail of human GPR35a. The above set of experiments involving both wild type and phosphorylation deficient version of hGPR35a employed different agonists, partial agonist, and antagonist and thus accurate

pharmacology of the hGPR35a was depicted. This certainly validated the accuracy of phospho-site–specific antisera in cell lines expressing human orthologue of GPR35.

The GPR35 receptor is distinctive in a number of ways that make translation challenging. Humans express two distinct protein isoform sequences as opposed to the single protein isoform expressed by rodents. The pharmacology of the GPR35 orthologues differs greatly between rodents and humans. Moreover, there are GPR35 agonists and antagonists whose activity is species-specific. In this chapter, an attempt was made to validate the species selectivity of hGPR35a partial agonist pamoic acid and antagonist CID-2745687. As pamoic acid was identified as a partial agonist of hGPR35a, it was used to stimulate the mGPR35 in a cell line stably expressing mGPR35-HA. After immunoblotting with mGPR35pSer^{298}/pSer^{301} antiserum, there was no phosphorylation signal detected. This proved the inability of pamoic acid to phosphorylate the mouse orthologue of GPR35. Again, CID-2745687 was claimed to show antagonism only for hGPR35a. After using the antagonist molecule CID-2745687, prior to the addition of agonist zaprinast, there was still a visible phosphorylation signal detected by mGPR35pSer^{298}/pSer^{301} antiserum in mouse orthologue of receptor suggesting that this antagonist is only human species selective of the receptor. In this way, validation of species selectivity of agonist and antagonist were documented.

After successfully characterising the phosphorylation site specific antisera for both orthologues of GPR35 by immunoblotting techniques, an effort was made to achieve the same results in an immunocytochemical assay with these antibodies. In Flp-In TREx 293 cells stably expressing hGPR35a-HA, zaprinast was employed to stimulate the receptor and specific signal was detected not only in punctate intracellular vesicles but also at the cell surface upon applying hGPR35a-pSer^{300}-pSer^{303}antisera. A similar sort of experiment was also carried out in Flp-In TREx 293 cells induced to express human GPR35-PDM-HA. Immunocytochemical investigations using hGPR35a-pSer^{300}-pSer^{303}antisera failed to recognise hGPR35-PDM-HA, although simultaneous detection by anti-HA antibody ensured the presence of receptor protein. The above experiments successfully confirmed that hGPR35a-pSer^{300}-pSer^{303}antisera could clearly detect phosphorylation signals of hGPR35a-HA in an immunocytochemical based assay.

Due to the considerable differences in the pharmacology of the GPR35 orthologues in human and mouse, phosphorylation site specific antisera were also employed in immunocytochemical experiments to detect the phosphorylation status of mGPR35-HA. Again, in In Flp-In TREx 293 cells stably expressing mGPR35-HA, mGPR35-pSer^{298}-pSer^{301}antisera detected the relevant receptors only after being stimulated with agonist zaprinast. The distinct signal of phosphorylated mGPR35 construct was mostly seen at the cell surface and in punctate intracellular vesicles. When a similar study was undertaken in a Flp-In TREx system expressing mouse GPR35-PDM-HA, mGPR35-pSer^{298}-pSer^{301}antisera could not detect the receptor, although the persistent presence of the receptor protein was ensured by anti-HA antibody. The aforementioned tests successfully demonstrated that mGPR35-pSer^{298}-pSer^{301}antisera are capable of accurately detecting mGPR35a-HA phosphorylation signals in an immunocytochemical study.

As phosphorylation site specific antibody had been used in immunoblot and immunocytochemical studies throughout this chapter to identify the post activation status of GPR35, there is a requirement of appropriate control to ensure that the antibodies actually are identifying the pSer^{300}, pSer^{303}, or both sites. For this reason, a phosphatase enzyme called Lambda protein phosphatase was employed. This enzyme usually chops or releases phosphate groups from phosphorylated serine or threonine of the receptor protein and, in this way, eliminates any scope of phosphorylation. In this chapter, a cell line stably expressing human GPR35a-eYFP was stimulated with agonist. Following treatment with Lambda protein phosphatase and separated by SDS-PAGE, hGPR35a-pSer^{300}-pSer^{303}antisera failed to detect the receptor. On the other hand, phospho-site specific antisera detected the protein samples that were untreated with λ-PPase. From this study, it is clear that as λ-PPase releases phosphate groups from phosphorylated serine, threonine, and tyrosine residues in proteins (Zhuo et al., 1993), and hGPR35a-pSer^{300}-pSer^{303}antisera was unsuccessful in identifying the receptor. The antisera actually detected the pSer^{300}, pSer^{303} of hGPR35a.

Throughout the phosphorylation studies with both orthologues of GPR35, differential N-glycosylation of the receptor protein was observed. Different glycosylation states of the receptor GPR35 were also evident previously (Jenkins et al., 2011). After observing multiple forms of GPR35, the enzyme N-glycosidase F was employed. When the samples were resolved by SDS-PAGE, carbohydrates

were removed and a single anti-HA immunoreactive band was visible. This study confirmed the multiple forms of the receptor upon glycosylation.

After gaining proper knowledge from a combination of mass spectrometry, detection of amino acids that undergo [^{32}P] incorporation and mutagenesis for defining the contribution of particular amino acids in arrestin recruitment, designing and development of phosphorylation-site-specific antisera was accomplished. These antisera were then successfully employed as biosensors to identify and recognise the post-activation status of both human and mouse orthologue of GPR35.

Finally, it can be stated that phospho-site-specific antisera against the area enclosing Ser^{303} in human (Ser^{301} in mouse) GPR35a were effective sensors for determining the activation status of the receptors in both immunoblotting and immunocytochemical experiments. In addition, these antisera only recognised mature versions of GPR35. From the outcomes of all of the experiments in this chapter, it can be claimed with confidence that these antibodies could be helpful tools to assess target engagement in drug discovery and target validation operations.

The recent investigations offer a thorough examination of the mechanisms of GPR35 phosphorylation as well as novel reagents that will be extremely helpful in elucidating pathophysiological functions of GPR35 and the possibility of therapeutically targeting them.

Chapter 5 Investigation of the role of G-protein receptor kinases (GRKs) in regulating phosphorylation of the orphan G protein-coupled receptor35 (GPR35)

5.1 Introduction

G protein-coupled receptors (GPCRs) are cell surface proteins that play key roles in allowing cells to respond to external signals and cues. They are responsible for activating cellular responses to numerous bioactive molecules, including odorants, pheromones, hormones, and neurotransmitters (Lefkowitz, 2007). GPCRs interact with many transducers, such as heterotrimeric G proteins, GPCR kinases (GRKs), and arrestins. GPR35 is a poorly characterised member of the rhodopsin like, class A subfamily of GPCRs, which because of its expression pattern is an attractive target for the development of novel therapeutics (Jenkins et al., 2012, Milligan, 2023). Recently, this orphan receptor has attracted great interest as a therapeutic target in conditions ranging from non-alcoholic steatohepatitis to lower intestinal inflammation (Quon et al., 2020, Milligan, 2023).

An essential part of GPCR signalling is the agonist-dependent phosphorylation of receptor intracellular domains, which has a significant impact on the desensitisation of G protein signalling, the internalisation and recycling of the receptor, and the receptor's ability to stimulate G protein independent signalling (Nobles et al., 2011). Since the phosphorylation of the active receptor by specialised kinases (GRKs) and subsequent binding of arrestin proteins end the signalling of most GPCRs via G proteins, (Figure 5.1), the in-depth analysis of the sites and mechanism of agonist regulated phosphorylation of GPCRs and the contribution of an individual or multiple GRK isoforms in regulating the phosphorylation are of paramount importance.

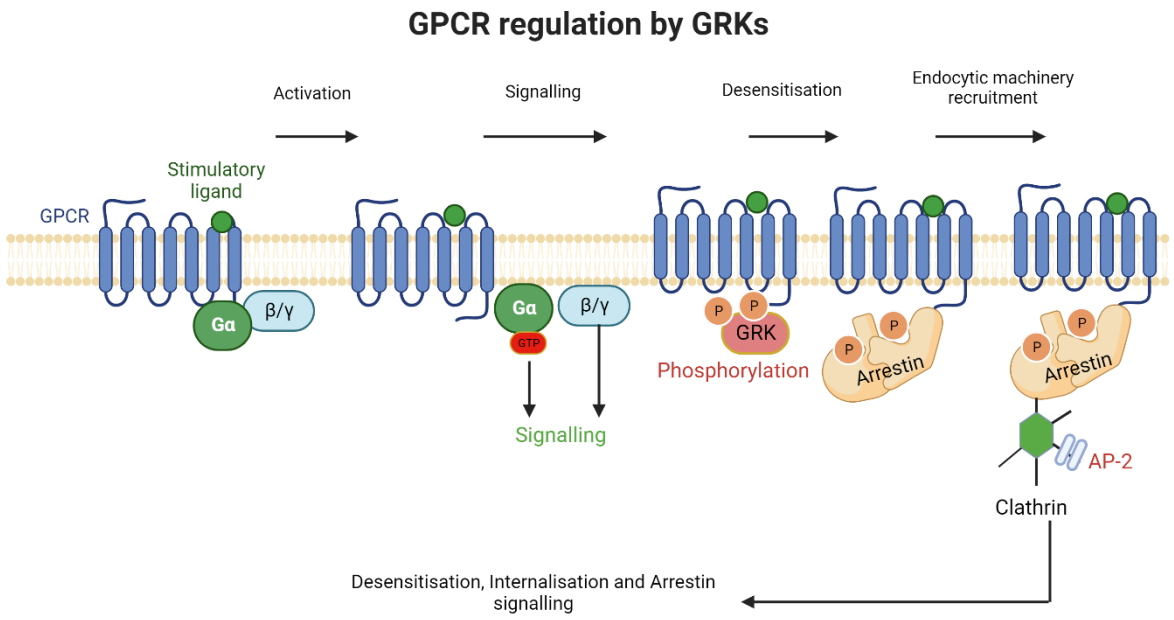

Figure 5.1 Demonstration of GRK mediated regulation of GPCRs
GPCRs are transmembrane proteins that are primarily found in plasma membrane. Agonist binding activates GPCRs. Active receptor binds inactive heterotrimeric G protein consisting of α-, β-, and γ-subunits. Receptor binding leads to formation of GTP-liganded G protein which then dissociates from the receptor as a distinct α-subunit-GTP and βγ-dimer, both of which can interact with different effector proteins to initiate signalling. Active GPCRs are detected by specialised GPCR kinases (GRKs) that phosphorylate many GPCRs at the C-terminus. Arrestins bind active phosphorylated GPCRs and via direct contacts recruit main components of the endocytic machinery of the coated pit, clathrin, and clathrin adaptor AP-2, thereby promoting receptor internalisation. Moreover, arrestin can also induce G protein-independent signalling. This figure was created with BioRender.com.

Two kinds of serine/threonine kinases at least control the phosphorylation of GPCRs. The first type consists of second messenger-dependent kinases like PKA or PKC that can cause heterologous desensitisation by phosphorylating receptors independently of receptor-ligand interaction (Yang et al., 2017). The second class consists of the GPCR kinases, a family of seven second messenger-independent kinases (GRK1 to GRK7). They control the phosphorylation of GPCRs in an agonist-dependent way (Yang et al., 2017).

The unique regulator of the G protein signalling homology (RH) domain, which flanks the kinase domain and controls GPCR phosphorylation, distinguishes GRKs from other members of the AGC kinase superfamily. The RH domain is made up of two subdomains: a bundle subdomain that forms intramolecular contacts with the kinase C-lobe and a terminal subdomain whose peptide sequence feeds into the kinase N-lobe. Additionally, GRKs feature an N-terminal α-helix (αN-helix), which is required for kinase function. The GRK C-terminus differs amongst subfamilies and mediates lipid binding for membrane localisation and GPCR targeting (Sulon and Benovic, 2021, Komolov and Benovic, 2018). It has been demonstrated that

binding to active GPCRs causes GRKs to become allosterically active (Palczewski et al., 1991). Although the exact mechanism of this interaction has not yet been determined for each receptor, x-ray crystallography and cryo-EM structure of GPCRs-GRKs certainly provide insights that interaction mainly happens through the insertion of an N-terminal α-helix of GRKs into the GPCR's cytoplasmic cavity. This technique of GRK-binding is extremely intriguing since G proteins and arrestins probe for active GPCR conformations in a similar manner, even though structural evidence is not always definitive (Cato et al., 2021). Active GPCRs are phosphorylated at their intracellular locations as a result of GRK-binding in a cellular setting. There are two families of non-visual GRKs (Homan and Tesmer, 2014). GRK2 and GRK3 constitute the GRK2 family and are expressed in the cytosol. Following GPCR activation, GRK2 and 3 are attracted to the membrane, which is made possible by the creation of GPCR complexes and stabilising connections with Gβγ-subunits (Tesmer et al., 2005, Kawakami et al., 2022). GRK4, 5, and 6 are members of the GRK4 family of kinases, which are typically membrane-associated.

Although the critical roles of GRKs in the phosphorylation and regulation of many GPCRs are widely acknowledged in the scientific community, the precise contribution of particular GRKs has frequently been poorly investigated and described (Sulon and Benovic, 2021). The regular co-expression of several GRK isoforms and the constrained selection of well-studied small molecule inhibitors of particular GRKs or subsets of the larger group have both contributed to this. Significant obstacles include accurately identifying phosphorylation sites and connecting them to the activity of particular GRKs or other protein kinases, as well as the regulation of particular physiological responses. Utilising mass spectrometry-based phospho-proteomics, our group has already addressed this obstacle by enabling the rational design of receptor phospho-site specific antibodies (Marsango et al., 2022, Divorty et al., 2022).

GPR35's agonist-induced phosphorylation is located inside the relatively short intracellular C-terminal tail, and it has been mapped by the use of mutagenesis, mass spectrometry, and [^{32}P] labelling (Divorty et al., 2022). These studies indicated that phosphorylation of Ser^{300} and Ser^{303} in human GPR35a, and of the equivalent residues in the mouse and rat orthologues, were important to successful interactions of the receptor with arrestin-3. Additionally,

phosphorylation of these residues occurred in an almost agonist-dependent manner. Although mass spectrometry, [^{32}P] labelling and mutagenesis contributed a lot to getting insight into GPR35 phosphorylation, we still have limited knowledge about the specific contribution of individual GRK in phosphorylation and regulation of this receptor. To further pinpoint the contribution of individual or a group of GRKs in GPR35 phosphorylation, I used combinations of GRK subtype knock-out cell lines (Drube et al., 2022) and reconstitution of function with individual GRKs, a pSer^{300}-pSer^{303} human GPR35a directed antiserum and a group of selective small molecule GRK inhibitors (Uehling et al., 2021, Varney et al., 2022) and ultimately proved that GRK5 and 6 are the key mediators of both the phosphorylation of Ser^{300} and Ser^{303} in human GPR35 and of the effective interactions of this receptor with arrestins, a process directly related to receptor internalisation. Arrestins play significant roles in the regulation of GPCRs. Although GRKs mediated phosphorylation reduces signalling via the G protein of some receptors like β_2 Adrenergic receptor (Benovic et al., 1989), it did not stop it. Therefore, arrestins are a second group of players who are suspected.

5.1.1 Aims

For a long time, it has been understood that the GRK family plays a crucial role in the regulation of GPCRs and in fostering connections with arrestin adaptor proteins (Gurevich and Gurevich, 2019). Despite this, there is little known about the nature of the GRKs that interact with and control specific receptors and phosphorylated residues. Additionally, it is yet unclear how the concept of phosphorylation "bar-coding" relates to the phosphorylation of certain serine and/or threonine residues within the intracellular parts of GPCRs. Although a set of phosphorylation codes has been validated to serve as a common mechanism for phosphorylation-dependent recruitment of arrestins by GPCRs (Zhou et al., 2017), there remain many challenges to a clear understanding of cellular response variations to agonists in different cell types and tissues (Prihandoko et al., 2015, Butcher et al., 2011). Fortunately, there have been new developments that are helping to address these problems. Prominent among these has been the capacity to define locations of controlled phosphorylation by unbiased mass spectrometry (Marsango et al., 2022). The creation of genome-edited cell lines lacking expression of one or more of the ubiquitously expressed GRK isoforms, GRK2, GRK3, GRK5 and GRK6 also offers new approaches for defining GRK selectivity and

functional restoration (Drube et al., 2022). Moreover, significant knowledge has been gained via the creation of both selective small molecule GRK inhibitors (Uehling et al., 2021) and similarly, phospho-site specific antisera (Divorty et al., 2022) that identify locations of controlled or constitutive phosphorylation within GPCRs. As GPR35 is expressed significantly in the crypts of the colon and lower gut, there is strong scientific evidence that agonism of GPR35 might be an effective therapeutic strategy in the treatment of ulcerative colitis and related disorders. Thus, a major goal is to clearly grasp how GRK isoforms control GPR35 phosphorylation and ultimately regulation.

The main objectives of this chapter were

To investigate and confirm the contribution of GRKs for the efficient interaction between hGPR35a and arrestin

To determine the specific contribution of a sub-group of GRKs to allow agonist mediated hGPR35a and arrestin interaction in genome edited HEK293-derived cell lines engineered to lack expression of either GRK2 and GRK3 (ΔGRK2/3) or GRK5 and GRK6 (ΔGRK5/6)

Determination of the contribution of individual reconstituted GRK in genome edited knock out cells lacking expression of all endogenous GRKs

Investigation of the phosphorylation of human and mouse orthologues of GPR35 by phospho site specific antibodies and a GPR35 C-terminal antibody

Measurement of the efficacy of different GRK inhibitor compounds in abolishing receptor phosphorylation

Determination of the ability of different GRK inhibitors to prevent arrestin recruitment by GPR35

Assessment of the contribution of GRKs in receptor phosphorylation by agonist induced immunocytochemical study.

5.2 Results

5.2.1 Investigating the contribution of one or more GRK isoforms in agonist-induced interactions between human GPR35a and arrestin

Parental 293 cells were transiently transfected to co-express human (h)GPR35a, tagged at the C-terminus with eYFP (hGPR35a-eYFP), and arrestin-3 tagged with Renilla luciferase (arrestin-3-RLuc) (Figure 5.2 A). In the presence of a luciferase substrate, the addition of the GPR35 agonist lodoxamide, which displays high potency at human GPR35 (MacKenzie et al., 2014), resulted in a concentration-dependent increase in measured bioluminescence resonance energy transfer (BRET) (Figure 5.2A) with pEC_{50} 8.06 ± 0.06 (mean± SEM, n=3 for wild type). Equivalent studies using a previously characterised C-terminal phospho-acceptor site-deficient mutant of hGPR35a (hGPR35a-PDM-eYFP) (Divorty et al., 2022) in which all 5 of the serine/threonine residues within the receptor C-terminal tail had been changed to alanines resulted in no detectable increase in BRET signal (Figure 5.2A). One or more GRK family members were necessary for the receptor and arrestin-3 to engage in response to lodoxamide. This was demonstrated by the fact that even when using wild-type hGPR35a-eYFP, only a very weak response to lodoxamide was seen when such studies were carried out in a clone of HEK293 cells that had been genetically modified to lack all four of the widely expressed GRK isoforms (ΔGRK2/3/5/6) (Drube et al., 2022) (Figure 5.2A). As anticipated from the above, no response to lodoxamide was observed when hGPR35a-PDM-eYFP and arrestin-3-RLuc were co-introduced into ΔGRK2/3/5/6 HEK293 cells (Figure 5.2A). Similar outcomes (lodoxamide pEC_{50} 7.71 ± 0.07 (mean± SEM, n=3 for wild type) were produced when arrestin-3-RLuc was substituted with arrestin-2-Rluc (Figure 5.2B).

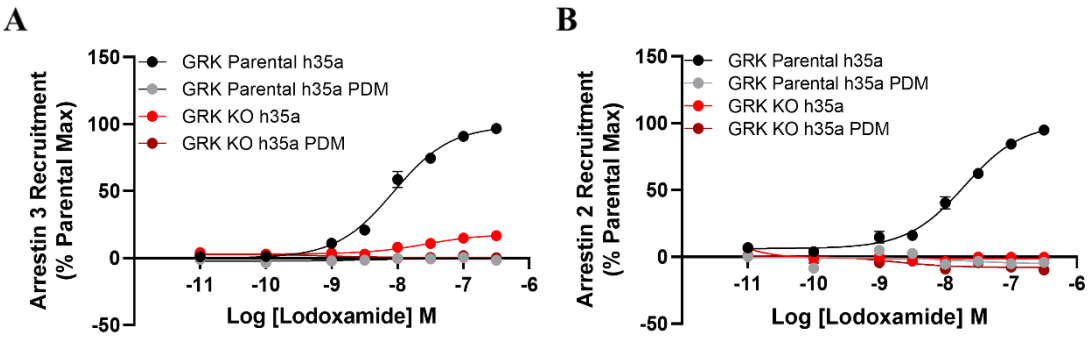

Figure 5.2 Agonist-induced interactions between human GPR35a and arrestin-3 and arrestin-2 require the presence of one or more GRK isoforms
Parental HEK293 cells were transfected transiently to express either hGPR35a-eYFP (black circles) or hGPR35a-PDM-eYFP (grey circles) and arrestin-3-RLuc **(A)** or arrestin-2-RLuc **(B)**. A clone genome-edited to lack expression of each of GRK2, GRK3, GRK5 and GRK6 (ΔGRK2/3/5/6) was transfected transiently to express either hGPR35a-eYFP (red circles) or hGPR35a-PDM-eYFP (maroon circles) and arrestin-3-RLuc or arrestin-2-RLuc. Cells were exposed to the indicated concentrations of lodoxamide for 5 min and after substrate addition BRET was measured. Data are the mean ± SEM of outcomes from three independent experiments.

5.2.2 Assessment of the specific contribution of a sub-group of GRKs to allow agonist-mediated hGPR35a and arrestin interaction in engineered HEK293-derived cell lines

5.2.2.1 Contribution of a sub-group of GRKs in arrestin recruitment of hGPR35a and small molecule inhibition of these kinases phenocopies genetic knock-out

GRK2 and GRK3 form a subfamily of the widely expressed GRKs, as do GRK5 and GRK6 (Sulon and Benovic, 2021, Benovic, 2021). To define which GRK isoform(s) might promote agonist-induced hGPR35a/arrestin-3 and arrestin-2 interactions I initially used a combination of HEK293-derived cell lines engineered to lack expression of either GRK2 and GRK3 (ΔGRK2/3) or GRK5 and GRK6 (ΔGRK5/6) (Drube et al., 2022), alongside selective small molecule inhibitors. When introduced into ΔGRK5/6 cells, hGPR35a-eYFP and arrestin-3-RLuc did not cause lodoxamide to generate BRET, but rather phenocopied the findings in ΔGRK2/3/5/6 cells (Figure 5.3A). By contrast, after co-transfection of hGPR35a-eYFP and arrestin-3-RLuc into ΔGRK2/3 cells, the addition of lodoxamide generated BRET signals (Figure 5.3A) very similar in potency (pEC_{50} 8.09 ± 0.03 (mean± SEM, n=3) and, indeed, slightly larger in magnitude, than those in parental HEK293 cells. Compound 101 (3-[[[4-methyl-5-(4-pyridyl)-4H-1,2,4-triazole-3-yl] methyl] amino]-N-[2-(trifuoromethyl) benzyl] benzamidehydrochloride) is a well-studied, small molecule GRK2/3 selective inhibitor (Lowe et al., 2015, Thal et al.,

2011). Pre-addition of compound 101 (10 μM) did not affect the ability of lodoxamide to enhance hGPR35a-eYFP-arrestin-3-RLuc connections in either wild-type or ΔGRK2/3 cells (Figure 5.3B). Inhibitors of GRK5/6 have not been as extensively researched and produced. However, 'compound 19' ((S)-N2-(1-(5-chloropyridin-2-yl) ethyl)-N4-(5-ethyl-1H-pyrazol-3-yl)-5-methoxyquinazoline-2,4-diamine) (10 μM) reported as one of a series of GRK5/6-selective inhibitors (Uehling et al., 2021, Varney et al., 2022) was able to fully prevent lodoxamide-mediated hGPR35a-eYFP-arrestin-3-RLuc interactions in both parental and ΔGRK2/3 293 cells (Figure 5.3B). Similar sets of experiments were conducted with hGPR35a and arrestin-2. Here, also after co-transfection of hGPR35a-eYFP and arrestin-2-RLuc into ΔGRK2/3 cells, addition of lodoxamide generated BRET signals (Figure 5.3C) very similar in potency (pEC_{50} 7.76 ± 0.06 (mean± SEM, n=3) and, indeed, slightly larger in magnitude, than those in parental HEK293 cells, while almost no BRET signal in either ΔGRK5/6 or ΔGRK2/3/5/6 cells was noticed after lodoxamide induced hGPR35a/arrestin-2 interactions (Figure 5.3C). Similar results were obtained when arrestin-3-RLuc was substituted with arrestin-2-RLuc following the addition of inhibitor compounds 101 or 19 (Figure 5.3D).

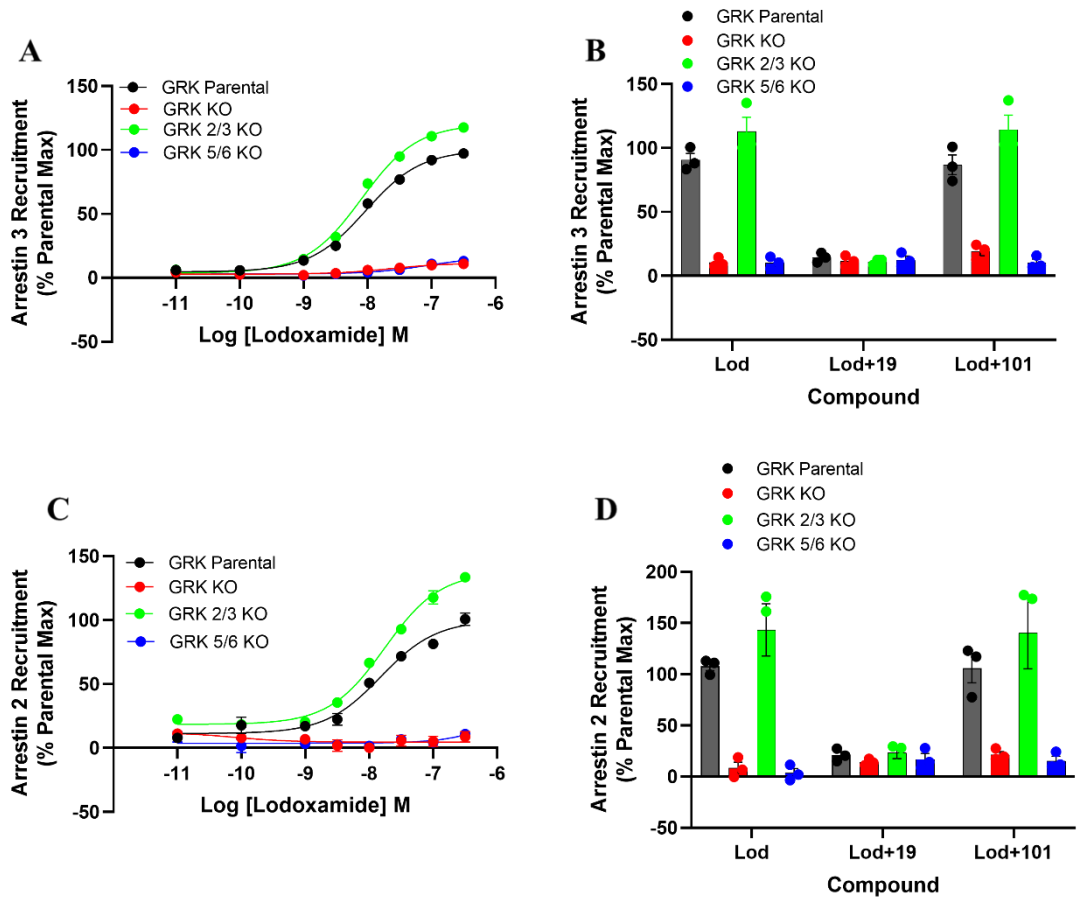

Figure 5.3 GRK5 and/or GRK6 but not GRK2 and/or GRK3 are essential to allow agonist-promoted human GPR35a-arrestin-3 and arrestin-2 interactions
Studies akin to **Figure 5.2** were performed after transient co-expression of hGPR35a-eYFP and **(A) (B)** arrestin-3-RLuc and **(C) (D)** arrestin-2-RLuc into each of parental HEK293 cells (black circles) or a clone genome-edited to lack expression of GRK2 and GRK3 (ΔGRK2/3) (green circles), GRK5 and GRK6 (ΔGRK5/6) (blue circles) or all four of these GRKs (ΔGRK2/3/5/6) (red circles). **(A)** and **(C)**, Cells were exposed to the indicated concentrations of lodoxamide for 5 min and after substrate addition BRET was measured. Data are the mean ± SEM of outcomes from three independent experiments. **(B)** and **(D)**, Cells were exposed to 100 nM lodoxamide for 5 min after pre-exposure or not to either compound 19 or compound 101 (each at 10 μM) for 30 min. Data show individual outcomes from three independent studies.

5.2.2.2 Comparative effects of a group of kinase inhibitors on arrestin recruitment

From the previous experiment, it was found that GRK5/6 inhibitor compound 19 was able to prevent the agonist-mediated arrestin recruitment for hGPR35a. On the other hand, compound 101, a well-known GRK2/3 inhibitor could not do this. I then decided to use some additional compounds from this series, including compounds 15, 16, 17 and 18 along with 19 (Uehling et al., 2021) to assess their inhibitory potential of both arrestin-3 and arrestin-2. Compound 101 was also used in this study. From the experiments, it was found that compound 15 and compound 19 (each at 10 μM) fully prevented lodoxamide induced hGPR35a-eYFP-arrestin-3-RLuc interactions in both parental and ΔGRK2/3 293 cells. Compound 16 and

compound 17 (each at 10 μM) also showed prominent activity in preventing lodoxamide induced arrestin-3 recruitment. The other member of this series compound 18 and GRK2/3 inhibitor compound 101 were without any effects to inhibit arrestin recruitment in both parental and ΔGRK2/3 293 cells (Figure 5.4A). When a similar experiment was conducted with all the compounds in inhibition of arrestin-2 recruitment, equivalent findings were replicated (Figure 5.4B).

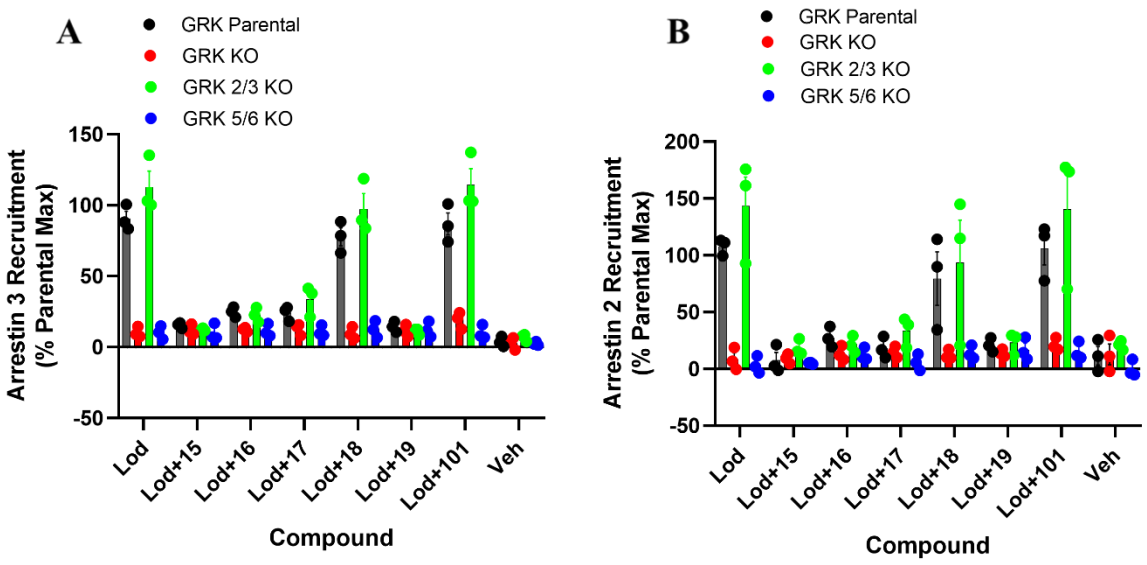

Figure 5.4 A selection of compounds with GRK5/6 inhibitory activity prevent interactions between human GPR35a and arrestin-3 and arrestin-2
Studies akin to **Figure 5.3** were performed after transient co-expression of hGPR35a-eYFP and **(A)** arrestin-3-RLuc and **(B)** arrestin-2-RLuc into each of parental HEK293 cells (black circles) or a clone genome-edited to lack expression of GRK2 and GRK3 (ΔGRK2/3) (green circles), GRK5 and GRK6 (ΔGRK5/6) (blue circles) or all four of these GRKs (ΔGRK2/3/5/6) (red circles). Cells were exposed to 100 nM lodoxamide for 5 min after pre-treatment with either vehicle or the indicated GRK5/6 inhibitor compounds (15-19) and compound 101 (each at 10 μM) for 30 min. After substrate addition BRET was measured. Data show individual outcomes from three independent studies.

5.2.3 Investigation of the role of kinase reconstitution in genome edited HEK293-derived cell lines on agonist-induced interactions between human GPR35a and arrestin

5.2.3.1 Comparison among a group of kinase inhibitors on arrestin recruitment upon reconstitution of GRKs

For investigating the role of particular GRKs after reconstitution and to explore the inhibitory capacity of the kinase inhibitors, ΔGRK2/3/5/6 cells were transfected transiently with human GPR35a-eYFP and arrestin-3-RLuc alongside LgBiT-tagged forms of each of the ubiquitously expressed GRKs. Here, pre-

treatment with compound 101 (10 μM) could not inhibit GRK5/6 mediated arrestin-3 recruitment by lodoxamide. However, the addition of compound 19 (10 μM) prior to treatment with lodoxamide was able to fully prevent GRK5/6 mediated interaction of hGPR35a with arrestin-3 (Figure 5.5A). Equivalent results were found with compound 101 and compound 19 in arrestin-2 recruitment inhibition, suggesting important roles of GRK5 and 6 in hGPR35a phosphorylation (Figure 5.5B). To extend this analysis, I wished to use some other kinase inhibitor compounds from this series. Here again, I transfected human GPR35a-eYFP and arrestin-3-RLuc alongside GRK2,3,5, and 6 with LgBiT-tags into ΔGRK2/3/5/6 cells. It was found that compound 15 and compound 19 (each at 10 μM) fully prevented lodoxamide induced GRK5/6 mediated hGPR35a-eYFP-arrestin-3-RLuc interactions. Compound 16 and compound 17 (each at 10 μM) also demonstrated inhibition of GRK5/6 mediated arrestin-3 recruitment. Another compound from this series, compound 18 showed modest inhibitory activity, whilst the GRK2/3 inhibitor, compound 101 did not show any effect on GRK5/6 mediated arrestin-3 interaction with hGPR35a (Figure 5.5C). Similar findings were obtained when the inhibitory potentials of the kinase inhibitors were measured on GRK reconstitution mediated arrestin-2 interaction with hGPR35a (Figure 5.5D).

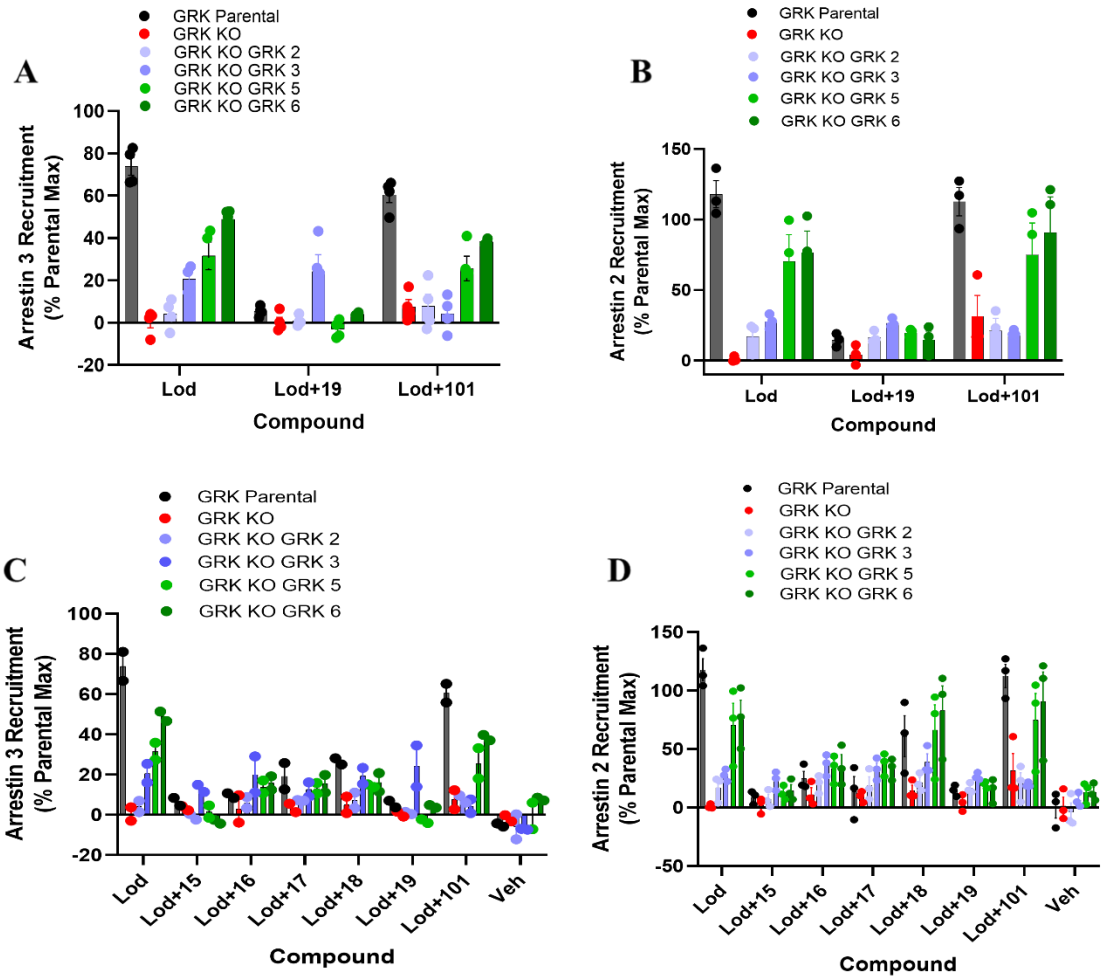

Figure 5.5 GRK5 and/or GRK6 play key roles in allowing agonist-promoted human GPR35a-arrestin-3 and arrestin-2 interactions and these interactions are prevented by GRK5/6 inhibitors

ΔGRK2/3/5/6 cells were transfected transiently with combinations of human GPR35a-eYFP and **(A)** and **(C)** arrestin-3-RLuc and **(B)** and **(D)** arrestin-2-RLuc alongside LgBiT-tagged forms of each of GRK2 (light blue circles), GRK3 (deep blue circles), GRK5 (light green circles), and GRK6 (deep green circles). **(A**) and **(B)** Cells were exposed to 100 nM lodoxamide for 5 min after pre-exposure or not to either compound 101 or compound 19 (each at 10 μM) for 30 min. **(C)** and **(D)** Cells were exposed to 100 nM lodoxamide for 5 min after pre-treatment with either vehicle or the indicated GRK5/6 inhibitor compounds (15-19) and compound 101 (each at 10 μM) for 30 min. After substrate addition BRET was measured. Data for wild type HEK293 (black circles) and ΔGRK2/3/5/6 cells without the introduction of a GRK (red circles) were provided for reference. Data show individual outcomes from three independent studies.

5.2.3.2 GRK5 and GRK6 reconstitution significantly influences arrestin recruitment

To further verify the outcomes obtained from the individual GRK isoforms, I transiently introduced hGPR35a-eYFP and arrestin-3-RLuc into ΔGRK2/3/5/6 293 cells alongside plasmids able to express each of GRK2, GRK3, GRK5 and GRK6. In this case, the hGPR35a-eYFP/arrestin-3 interactions produced by lodoxamide was

substantially restored by introducing either GRK5 or GRK6. In contrast, the effects of introducing GRK2 or GRK3 were significantly less noticeable (Figure 5.6A). Similar findings were replicated when similar experiments were conducted to measure the recruitment of arrestin-2 (Figure 5.6B). The outcome of these studies strongly supports that GRK5/6 are mainly responsible for arrestin recruitment to hGPR35a. As experiments were performed in cells that have been genome edited to lac expression of all commonly used GRKs, there is no influence of endogenous kinases, thereby pinpointing the contribution of each reconstituted GRK.

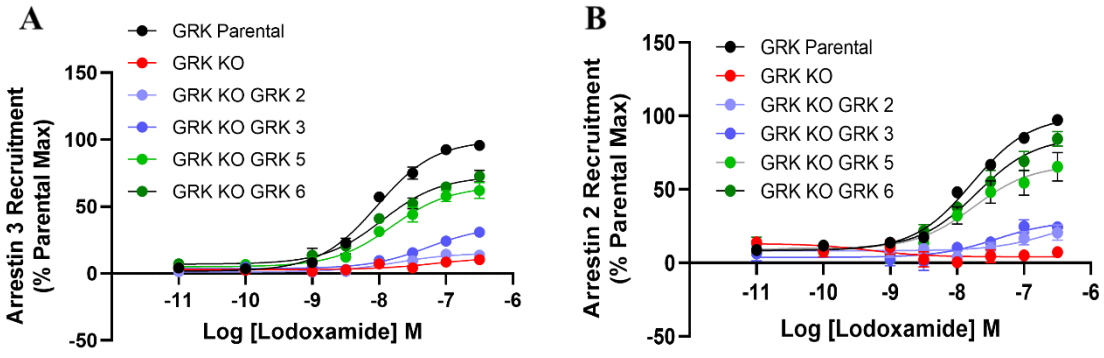

Figure 5.6 Both GRK5 and GRK6 can allow agonist-mediated human GPR35a-arrestin-3 and arrestin-2 interactions
ΔGRK2/3/5/6 cells were transfected transiently with combinations of human GPR35a-eYFP and **(A)** arrestin-3-RLuc and **(B)** arrestin-2-RLuc alongside LgBiT-tagged forms of each of GRK2 (light blue circles), GRK3 (deep blue circles), GRK5 (light green circles), and GRK6 (deep green circles). Subsequently the ability of varying concentrations of lodoxamide to promote BRET signals reflecting GPR35a-eYFP-arrestin-3-RLuc/arrestin-2-RLuc proximity and/or interactions were recorded. Data for wild type HEK293 (black circles) and ΔGRK2/3/5/6 cells without the introduction of a GRK (red circles) were provided for reference. Data are the mean ± SEM of outcomes from three independent experiments.

5.2.3.3 GRK5/6 inhibitor compound 19 prevents arrestin recruitment to hGPR35a

To support the role of GRK5/6 in arrestin recruitment to hGPR35a, I employed different concentrations of compound 19 (GRK5/6 inhibitor) to assess its arrestin inhibitory activity. GRK2/3 blocker, compound 101 was also used. Here, in ΔGRK2/3/5/6 293 cells that had been transiently transfected with either GRK2 or GRK3, the limited extent of lodoxamide-induced hGPR35a-eYFP-arrestin-3-RLuc interactions was inhibited by pre-treatment with compound 101 (pIC_{50} 6.20 ± 0.59 (mean± SEM, n=3) for GRK2 and (pIC_{50} 6.13 ± 0.25 (mean± SEM, n=3) for GRK3 (Figure 5.7A). On the other hand, following introduction of GRK5 or GRK6 into ΔGRK2/3/5/6 293 cells, lodoxamide-induced hGPR35a-eYFP/arrestin-3-RLuc

interactions were again inhibited by compound 19 in a concentration-dependent manner with (pIC_{50} 5.34 ± 0.15 (mean± SEM, n=3) for GRK5 and (pIC_{50} 4.95 ± 0.29 (mean± SEM, n=3) for GRK6 (Figure 5.7A). When I did similar assays where hGPR35a interacted with arrestin-2, again the limited extent of lodoxamide-induced hGPR35a-eYFP-arrestin-2-RLuc interactions by GRK2 or GRK3, was inhibited by pre-treatment with compound 101 (pIC_{50} 7.04 ± 0.41 (mean± SEM, n=3) for GRK2 and (pIC_{50} 6.54 ± 0.25 (mean± SEM, n=3) for GRK3 (Figure 5.7B). By contrast, lodoxamide-induced hGPR35a-eYFP/arrestin-2-RLuc interactions were again inhibited by compound 19 in a concentration-dependent manner after the introduction of GRK5 or GRK6 into ΔGRK2/3/5/6 293 cells, with (pIC_{50} 5.72± 0.07 (mean SEM, n=3) for GRK5 and (pIC_{50} 5.66± 0.08 (mean SEM, n=3) (Figure 5.7B). As indicated concentrations of compound 19 can fully inhibit agonist induced arrestin-3 and arrestin-2 interaction with hGPR35a, it strongly supports the hypothesis that GRK5/6 play key roles in the arrestin recruitment and, thereby, phosphorylation of GPR35.

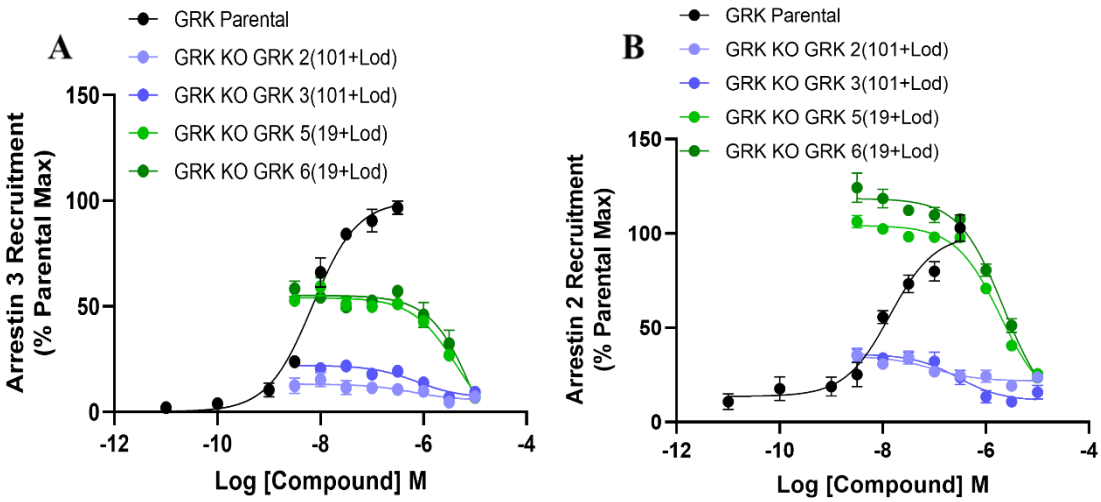

Figure 5.7 Compound 19 prevents GRK5/6 mediated, lodoxamide-induced human GPR35a-arrestin-3 and arrestin-2 interactions

ΔGRK2/3/5/6 cells were transfected to co-express hGPR35a-eYFP and **(A**) arrestin-3-RLuc and **(B)** arrestin-2-RLuc alongside GRK2 (light blue circles), GRK3 (deep blue circles), GRK5 (light green circles) and GRK6 (deep green circles). Before addition of lodoxamide (100 nM, 5 min) cells were pre-treated for 30 min with varying concentrations of either compound 19 (GRK5 and GRK6) or compound 101 (GRK2 and GRK3). Data were presented as % of the effect of lodoxamide in the absence of compound 19 or 101 in Parental 293 cells. A concentration-response curve of lodoxamide-induced **(A**) hGPR35a-eYFP arrestin-3-RLuc interactions and **(B)** hGPR35a-eYFP arrestin-2-RLuc interactions in parental 293 cells were shown for reference. Data are the mean ± SEM of outcomes from three independent experiments.

5.2.3.4 Compound 19 and compound 101 are GRK5/6 and GRK2/3 selective inhibitors respectively; Compound 19 can also inhibit arrestin interaction in HEK 293 cells in a concentration dependent way

As shown in the previous section, compound 19 blocks GRK5/6 mediated arrestin recruitment and compound 101 inhibits GRK2/3 regulated interaction of the receptor with arrestins. I was interested in validating if the above two classes of kinase inhibitors are selective to specific kinases or not. For this, ΔGRK2/3/5/6 293 cells were transiently co-transfected with hGPR35a-eYFP/arrestin-3-RLuc and either GRK2 or GRK3. Compound 19 was employed to inhibit lodoxamide-induced hGPR35a-eYFP/arrestin-3-RLuc interactions. In this case, compound 19 was unable to prevent arrestin recruitment (Figure 5.8A). Similarly, I transiently co-transfected hGPR35a-eYFP/arrestin-3-RLuc into ΔGRK2/3/5/6 293 cells along with either GRK5 or GRK6 and employed compound 101. Compound 101 did not block the arrestin interaction with hGPR35a mediated by GRK5/6 (Figure 5.8A).

I also used compound 19 and compound 101 to assess their effects in HEK 293 cells without any reconstituted GRKs. Here, the effect of lodoxamide to promote such interactions was markedly compromised by the presence of increasing concentrations of the GRK5/6 inhibitor compound 19 (pIC_{50} 5.80± 0.08 (mean± SEM, n=3), but affected only in a marginal way by increasing concentrations of the GRK2/3 inhibitor compound 101 (Figure 5.8B).

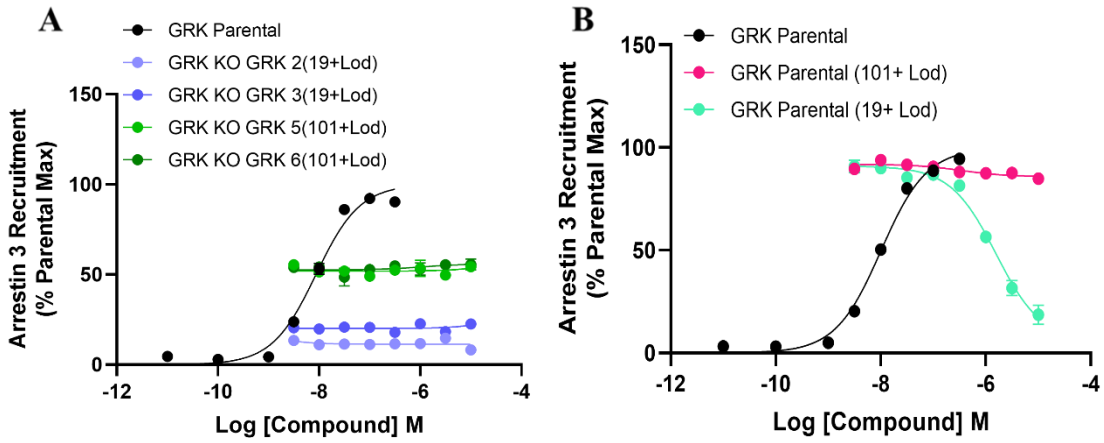

Figure 5.8 Validation of selectivity of GRK inhibitory action of compound 19 and compound 101 and demonstration of the activity of compound 19 in preventing lodoxamide-induced hGPR35a-arrestin-3 interactions in 293 cells in a concentration-dependent manner
(A) ΔGRK2/3/5/6 cells were transfected to co-express hGPR35a-eYFP and arrestin-3-RLuc alongside GRK2 (light blue circles), GRK3 (deep blue circles), GRK5 (light green circles) and GRK6 (deep green circles). Before addition of lodoxamide (100 nM, 5 min) cells were pre-treated for 30 min with varying concentrations of either compound 19 (GRK2 and GRK3) or compound 101 (GRK5 and

GRK6). **(B)** Parental HEK293 cell (black circles) were transfected transiently to express hGPR35a-eYFP and arrestin-3-RLuc. Before addition of lodoxamide (100 nM, 5 min) cells were pre-treated for 30 min with varying concentrations of either compound 19 or compound 101. Data are presented as % of the effect of lodoxamide in parental 293 cells in the absence of compound 19 or 101 for both **(A)** and **(B).** Arrestin 3 inhibitory activities of compounds 19 and 101 are shown by (very light green circles and pink circles respectively). A concentration-response curve of lodoxamide-induced hGPR35a-eYFP- arrestin-3-RLuc interactions in parental 293 cells (black circles) was shown for reference for both **(A)** and **(B)**. Data are the mean ± SEM of outcomes from three independent experiments.

5.2.4 Expression pattern of GRKs

5.2.4.1 Transfected GRK expression patterns in cell lines produced from HEK293

In previous sections, I reconstituted different GRKs with LgBiT tag in parental 293 derived cell lines to investigate their individual contribution. As each of the introduced GRK isoforms was fused to the large BiT (LgBiT) fragment (Palmer et al., 2022) of the NanoBiT® complementation technology (Dale et al., 2019, Guo et al., 2022), I was able to use an anti-LgBiT monoclonal antibody to detect the relative levels of each GRK (Figure 5.9). With this, it is possible to determine whether the variation in the extent of reconstitution could reflect intrinsic differences in the actions of the various GRKs or might simply reflect transfection and expression level difference between them. Following transfection of either parental HEK293 cells (Figure 5.9A) or ΔGRK2/3/5/6 293 (Figure 5.9B) cells, comparatively equal amounts of each GRK were detected.

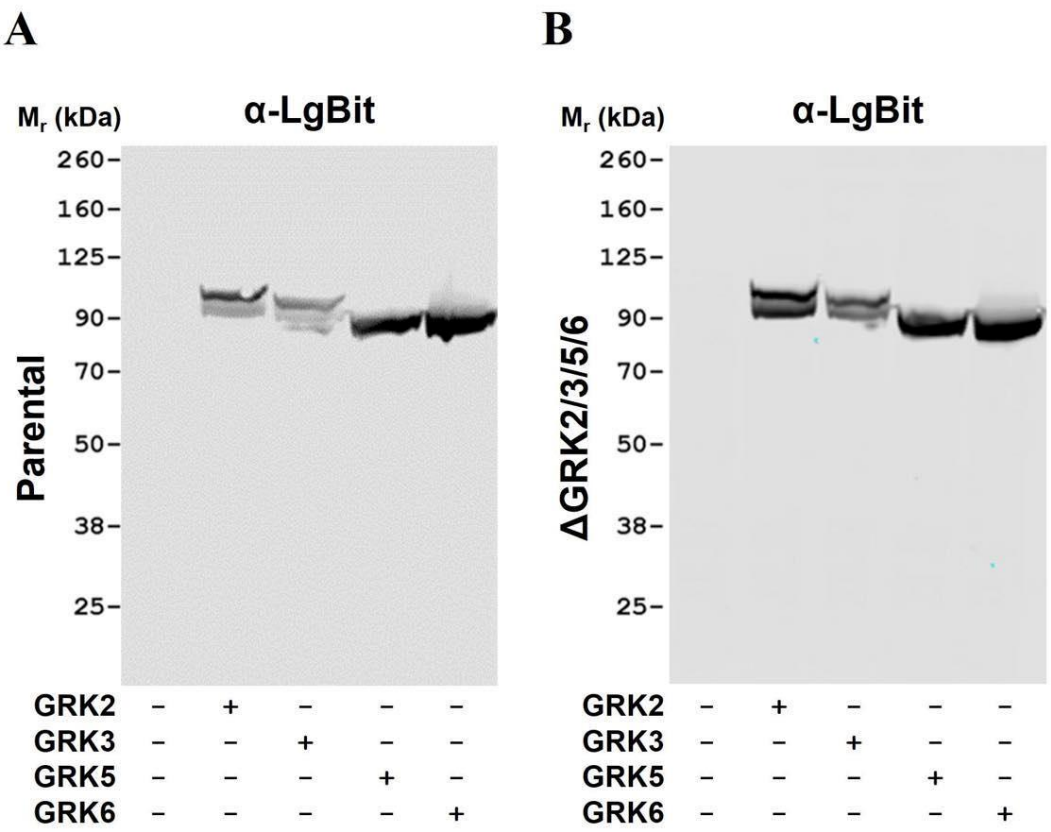

Figure 5.9 Expression patterns of transfected GRKs in HEK293-derived cell lines
Following transfections akin to those in **Figure 5.6**, cell lysates were produced and resolved by SDS-PAGE. These (**A**, parental HEK293, **B**, ΔGRK2/3/5/6 cells) were then immunoblotted with an anti-LgBiT antibody. The identity of the introduced GRK is noted in each case. GRK, G protein–coupled receptor kinase; HEK, Human embryonic kidney; LgBiT, large BiT.

5.2.4.2 Expression pattern of endogenous and transfected GRKs with GRK isoform-directed antibodies

Studies akin to Figure 5.9, experiments were performed using GRK isoform-directed antibodies instead of anti-LgBiT monoclonal antibody. Results of the immunoblots demonstrated successful expression of each isoform, with a degree of previously reported cross-reactivity with GRK5 for the nominally GRK6 directed antibody in both ΔGRK2/3/5/6 (Figure 5.10A) and parental 293 cells (Figure 5.10B) (Reichel et al., 2022). The fusion of the GRKs with the LgBiT sequence added an extra 18 kDa of molecular mass, which enabled immunoblots using GRK-isoform antibodies to simultaneously detect the relative amounts of the inserted GRK-LgBiT species forms and endogenous levels of each GRK in the parental HEK293 cells (Figure 5.10B). According to these investigations, the introduced GRKs levels were comparable to (GRK3, GRK6), or rather higher (GRK2, GRK5) than endogenous levels in the parental cells.

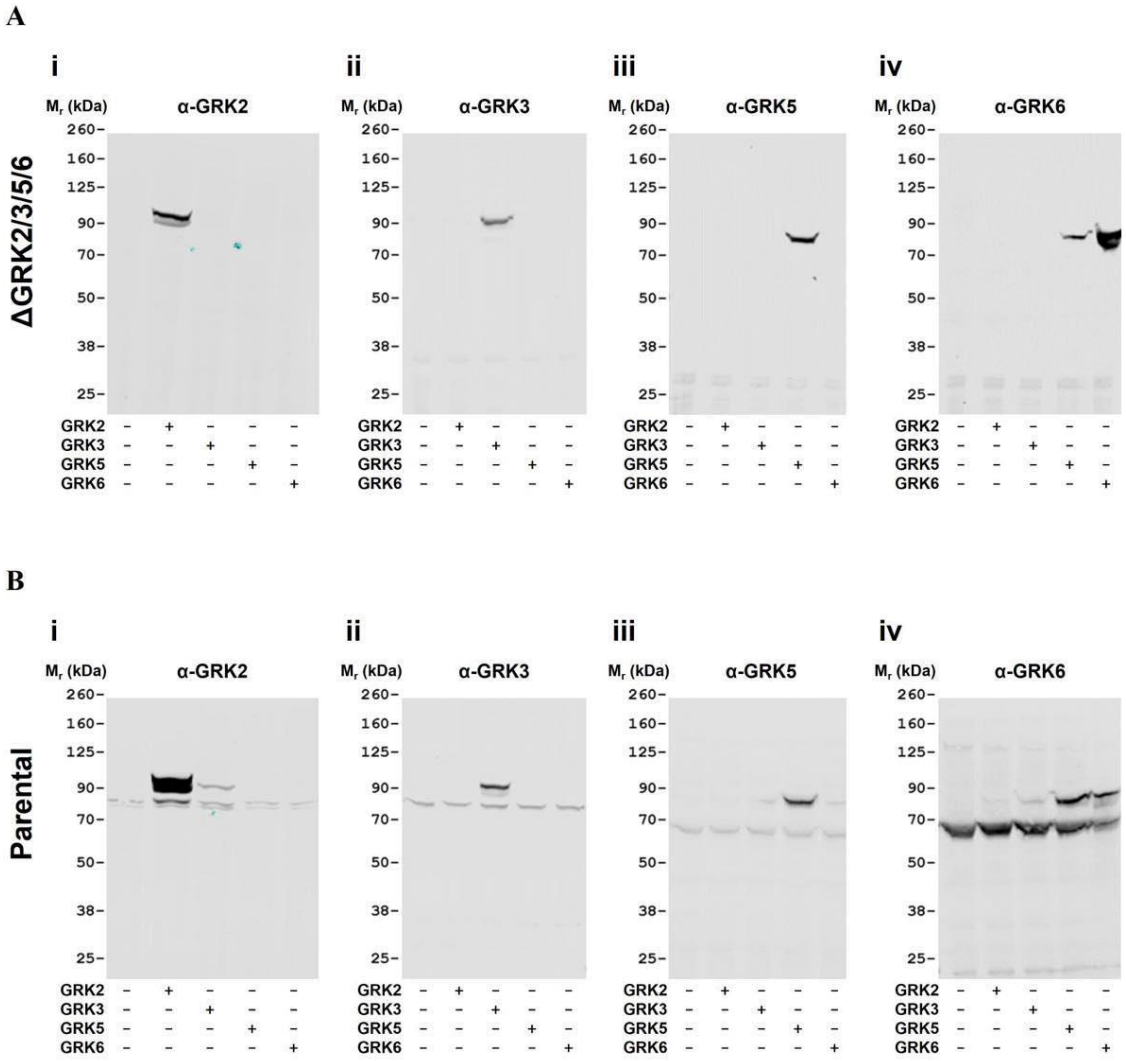

Figure 5.10 Expression patterns of endogenous and transfected GRKs in HEK293-derived cell lines detected by anti-GRK antibodies
Following transfections akin to those in **Figure 5.6** and **Figure 5.9**, cell lysates were produced and resolved by SDS-PAGE. These (**A**, ΔGRK2/3/5/6 cells **B**, parental HEK293 cells) were then immunoblotted with antibodies against GRK2 **(i)**, GRK3 **(ii)**, GRK5 **(iii)** and GRK6 **(iv)**. In **B** relative levels of endogenous GRKs and the introduced LgBiT-tagged forms can be observed for each isoform.

5.2.5 Assessment of the role of GRK5/6 inhibitor compound 19 in GPR35 phosphorylation

5.2.5.1 Phosphorylation of human GPR35a at pSer^{300}-pSer^{303} is prevented by compound 19

In human GPR35, each of the hydroxyamino acids in the intracellular C-terminal tail that contribute to interactions with arrestins have been characterised (Divorty et al., 2022). Although Ser^{287}, Ser^{300}, Ser^{303}, and Thr^{307} were all independently proven to have a substantial impact when changed to Ala, the combination of

Ser^{300} and Ser^{303} changes resulted in a receptor type that had minimal ability to engage with arrestin-3 (Divorty et al., 2022). Our group created an antiserum to selectively recognise $pSer^{300}$-$pSer^{303}$ hGPR35a as part of our earlier investigations, and we demonstrated that this antiserum only recognises hGPR35a post-agonist activation (Divorty et al., 2022). Then, using doxycycline as an inducer, I created a stable transfected Flp-In TREx 293 cell line that expresses hGPR35a with an HA tag at its C-terminus (hGPR35a-HA). Lodoxamide (100 nM, 5 min) was added, and when the receptor was captured using HA-trap, the receptor could be detected in immunoblots by the anti-$pSer^{300}$-$pSer^{303}$ antiserum (Figure 5.11A). As previously reported (Divorty et al., 2022), this was a pair of well resolved species that reflect differential N-glycosylation (Figure 5.11A). Compound 19 pre-treatment of the cells completely prevented the $pSer^{300}$-$pSer^{303}$ phosphorylation induced by lodoxamide (Figure 5.11A). In contrast, compound 101 treatment decreased the anti-$pSer^{300}$-$pSer^{303}$ antiserum's recognition but did not completely eliminate it (Figure 5.11A). In addition, we created an antiserum directed against the distal end of the hGPR35a C-terminal tail. While being intended as a structural antiserum, this reagent did not exhibit the expected property that recognition of the receptor protein would be unaffected by the activation or phosphorylation state of the receptor (Figure 5.11B). Lodoxamide treatment decreased this antiserum's detection of hGPR35a-HA in parallel immunoblots (Figure 5.11B). This may suggest that the incorporation of negative charges caused by lodoxamide, reflecting the phosphorylation of residues like Ser^{300} and Ser^{303}, may obstruct the antiserum's ability to recognise an epitope. This idea is supported by the fact that pre-treating cells with compound 19 before adding lodoxamide did not cause such a drop in the antiserum's ability to recognise hGPR35a-HA (Figure 5.11B). In comparison, pre-treatment with compound 101 prior to the addition of lodoxamide produced a limited reduction in the effect of lodoxamide (Figure 5.11B). I carried out additional parallel immunoblots using an anti-HA antibody to verify that these observations were not loading artefacts or that the treatment with lodoxamide in the presence or absence of the GRK inhibitors had not changed the overall amount of hGPR35a-HA protein. These demonstrated similar receptor construct levels under all testing settings (Figure 5.11C).

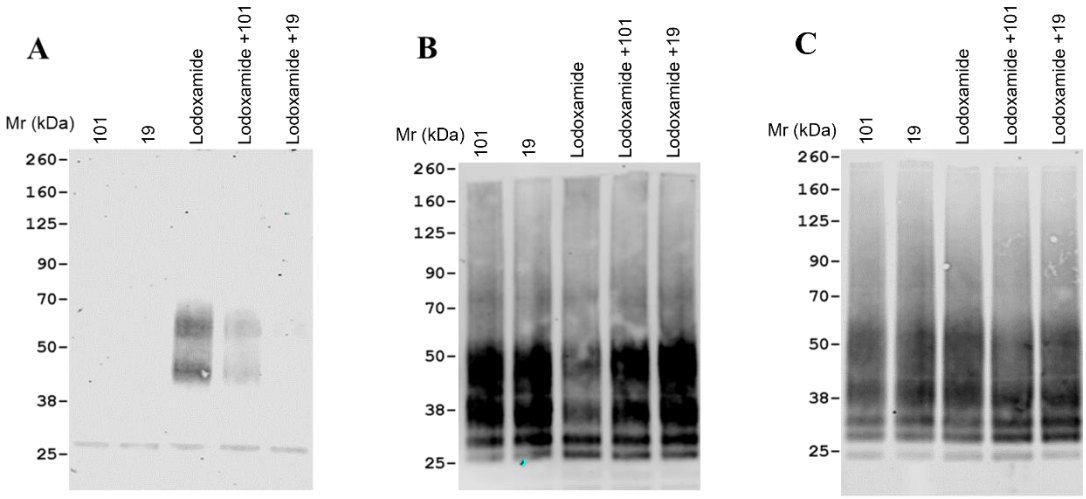

Figure 5.11 Recognition of agonist-activated human GPR35a by an anti-human GPR35-pSer^{300}-pSer^{303} antiserum is prevented by compound 19
A Flp-In TREx 293 cell line induced to express human GPR35a-HA was treated with lodoxamide (100 nM), compound 101, compound 19 (each at 10 μM) or lodoxamide plus compound 19 or compound 101. Subsequently, after anti-HA immunoprecipitation, samples were resolved by SDS-PAGE and immunoblotted to detect **(A)** hGPR35a-pSer^{300}-pSer^{303}, **(B)** the C-terminal region of GPR35a or, **(C)** the HA epitope tag. Results are representative of three independent experiments. HA, haemagglutinin

5.2.5.2 Phosphorylation of mouse GPR35 at pSer^{298}-pSer^{301} is prevented by compound 19

GPR35 is a unique receptor in several aspects that make translation difficult. Rodents only express one version of a protein, whereas humans express two different protein isoform sequences. The pharmacology of the GPR35 orthologues in humans and rodents are significantly different from one another. For this reason, I was interested in extending this study to the mouse orthologue of GPR35 and explore this more extensively. Compared to human GPR35, the C-terminal tail of mouse GPR35 has more potential phosphorylation sites (Divorty et al., 2022). However, amino acids equivalent to Ser^{300} and Ser^{303} (Ser^{298} and Ser^{301} in the mouse orthologue) are conserved and their phosphorylation is equally, if not even more, important for interactions with arrestin-3 (Divorty et al., 2022). As a result, I performed sets of studies with mouse GPR35-HA. Here, I used a unique antiserum that recognises mouse GPR35 pSer^{298}-pSer^{301} and is phospho-specific (Divorty et al., 2022). Compound 19 was pre-treated in stably transfected Flp-In TREx 293 cells that were induced to express mouse GPR35-HA before the addition of the mouse GPR35 active agonist zaprinast (Divorty et al., 2022). I used zaprinast for these tests because lodoxamide has only moderate potency at mouse GPR35 and

because this was the ligand utilised by (Divorty et al., 2022) for prior research on the mouse orthologue. Compound 19 fully eliminated zaprinast-induced recognition of mouse GPR35-HA by the anti-pSer^{298}-pSer^{301} antiserum (Figure 5.12A). The non-phospho-site GPR35 C-terminal tail antiserum almost completely failed to recognise mGPR35-HA after treatment with zaprinast, an effect that was even more evident than when employing hGPR35a-HA (Figure 5.12B). Pre-treatment with compound 19 fully prevented the zaprinast-induced loss of recognition by this antiserum (Figure 5.12B). Unlike the partial effect in cells expressing hGPR35a-HA, here compound 101, although again partially limiting detection of mouse GPR35-HA by the mouse GPR35 pSer^{298}-pSer^{301} antiserum (Figure 5.12A), did not partially restore identification of mouse GPR35-HA by the structural anti-GPR35 antiserum (Figure 5.12B). Parallel immunoblots using anti-HA once more demonstrated equal loading of proteins onto the gels (Figure 5.12C).

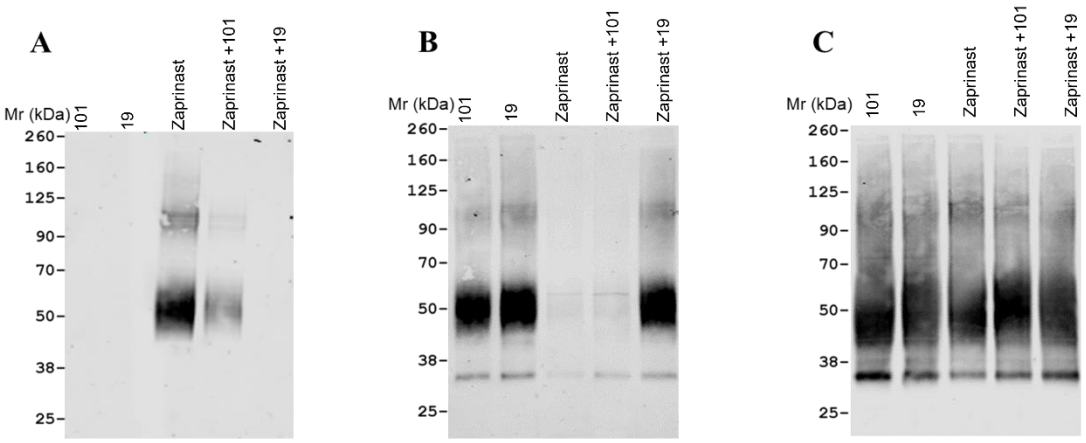

Figure 5.12 Recognition of agonist-activated mouse GPR35 by an anti-mouse GPR35-pSer^{298}-pSer^{301} antiserum is prevented by compound 19
Experiments akin to **Figure 5.11** were performed using a Flp-In TREx 293 cell line induced to express mouse GPR35-HA. Zaprinast (10 μM), which is an agonist at mouse GPR35 replaced Iodoxamide. Pre-treatment with compound 101, or compound 19 (each at 10 μM) was for 30 min. Immunoblots of anti-HA immunoprecipitated samples are shown. **(A)** mGPR35-pSer^{298}-pSer^{301}, **(B)** the C-terminal region of GPR35 or, **(C)** the HA epitope tag. Results are representative of three independent experiments. HA, haemagglutinin

5.2.6 Investigation of the direct involvement of GRK5 and GRK6 in human GPR35a phosphorylation

After exploring both (human and mouse) orthologues of GPR35, I wished to return to the human orthologue of the receptor to investigate the direct and specific contribution of GRK5 and GRK6 in hGPR35a phosphorylation. I transiently introduced LgBiT-tagged forms of GRK2, GRK3, GRK5 or GRK6, along with hGPR35a-HA, into ΔGRK2/3/5/6 293 cells. Lodoxamide (100 nM, 5 min) was administered to the cells before the receptor was bound with anti-HA beads. Subsequent immunoblots with anti-HA confirmed equivalent transfection and capture of the receptor (Figure 5.13A). Parallel immunoblots with anti-hGPR35a pSer^{300}-pSer^{303} showed that the presence of GRK5 and, in particular, GRK6, enhanced phosphorylation of these sites, but that GRK2 and GRK3 had no discernible impact (Figure 5.13B). If cells had been treated with compound 19 prior to agonist treatment, these effects were completely inhibited (Figure 5.13C). Overall, results from these experiments, strongly support the important role of GRK5 and GRK6 in the phosphorylation and regulation of human GPR35a.

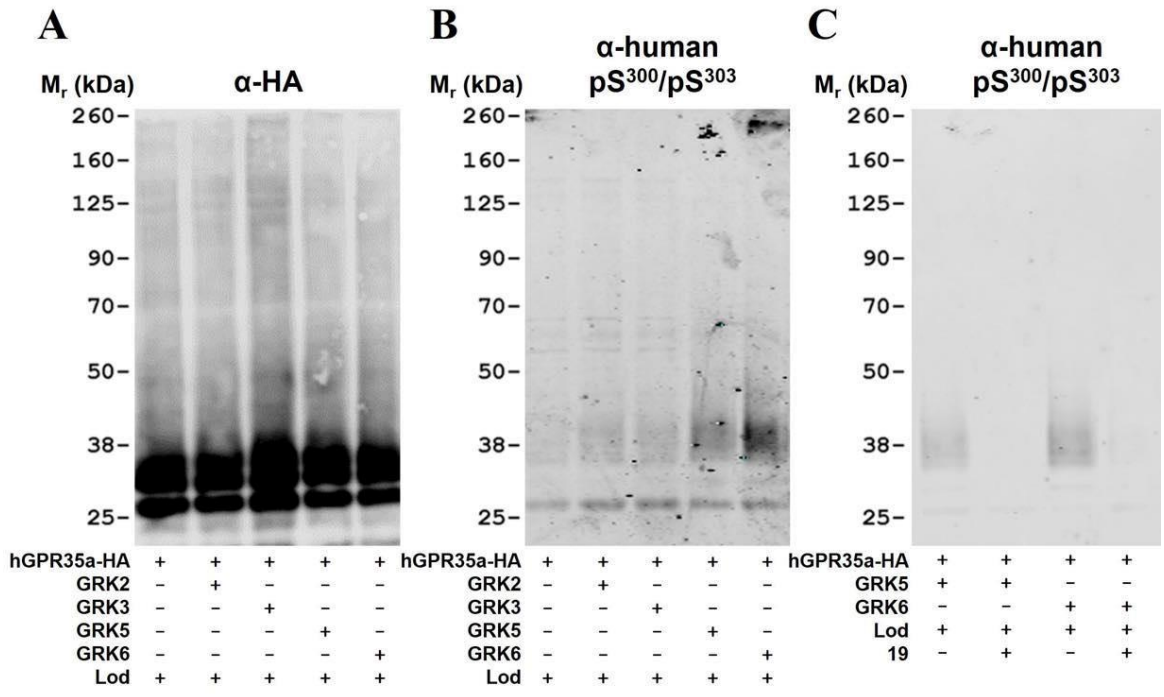

Figure 5.13 GRK5 and GRK6 directly promote hGPR35a phosphorylation at Ser^{300} and Ser^{303}
ΔGRK2/3/5/6 cells were transfected transiently with combinations of human GPR35a-HA (all lanes) and LgBiT-tagged forms of individual GRK isoforms as noted (+). After treatment with lodoxamide (100 nM, 5 min) (Lod+) samples were captured with anti-HA beads and resolved by SDS-PAGE. These were subsequently immunoblotted to detect **(A)** the HA epitope tag or **(B)** pSer^{300}-pSer^{303}-hGPR35a-HA. In similar studies **(C)**, ΔGRK2/3/5/6 cells co-expressing hGPR35a-HA and LgBiT-tagged forms of either GRK5 or GRK6 (+) were treated without (−) or with (+) compound 19 (10 μM,

30 min) ahead of exposure to lodoxamide. Anti-HA bead immunoprecipitated samples were immunoblotted with the pSer^{300}-pSer^{303}-hGPR35a-HA antiserum after SDS-PAGE. Note: the lower apparent molecular mass of hGPR35a-HA following transient transfection compared to when expressed stably (Figure **5.11**). This may reflect differing degrees of maturation and posttranslational modification. GRK, G protein–coupled receptor kinase; HA, haemagglutinin; LgBiT, large BiT.

5.2.7 Role of GRK2/3 inhibitor compound 101 in inhibiting GPR35 phosphorylation

5.2.7.1 Compound 101 also partially inhibits GSK 938 induced hGPR35a phosphorylation

Among the small molecule kinase inhibitors, compound 101 is GRK2/3 selective (Thal et al., 2011, Lowe et al., 2015). As this compound is well-studied, initially I utilised this compound to prevent agonist mediated phosphorylation of hGPR35a. For this, I developed a stably transfected Flp-In TREx 293 cell line that expresses hGPR35a with an enhanced yellow fluorescent protein (eYFP) tag at its C-terminus using doxycycline as an inducer (hGPR35a-eYFP). When the receptor was enriched using GFP-trap, immunoblot with an anti-GFP antibody demonstrated equal loading of proteins onto the gels (Figure 5.14A). After stimulating the receptor with two potent agonists, (lodoxamide and GSK 938) (each at 100 nM, 5 min) and a suggested endogenous ligand of GPR35, 5-HIAA (De Giovanni et al., 2022) (10 µM, 5 min), the phosphorylated receptor was visible upon treatment with lodoxamide and GSK 938 using anti-pSer^{300}-pSer^{303} antiserum (Figure 5.14B). Although 5-HIAA is claimed as a potent endogenous ligand of GPR35 (De Giovanni et al., 2022, De Giovanni et al., 2023a), this molecule, a metabolite of serotonin, even at 10 µM did not phosphorylate hGPR35a. Moreover, treatment with compound 101 decreased, but did not completely eradicate, recognition of agonist-induced phosphorylation by the anti-pSer^{300}-pSer^{303} antiserum (Figure 5.14B). After applying the non-phospho structural antiserum of GPR35 which is directed against the distal end of the hGPR35a C-terminal tail, I again saw the receptor hGPR35a across the panel but with reduced recognition in samples treated with lodoxamide or the GSK 938. This may suggest that the incorporation of negative charges caused by lodoxamide and GSK 938, reflecting the phosphorylation of residues like Ser^{300} and Ser^{303}, may obstruct the antiserum's ability to recognise an epitope. The purpose of these investigations was to ensure constant phosphorylation patterns of hGPR35a upon treatment with additional potential agonist ligands.

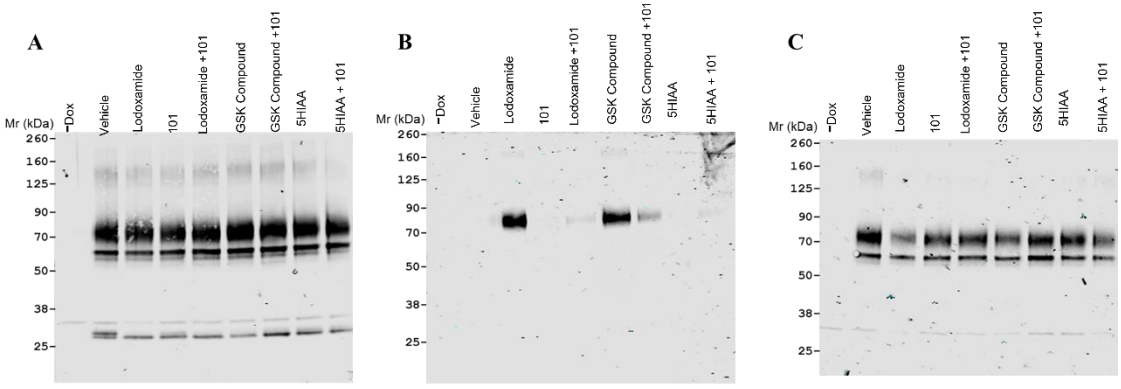

Figure 5.14 Recognition of agonist-activated human GPR35a by an anti-human GPR35-pSer^{300}-pSer^{303} antiserum is partially ablated by compound 101
A Flp-In TREx 293 cell line induced to express human GPR35a-eYFP was treated with vehicle, lodoxamide (100 nM), GSK 938 (100 nM), 5HIAA (10 μM), compound 101 (10 μM) or above mentioned 3 ligands plus compound 101. Following capture of the receptor construct via a GFP-trap, samples were resolved by SDS-PAGE and immunoblotted to detect **(A)** the eYFP epitope tag, **(B)** hGPR35a-pSer^{300}-pSer^{303} or, **(C)** the C-terminal region of GPR35a. Results are representative of three independent experiments.

5.2.7.2 Compound 101 shows very poor activity to inhibit agonist induced mGPR35 phosphorylation

As the pharmacology of GPR35 is distinct between the human and mouse orthologue, I assessed the GRK2/3 selective inhibitor compound 101 for effects on phosphorylation of mouse GPR35. In order to accomplish this, I developed a stable transfected Flp-In TREx 293 cell line that expresses mouse GPR35 with an HA tag at its C-terminus (mGPR35-HA). After the receptor was captured using HA-trap, an immunoblot employing an anti-HA antibody showed that the proteins were loaded equally onto the gels (Figure 5.15A). After stimulating the receptor with two potent mGPR35 agonists zaprinast and pemirolast (each at 10 μM, 5 min), the phosphorylated receptor was detectable by using the anti-pSer^{298}-pSer^{301} antiserum (Figure 5.15B). Treatment with compound 101 could not reduce the recognition of agonist induced phosphorylation by the anti-pSer^{298}-pSer^{301} antiserum (Figure 5.15B).

After employing the non-phospho structural antiserum of GPR35, I again observed the receptor mGPR35 across the panel but with reduced recognition in samples treated with zaprinast and pemirolast. This might reflect the phosphorylation of residues Ser^{298} and Ser^{301} due to the incorporation of negative charge by zaprinast and pemirolast, thereby limiting the antiserum's ability to recognise the epitope. As compound 101 (a GRK2/3 blocker) did not have any significant effects in

inhibiting phosphorylation, this compound also could not prevent the agonist-induced loss of recognition by this non-phospho structural antiserum of GPR35 (Figure 5.15C).

Overall, the GRK2/3 inhibitor compound 101 did not show very significant inhibitory effects in phosphorylation of both orthologues of GPR35 suggesting the poor contribution of GRK2/3 in GPR35 phosphorylation.

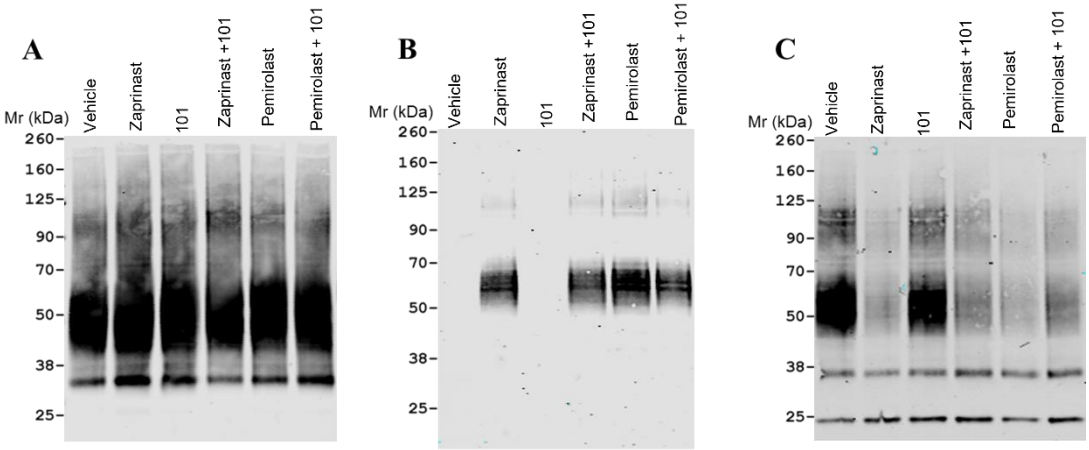

Figure 5.15 Recognition of agonist-activated mouse GPR35 by an anti-mouse GPR35-pSer^{298}-pSer^{301} antiserum is partially ablated by compound 101
Experiments similar to Figure 5.14 were performed using a Flp-In TREx 293 cell line induced to express mouse GPR35-HA. Zaprinast and pemirolast which are both agonists at mouse GPR35 were used in this study (each at 10 μM). Vehicle and compound 101 (10 μM) alone were also added. Pre-treatment with compound 101 (10 μM) was for 30 min before ligand addition. Immunoblots of anti-HA immunoprecipitated samples are shown. **(A)** the HA epitope tag, **(B)** mGPR35-pSer^{298}-pSer^{301} or, **(C)** the C-terminal region of GPR35. Results are representative of three independent experiments.

5.2.8 Investigation of the comparative contribution of two classes of kinase inhibitors in preventing phosphorylation of GPR35

5.2.8.1 Direct comparison between compound 101 (GRK2/3 inhibitor) and compound 19 (GRK5/6 inhibitor) in preventing mouse GPR35 phosphorylation using multiple agonists

While GRK5 and GRK6 are membrane-localised (Komolov and Benovic, 2018), GRK2 and GRK3 are primarily cytosolic and translocate to the plasma membrane. Plasma membrane translocation is supported by interaction with βγ subunits of activated G-proteins (Tesmer et al., 2005, Drube et al., 2022). Hence, GRK5/6 and GRK2/3 are different in nature, I was interested in using two classes of kinase inhibitors in parallel to investigate the effect of distinct agonists on the phosphorylation

status of GPR35. Here, the use of different agonists was crucial to ensure that the phosphorylation pattern of the receptor did not change throughout treatment with various agonists and two types of kinase inhibitors.

In this set of studies, a stably transfected Flp-In TREx 293 cell line that expresses mouse GPR35 with a HA tag in its C-terminus (mGPR35-HA) was used. After the receptor was captured using the HA-trap, an immunoblot employing an anti-HA antibody showed equivalent levels of the receptor construct throughout this study (Figure 5.16A). Here, cells were stimulated with two potent agonists zaprinast (10 μM) and GSK 938 (100 nM). When employing the mouse GPR35 directed pSer^{298}-pSer^{301} antiserum, phosphorylated receptors were observed in immunoblots (Figure 5.16B). Compound 19 fully eliminated zaprinast and GSK 938 induced recognition of mouse GPR35-HA by the anti-pSer^{298}-pSer^{301} antiserum. By contrast, pre-treatment with compound 101 reduced but did not fully ablate the agonist induced recognition of phosphorylation signal (Figure 5.16B). The non-phospho-site GPR35 C-terminal tail antiserum almost completely failed to recognise mGPR35-HA after treatment with either zaprinast or the GSK 938 (Figure 5.16C). Compound 19 pre-treatment completely stopped the loss of recognition caused by zaprinast and GSK 938 by this antiserum. Compound 101 pre-treatment before the addition of the agonists slightly prevented the agonist induced loss of phosphorylation signals (Figure 5.16C).

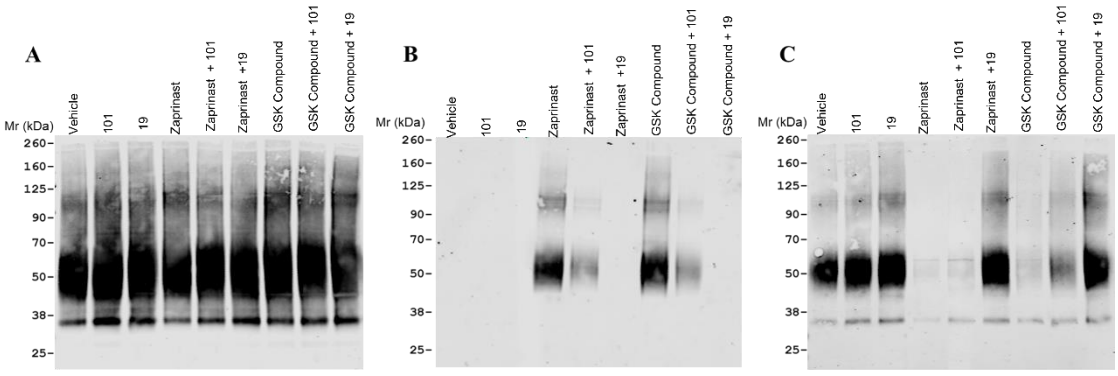

Figure 5.16 Comparison of effects of compounds 101 and 19 in limiting detection of agonist-activated mouse GPR35 by an anti-mouse GPR35-pSer^{298}-pSer^{301} antiserum upon treatment with agonists

Experiments similar to Figure 5.12 were performed using a Flp-In TREx 293 cell line induced to express mouse GPR35-HA. Zaprinast (10 μM) and GSK 938 (100 nM) which are both agonists at mouse GPR35 were used. Vehicle, compound 101 (10 μM) and compound 19 (10 μM) were also added. Pre-treatment with compound 101, or compound 19 (each at 10 μM) was for 30 min before the addition of the above mentioned agonists. Immunoblots of anti-HA immunoprecipitated samples

are shown. **(A)** the HA epitope tag, **(B)** mGPR35-pSer^{298}-pSer^{301} or, **(C)** the C-terminal region of GPR35. Results are representative of three independent experiments.

5.2.8.2 Assessment of effects of a series of GRK5/6 blockers on mouse GPR35 phosphorylation

To extend the above results with compound 19, I utilised other compounds from this series (compounds 15-18) to assess their regulation of mouse GPR35 phosphorylation.

Here again, the mouse GPR35 with a HA tag at its C-terminus (mGPR35-HA) was expressed by a stably transfected Flp-In TREx 293 cell line. After the receptor was captured using the HA-trap, an immunoblot employing an anti-HA antibody demonstrated similar amounts of the receptor construct throughout this investigation (Figure 5.17A). Here, the mouse GPR35 active agonist zaprinast (10 μM) was used. Phosphorylated receptors were identified in immunoblots when using the mouse GPR35 directed antisera pSer^{298}-pSer^{301} (Figure 5.17B). Zaprinast-induced identification of mouse GPR35-HA by the anti-pSer^{298}-pSer^{301} antiserum was abolished by pre-treating each of the compounds (15-18) from this series (Figure 5.17B). After zaprinast treatment, the non-phospho-site GPR35 C-terminal tail antiserum almost completely failed to recognise mGPR35-HA (Figure 5.17C). Pre-treatment with compounds (15-18) variably prevented the zaprinast induced loss of recognition by this antiserum (Figure 5.17C).

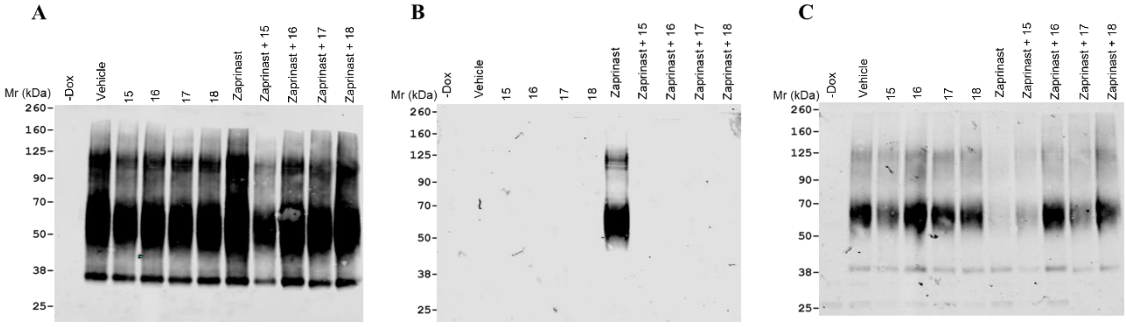

Figure 5.17 Inhibitory activity of a series of GRK5/6 inhibitor compounds in limiting the detection of agonist-activated mouse GPR35 by an anti-mouse GPR35-pSer^{298}-pSer^{301} antiserum upon treatment with zaprinast
Experiments similar to **Figure 5.16** were performed using a Flp-In TREx 293 cell line induced to express mouse GPR35-HA. Zaprinast (10 μM), was used to stimulate the receptor. Pre-treatment with compounds 15-18 (each at 10 μM) were for 30 min before adding zaprinast. Immunoblots of anti-HA immunoprecipitated samples are shown. **(A)** the HA epitope tag, **(B)** mGPR35-pSer^{298}-

pSer^{301} or, **(C)** the C-terminal region of GPR35. Results are representative of three independent experiments.

5.2.8.3 Confirmation of inhibitory potential of a selection of compounds for mouse GPR35 phosphorylation

To extend the results of Figure 5.17, I used a cell line that stably expressed mouse GPR35 with an enhanced yellow fluorescent protein (eYFP) tag at its C terminal. After the receptor was enriched using the GFP-trap, an immunoblot employing an anti-GFP antibody demonstrated consistent levels of the receptor construct throughout this investigation (Figure 5.18A, C). In this case, the mouse GPR35 active agonist zaprinast (10 μM) was used. Using the mouse GPR35 directed antisera pSer^{298}-pSer^{301}, phosphorylated receptors can be detected in immunoblots (Figure 5.18B, D). By pre-treating with compound 15 and compound 18, zaprinast-induced identification of mouse GPR35-eYFP by the anti-pSer^{298}-pSer^{301} antiserum was eliminated (Figure 5.18B). Zaprinast-induced identification of mouse GPR35-eYFP by the anti-pSer^{298}-pSer^{301} antiserum was also abolished by pre-treating with compound 16 and compound 17 (Figure 5.18D)

Overall, from the above experimental studies, it is clearly observed that almost all GRK 5/6 inhibitor compounds (15,16,17,18,19) were able to inhibit phosphorylation of GPR35 with varying levels of ability. By contrast, the well-studies GRK2/3 inhibitor compound 101 failed to inhibit GPR35 phosphorylation. Taken together from these findings, I can claim that GPR35 phosphorylation is mainly GRK5/6 mediated.

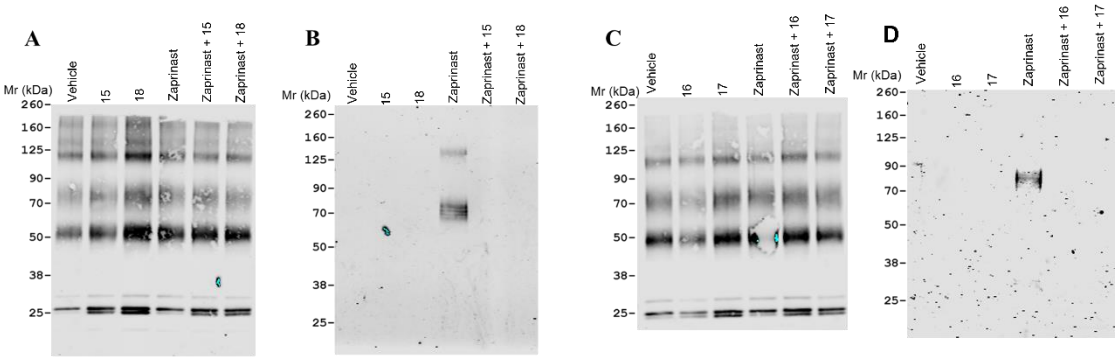

Figure 5.18 Confirmation of the inhibitory potential of a selection of compounds in limiting signals raised by an anti-mouse GPR35-pSer^{298}-pSer^{301} antiserum upon agonist activation
Experiments similar to Figure 5.17 were performed using a Flp-In TREx 293 cell line induced to express mouse GPR35-eYFP. Zaprinast (10 μM) was used to stimulate the receptor. Pre-treatment with compounds 15-18 (each at 10 μM) were for 30 min before the addition of zaprinast. Immunoblots

after GFP-trap immunoprecipitated samples were shown. **(A)** the eYFP epitope tag (samples treated with compound 15 and 18), **(C)** the eYFP epitope tag (samples treated with compound 16 and 17), **(B)** mGPR35-pSer^{298}-pSer^{301} (effects of compound 15 and 18), **(D)** mGPR35-pSer^{298}-pSer^{301} (effects of compound 16 and 17). Results are representative of three independent experiments.

5.2.9 Comparative expression pattern of ubiquitously expressed GRKs across the isoforms of human GPR35

The human GPR35 gene is located on chromosome 2q37.3 and can be expressed as several transcripts resulting from differential promoter usage and alternative splicing (Schihada et al., 2022). Among all the transcripts, only two mRNAs encode GPR35b (also referred to as "GPR35 long"), while all other known/annotated transcripts encode the reference isoform GPR35a (also known as "GPR35 short"). Hence, human GPR35 has two isoforms where GPR35b has a longer extracellular domain but is otherwise identical in sequence (Quon et al., 2020). Although the location of GPR35a and GPR35b mRNA expression in human tissues has been identified, their possible unique activities are unknown because of their strikingly comparable pharmacology and, when studied, signalling pathways (Quon et al., 2020, Milligan, 2023). For this reason, I directly compared the expression pattern of all commonly expressed GRKs (GRK2, GRK3, GRK5 and GRK6) by reconstituting these with both short (hGPR35a) and long (hGPR35b) isoforms in parental 293 cells.

In this study, I took advantage of using an anti-LgBiT monoclonal antibody to detect the relative levels of each GRK across both isoforms, as all of the introduced GRK isoforms was fused to the large BiT (LgBiT) fragment (Palmer et al., 2022) of the NanoBiT® complementation technology (Guo et al., 2022, Dale et al., 2019). Following co-transfection of all the GRKs with both short and long GPR35 isoforms, there were no significant variation of expression levels noticed when compared between the two isoforms of human GPR35 (Figure 5.19).

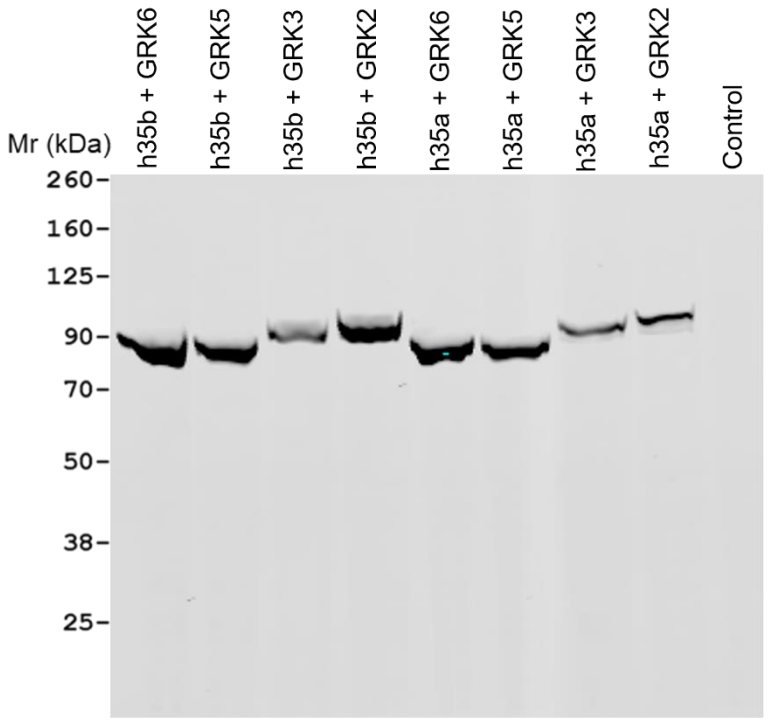

Figure 5.19 Expression patterns of transfected GRKs in parental HEK293 cell lines by two isoforms of hGPR35
After transfections similar to those in **Figure 5.9**, cell lysates were produced and resolved by SDS-PAGE. Two isoforms of hGPR35 (hGPR35a and hGPR35b) with ubiquitously expressed GRK2, GRK3, GRK5 and GRK6 as well as an untransfected control were then immunoblotted with an anti-LgBiT antibody.

5.2.10 Investigation of the effects of GRK5 and GRK6 and specific kinase inhibitors in translocation of the proteins across plasma membrane and cytosol

It is known from previous discussion that the GRK2 family, which consists of GRK2 and GRK3, is expressed in the cytoplasm. However, the GRK4 family of kinases, which includes GRK4, GRK5, and GRK6, are typically membrane-associated (Matthees et al., 2021). In this section, I attempted to separate the protein into plasma membrane and cytosol and determine the protein translocation effects of two membrane associated kinase GRK5/6 in presence or absence of kinase inhibitor compound 19. Here, after co-transfection of hGPR35a-HA with either GRK5 or GRK6 in ΔGRK2/3/5/6 cells, the protein concentrations in plasma membrane were higher in the samples upon pre-treatment with compound 19 with lodoxamide compared to lodoxamide only after immunoblotted with an anti-LgBiT

antibody (Figure 5.20 Membrane). On the other hand, when ΔGRK2/3/5/6 cells were co-transfected with hGPR35a-HA with either GRK5 or GRK6, the protein concentrations in cytoplasm were lower in the samples upon pre-treatment with compound 19 with lodoxamide compared to lodoxamide only after immunoblotted with an anti-LgBiT antibody (Figure 5.20 Cytoplasm). These findings indicate that, the pre-coupling of membrane associated GRK5 and GRK6 with GPR35 were prevalent and the pre-coupling incidence decrease in an agonist dependent manner but pre-treatment with GRK5/6 specific inhibitor, compound 19 before the addition of agonist increases the plasma membrane localisation of both GRK5 and GRK6 (Figure 5.20 Membrane). This study also claims that, as GRK5/6 are membrane anchored in nature, so in cytoplasm, the scenario seems to be almost reverse compared to plasma membrane (Figure 5.20 Cytoplasm). The total protein concentration of the lysate was used as a control indicating equal amount of proteins across the study (Figure 5.20 Total Lysate Protein).

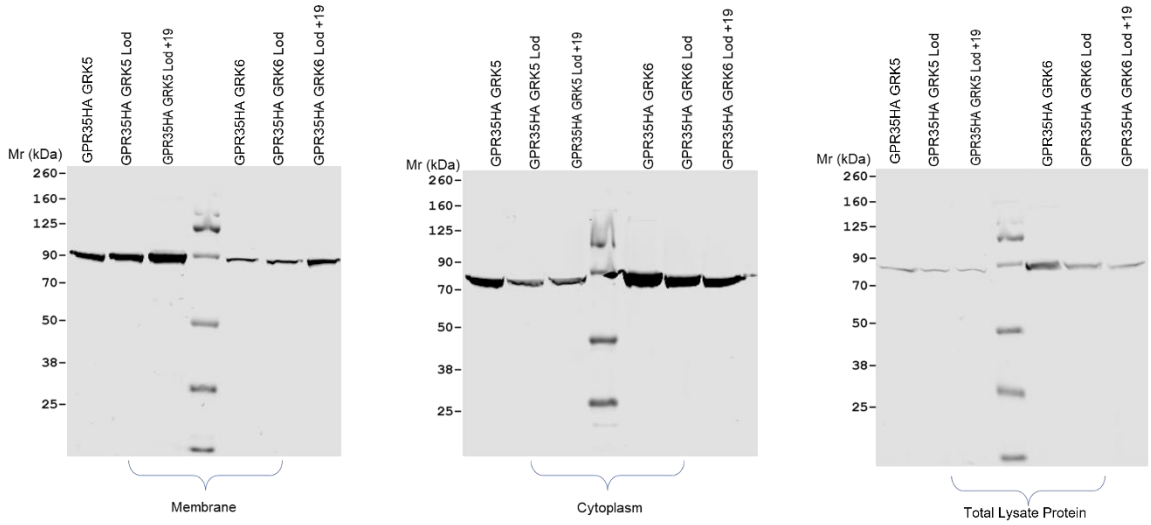

Figure 5.20 Separation and comparison of protein concentration in the plasma membrane and cytosol after transfection with GRK5 and GRK6 with or without inhibitor compound 19 upon stimulation by Lodoxamide

Experiment was performed in a cloned cell line whose genome has been altered to prevent the expression of each of the ubiquitous GRK2, GRK3, GRK5 and GRK6. ΔGRK2/3/5/6 cells were transfected with hGPR35a with a HA tag at the C-terminus of the receptor along with GRK5 and GRK6. Proteins were separated into plasma membrane and cytoplasm as well as a control of total lysate. The effects of lodoxamide with or without the inhibitor compound 19 was shown and immunoblotted with an anti-LgBiT antibody.

5.2.11 Validation of the inhibitory effects of kinase inhibitors in preventing arrestin recruitment in HEK-293 cells

I already investigated the phosphorylation inhibitory activities of all GRK inhibitors in immunoblots in section 5.2.8. As phosphorylation of the active receptor by G-protein receptor kinase (GRKs) is closely related with the binding of arrestin protein, an effort was taken to assess the arrestin-3 recruitment inhibitory activities of the kinase inhibitors in parental 293 cells. In this study, I used both human and mouse orthologues of GPR35 and measured arrestin-3 interaction with the receptor in a BRET based arrestin experiment.

In case of human GPR35, parental 293 cells were transiently transfected to co-express human (h)GPR35a, tagged at the C-terminus with eYFP (hGPR35a-eYFP), and arrestin-3 tagged with Renilla luciferase (arrestin-3-RLuc) (Figure 5.21A). Here, compound 15 and compound 19 strongly reduced lodoxamide-induced hGPR35a-eYFP/arrestin-3-RLuc interactions in parental 293 cells in a concentration-dependent manner. Compound 16 and compound 17 showed moderate activity in preventing agonist mediated recruitment of arrestin-3 to hGPR35a but pre-treatment with compound 18 and GRK 2/3 inhibitor compound 101 had no effects (Figure 5.21A). To verify any additive or synergistic effects of two different classes of kinase inhibitors, I used compound 101 (GRK2/3 inhibitor) at 10 μM concentration with different concentrations of GRK5/6 inhibitors. There were no significant additive effects found (Figure 5.21A). CID-2745687, a human GPR35 specific antagonist was also used in this experiment as a control. Pre-treatment of CID-2745687 for 15 min completely abolished lodoxamide induced arrestin-3 recruitment with hGPR35a (Figure 5.21A).

The same set of experiment was conducted with mouse orthologue of the receptor. Here, mouse GPR35 tagged at the C-terminus with eYFP (mGPR35-eYFP), and arrestin-3 tagged with Renilla luciferase (arrestin-3-RLuc) were transiently co-transfected into parental 293 cells (Figure 5.21B). From the experiment, it was found that compound 19 and compound 15 again showed their promising characteristics to inhibit GSK 938 induced arrestin-3 recruitment in a concentration-dependent manner. Compound 16 and compound 17 from this series were moderately active inhibitors of arrestin-3 recruitment for mGPR35. Compound 18 had a marginally better effect on mouse GPR35 than on human

counterpart in terms of preventing arrestin-3 interaction mediated by the agonist. As usual, compound 101 (GRK 2/3 inhibitors) was not as active in this environment as it was in humans (Figure 5.21B). Since the antagonist CID-2745687 was human GPR35 specific, it was unable to significantly reduce arrestin-3 recruitment caused by agonist in mouse GPR35, demonstrating its human specificity (Figure 5.21B). I combined compound 101 (GRK2/3 inhibitor) at a 10 μM concentration with various concentrations of GRK5/6 inhibitors to see if there were any additive or synergistic effects between the two families of kinase inhibitors. There were significant synergistic effects found between the two classes of kinase inhibitors (Figure 5.21B) although the additive effects were not so pronounced when the experiment was conducted with human orthologue of the receptor. In order to come into a conclusion about this discrepancy, replication of this type of experiment is required.

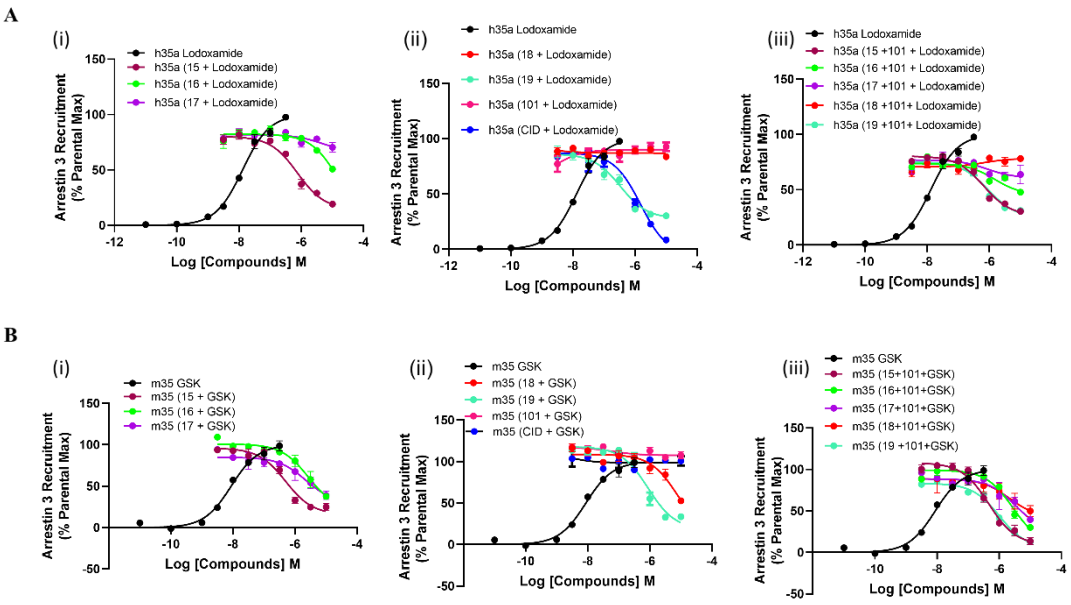

Figure 5.21 Demonstration and validation of the activity of GRK5/6 blockers, GRK2/3 blockers, and a combination of two classes of inhibitors and GPR35 antagonist CID-2745687 in preventing agonist-induced GPR35-arrestin-3 interactions in 293 cells
Parental HEK293 cell (black circles) was transfected transiently to express **(A)** hGPR35a-eYFP and **(B)** mGPR35-eYFP arrestin-3-RLuc. Prior to addition of lodoxamide (100 nM, 5 min) for hGPR35a-eYFP and GSK 938 (100 nM, 5 min) for mGPR35-eYFP cells were pre-treated for 30 min with varying concentrations of compounds (15, 16, 17) **(i),** (18,19, 101 and CID-15 min treatment) **(ii)** and combination of these two classes of inhibitors **(iii).** Data were presented as % of the effect of lodoxamide in parental 293 cells in the absence of inhibitor compound. Arrestin 3 inhibitory activities of compounds 15 (maroon circles), 16 (green circles), 17 (purple circles), 18 (red circles), 19 (paste circles), 101 (pink circles) and antagonist CID-2745687 (black circles) are represented respectively. A concentration-response curve of lodoxamide-induced hGPR35a-eYFP-arrestin-3-RLuc interactions in parental 293 cells (black circles) was shown for reference. The experiment was performed once only (n=1).

5.2.12 Agonist-induced immunocytochemical detection of both human and mouse GPR35 is mediated by GRK5/6

As an extension to the immunoblot studies for the determination of phosphorylation of GPR35, immunocytochemical studies were performed using hGPR35a-pSer^{300}-pSer^{303}, mGPR35-pSer^{298}-pSer^{301} and non-phospho-site GPR35 C-terminal tail antisera.

5.2.12.1 Mouse GPR35 phospho-site–specific antisera and non-phospho-site GPR35 C-terminal tail antisera function as biosensors of agonist activated, fully matured mGPR35

In Flp-In TREx 293 cells induced to express mouse GPR35-HA, non-phospho-site GPR35 C-terminal tail antisera detected the corresponding receptors upon treated with vehicle (Figure 5.22A). In the same system, mGPR35-pSer^{298}-pSer^{301} antisera detected the corresponding receptors in an agonist (zaprinast)-dependent manner in immunocytochemical studies (Figure 5.22B). Compound 19 pre-treatment inhibited the mGPR35-pSer^{298}-pSer^{301} antisera's ability to immunocytochemically identify the receptors, which was triggered by the administration of the proper agonist zaprinast (Figure 5.22B) but the same immunocytochemical detection of the receptors was restored by non-phospho-site GPR35 C-terminal tail antisera (Figure 5.22A). Simultaneous detection of each orthologue by anti-HA verified the constant presence of receptor protein even after treatment with agonist and kinase inhibitor (Figure 5.22A, B).

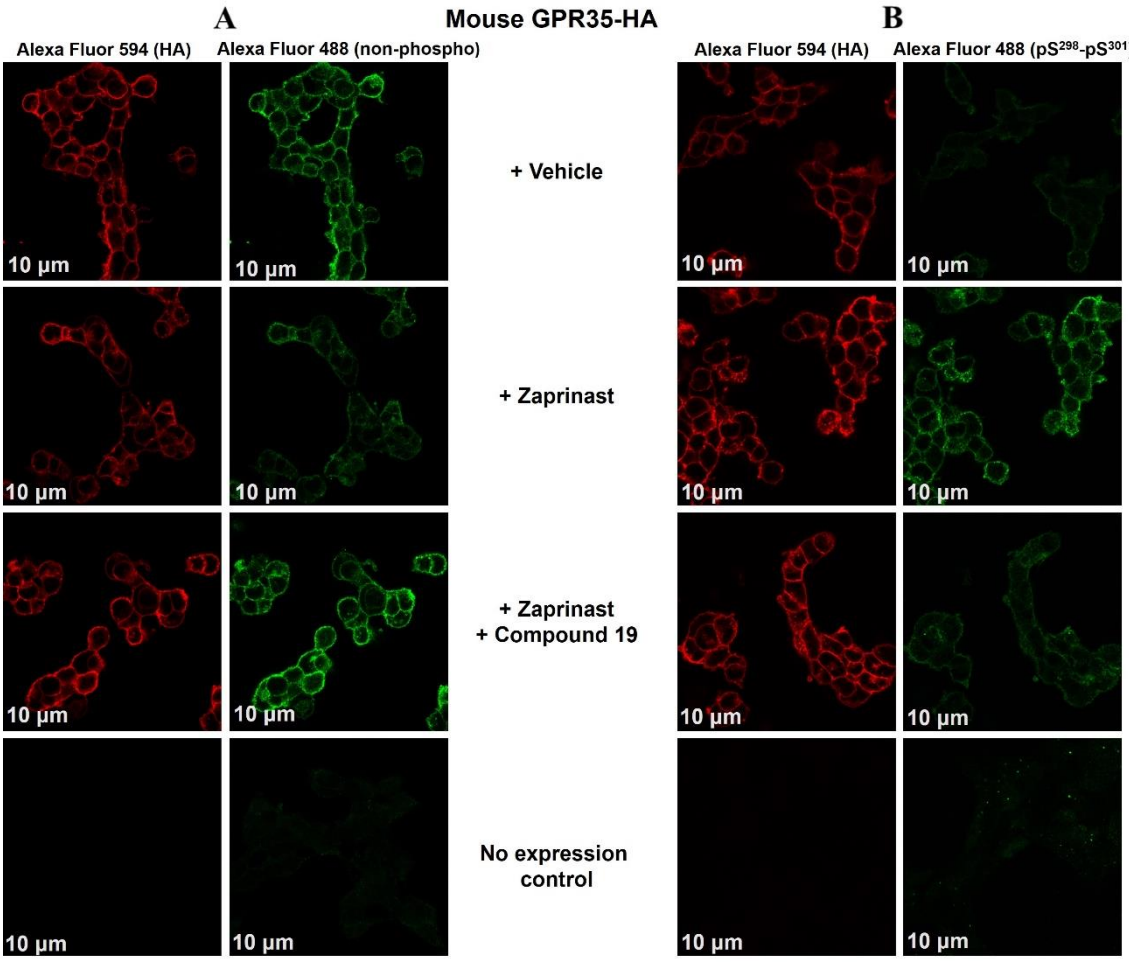

Figure 5.22 Mouse GPR35 phospho-site–specific antisera pSer^{298}-pSer^{301} and non-phospho-site GPR35 C-terminal tail antiserum detect the post activation status of mGPR35 in immunocytochemical studies
Cells as in **Figure 5.22** able to express mGPR35-HA were either uninduced (−dox) or induced by treatment with doxycycline (+dox) and then treated with either vehicle or zaprinast and zaprinast with GRK inhibitor compound 19. Such cells were then used in immunocytochemical studies employing **(A)** Non-phospho-site GPR35 C-terminal tail antiserum and **(B)** mGPR35-pSer^{298}/pSer^{301}. In both **(A)** and **(B)** sections of this figure, samples were stained with Alexa Fluor 594 (HA) (*left panels*) and Alexa Fluor 488 (Non-phospho GPR35 and pSer^{298}-pSer^{301}) (*right panels*). Scale bar = 10 µm. Representative images are shown. mGPR35, mouse GPR35.

5.2.12.2 Human GPR35 phospho-site–specific antisera and non-phospho-site GPR35 C-terminal tail antisera detect the post activation status of hGPR35a

In Flp-In TREx 293 cells induced to express human GPR35-HA, non-phospho-site GPR35 C-terminal tail antisera detected the corresponding receptors upon treated with vehicle (Figure 5.23A). In the same system, immunocytochemical investigations using hGPR35a-pSer^{300}-pSer^{303}antisera identified the relevant receptors in a way that was agonist (lodoxamide)-dependent (Figure 5.23B). In cells induced to express human GPR35a-HA, hGPR35a-pSer^{300}-pSer^{303} antisera indicated a level of detection in the absence of lodoxamide that may imply a

degree of constitutive phosphorylation of the receptor in this setting (Figure 5.23A). Pre-treatment with compound 19 prevented hGPR35-pSer^{300}-pSer^{303} antisera from immunocytochemically detecting the receptors after adding the suitable agonist lodoxamide (Figure 5.23B) however, non-phospho-site GPR35 C-terminal tail antisera restored the same immunocytochemical detection of the receptors (Figure 5.23A). The persistent existence of the receptor protein, even after treatment with an agonist and a kinase inhibitor was established by the simultaneous detection of each orthologue by anti-HA (Figure 5.23A, B).

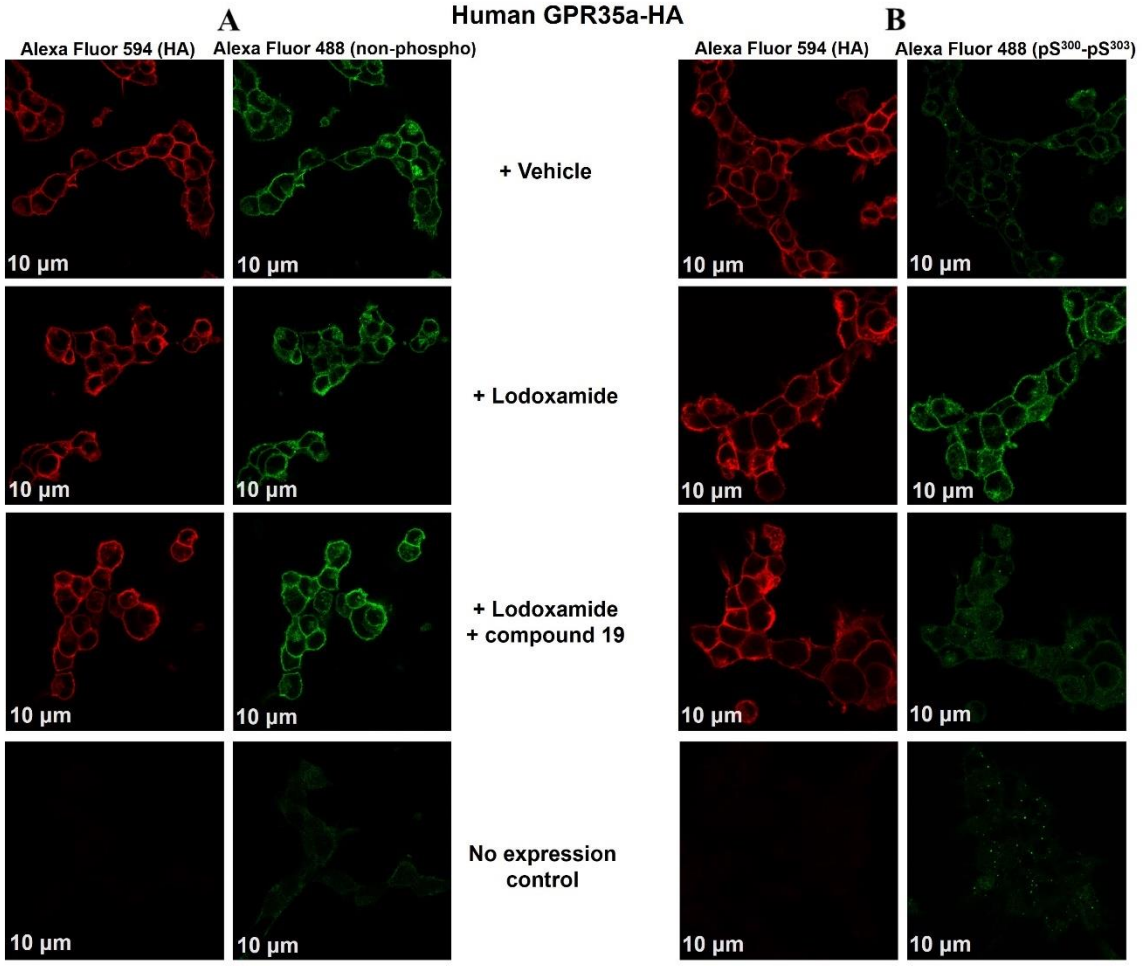

Figure 5.23 Human GPR35a phospho-site–specific antisera pSer^{300}-pSer^{303} and non-phospho-site GPR35 C-terminal tail antiserum detect the post activation status of hGPR35a in immunocytochemical studies

Cells as in **Figure 5.23** able to express hGPR35a-HA were either uninduced (−dox) or induced by treatment with doxycycline (+dox) and then treated with either vehicle or lodoxamide and lodoxamide with GRK inhibitor compound 19. Such cells were then used in immunocytochemical studies employing **(A)** Non-phospho-site GPR35 C-terminal tail antiserum and **(B)** hGPR35-pSer^{300}/pSer^{301}. In both **(A)** and **(B)** sections of this figure, samples were stained with Alexa Fluor 594 (HA) (*left panels*) and Alexa Fluor 488 (Non-phospho GPR35 and pSer^{300}/pSer^{301}) (*right panels*). Scale bar = 10 µm. Representative images are shown. hGPR35a, human GPR35a.

5.2.12.3 Agonist mediated immunocytochemical detection of both human and mouse GPR35 is prevented by inhibition of GRK5/6

The human pSer^{300}-pSer^{303} GPR35a and mouse pSer^{298}-pSer^{301} GPR35 antisera also detect the corresponding receptors in an agonist-dependent manner in immunocytochemical studies (Divorty et al., 2022). For direct comparison of the phosphorylation pattern of both orthologues of GPR35, appropriate agonist and GRK 5/6 inhibitor, compound 19 were employed. In Flp-In TREx 293 cells induced to express either hGPR35a-HA or mGPR35-HA pre-treatment with compound 19 prevented immunocytochemical detection of the receptors by these antisera that were induced by the addition of appropriate agonist ligands (Figure 5.24). Parallel detection of each orthologue by anti-HA confirmed that the loss of agonist-induced detection by the phospho-site specific antisera in the presence of the compound did not reflect loss of receptor protein (Figure 5.24).

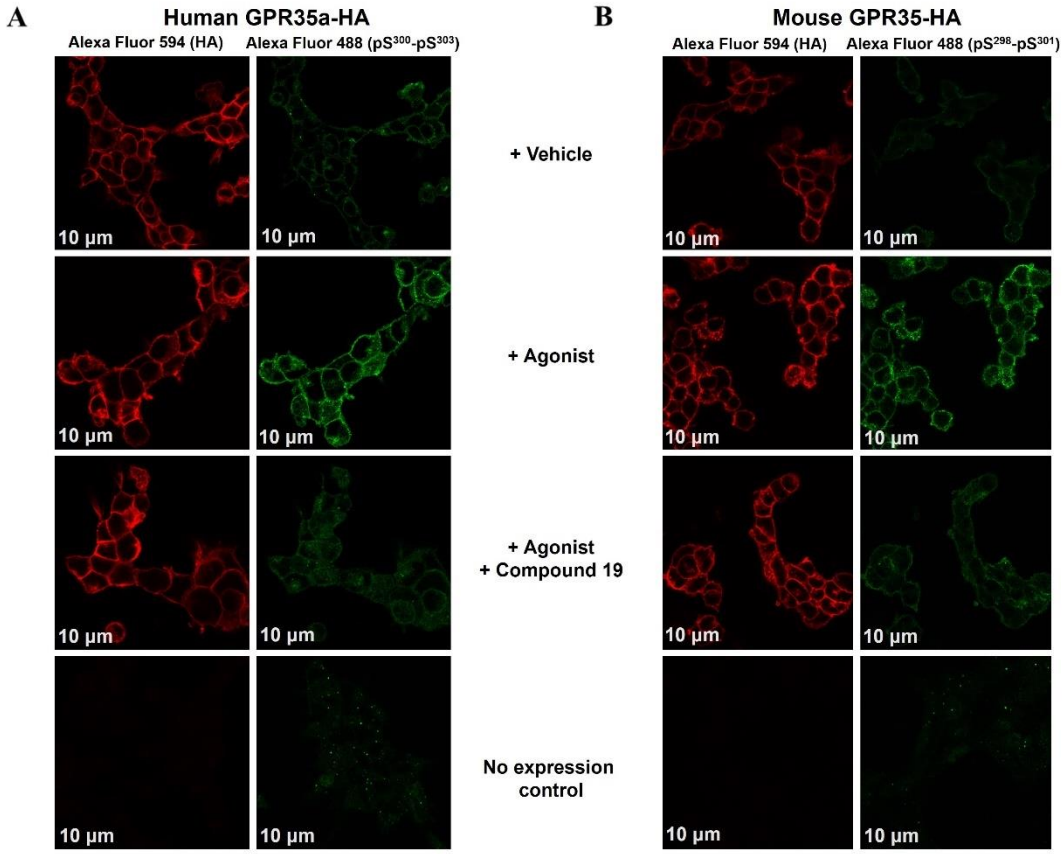

Figure 5.24 Direct comparison of phosphorylation between human and mouse orthologue of GPR35 by phospho-site–specific antisera in immunocytochemical studies
Cells as in **Figure 5.24** able to express **(A)** hGPR35a-HA and **(B)** mGPR35-HA were either uninduced (−dox) or induced by treatment with doxycycline (+dox) and then treated with either vehicle or suitable agonist and agonist with GRK inhibitor compound 19. Such cells were then used in immunocytochemical studies employing **(A)** hGPR35a-pSer^{300}/pSer^{301} or **(B)** mGPR35- pSer^{298}-pSer^{301}. In both **(A)** and **(B)** sections of this figure, samples were stained with Alexa Fluor 594 (HA)

(*left panels*) and Alexa Fluor 488 (pSer^{300}/pSer^{301} and pSer^{298}-pSer^{301}) (*right panels*). Scale bar = 10 µm. Representative images are shown.

5.2.13 Alphafold models of GPR35-GRK selectivity indicate selective interactions with GRK5/6

Overall, all of the investigations so far conducted, demonstrated important functions for GRK5 and 6, with little to no involvement of GRK2 and/or GRK3 in the phosphorylation of these particular sites or the interaction of hGPR35a with arrestins. To attempt to consider this at a more mechanistic and molecular level, I took the help of 'Alphafold' deep learning algorithm (Jumper et al., 2021, Mirdita et al., 2022) for prediction examination of GRK2, GRK3, GRK5, GRK6 with hGPR35a. From this predictive modelling of the interaction of human GPR35 with GRKs, it was clear that the extreme N-terminal region of GRK5 occupies the same methionine pocket on the intracellular face of hGPR35a that accommodates the $G\alpha_{13}$ C-terminal helix (Duan et al., 2022). But in these models, while GRK6's N-terminus overlaps with GRK5, GRK2 and GRK3 do not (Figure 5.25). Those models at least agree with the experimentally determined GRK-selectivity profile for GPR35.

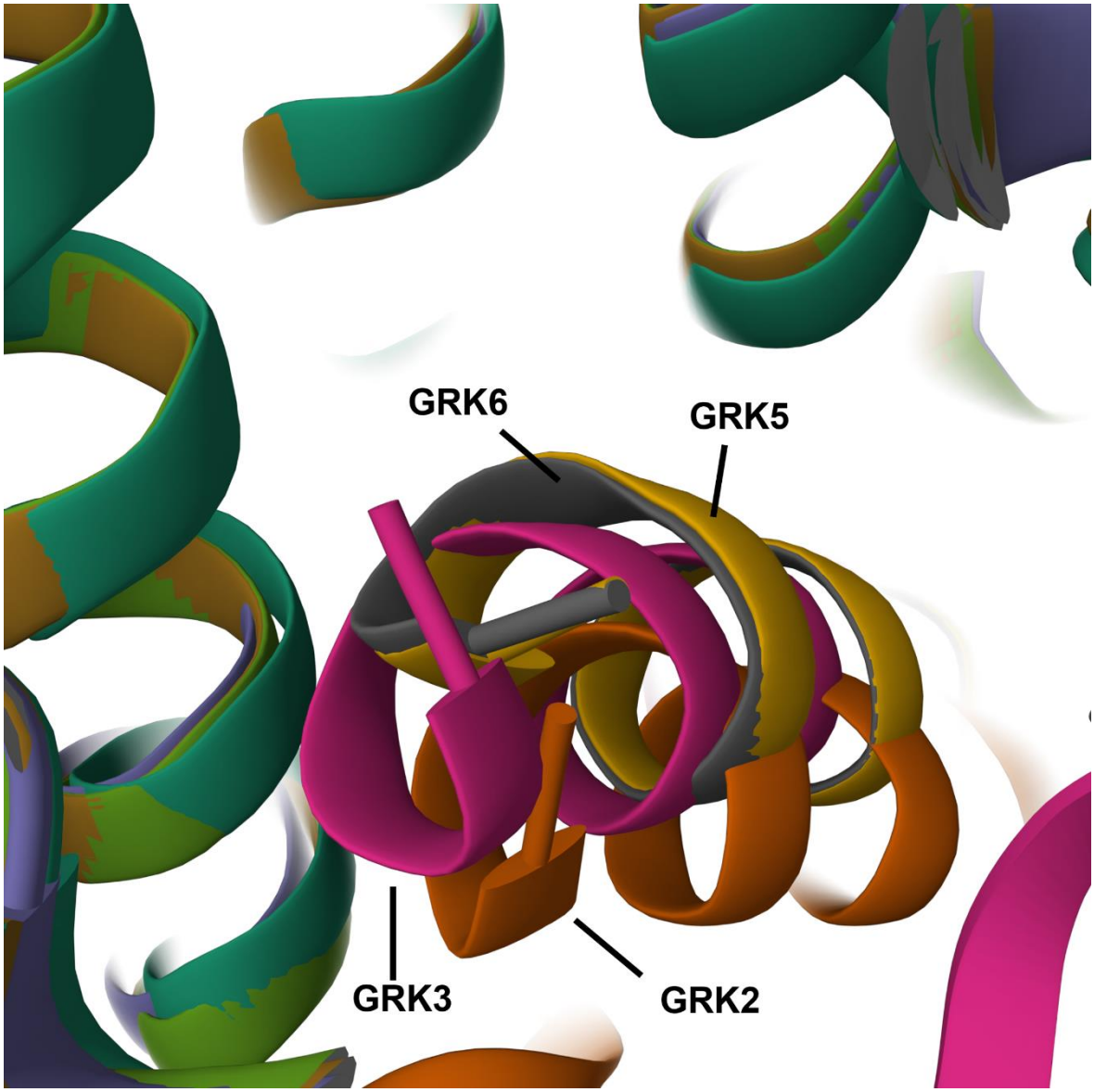

Figure 5.25 Alphafold prediction shows distinct peptide positioning and alignment of GRK isoforms, consistent with receptor selectivity
Alphafold modelling predicts distinct peptide positioning and alignment of GRK2 (orange) and GRK3 (pink) isoforms compared to GRK5 (yellow) or GRK6 (grey), consistent with agonist induced GPR35 selectivity. This artificial modelling prediction was carried out with the help of Dr. Tezz Quon.

It is also evident from the summary table that GRK5 and/or GRK6 but not GRK2 and/or GRK3 are essential to allow agonist-promoted GPR35-arrestin-3 interaction as well as phosphorylation. pEC_{50} and %Emax of lodoxamide in parental 293 cells, GRK KO, GRK2/3 KO and GRK5/6 KO cells are shown in the following table (Table 5.1)

	Parental 293	GRK KO	GRK 2/3 KO	GRK 5/6 KO
pEC_{50}	8.03 ±0.02	7.60±0.17 P=0.07 (ns)	8.09±0.02 P=0.97 (ns)	7.03±0.16 P<0.01 (**)
%Emax	100±0.01	11.83±4.16 P<0.001 (***)	120.2±0.92 P<0.01 (**)	16.89±1.81 P<0.001 (***)

Table 5.1 Comparison of pEC_{50} and %Emax of lodoxamide at different cell lines in human GPR35a-arrestin-3 interactions
pEC_{50} and %Emax of lodoxamide were compared at parental 293 and different GRK KO cell lines using BRET based human GPR35a-arrestin-3 recruitment assays. Results are expressed as mean ± SEM of three individual experiments. Data were analysed by one-way ANOVA followed by Dunnett's multiple comparisons test where the value for parental 293 cells was used as control. ns = non-significant, * p<0.05, ** p<0.01, ***p<0.001.

5.3 Discussion

Increasing amounts of data show that GPCR phosphorylation is a complicated process involving a variety of protein kinases that can phosphorylate the same receptor at various locations and that this leads to varied signalling effects (Tobin, 2008). It has also long been understood that GRK family members play a crucial role in GPCR regulation and in fostering connections with arrestin adaptor proteins (Gurevich and Gurevich, 2019, Benovic, 2021, Sulon and Benovic, 2021). Despite this, there is little known about the nature of the GRKs that interact with and control specific receptors and phosphorylated residues. Additionally, it is yet unclear how the concept of phosphorylation "bar-coding" relates to the phosphorylation of certain serine and/or threonine residues within the intracellular parts of GPCRs. Nonetheless, this could explain why distinct cell types and tissues can exhibit diverse biological reactions to agonists (Butcher et al., 2011, Prihandoko et al., 2015).

As GPR35 is a therapeutically important orphan GPCR and a potential target for lower gut inflammation to non-alcoholic steatohepatitis, gaining a comprehensive grasp of how GRK isoforms regulate GPR35 is essential. Although a significant variety of synthetic ligands, as well as the naturally occurring tryptophan metabolite kynurenic acid can activate this receptor, it is currently classified as an orphan GPCR (Quon et al., 2020, Milligan, 2023). Despite this, there is a great deal of interest in the idea that agonists of GPR35 could be useful in the treatment of ulcerative colitis and related disorders due to the protein's significant

expression in colon crypts and the obvious correlation between inflammatory diseases of the lower gut and a single nucleotide polymorphism that results in a T108M variation in transmembrane III of the protein (Quon et al., 2020). As multiple GRK isoforms are often routinely co-expressed and there is an obvious scarcity of well-characterised small molecules kinase inhibitors, a battery of complementary approaches including the creation of genome-edited cell lines devoid of expression of GRK2, GRK3, GRK5, and GRK6, the ubiquitously expressed GRK isoforms (Drube et al., 2022) and defining GRK selectivity by functional reconstitution, development and utilisation of both selective small molecule GRK inhibitors (Uehling et al., 2021, Varney et al., 2022), generation of phospho-site specific antisera that detect sites of regulated phosphorylation within GPR35 have been applied successfully (Divorty et al., 2022) for this therapeutically important receptor to highlight the contribution of specific GRK.

In this chapter, it has been proven initially that contribution of one or more GRK isoforms is necessary for agonist-induced interactions between human GPR35a and arrestin proteins. Furthermore, the accessibility of 293-derived cell lines devoid of expression of different GRKs showed that, whereas the absence of both GRK5 and GRK6 nearly completely removed agonist-induced receptor-arrestin associations, the removal of both GRK2 and GRK3 did not decrease such interactions. Furthermore, reconstitution tests using individual GRK isoforms were made possible by the ΔGRK2/3/5/6 HEK293 cells, and these showed that GRK5 and GRK6 were practically equally effective. Upon using 'Alphafold' deep learning algorithm (Jumper et al., 2021, Mirdita et al., 2022), molecular level and mechanistic analysis demonstrated that GRK5 and GRK6 interacted with hGPR35a strongly and effectively than GRK2 and GRK3 thus supporting our experimental findings. Even though compound 101 is a well-researched and well-proven selective inhibitor of GRK2 and GRK3 (Thal et al., 2011, Lowe et al., 2015), until recently, there have been few options available for selective small molecule inhibition of GRK5 and GRK6. The set of quinazoline-based inhibitors reported by (Uehling et al., 2021) has, however, provided a way to deal with this issue. In both immunoblotting and immunocytochemistry studies, Compound 19 and other compounds in this series successfully blocked the detection of agonist-mediated phosphorylation of the human and mouse orthologue by the hGPR35a $pSer^{300}$/$pSer^{303}$ antiserum and the equivalent mouse directed antiserum. They also

prevented agonist-induced interactions of human GPR35a with either arrestin-2 or arrestin-3. The established inhibitor molecule compound 101 was not effective either in inhibiting GPR35 phosphorylation and/or preventing receptor-arrestin interaction.

To pinpoint the contribution of individual GRK in GPR35 phosphorylation, I reintroduced a single GRK at a time into ΔGRK2/3/5/6 HEK293 cells. These GRKs were tagged with LgBiT at their N-terminal. To confirm the relative similar expression of each GRK, I used an anti-LgBiT monoclonal antibody. I also used GRK isoform directed antibody to detect the expression pattern of endogenous and transfected GRK in HEK 293 derived cell lines.

To measure the direct involvement of GRK5 and GRK6 in human GPR35 phosphorylation, I transiently introduced LgBiT-tagged forms of GRK2, GRK3, GRK5 or GRK6, along with hGPR35a-HA, into ΔGRK2/3/5/6 293 cells. Immunoblotting with anti-hGPR35a pSer^{300}-pSer^{303} showed that the presence of GRK5 and, in particular, GRK6, enhanced the phosphorylation of these sites, but that GRK2 and GRK3 had no discernible impact. I also demonstrated that If cells had received compound 19 before agonist treatment, these effects would have been completely inhibited.

One thing that needs to be mentioned is that compound 19 pre-treatment totally blocked the receptor's ability to be recognised by the phospho-site-specific antisera used following stimulation by an agonist, whereas pre-treatment with the GRK2/3 inhibitor compound 101 partially limited such recognition for both human GPR35a and mouse GPR35. This may seem contradictory given that compound 101 has no impact on arrestin recruitment. Yet I do not have a clear explanation for this, as previously mentioned, there are 5 phospho-acceptor sites in the C-terminal tail of human GPR35a (and indeed 9 in the C-terminal tail of mouse GPR35). Our group has previously demonstrated that all five residues in the human receptor can be phosphorylated in an agonist-dependent way, even though phosphorylation mediated by Ser^{303} is particularly crucial for interactions with arrestins (Divorty et al., 2022). In addition, it was found that after agonist treatment and subsequent phosphorylation, the antisera designed to recognise the receptor's unmodified C-terminal tail identified mouse GPR35 very poorly and human GPR35a less well. Hence, it is feasible that one or more of the additional

phospho-acceptor residues may be phosphorylated by GRK2/3, which may reduce the epitope's ability to be recognised by the $pSer^{301}$/$pSer^{303}$ antiserum. Indeed, the antigen used to generate the human antiserum (KAHKpSQDpSLCVTL) contains a further phospho-acceptor residue, whilst the mouse GPR35-directed $pSer^{298}$/$pSer^{301}$-GPR35 antiserum, was raised against the sequence TPHKpSQDpSQILSLT that contains an additional 2 phospho-acceptor residues.

The recent investigations highlight how crucial GRK5 and GRK6 are for increasing the agonist-dependent phosphorylation of, at the very least, Ser^{300} and Ser^{303} in human GPR35a (and residues Ser^{298} and Ser^{301} in the mouse orthologue). These residues are crucial for the agonist-induced interaction of these GPR35 orthologues with arrestins, according to mutational research also. However, it is crucial to note that all of the published investigations used HEK293-derived cells that were both wild type and genome-engineered. The idea that various kinases may stimulate various phosphorylation patterns in various cell types and tissues is beginning to take shape (Matthees et al., 2021) and It is now understood that, depending on the phosphorylation pattern, each of the widely expressed arrestin isoforms can interact with the same GPCR in a different way (Haider et al., 2022). The level of functional selectivity that results from this is likely to help explain why the same ligand-receptor combination can have distinct effects in various cells and tissues. The focus now needs to be on determining whether or if physiologically relevant tissues do produce this differential patterning and, if they do, what effects it might have on cell type and tissue function.

Overall, the cell-based investigations conducted in this chapter demonstrated important functions for GRK5 and 6, with little to no involvement of GRK2 and/or GRK3 in the phosphorylation of these particular sites or the interaction of GPR35 with arrestins. The findings of this chapter offer distinct and comprehensive insights into GPR35 modulation, a receptor that is currently generating significant interest as a potential new therapeutic target for conditions like ulcerative colitis.

Chapter 6 Split Nanoluciferase based complementation assay for systematic profiling of GPR35 GRK interaction

6.1 Introduction

G protein-coupled receptor kinases (GRKs) constitute a family of seven serine/threonine protein kinases that specifically recognise and regulate the phosphorylation of G protein-coupled receptors (GPCRs) in an agonist-dependent manner (Yang et al., 2017, Ribas et al., 2007). These GPCR kinases (GRK1 to GRK7) are also known as second messenger-independent kinases. GRK-mediated receptor phosphorylation is one of the well-characterised mechanisms for GPCR desensitisation. Receptor phosphorylation triggers the binding of arrestin proteins, which arrest the G protein dependent signalling, leading to rapid homologous desensitisation (Ribas et al., 2007). Recruitment of arrestin to the phosphorylated GPCRs frequently represents an early event in GPCR internalisation from the cell surface. Most commonly GPCR internalisation involves recruitment of the main components of the endocytic machinery of the coated pit, clathrin and clathrin adaptor AP-2. The internalised receptor is deactivated by the loss of agonist in the acidic environment of the endosome. This facilitates arrestin dissociation, which makes receptor-attached phosphates accessible for the phosphatases allowing the receptor to be recycled back to the plasma membrane and reused. Apart from this role, arrestin can also induce G protein-independent signalling like agonist-regulated mitogen-activated protein kinase (MAPK) scaffolds (Gurevich and Gurevich, 2019, Calebiro and Godbole, 2018) which has gained renewed interest within the scientific community.

GRKs are serine/threonine protein kinases that belong to the AGC kinase superfamily. GRKs share a modular structure where a central catalytic domain sits within a regulator of G protein signalling homology (RH) domain that is surrounded by a short N-terminal α-helical domain and a variable C-terminal lipid-binding region (Komolov and Benovic, 2018). This fundamental structure is conserved in all GRKs. The GRKs can be classified into three main groups based on sequence homology: visual GRK or rhodopsin kinase subfamily (GRK1 and GRK7), GRK2 or the ß-adrenergic receptor kinases subfamily (GRK2 and GRK3) and the GRK4 subfamily (GRK4, GRK5 and GRK6). All these kinases have certain characteristics in common, but they are all distinct enzymes with specific regulatory properties. GRK2, 3, 5 and 6 are ubiquitously expressed in mammalian tissues, whereas GRK1, 4 and 7 are confined to specific organs. GRK1 and 7 are expressed in retinal rods and cones, respectively, and GRK4 is present in the testis, cerebellum, and kidney

(Gurevich and Gurevich, 2019, Ribas et al., 2007, Sallese et al., 1997). Among all the GRKs, four of them are membrane anchored, namely GRK1 and GRK7 where the C-terminal region mediates membrane localisation by prenylation and GRK4 and GRK6, which are post-translationally palmitoylated by the C-terminal lipid-binding region leading to a constitutive membrane associated localisation (Figure 6.1). It is also worth mentioning that GRK4 and GRK6 are expressed as multiple splice-variant forms that can lead to a different structural domain organisation. GRK2 and GRK3 are recruited directly through their pleckstrin homology (PH) domain in the C-terminal, which binds the $G_{\beta\gamma}$ dimer and membrane phospholipid PIP2 and are thus made accessible following G protein activation and dissociation (Figure 6.1). As GRK2 and 3 are cytosolic proteins, these specific interactions usually help to maintain a membrane-bound population of GRK2 prior to the agonist-dependent overt GRK2 translocation (Penela et al., 2003). GRK5 is also membrane-associated through a PIP2 binding domain present on its N-terminus and binds phospholipids constitutively via its carboxy terminal domain. Recently, it has been observed that GRK5 contains an amphipathic helix membrane binding domain located in its C-terminal region, which is vital for its function and proper localisation at the membrane (Ribas et al., 2007, Palmer et al., 2022, Thiyagarajan et al., 2004).

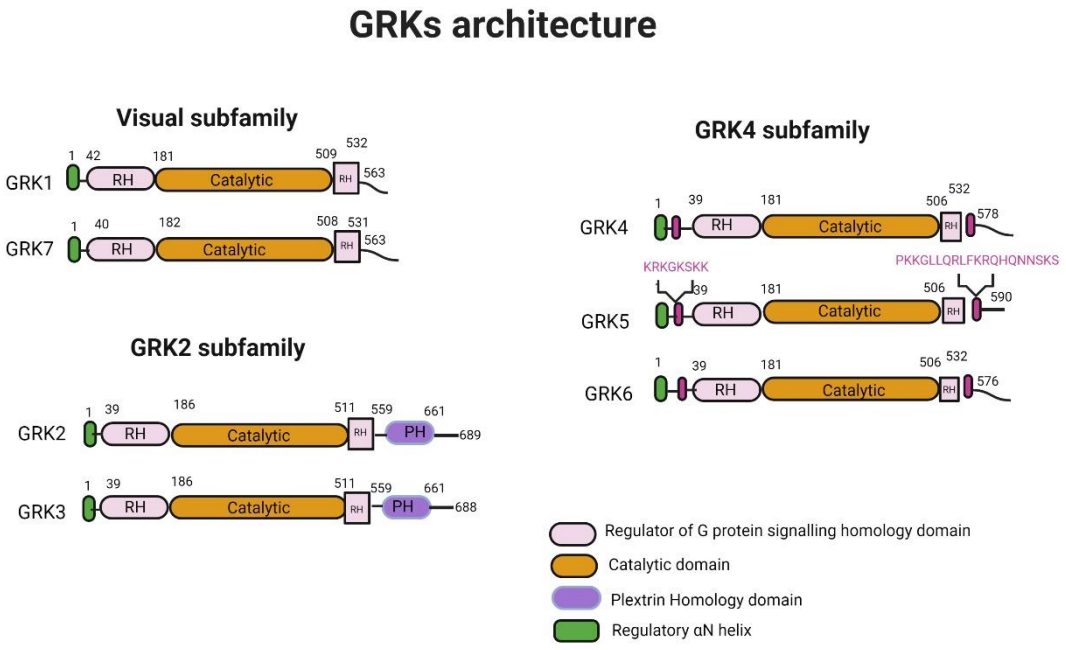

Figure 6.1 Architecture of GRKs

Based on sequence homology, GRKs are divided into 3 subfamilies and composed of two main domains, regulator of G protein signalling homology domain (RH) and catalytic domains. The first 20 residues of the αN-helix, which connects the N and C lobes of the catalytic domain, have a regulatory function. The C-terminal fragment mediates the membrane localisation of GRKs. Two polybasic areas are present at the N- and C-termini of the GRK4 subfamily, and GRK5 depends on these regions to interact with negatively charged phospholipids. The PH domain of GRK2 and GRK3 interacts with Gβγ subunits and acidic phospholipids. The idea of the figure was adopted from (Komolov and Benovic, 2018).This figure was created with BioRender.com.

In addition to phosphorylation and regulation of GPCRs, GRKs have already proven themselves as potential therapeutic targets in diseases, with studies from the Tesmer and Koch groups highlighting the importance of GRK2 in cardiovascular disease. They particularly showed a clear insight that paroxetine-mediated inhibition of GRK2 could improve cardiovascular signalling and function in a mouse model of heart failure (Schumacher et al., 2015). GRKs also influence physiological and pathological systems due to their role in receptor signalling and trafficking pathways for example, GRK5 can act as a cytoprotective in the regulation of protease activated receptor-1 (PAR1). In this case, GRK5 mediates arrestin-biased signalling in endothelial cells that is crucial for cytoprotection (Sulon and Benovic, 2021). GRK5 has also a vital role in pathological cardiac hypertrophy where GRK5 interacts with calmodulin that results in nuclear translocation associated with cardiac hypertrophy (Gold et al., 2013). GRK5 also contributes to pathological cardiac hypertrophy by activating the nuclear factor of activated T cells transcription factor in a phosphorylation independent manner by direct interaction (Gurevich and Gurevich, 2019).

The engagement of GRKs and subsequent interaction with the isoforms of arrestin are mandatory and crucial for agonist mediated phosphorylation of most of the GPCRs (Gurevich and Gurevich, 2019). These effector proteins (seven GRKs and four arrestins) are limited in number, but they can regulate around 800 members of the GPCR family (Palmer et al., 2022). Although it is well accepted in the scientific arena about the key roles of GRKs in the phosphorylation and regulation of many G protein-coupled receptors (GPCRs), the precise role of distinct GRKs has frequently been inadequately investigated and characterised (Sulon and Benovic, 2021). The routine co-expression of multiple GRK isoforms and the constrained selection of well-studied small molecule inhibitors of particular GRKs or subsets of the larger group have both contributed to this. The accurate identification of phosphorylation sites and linking this to the activity of specific

GRKs, or other protein kinases, as well as the control of specific physiological responses, represent significant hurdles. Using mass spectrometry-based phospho-proteomics, our group has already overcome this difficulty by enabling the rational design of receptor phospho-site specific antibodies (Marsango et al., 2022, Divorty et al., 2022).

GPR35 is a therapeutically important orphan GPCR which is a potential target for lower gut inflammation to non-alcoholic steatohepatitis (Quon et al., 2020). The relatively short intracellular C-terminal tail of GPR35 contains a cluster of sites of agonist-induced phosphorylation, which have been mapped using a combination of mass spectrometry, [^{32}P]labelling, and mutagenesis (Divorty et al., 2022). These investigations demonstrated that phosphorylation of Ser^{300} and Ser^{303} in human GPR35a and of the equivalent residues in the mouse and rat orthologues were key to effective interactions of the receptor with arrestin-3. Additionally, agonist dependence was nearly solely responsible for the phosphorylation of these residues. To further pinpoint the contribution of an individual or a group of GRKs in GPR35 phosphorylation, I used combinations of GRK subtype knock-out cell lines (Drube et al., 2022) and reconstitution of function with individual GRKs, a pSer^{300}-pSer^{303} human GPR35a directed antiserum and a group of selective small molecule GRK inhibitors (Uehling et al., 2021) and finally demonstrated that GRK5 and 6 are the key mediators of both the phosphorylation of Ser^{300} and Ser^{303} in human GPR35 and of the effective interactions of this receptor with arrestins, a process directly related to receptor internalisation (Chapter 5). Although all these new tools and novel techniques have aided a lot in the investigation of the contribution of a single or multiple GRKs for GPR35 phosphorylation, a standardised method is still required to clearly and methodically explain the GPR35-GRK interaction pattern. In this case, the split nanoluciferase based complementation assay has been employed for direct and systematic profiling of GPR35-GRK interaction.

6.1.1 Aims

As the important role of GRK5 and 6 in the regulation of GPR35 by particularly phosphorylating Ser^{300} and Ser^{303} in human GPR35a and subsequent interaction with the arrestin protein have been validated in Chapter 5, I finally wished to explore potential GPR35-GRK interactions more directly. To do so, I took advantage of the split nanoluciferase based complementation technology.

Basically, it is a protein-protein interaction assay where nanoluciferase (Nluc) recombines quickly and produces a strong luminescent signal upon supplemented with the corresponding substrate (Dixon et al., 2016). The fundamental design of this split nanoluciferase technique is that GRK is N-terminally or C-terminally tagged with a fragment of the Nanoluciferase (NLuc) enzyme, coined the LgBiT fragment (18 kDa), while the GPCR of interest is C-terminally tagged with the complementary 11-residue fragment, namely the SmBiT tag (Palmer et al., 2022). The LgBiT and SmBiT subunits are expressed as fusions to target proteins of interest and have each been independently optimised for stability and minimum self-association (Dixon et al., 2016). Target protein interaction makes it easier for subunit complementation to recreate a bright, luminescent enzyme (Figure 6.2). This complementation, which is completely reversible, enables the monitoring of protein attachment and dissociation across a wide dynamic range. To replicate this principle in GPR35, I generated a form of GPR35 which was C-terminally fused with the 11 amino acid small BiT (SmBiT) fragment of the NanoBiT® complementation technology. Upon co-expression of such a form of a receptor and a LgBiT-tagged form of a GRK, generation of luminescence upon addition of an appropriate substrate is consistent with NanoBiT complementation and, by extension, the proximity of the proteins linked to the corresponding SmBiT and LgBiT fragments (Palmer et al., 2022). The main aims of this chapter were:

To investigate the direct interaction between human and mouse GPR35 (wild type) with different GRKs using different parental 293 derived cell lines

To assess the systematic interaction between the phosphorylation deficient version of human and mouse GPR35 (PDM) with different GRKs

To investigate the signalling of GRK6 and GRK5 (particularly) with GPR35 by mutating some amino acids or truncating some portions to alter the plasma membrane localisation of GRK5

To particularly assess the pre-coupling behaviour and membrane-anchored nature of GRK5

To establish the significant contribution of GRK5 (compared to other GRKs) for interaction with GPR35 and support the findings obtained from chapter 5

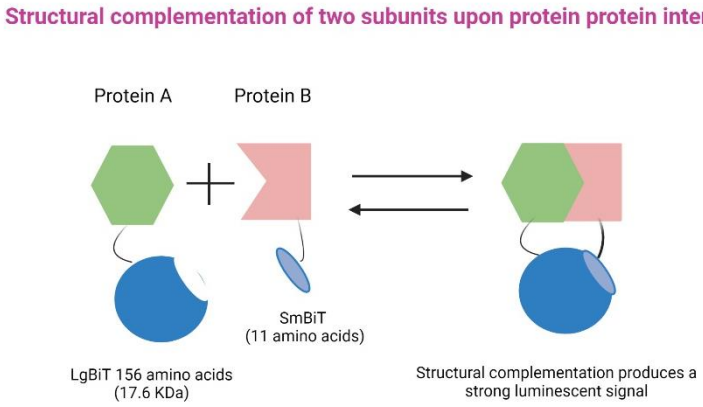

Figure 6.2 Generation of strong luminescence signal following structural complementation of two protein subunits
Here, protein A and protein B were fused with LgBiT and SmBiT respectively. LgBiT and SmBiT's structural complementation as a result of the interaction between the two fusion proteins creates an active enzyme with a strong, luminous signal. This figure was created with BioRender.com.

6.2 Results

6.2.1 Investigating the interaction between human GPR35 with GRKs

6.2.1.1 Assessment of interaction between hGPR35-SmBiT and GRK 2,3,5 and 6-LgBiT in ΔGRK2/3/5/6 293 cells

The human GPR35 gene is located on chromosome 2 and can be expressed as several transcripts resulting from differential promoter usage and alternative splicing (Schihada et al., 2022). The human GPR35 gene can be transcribed and translated into three variants. Variants 2 and 3 both encode the same longer isoform, GPR35b, which varies from GPR35a by an additional N-terminal extension of 31 amino acids. As a result, GPR35b has a longer extracellular domain but is otherwise identical in sequence (Quon et al., 2020). As I already know from the previous chapter, hGPR35 is phosphorylated mainly by GRK5 and GRK6; I attempt to investigate the direct and systematic interactions between hGPR35 and different GRKs. Since hGPR35 has two isoforms (hGPR35a and hGPR35b), experiments were conducted using both isoforms of hGPR35 with SmBiT tag at the C-terminal and different ubiquitously expressed GRKs with LgBiT tag at the N-terminal.

When I transiently expressed either LgBiT-tagged GRK2 or GRK3 with hGPR35a-SmBiT into ΔGRK2/3/5/6 293 cells, basal luminescence was low. By contrast, basal

luminescence following co-expression of the receptor with LgBiT-tagged forms of GRK5 or GRK6 was substantially higher (Figure 6.3A(i)). This is consistent with either a level of pre-coupling of the receptor with GRK5 and GRK6 or a 'bystander' effect produced because GRK5 and GRK6 are intrinsically targeted to the plasma membrane (Thiyagarajan et al., 2004). In the case of both GRK2 and GRK3, luminescence was increased modestly, in a concentration-dependent manner, by the addition of GPR35 agonist lodoxamide with pEC_{50} = 7.9 for GRK2 and 7.8 for GRK3 (Figure 6.3A(i)). By contrast, for GRK6 and, particularly, GRK5, a marked and concentration-dependent reduction of luminescence was produced upon the addition of lodoxamide, with pEC_{50} = 8.18 for GRK5 (Figure 6.3 A(i)). These initial high basal signals may be because of pre-coupling of hGPR35a with GRK5 and GRK6 and subsequent signal reduction may be due to disruption of such interactions with increasing concentration of agonist.

Upon addition of indicated concentration of GRK2/3 inhibitor, compound 101 (3-[[[4-methyl-5-(4-pyridyl)-4H-1,2,4-triazole-3-yl] methyl] amino]-N-[2-(trifuoromethyl) benzyl] benzamidehydrochloride) for 30 min followed by a fixed concentration of lodoxamide (100 nM, 5 min), the luminescence was not altered significantly for GRK2 and GRK3 compared to luminescence generated by lodoxamide only (Figure 6.3A(ii)). This may be because of the ATP-competitive nature of the kinase inhibitors (Vulpetti and Bosotti, 2004) and compound 101 indeed does not antagonise the action of GPR35 agonist lodoxamide. But interestingly and surprisingly, following treatment with indicated concentration of GRK5/6 inhibitor, compound 19 ((*S*)-*N*2-(1-(5-chloropyridin-2-yl) ethyl)-*N*4-(5-ethyl-1*H*-pyrazol-3-yl)-5-methoxyquinazoline-2,4-diamine) for 30 min followed by a fixed concentration of lodoxamide (100 nM, 5 min), the luminescence was increased significantly for GRK5 and at a modest level for GRK6 (Figure 6.3 A(ii)) compared to luminescence generated by lodoxamide only which were actually concentration-dependent reduction of signal. Again, this may be because of the inherent characteristic of the kinase inhibitor. As compound 19, a GRK5/6 inhibitor competes with ATP, it shows no antagonism with lodoxamide. By carefully analysing, it was found that the increasing trend of luminescence by different concentrations of compound 19 for GRK5 and GRK6 is obvious. The curve seems to be of an opposite pattern of the lodoxamide curve for GRK5 and GRK6 only because they are pre-coupled initially and then there is the occurrence of

ligand mediated disruption of such interactions. If there is no incidence of pre-coupling, then it is anticipated that the concentration curve of compound 19 will be almost similar to the lodoxamide curve.

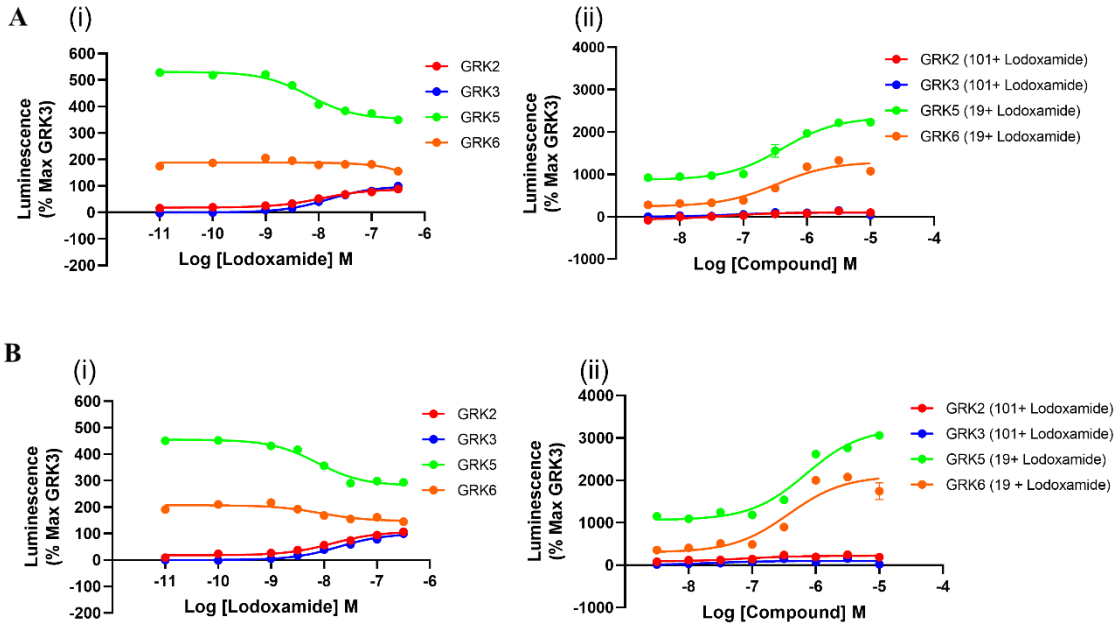

Figure 6.3 Assessment of direct interaction between hGPR35-SmBiT and GRK 2,3,5 and 6-LgBiT in ΔGRK2/3/5/6 293 cells using NanoBiT complementation technology

ΔGRK2/3/5/6 cells were transfected to co-express either **(A)** hGPR35a-SmBiT and **(B)** hGPR35b-SmBiT and GRK 2 (red circles),3 (blue circles),5 (green circles) and 6 (orange circles) each tagged with LgBiT. **(i)** Cells were exposed to the indicated concentrations of lodoxamide for 5 min and after substrate addition luminescence was measured. **(ii)** Prior to the addition of lodoxamide (100 nM, 5 min) cells were pre-treated for 30 min with varying concentrations of either compound 19 (GRK5 and GRK6) or compound 101 (GRK2 and GRK3). Data are presented as % of the effect of lodoxamide (300 nM) in GRK3 co-transfected cells. The experiment was performed once only (n=1).

Studies akin to the Figure 6.3A, GRK recruitment assay were undertaken employing long isoform of human GPR35 or hGPR35b. Here again, upon transient transfection of either LgBiT-tagged GRK2 or GRK3 with hGPR35b-SmBiT into ΔGRK2/3/5/6 293 cells, basal luminescence was low initially and then luminescence was increased modestly, in a concentration-dependent manner, by addition of GPR35 agonist lodoxamide with pEC_{50} = 7.8 for GRK2 and 7.7 for GRK3 (Figure 6.3B(i)). On the other hand, after co-expression of the receptor hGPR35b-SmBiT with LgBiT-tagged versions of GRK5 or GRK6, basal luminescence was noticeably increased, but the addition of lodoxamide resulted in a significant and concentration-dependent reduction of luminescence for GRK6 and, particularly GRK5 pEC_{50} = 8.13 (Figure 6.3B(i)).

The luminescence for GRK2 and GRK3 was not significantly changed after adding the prescribed concentration of GRK2/3 inhibitor, compound 101, for 30 min, followed by a fixed concentration of lodoxamide (100 nM, 5 min) (Figure 6.3B(ii)). However, intriguingly, and unexpectedly, the luminescence was significantly increased for GRK5 and at a modest level for GRK6 upon the addition of the indicated concentration of GRK5/6 inhibitor, compound 19, for 30 min followed by a fixed concentration of lodoxamide (100 nM, 5 min) (Figure 6.3B(ii)), as opposed to luminescence generated by lodoxamide alone, which were concentration-dependent reductions of the signal. We anticipate the same molecular process is replicated here like Figure 6.3A.

It is worth mentioning that raw luminescence values were significantly lower when the assays were done with hGPR35b compared to hGPR35a.

The key results of lodoxamide induced interaction between hGPR35 isoforms and different GRKs are shown in the following table (Table 6.1).

%Emax	hGPR35a	hGPR35b
GRK2	87.86	107.6
GRK3	100	100
GRK5	352.2	280.8
GRK6	Variable	147.3

Table 6.1 Comparison of lodoxamide induced interaction between hGPR35 isoforms and different GRKs in ΔGRK2/3/5/6 293 cells using NanoBiT complementation technology
%Emax of lodoxamide was compared after hGPR35a-SmBiT and hGPR35b-SmBiT were co-expressed with GRK2, 3, 5 and 6 in ΔGRK2/3/5/6 293 cells. Data are presented as % of the effect of lodoxamide (300 nM) in GRK3 co-transfected cells. The experiment was performed once only (n=1).

6.2.1.2 Assessment of interaction between hGPR35-SmBiT and GRK 2,3,5 and 6-LgBiT in parental 293 cells

All the experiments in the previous sections 6.2.1.1, were conducted in parental 293 derived cell lines that were genome edited to lack expression of all the ubiquitously expressed GRKs such as GRK2,3,5 and 6. The aim of using this genome edited cell line was to pinpoint the interaction between introduced GRK and hGPR35 without the effects of ubiquitously expressed endogenous GRKs. As the main principle of the protein sub-unit system is the complementation of the two sub-units and generation of luminescence upon the addition of an appropriate

substrate, the proximity of the proteins linked to the corresponding SmBiT and LgBiT fragments is the key. For this reason, I attempted to replicate the same series of experiments of Figure 6.3 in parental HEK 293 cells.

Here in parental HEK 293 cells, all universally expressed GRK2,3,5 and 6 tagged with LgBiT were co-transfected with either hGPR35a-SmBiT (Figure 6.4A(i)) or hGPR35b-SmBiT (Figure 6.4B(i)). The same pattern of the lodoxamide curve was found in parental cells compared to ΔGRK2/3/5/6 293 cells for both isoforms of hGPR35. pEC_{50} value of lodoxamide were 7.9 for GRK2, 7.9 for GRK3, 8.4 for GRK5 and 8.9 for GRK6 when they were complemented with hGPR35a. Again, the pEC_{50} value of lodoxamide were 7.8 for GRK2, 7.9 for GRK3, 8.5 for GRK5 and 8.4 for GRK6 when they were complemented with hGPR35b. Although the nature of agonist response was similar, the raw luminescence values were significantly lower in HEK 293 cells compared to genome edited cells. These may be because of the possible interference of the endogenous kinase to the introduced GRKs.

Upon addition of inhibitor compounds 101 or 19 for 30 min, followed by a fixed concentration of lodoxamide (100 nM, 5 min) the pattern of curve was similar in parental cells compared to ΔGRK2/3/5/6 293 cells for both hGPR35a (Figure 6.4A(ii)) and hGPR35b (Figure 6.4B(ii)) although in comparison to genome edited knock-out cells, the raw luminescence values in HEK 293 cells were much lower.

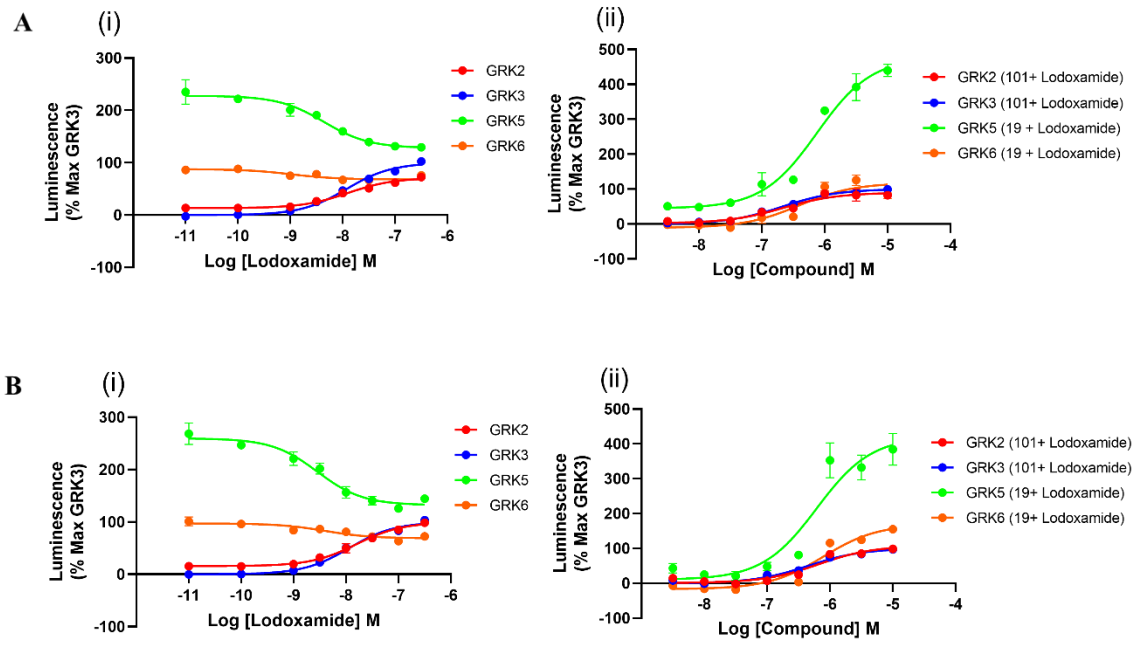

Figure 6.4 Interaction between hGPR35-SmBiT and GRK 2,3,5 and 6-LgBiT in parental HEK 293 cells

Parental HEK293 cells were transfected to co-express either **(A)** hGPR35a-SmBiT and **(B)** hGPR35b -SmBiT and GRK 2 (red circles),3 (blue circles),5 (green circles) and 6 (orange circles) each tagged with LgBiT. **(i)** Cells were exposed to the indicated concentrations of lodoxamide for 5 min and after substrate addition luminescence was measured. **(ii)** Prior to the addition of lodoxamide (100 nM, 5 min) cells were pre-treated for 30 min with varying concentrations of either compound 19 (GRK5 and GRK6) or compound 101 (GRK2 and GRK3). Data are presented as % of the effect of lodoxamide (300 nM) in GRK3 co-transfected cells. The experiment was performed once only (n=1).

6.2.2 The effects of phosphorylation on human GPR35 interaction with GRKs

6.2.2.1 Measurement of interaction between hGPR35a PDM-SmBiT and GRK 2,3,5 and 6-LgBiT in ΔGRK2/3/5/6 293 cells

From my observations in the previous sections, I have found that the GRK5 and GRK6 recruitment profile with both isoforms of human GPR35 in parental 293 cells or genome edited ΔGRK2/3/5/6 cells followed an agonist concentration-dependent reduction of luminescence. To investigate the potential reason for this signal reduction, an attempt was made to generate the phosphorylation deficient version of the hGPR35a construct, which is known as hGPR35a PDM-SmBiT. Here, all 5 potential phosphorylation sites in the C-terminal tail of hGPR35a had been mutated to alanine. The idea behind this generation of phosphorylation deficient mutant of hGPR35a (hGPR35a PDM-SmBiT) came from the initial thought that reduction of the signal by GRKs, specially by GRK5 is due to internalisation and, therefore, phosphorylation of the receptor.

In this assay, as usual and expected basal luminescence was low when LgBiT-tagged GRK2 or GRK3 was transiently expressed in ΔGRK2/3/5/6 293 cells with hGPR35a PDM-SmBiT and then luminescence was increased modestly and gradually, in a concentration-dependent manner, by addition of GPR35 agonist lodoxamide with pEC_{50} = 8.3 for GRK2 and 8.1 for GRK3. In the case of the interaction of hGPR35a PDM-SmBiT with GRK5 and GRK6, our expectation was that the luminescence signal would not be reduced. Surprisingly, I found a similar scenario of the previous section. Here, the basal luminescence was considerably raised after co-expression of the receptor hGPR35a PDM-SmBiT with LgBiT-tagged copies of GRK5 or GRK6, while the addition of lodoxamide caused a large and concentration-dependent reduction of luminescence for GRK5 and modestly for GRK6 with pEC_{50} = 8.5 for GRK5 and 8.4 for GRK6 (Figure 6.5(i)). As the result of the phosphodeficient version of the receptor was similar to the wild type, so I could preliminarily claim that phosphorylation has really no significant contribution in GRKs recruitment assay, at least in this setting. One possible explanation of this finding is that in the phosphorylation deficient version of hGPR35a, amino acids (serine and threonine) in the C-terminal chain have been mutated to alanine only. But from my recent study (Ganguly et al., 2023), when I predicted the GPR35-GRK interaction using the 'Alphafold' deep learning algorithm (Jumper et al., 2021, Mirdita et al., 2022), this approach suggests that GRK5 and GRK6's extreme N-terminal regions reside in the same methionine pocket as the Ga_{13} C-terminal helix (Duan et al., 2022).

The pattern of the curve was identical in hGPR35a PDM-SmBiT transfected ΔGRK2/3/5/6 293 cells in comparison to hGPR35a SmBiT transfected ΔGRK2/3/5/6 cells after the addition of inhibitor compounds 101 or 19 for 30 min, followed by a fixed concentration of lodoxamide (100 nM, 5 min) (Figure 6.5(ii)).

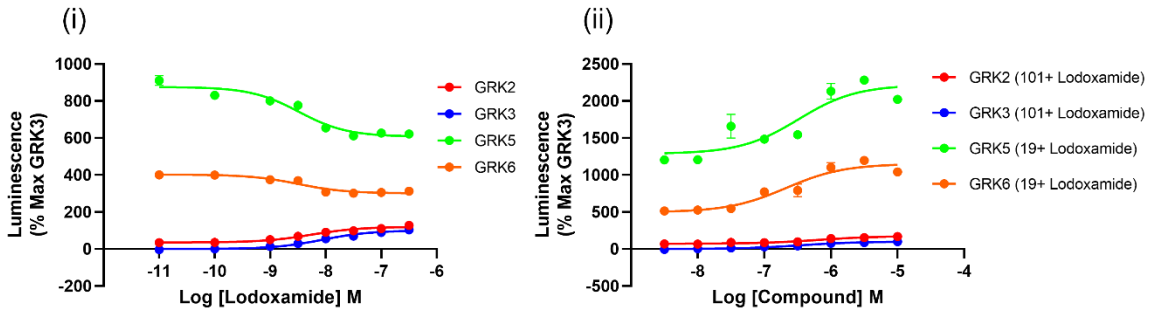

Figure 6.5 Interaction between hGPR35a PDM-SmBiT and GRK 2,3,5 and 6 LgBiT in ΔGRK2/3/5/6 293 cells

ΔGRK2/3/5/6 cells were transfected to co-express hGPR35a PDM-SmBiT and GRK 2 (red circles),3 (blue circles),5 (green circles) and 6 (orange circles) each tagged with LgBiT. **(i)** Cells were exposed to the indicated concentrations of lodoxamide for 5 min and after substrate addition luminescence was measured. **(ii)** Prior to the addition of lodoxamide (100 nM, 5 min), cells were pre-treated for 30 min with varying concentrations of either compound 19 (GRK5 and GRK6) or compound 101 (GRK2 and GRK3). Data are presented as % of the effect of lodoxamide (300 nM) in GRK3 co-transfected cells. The experiment was performed once only (n=1).

6.2.2.2 Measurement of interaction between hGPR35a-SmBiT and GRK 2,3,5 and 6-LgBiT in parental 293 cells genome edited to lack expression of both arrestin-2 and arrestin-3

As depicted from the previous result, using a phosphorylation deficient mutant of GPR35, hGPR35a PDM SmBiT was unsuccessful in reversing the signal reduction of GRK5 (particularly) and GRK6 also. From my previous knowledge and literature search, I conducted the experiment in parental 293 cells that have been genome edited to lack expression of both arrestin-2 and arrestin-3. As there is some evidence (Sánchez-Fernández et al., 2013) that a totally phosphorylation deficient mutant of the receptor could still recruit arrestin protein and thereby can be internalised, so in this case, again, I took an effort to transfect LgBiT-tagged GRK2/3/5 and 6 with SmBiT-tagged hGPR35a in arrestin-2 and arrestin-3 knock-out cell lines and thereby eliminating every possibility of phosphorylation, internalisation and therefore signal reduction. When GRK2 and GRK3 with LgBiT-tagged were co-transfected with SmBiT-tagged hGPR35a in a genome edited cell line, the initial luminescence value was low as usual and the addition of the GPR35 agonist lodoxamide, with pEC_{50} values of 7.2 for GRK2 and 7.5 for GRK3, moderately and gradually increased luminescence in a concentration-dependent manner. After this, when the receptor hGPR35a-SmBiT with copies of GRK5 or GRK6 that were LgBiT-tagged, were co-expressed in arrestin-2 and arrestin-3 knock-out cell lines, the basal luminescence was again noticeably increased for GRK5 and moderately for GRK6; however, the addition of lodoxamide resulted in

a significant and concentration-dependent reduction of luminescence for GRK5 and moderately for GRK6 with pEC_{50} = 7.9 for GRK5 and 7.7 for GRK6 (Figure 6.6(i)).

Comparing the hGPR35a-SmBiT transfected to arrestin-2 and arrestin-3 knock-out cell lines to hGPR35a PDM-SmBiT transfected to ΔGRK2/3/5/6 cells, the curve pattern was identical after the addition of inhibitor compounds 101 or 19 for 30 min, followed by a fixed concentration of lodoxamide (100 nM, 5 min) (Figure 6.6(ii)).

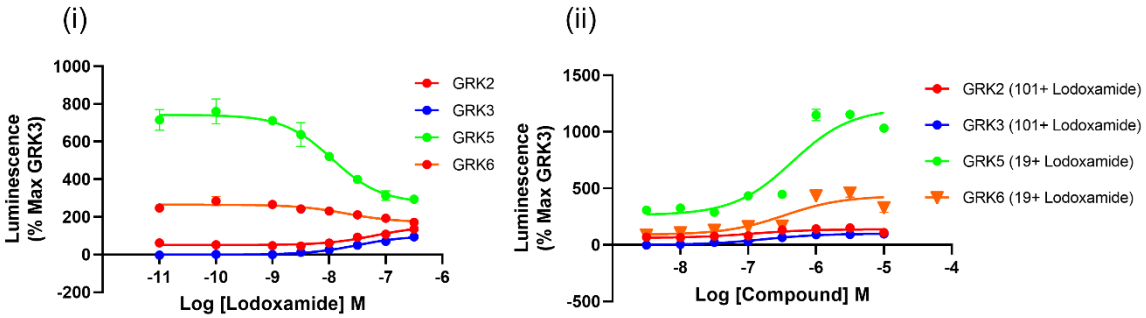

Figure 6.6 Measurement of interaction between hGPR35a-SmBiT and GRK 2,3,5 and 6-LgBiT in parental 293 cells that have been genome edited to lack expression of both arrestin-2 and arrestin-3

Arrestin-2 and arrestin-3 knock-out cells were transfected to co-express hGPR35a-SmBiT and GRK 2 (red circles),3 (blue circles),5 (green circles) and 6 (orange circles) each tagged with LgBiT. **(i)** Cells were exposed to the indicated concentrations of lodoxamide for 5 min and after substrate addition, luminescence was measured. **(ii)** Prior to the addition of lodoxamide (100 nM, 5 min) cells were pre-treated for 30 min with varying concentrations of either compound 19 (GRK5 and GRK6) or compound 101 (GRK2 and GRK3). Data are presented as % of the effect of lodoxamide (300 nM) in GRK3 co-transfected cells. The experiment was performed once only (n=1).

6.2.2.3 Interaction between hGPR35a-SmBiT and hGPR35a PDM-SmBiT with GRK 2,3,5 and 6-LgBiT (C orientations) in ΔGRK2/3/5/6 293 cells

It is already known that in the NanoBiT® complementation technology, the GPCR of interest is C-terminally tagged with the complementary 11-residue fragment, referred to as the SmBiT tag, while GRK is N-terminally or C-terminally tagged with a fragment of the Nanoluciferase (NLuc) enzyme, dubbed the LgBiT fragment (18 kDa) (Palmer et al., 2022). I have so far used the GRKs with LgBiT at the N-terminal in every experiment. Although the above groups mention that GRK with N-terminal LgBiT provides the highest specific signal to background readouts, I took a chance to test the other orientation of LgBiT. In this experiment, I used LgBiT-tagged GRK2/3/5 and 6 at the C-terminal with SmBiT-tagged hGPR35a also at the C-terminal.

When I transiently expressed either LgBiT-tagged at the C-terminal of GRK2 or GRK3 with hGPR35a-SmBiT into ΔGRK2/3/5/6 293 cells, there was almost no luminescence or signal across the entire concentration range of agonist lodoxamide. By contrast, basal luminescence following co-expression of the receptor with LgBiT-tagged (C-terminal) forms of GRK5 or GRK6 was substantially higher, however, the inclusion of lodoxamide produced a moderate concentration-dependent reduction of luminescence for GRK5 and GRK6 with pEC_{50} = 8.7 for GRK5 and 8.9 for GRK6 (Figure 6.7A). The most interesting observation found from this experiment is that the raw luminescence signal is greater for GRK6 than GRK5 but in our all-previous sets of experiments, the signal of GRK5 always outcompetes GRK6. These phenomena occurred may be because of the conformational change of the LgBiT fragments in GRKs.

Like Figure 6.7A, now I was interested in utilising hGPR35a PDM-SmBiT instead of hGPR35a-SmBiT. Here, when ΔGRK2/3/5/6 293 cells transfected with either LgBiT-tagged at C-terminal of GRK2 or GRK3 with hGPR35a PDM-SmBiT, again for the full spectrum of agonist lodoxamide concentrations, there was almost no luminescence or signal. In contrast, basal luminescence following co-expression of the receptor with LgBiT-tagged (C-terminal) forms of GRK5 or GRK6 was significantly higher. However, the inclusion of lodoxamide produced a moderate concentration-dependent reduction of luminescence for GRK5 and GRK6, with pEC_{50} = 7.9 for GRK5 and pEC_{50} = 8.0 for GRK6 (Figure 6.7B(i)).

There was almost no luminescence or signal for GRK2 and GRK3 again after adding the prescribed concentration of GRK2/3 inhibitor, compound 101, for 30 min, followed by a fixed concentration of lodoxamide (100 nM, 5 min) (Figure 6.7B (ii)). However, the luminescence was significantly increased for GRK6 and at a modest level for GRK5 upon the addition of the indicated concentration of GRK5/6 inhibitor, compound 19, for 30 min followed by a fixed concentration of lodoxamide (100 nM, 5 min) (Figure 6.7B (ii)).

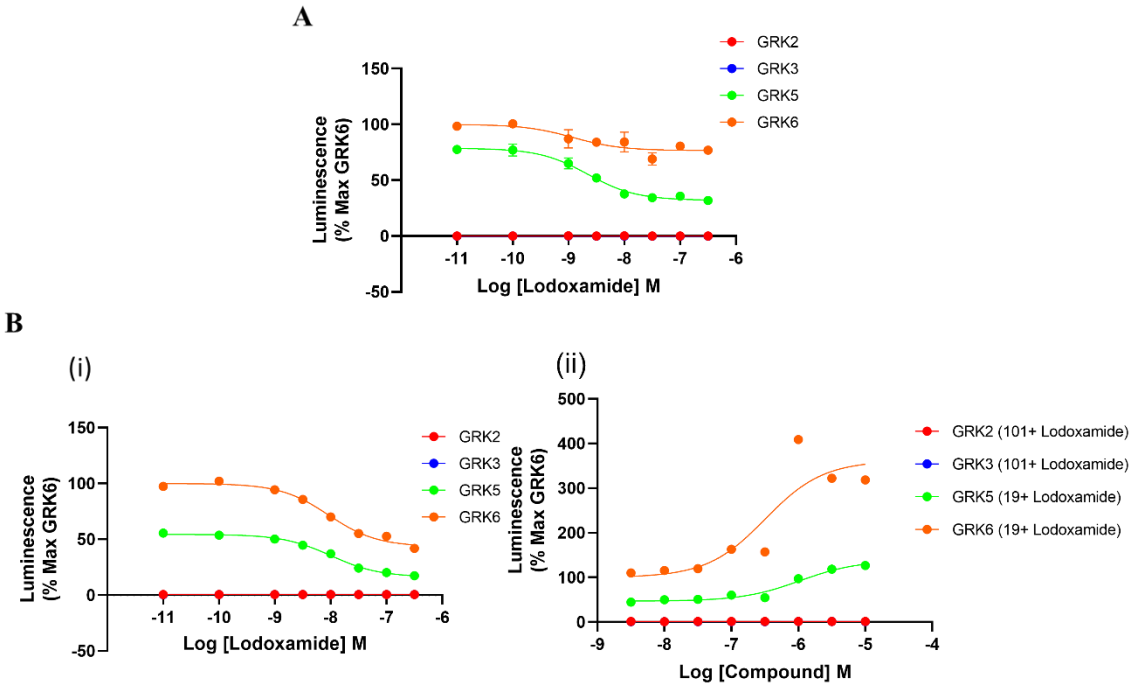

Figure 6.7 Measurement of interaction between hGPR35a-SmBiT and hGPR35a PDM-SmBiT with GRK 2,3,5 and 6-LgBiT (C orientations) in ΔGRK2/3/5/6 293 cells

ΔGRK2/3/5/6 cells were transfected to co-express **(A)** hGPR35a-SmBiT and **(B)** hGPR35a PDM-SmBiT and GRK 2 (red circles),3 (blue circles),5 (green circles) and 6 (orange circles) each tagged with LgBiT (C orientations). **(A)** and **(B) (i)** Cells were exposed to the indicated concentrations of lodoxamide for 5 min and after substrate addition luminescence was measured. **(B) (ii)** Prior to addition of lodoxamide (100 nM, 5 min) cells were pre-treated for 30 min with varying concentrations of either compound 19 (GRK5 and GRK6) or compound 101 (GRK2 and GRK3). Data are presented as % of the effect of lodoxamide (300 nM) in GRK6 co-transfected cells. The experiment was performed once only (n=1).

6.2.2.4 Investigation of interaction between hGPR35a-SmBiT with GRK 2,3,5 and 6-LgBiT in HEK 293 cells genome edited to lack expression of G-proteins

After trying with phosphodeficient versions of hGPR35a, using cell line genome edited to lack expression of arrestin-2 and arrestin-3, or trying with different orientations of LgBiT, there was still signal reduction for GRK5 and GRK6. I then attempted to use the concept of using a parental 293 derived cell line that is genome edited to lack expression of G_q, G_{11}, G_{12} and G_{13}. The original concept is that for some receptors, for example, angiotensin II type-2 receptor (AT1R), GRK5/6 availability for ligand-bound AT1R is negatively regulated by G_q, a family of heterotrimeric G-protein. Upon pharmacological inhibition or genetic loss of G_q, GRK5 and GRK6 signals increase rather than decrease (Kawakami et al., 2022).

In this assay, upon transient transfection of either LgBiT-tagged GRK2 or GRK3 with hGPR35a-SmBiT into $\Delta G_{q/11/12/13}$ cells, basal luminescence was low initially and then luminescence was increased modestly, in a concentration-dependent manner, by addition of GPR35 agonist lodoxamide with pEC_{50} = 6.9 for GRK2 and 7.8 for GRK3 (Figure 6.8(i)). On the other hand, after co-expression of the receptor hGPR35a-SmBiT with LgBiT-tagged versions of GRK5 or GRK6, basal luminescence was noticeably increased, but the inclusion of lodoxamide produced a significant and concentration-dependent reduction of luminescence for GRK6 (pEC_{50} = 8.5) and, particularly, GRK5 (pEC_{50} = 8.3) (Figure 6.8(i)). So, from this experiment, it was clear that even after using $\Delta G_{q/11/12/13}$ cells, there are still signal reductions of GRK5 and GRK6.

The luminescence for GRK2 and GRK3 was not significantly changed after adding the prescribed concentration of GRK2/3 inhibitor, compound 101, for 30 min, followed by a fixed concentration of lodoxamide (100 nM, 5 min) (Figure 6.8(ii)). However, the luminescence was significantly increased for GRK5 and at a modest level for GRK6 upon the addition of the indicated concentration of GRK5/6 inhibitor, compound 19, for 30 min followed by a fixed concentration of lodoxamide (100 nM, 5 min) (Figure 6.8(ii)).

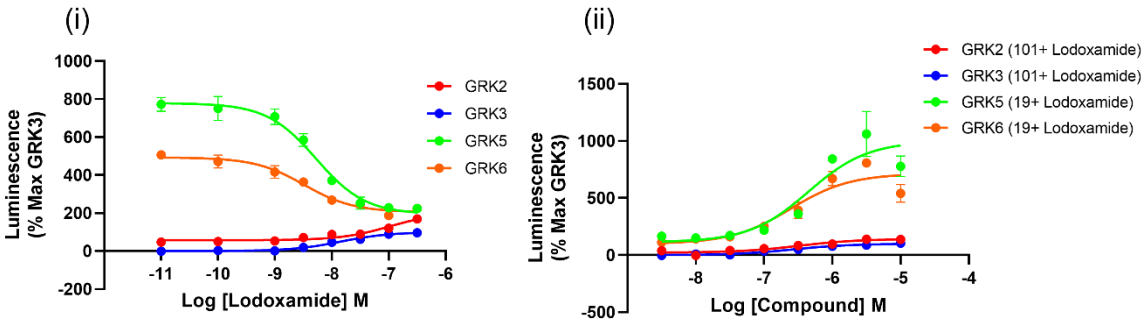

Figure 6.8 Interaction between hGPR35a-SmBiT and GRK 2,3,5 and 6-LgBiT in parental 293 cells that have been genome edited to lack expression of G_q, G_{11}, G_{12} and G_{13}

$\Delta G_{q/11/12/13}$ cells were transfected to co-express hGPR35a SmBiT and GRK 2 (red circles),3 (blue circles),5 (green circles) and 6 (orange circles) each tagged with LgBiT. **(i)** Cells were exposed to the indicated concentrations of lodoxamide for 5 min and after substrate addition luminescence was measured. **(ii)** Prior to the addition of lodoxamide (100 nM, 5 min) cells were pre-treated for 30 min with varying concentrations of either compound 19 (GRK5 and GRK6) or compound 101 (GRK2 and GRK3). Data are presented as % of the effect of lodoxamide (300 nM) in GRK3 co-transfected cells. The experiment was performed once only (n=1).

6.2.3 Investigating the interaction between human GPR35 with GRKs using partial agonist

6.2.3.1 Assessment of interaction between hGPR35a-SmBiT and GRK 2,3,5 and 6-LgBiT in ΔGRK2/3/5/6 293 cells with pamoic acid

So far, I used lodoxamide, a reference agonist for GPR35, in all these experiments. I utilised both isoforms of hGPR35, the phosphodeficient version of this receptor and even different genome edited cell lines that specifically lack expression of either GRKs or arrestin or G-proteins. But still there was agonist mediated signal reduction of GRK5 and GRK6 with hGPR35 interaction. To solve this issue, I now tried to switch the agonist ligand for GPR35 from full agonist lodoxamide to partial agonist pamoic acid.

In this assay, basal luminescence was initially low after transiently transfecting either GRK2 or GRK3 tagged with LgBiT with hGPR35a-SmBiT into ΔGRK2/3/5/6 293 cells. Luminescence was then very modestly increased, in a concentration-dependent manner, by the addition of hGPR35a partial agonist pamoic acid, with pEC_{50} = 6.9 for GRK2 and 7.0 for GRK3 (Figure 6.9(i)). On the other hand, basal luminescence was notably elevated after co-expression of the receptor hGPR35a-SmBiT with LgBiT-tagged versions of GRK5 or GRK6 but decreased gradually and concentration-dependently for GRK6 (pEC_{50} = 7.8) and particularly, GRK5 (pEC_{50}= 7.6) for pamoic acid (Figure 6.9(i)). Furthermore, it was evident from this experiment that there were still signal reductions of GRK5 and GRK6 even when utilising pamoic acid as an agonist, although the trend of this curve was less sharp than full agonist lodoxamide.

After applying the recommended concentration of the GRK2/3 inhibitor, compound 101, for 30 min, followed by a fixed quantity of pamoic acid (1 μM, 5 min), the luminescence for GRK2 and GRK3 did not vary appreciably (Figure 6.9(ii)). However, when the stated quantity of the GRK5/6 inhibitor, compound 19, was added for 30 min, followed by a fixed concentration of pamoic acid (1 μM, 5 min), the luminescence was dramatically elevated for GRK5 and at a modest level for GRK6 (Figure 6.9(ii)).

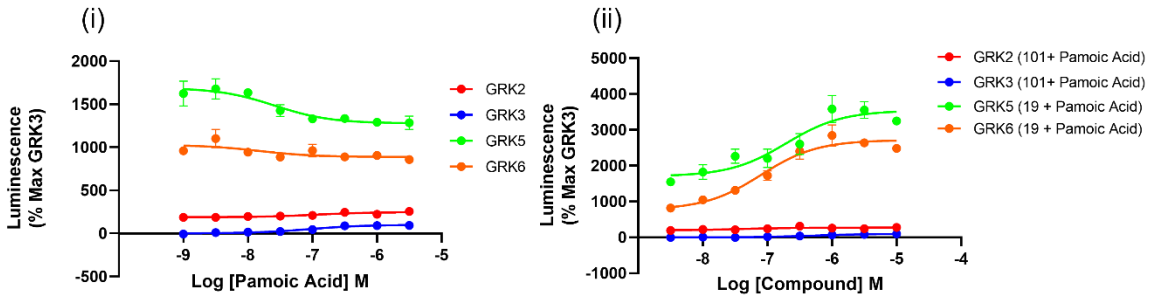

Figure 6.9 Assessment of interaction between hGPR35a-SmBiT and GRK 2,3,5 and 6-LgBiT in ΔGRK2/3/5/6 293 cells with hGPR35a partial agonist pamoic acid

ΔGRK2/3/5/6 cells were transfected to co-express either hGPR35a SmBiT and GRK 2 (red circles),3 (blue circles),5 (green circles) and 6 (orange circles) each tagged with LgBiT. **(i)** Cells were exposed to the indicated concentrations of pamoic acid for 5 min and after substrate addition luminescence was measured. **(ii)** Prior to the addition of pamoic acid (1 μM, 5 min) cells were pre-treated for 30 min with varying concentrations of either compound 19 (GRK5 and GRK6) or compound 101 (GRK2 and GRK3). Data are presented as % of the effect of pamoic acid (3 μM) in GRK3 co-transfected cells. The experiment was performed once only (n=1).

6.2.3.2 Measurement of interaction between hGPR35b-SmBiT and GRK 2,3,5 and 6-LgBiT in ΔGRK2/3/5/6 293 cells with pamoic acid

After using the partial agonist pamoic acid in hGPR35a-GRK interactions, I was keen to utilise this ligand to assess the interaction of hGPR35b (the long isoform of hGPR35) with different GRKs. Aside from the use of GRK selective inhibitors, an attempt was made to use hGPR35 specific antagonist molecule CID-2745687 in these interactions.

After transiently transfecting either GRK2 or GRK3 with hGPR35b-SmBiT into ΔGRK2/3/5/6 293 cells, basal luminescence was initially low in this test. The addition of the hGPR35b partial agonist pamoic acid very slightly increased luminescence in a concentration-dependent manner, with pEC_{50} = 7.2 for GRK2 and pEC_{50} = 7.1 for GRK3 (Figure 6.10(i)). However, increased baseline luminescence was gradually and concentration-dependently reduced for GRK6 and particularly GRK5 (pEC_{50} = 7.6) for pamoic acid after co-expression of the receptor hGPR35b-SmBiT with LgBiT-tagged versions of GRK5 or GRK6 (Figure 6.10(i)).

The luminescence for GRK2 and GRK3 did not significantly change after 30 min of using compound 101 at the prescribed concentration, followed by a constant dose of pamoic acid (1 μM, 5 min) (Figure 6.10(ii)). However, the luminescence was significantly increased for GRK5 and at a low level for GRK6 when the specified

amount of the GRK5/6 inhibitor, compound 19, was administered for 30 min, followed by a fixed concentration of pamoic acid (1 μM, 5 min) (Figure 6.10(ii)).

After 15 min of utilising hGPR35b antagonist CID-2745687 at the recommended concentration, followed by a steady dose of pamoic acid (1 μM, 5 min), the luminescence for GRK2 and GRK3 altered slightly compared to pamoic acid only curve (Figure 6.10(iii)). The reason behind this is probably CID-2745687 is antagonising the effects of pamoic acid in the recruitment of GRK2 and GRK3. Also, when the prescribed dose of the antagonist CID-2745687, was supplied for 15 min, followed by a fixed concentration of pamoic acid (1 μM, 5 min), the luminescence was not significantly changed for GRK5 and GRK6 compared to pamoic acid only curve (Figure 6.10(iii)). The overall effect of antagonist CID-2745687 in recruiting GRKs is not prominent because the original luminescence value generated by partial agonist pamoic acid is also moderate.

In this set of experiments, transfected with hGPR35b-SmBiT, raw luminescence values were comparatively lower because it is obvious that hGPR35b yields a lower signal. Overall, the raw luminescence was also lower because partial agonist pamoic acid was used instead of any full agonist.

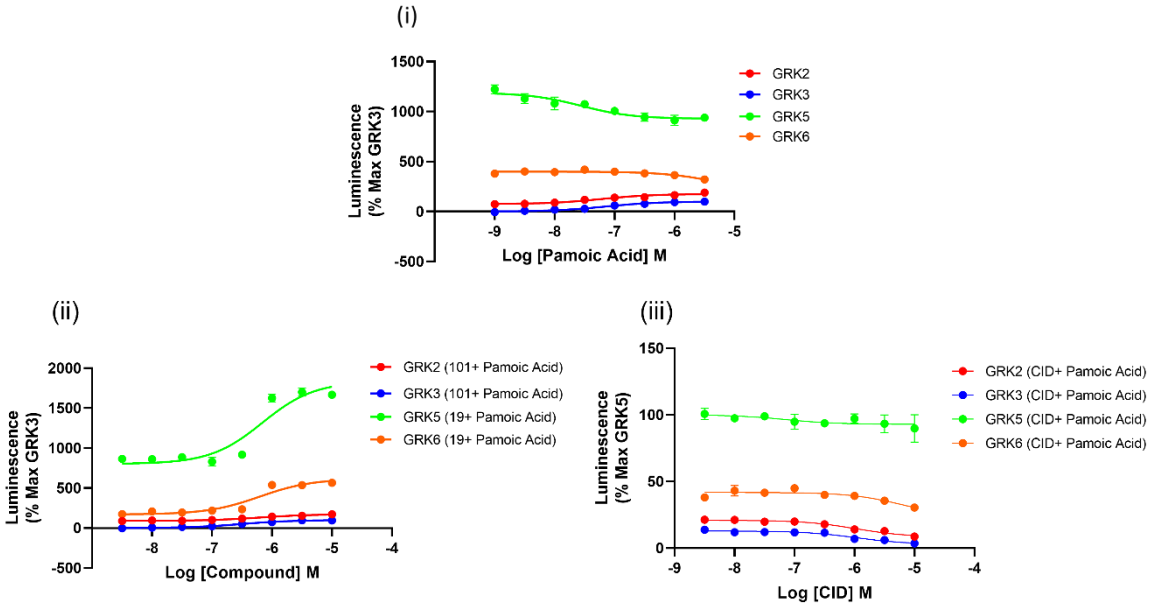

Figure 6.10 Assessment of interaction between hGPR35b-SmBiT and GRK 2,3,5 and 6-LgBiT in ΔGRK2/3/5/6 293 cells with hGPR35b partial agonist pamoic acid

ΔGRK2/3/5/6 cells were transfected to co-express either hGPR35b SmBiT and GRK 2 (red circles),3 (blue circles),5 (green circles) and 6 (orange circles) each tagged with LgBiT. **(i)** Cells were exposed to the indicated concentrations of pamoic acid for 5 min and after substrate addition luminescence

was measured. **(ii)** Prior to the addition of pamoic acid (1 μM, 5 min) cells were pre-treated for 30 min with varying concentrations of either compound 19 (GRK5 and GRK6) or compound 101 (GRK2 and GRK3). **(iii)** Cells were also treated with different concentration of hGPR35b antagonist CID-2745687 for 15 min before adding pamoic acid (1 μM, 5 min). Data are presented as % of the effect of pamoic acid (3 μM) in GRK3 co-transfected cells. The experiment was performed once only (n=1).

6.2.4 Investigating the interaction between human GPR35 with GRKs using novel potent agonist GSK 938

As the luminescence signal reduction of GRK5 and GRK6 with hGPR35 was still visible (although to a lower extent) upon introduction of the partial agonist pamoic acid, I was interested in utilising a new potent agonist of GPR35, developed by a company called GlaxoSmithKline pharmaceutical industry company. As this compound is not still available in the public domain, I was instructed to call it GSK 938 rather than its actual IUPAC name. From the initial studies, the compound was proven equipotent both for human and mouse orthologues of GPR35.

6.2.4.1 Assessment of interaction between hGPR35a-SmBiT and GRK 2,3,5 and 6-LgBiT in $\Delta G_{q/11/12/13}$ cells with GSK 938

In this assay, basal luminescence was initially low after transiently transfecting either GRK2 or GRK3 with hGPR35a-SmBiT into ΔGq/11/12/13 cells. Luminescence was then modestly increased, in a concentration-dependent manner, by the addition of GPR35 agonist GSK 938, with pEC_{50} = 7.0 for GRK2 and pEC_{50} = 8.2 for GRK3 (Figure 6.11(i)). On the other hand, basal luminescence was notably elevated after co-expression of the receptor hGPR35a-SmBiT with LgBiT-tagged versions of GRK5 or GRK6 but decreased significantly and concentration-dependently for GRK6 (pEC50 = 7.7) and, particularly for GRK5 (pEC_{50} = 7.9) (Figure 6.11(i)). Furthermore, it is evident from this experiment that there are still signal decreases of GRK5 and GRK6 even when utilising GSK 938 as an agonist.

After applying the recommended concentration of the GRK2/3 inhibitor, compound 101, for 30 min., followed by a fixed quantity of GSK 938 (100 nM, 5 min), the luminescence for GRK2 and GRK3 did not vary appreciably (Figure 6.11(ii)). However, when the stated quantity of the GRK5/6 inhibitor, compound 19, was added for 30 min, followed by a fixed concentration of GSK 938 (100 nM, 5 min), the luminescence was dramatically elevated for GRK5 and GRK6 (Figure 6.11(ii)).

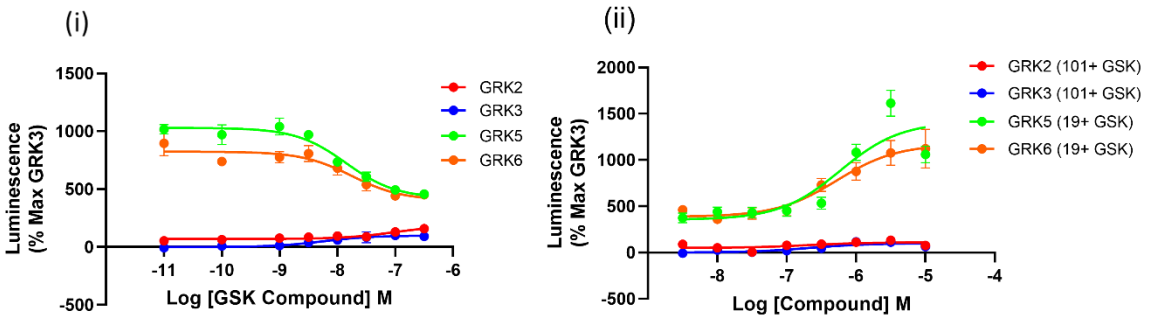

Figure 6.11 Interaction between hGPR35a-SmBiT and GRK 2,3,5 and 6-LgBiT in parental 293 cells that has been genome edited to lack expression of G_q, G_{11}, G_{12} and G_{13} with new potent agonist GSK 938

$\Delta G_{q/11/12/13}$ cells were transfected to co-express hGPR35a SmBiT and GRK 2 (red circles),3 (blue circles),5 (green circles) and 6 (orange circles) each tagged with LgBiT. **(i)** Cells were exposed to the indicated concentrations of GSK 938 for 5 min and after substrate addition luminescence was measured. **(ii)** Prior to the addition of GSK 938 (100 nM, 5 min) cells were pre-treated for 30 min with varying concentrations of either compound 19 (GRK5 and GRK6) or compound 101 (GRK2 and GRK3). Data are presented as % of the effect of GSK 938 (300 nM) in GRK3 co-transfected cells. The experiment was performed once only (n=1).

6.2.4.2 Measurement of interaction between hGPR35a-SmBiT and GRK 2,3,5 and 6-LgBiT in ΔGRK2/3/5/6 293 cells with GSK 938

As the signal reductions of GRK5 and GRK6 with hGPR35 were still evident, I changed the cell line from lacking expression of G-protein to lacking presence of all the ubiquitously expressed GRKs. I also added CID-2745687, the hGPR35 antagonist to block the effects of the potent agonist.

In this assay, basal luminescence was again initially low after transiently transfecting either GRK2 or GRK3 with hGPR35a-SmBiT into ΔGRK2/3/5/6 293 cells. Luminescence was then modestly increased, in a concentration-dependent manner, by the addition of GPR35 agonist GSK 938, with pEC_{50} = 7.9 for GRK2 and 7.9 for GRK3 (Figure 6.12(i)). On the other hand, basal luminescence was notably elevated after co-expression of the receptor hGPR35a-SmBiT with LgBiT-tagged versions of GRK5 or GRK6 but decreased significantly and concentration-dependently for GRK6 (pEC_{50} = 7.8) and, particularly for GRK5 (pEC_{50} = 7.8) (Figure 6.12(i)). Furthermore, it was evident from this experiment that there are still signal reductions of GRK5 and GRK6 even when utilising GSK 938 as an agonist in ΔGRK2/3/5/6 293 cells.

The luminescence for GRK2 and GRK3 did not significantly change after applying the suggested concentration of the GRK2/3 inhibitor, compound 101, for 30 min

followed by a constant amount of GSK 938 (100 nM, 5 min.) (Figure 6.12(ii)). However, the luminescence for GRK5 and GRK6 was significantly increased when the specified amount of the GRK5/6 inhibitor, compound 19, was administered for 30 min, followed by a fixed concentration of GSK 938 (100 nM, 5 min) (Figure 6.12(ii)).

The luminescence for GRK2 and GRK3 changed dramatically this time compared to the GSK 938 alone curve after 15 min of treatment with the hGPR35a antagonist CID-2745687 at the prescribed concentration followed by a steady dose of GSK 938 (100 nM, 5 min) (Figure 6.12(iii)). The probable cause is the ability of CID-2745687 to counteract the effects of GSK 938 in the recruitment of GRK2 and GRK3. Moreover, the luminescence for GRK5 and GRK6 also differed substantially from the curve of GSK 938 alone when the antagonist CID- 2745687 was administered as directed for 15 min, followed by a fixed concentration of GSK 938 (100 nM, 5 min) (Figure 6.12(iii)). As GSK 938 is very potent, antagonism by CID-2745687 is also clearly visible.

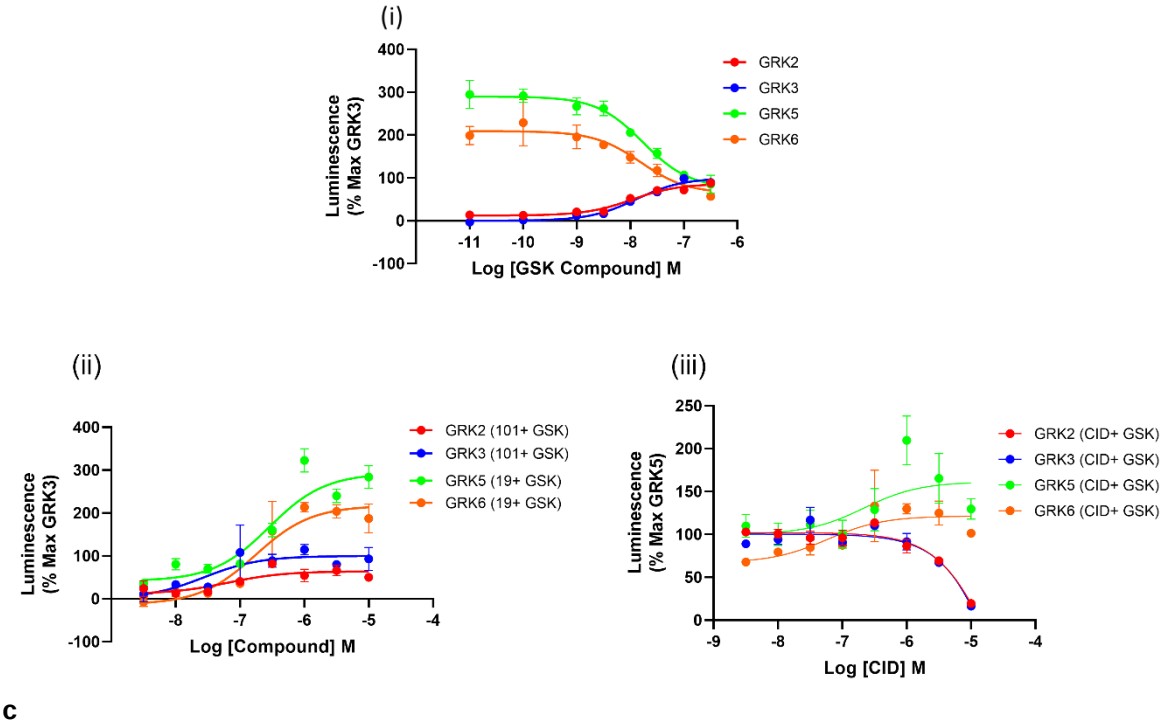

c

Figure 6.12 Assessment of interaction between hGPR35a-SmBiT and GRK 2,3,5 and 6-LgBiT in ΔGRK2/3/5/6 293 cells with GPR35 potent agonist GSK 938

ΔGRK2/3/5/6 cells were transfected to co-express either hGPR35a SmBiT and GRK 2 (red circles),3 (blue circles),5 (green circles) and 6 (orange circles) each tagged with LgBiT. **(i)** Cells were exposed to the indicated concentrations of GSK 938 for 5 min and after substrate addition luminescence was

measured. **(ii)** Prior to the addition of GSK 938 (100 nM, 5 min), cells were pre-treated for 30 min with varying concentrations of either compound 19 (GRK5 and GRK6) or compound 101 (GRK2 and GRK3). **(iii)** Cells were also treated with different concentrations of hGPR35a antagonist CID-2745687 for 15 min before adding GSK 938 (100 nM, 5 min). Data are presented as % of the effect of GSK 938 (300 nM) in GRK3 co-transfected cells. The experiment was performed once only (n=1).

6.2.5 Validation of luciferase complementation assay by deliberately introducing other GRKs with GPR35

6.2.5.1 Measurement of interaction between hGPR35a-SmBiT and GRK 1,4,5 and 7- LgBiT in ΔGRK2/3/5/6 293 cells with lodoxamide

In our recent study described in chapter 5, we employed different novel techniques and tools, such as combinations of mass spectrometry, [^{32}P] labelling, mutagenesis to specify the contribution of an individual or a family of GRKs for phosphorylation of GPR35. I also took the help of the combinations of GRK subtype knock-out cell lines, reconstitution of function with individual GRKs, human and mouse GPR35 directed antiserum and group of selective small molecule GRK inhibitors and proved that GRK5 and GRK6 are the key mediators of both the phosphorylation of Ser^{300} and Ser^{303} in human GPR35 and of the efficient connections between this receptor and arrestins, which is a key step in the internalisation of the receptor.

Now, I want to ensure that the same findings are also reproducible with the nanoluciferase based complementation assay. For this, the visual GRKs (GRK1 and GRK7) and GRK4 (limited presence in certain regions of the body like testis, cerebellum, and kidney), each with LgBiT tag at the N-terminal were transfected with hGPR35a-SmBiT in ΔGRK2/3/5/6 293 cells. GRK5 with LgBiT tag was also used as a reference. Lodoxamide, a standard agonist, was used in this experiment. Here, for the full spectrum of agonist lodoxamide concentrations, there was almost no luminescence or signal either for GRK1, GRK4 or GRK7 (Very limited). On the other hand, basal luminescence was significantly increased when the receptor was co-expressed with GRK5 tagged with LgBiT and then decreased gradually with increasing concentration of lodoxamide (pEC_{50} = 7.9) (Figure 6.13).

This experiment clearly validates the accuracy of the luciferase-based complementation assay system for direct and systematic profiling of GPCR-GRK interaction

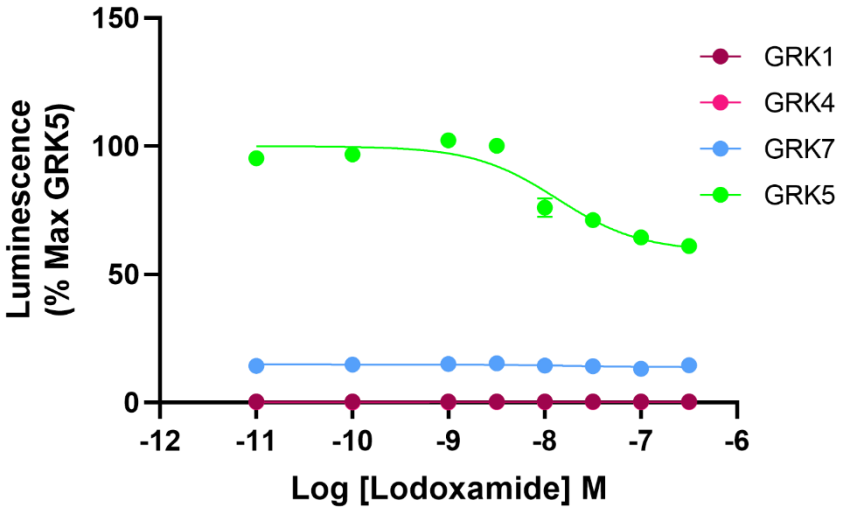

Figure 6.13 Validation of interaction between hGPR35a-SmBiT and GRK 1,4,5 and 7-LgBiT in ΔGRK2/3/5/6 293 cells

Arrestin-2 and arrestin-3 knock-out cells were transfected to co-express hGPR35a SmBiT and GRK 1 (maroon circles),4 (pink circles),5 (green circles) and 7 (light blue circles) each tagged with LgBiT. Cells were exposed to the indicated concentrations of lodoxamide for 5 min and after substrate addition luminescence was measured. Data are presented as % of the effect of lodoxamide (300 nM) in GRK5 co-transfected cells. Interaction between hGPR35a SmBiT and GRK5 LgBiT was used as a reference. The experiment was performed once only (n=1).

6.2.6 Investigating the interaction between mouse GPR35 with GRKs

GPR35 is a unique receptor in several aspects that make translation difficult. Rodents only express one version of a protein, whereas humans express two different protein isoform sequences. The pharmacology of the GPR35 orthologues in humans and rodents are significantly different from one another, with differences between rat and mouse GPR35 being just as noticeable as those between either of these species and human versions. For this reason, I was very keen to investigate the GRKs recruitment profile of mouse orthologues of GPR35 using a highly potent mouse GPR35 agonist GSK 938 and pemirolast

6.2.6.1 Assessment of interaction between mGPR35-SmBiT and GRK 2,3,5 and 6-LgBiT in ΔGRK2/3/5/6 293 cells

In this test, recruitment of all ubiquitously expressed GRKs was investigated with mouse orthologue of GPR35. Initially, upon transient transfection of either GRK2 or GRK3 (LgBiT tagged) with mGPR35-SmBiT into ΔGRK2/3/5/6 293 cells resulted in very low basal luminescence. The addition of the GPR35 agonist GSK 938 then slightly increased luminescence in a concentration-dependent manner, with pEC_{50} values of 8.9 for GRK2 and 8.5 for GRK3 (Figure 6.14(i)). The basal luminescence, on the other hand, was markedly increased following co-expression of the receptor mGPR35-SmBiT with LgBiT-tagged versions of GRK5 or GRK6, but it also decreased significantly and concentration-dependently for GRK6 (pEC_{50} = 8.5) and, particularly, for GRK5 (pEC_{50} = 8.6) (Figure 6.14(i)). Most importantly, it is noticeable that luminescence signal reduction of GRK5 and GRK6 are also prevalent in mouse orthologue of GPR35.

After using the recommended concentration of the GRK2/3 inhibitor, compound 101, for 30 min and then a constant amount of GSK 938 (100 nM, 5 min), the luminescence for GRK2 and GRK3 did not significantly alter (Figure 6.14(ii)). Nevertheless, when the prescribed dose of the GRK5/6 inhibitor, compound 19, was applied for 30 min, followed by a fixed concentration of GSK 938 (100 nM, 5 min), the luminescence for GRK5 and GRK6 was dramatically increased (Figure 6.14(ii)).

The luminescence for GRK2 and GRK3 did not change at all this time compared to the GSK 938 alone curve after 15 min of treatment with the GPR35 antagonist CID-2745687 at the prescribed concentration followed by a steady dose of GSK 938 (100 nM, 5 min) (Figure 6.14(iii). The probable cause may be the human receptor selective nature of the antagonist CID-2745687. Moreover, the luminescence curve for GRK5 and GRK6 were also almost flat line upon treatment with CID-2745687 for 15 min, followed by a fixed concentration of GSK 938 (100 nM, 5 min) (Figure 6.14(iii)) suggesting that the potent hGPR35 antagonist CID-2745687 is not active at mouse orthologue, thereby again validating the complex pharmacology of the receptor between humans and rodents.

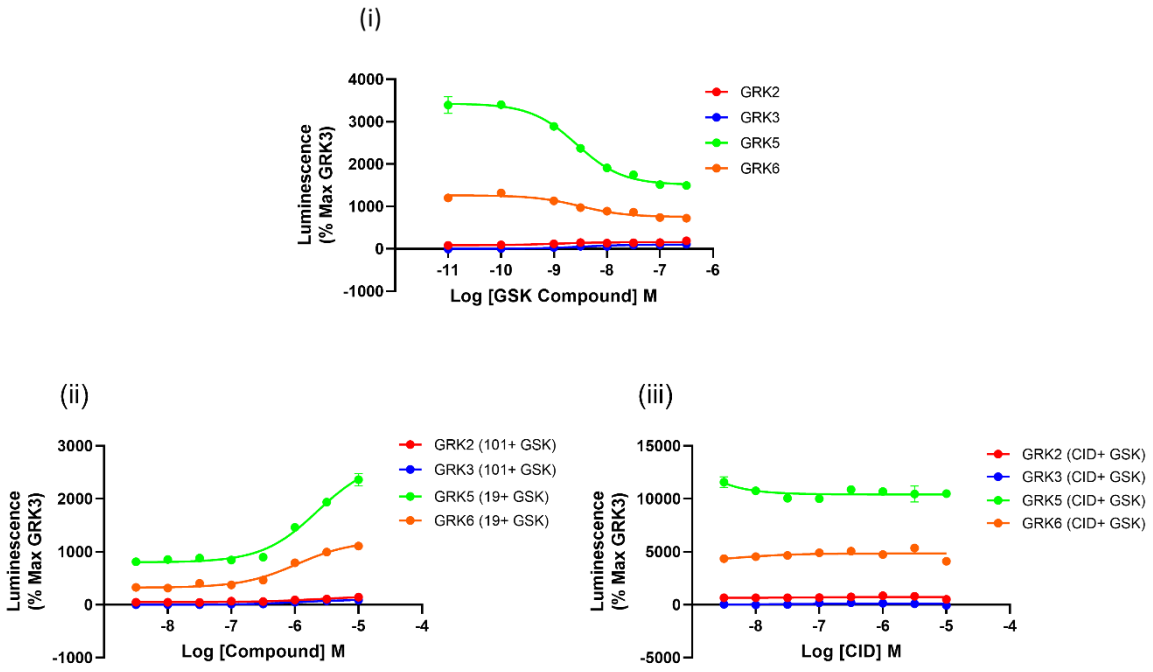

Figure 6.14 Assessment of interaction between mGPR35-SmBiT and GRK 2,3,5 and 6-LgBiT in ΔGRK2/3/5/6 293 cells with GPR35 potent agonist GSK 938 and validation of species selectivity of antagonist CID-2745687

ΔGRK2/3/5/6 cells were transfected to co-express either mGPR35 SmBiT and GRK 2 (red circles),3 (blue circles),5 (green circles) and 6 (orange circles) each tagged with LgBiT. **(i)** Cells were exposed to the indicated concentrations of GSK 938 for 5 min and after substrate addition luminescence was measured. **(ii)** Prior to the addition of GSK 938 (100 nM, 5 min) cells were pre-treated for 30 min with varying concentrations of either compound 19 (GRK5 and GRK6) or compound 101 (GRK2 and GRK3). **(iii)** Cells were also treated with different concentrations of GPR35 antagonist CID-2745687 for 15 min before adding GSK 938 (100 nM, 5 min). Data are presented as % of the effect of GSK 938 (300 nM) in GRK3 co-transfected cells. The experiment was performed once only (n=1).

6.2.6.2 Measurement of interaction between mGPR35 PDM-SmBiT and GRK 2,3,5 and 6-LgBiT in ΔGRK2/3/5/6 293 cells

During the assessment of mouse GPR35 interaction with GRK5 and GRK6, signal reduction was retained. So, an attempt was made to use phosphorylation deficient version of mouse GPR35 (mGPR35 PDM).

Using the mGPR35 PDM, the recruitment of all GRKs that are ubiquitously expressed was examined in this assay. LgBiT tagged GRK2 or GRK3 were transfected with SmBiT tagged mGPR35 PDM into ΔGRK2/3/5/6 293 cells. These initially led to very little basal luminescence with pEC_{50} values of 6.5 for GRK2 and 6.7 for GRK3. After the addition of the mGPR35 agonist pemirolast, the luminescence boosted marginally in a concentration-dependent manner (Figure 6.15(i)). The basal luminescence, on the other hand, was initially very high as usual and then dramatically decreased in a concentration-dependent manner for both GRK5 and GRK6 (pEC_{50} = 7.6 and 6.9, respectively) upon co-expression of the receptor mGPR35 PDM-SmBiT with these LgBiT-tagged variants of the GRK5 and GRK6 (Figure 6.15(i)).

After using the recommended concentration of the GRK2/3 inhibitor, compound 101, for 30 min and then a constant amount of pemirolast (3 μM, 5 min), the luminescence for GRK2 and GRK3 did not significantly alter (Figure 6.15(ii)). Nevertheless, when the prescribed dose of the GRK5/6 inhibitor, compound 19, was given for 30 min., followed by a fixed concentration of pemirolast (3 μM, 5 min), the luminescence for GRK5 and GRK6 was increased dramatically (Figure 6.15(ii)).

After 15 min of treatment with the GPR35 antagonist CID-2745687 at the recommended concentration, followed by a steady dose of pemirolast (3 μM, 5 min), the luminescence for GRK2 and GRK3 did not change at all this time compared to the pemirolast alone curve (Figure 6.15(iii). The selectivity of antagonist CID-2745687 for human receptors is thought to be the probable cause. A further indication that the potent hGPR35 antagonist CID-2745687 is inactive at mouse orthologues was confirmed by observing the luminescence curves for GRK5 and GRK6, which were nearly flat after being treated with CID-2745687 for 15 min, followed by a fixed concentration of pemirolast (3 μM, 5 min) (Figure 6.15(iii)).

This further validates the complex pharmacology of the receptor between mice and humans.

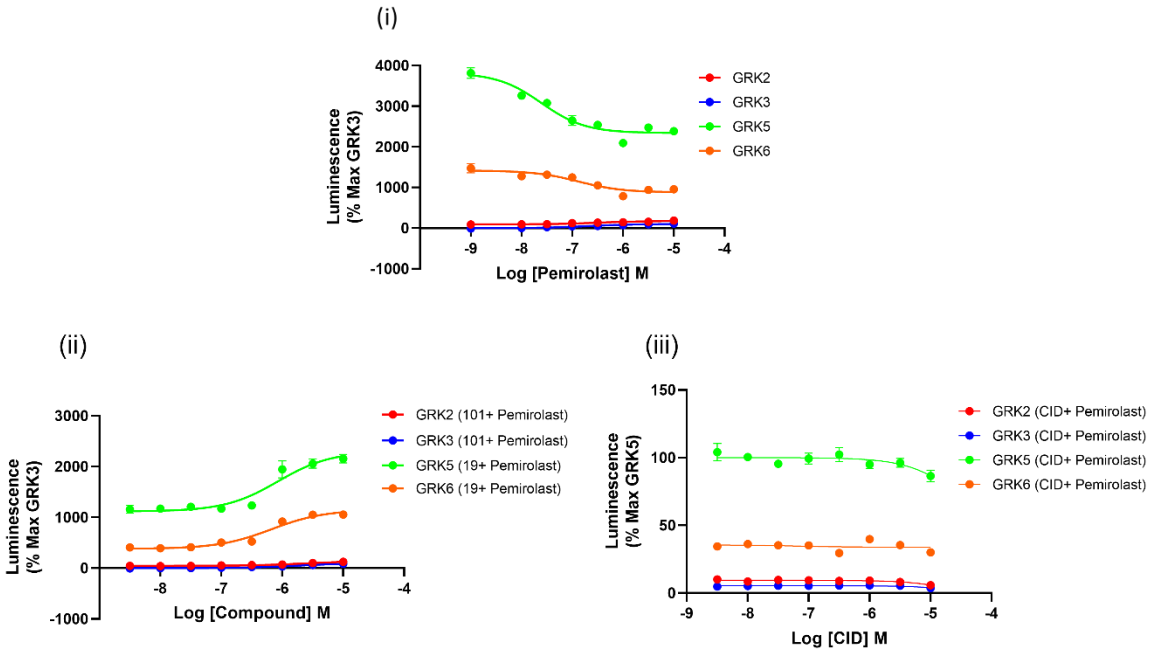

Figure 6.15 Measurement of interaction between mGPR35 PDM SmBiT and GRK 2,3,5 and 6 LgBiT in ΔGRK2/3/5/6 293 cells with mGPR35 potent agonist pemirolast

ΔGRK2/3/5/6 cells were transfected to co-express either mGPR35 PDM SmBiT and GRK 2 (red circles),3 (blue circles),5 (green circles) and 6 (orange circles) each tagged with LgBiT. **(i)** Cells were exposed to the indicated concentrations of pemirolast for 5 min and after substrate addition luminescence was measured. **(ii)** Prior to the addition of pemirolast (3 μM, 5 min) cells were pre-treated for 30 min with varying concentrations of either compound 19 (GRK5 and GRK6) or compound 101 (GRK2 and GRK3). **(iii)** Cells were also treated with different concentrations of GPR35 antagonist CID-2745687 for 15 min before adding pemirolast (3 μM, 5 min). Data are presented as % of the effect of pemirolast (10 μM) in GRK3 co-transfected cells. The experiment was performed once only (n=1).

6.2.7 Investigation of ligand mediated signal reduction of GRK5

6.2.7.1 Comparison of luminescence between full length and truncated GRK5

In this chapter I employed many different techniques to find out the actual cause of signal reduction of GRK5 (in particular) and GRK6. Approaches include generating a phosphorylation deficient receptor model, using genome editing cell lines, or alternative use of different ligands with distinct pharmacology. Now, I wanted to specifically focus on GRK5. GRK5 is localised in plasma membrane (Ribas et al., 2007). I have found from another study that a short C-terminal stretch of amino acids of GRK5 mediates plasma membrane localisation. A portion of GRK5's amino acids 546–565 may form an amphipathic helix, according to secondary structure predictions. The amphipathic helix is thought to have a hydrophobic patch on one face, hydrophilic amino acids on the other, and a number of basic amino acids around the hydrophobic patch. It is also found that amino acids 546–565 of GRK5 are sufficient to target the cytoplasmic green fluorescent protein (GFP) to the plasma membrane, and the hydrophobic amino acids are necessary for membrane targeting of GFP-546–565 (Thiyagarajan et al., 2004). As the region contained within amino acids 546–565 of GRK5 forms an amphipathic helix, I was keen to truncate this portion from the GRK5 to eliminate its membrane anchoring nature.

In this assay, hGPR35a SmBiT was transfected with full length GRK5 LgBiT and truncated GRK5 LgBiT. The basal signal of full length GRK5 was low as usual and decreased with increasing concentration of lodoxamide with pEC_{50} value of 8.2. But, when the same experiment was conducted with a truncated version of this GRK5, there was no significant signal generated (Figure 6.16(i)). This may be because of the dissociation of GRK5 from the plasma membrane.

When the prescribed dose of the GRK5/6 inhibitor, compound 19, was given for 30 min, followed by a fixed concentration of lodoxamide (100 nM, 5 min.), the luminescence for full-length GRK5 was dramatically increased, but for truncated GRK5, there were no effects (Figure 6.16(ii)).

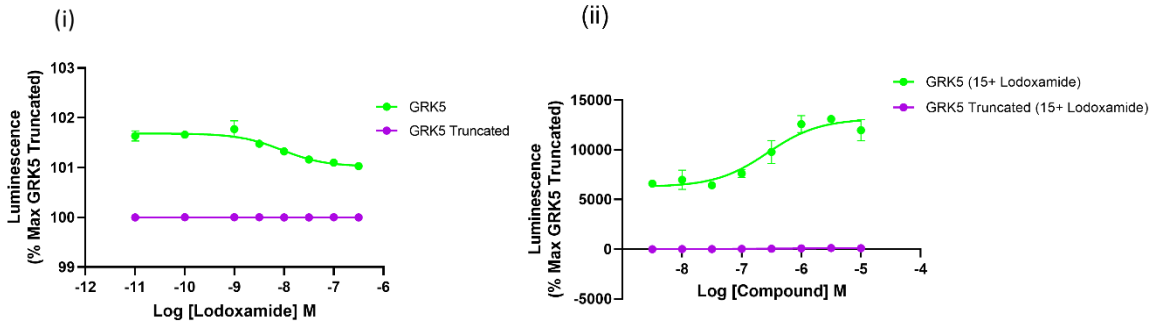

Figure 6.16 Comparison of luminescence between full length versus truncated GRK5 LgBiT with hGPR35a SmBiT

Studies akin to Figure 6.3, ΔGRK2/3/5/6 cells were transfected to co-express either hGPR35a SmBiT and GRK5 full length (green circles) and GRK5 truncated (purple circles) each tagged with LgBiT. (i) Cells were exposed to the indicated concentrations of lodoxamide for 5 min and after substrate addition luminescence was measured. (ii) Before the addition of lodoxamide (100 nM, 5 min) cells were pre-treated for 30 min with varying concentrations of compound 19 (GRK5). Data are presented as % of the effect of lodoxamide (300 nM) in GRK5 co-transfected cells. The experiment was performed once only (n=1).

6.2.7.2 Comparison of luminescence between full length and mutated GRK5

To further investigate the GRK5 signalling and its plasma membrane localisation, I have found that full-length GRK5-GFP is localised to the plasma membrane. However, when four basic residues (Lys ^{547}, Lys ^{548}, Lys ^{556}, and Arg ^{557}) that are assumed to border the hydrophobic patch were mutated to alanines, the resulting GRK5(basic)-GFP was located across the cytosol of cells with no noticeable plasma membrane association (Thiyagarajan et al., 2004). For this reason, I intentionally mutated the following residues (Lys ^{547}, Lys ^{548}, Lys ^{556}, and Arg ^{557}) to alanine. Moreover, mutated GRK5 has additional benefit as the integrity of GRK5 is maintained whereas in truncated GRK5, the membrane binding domain in the C-terminus has been deliberately eliminated. Although there is much possibility that the short C-terminal stretch of amino acids of GRK5 mediates only plasma membrane localisation, so truncation method is also useful unless this region has other functions.

In this assay, hGPR35a SmBiT was transfected with all commonly expressed GRKs with LgBiT (GRK2, GRK3, GRK5 and GRK6) and mutated GRK5. For all the ubiquitously expressed GRKs, the pattern was similar to that of the previous study. The luminescence signal of mutated GRK5 is not significantly different from the

original curve. pEC_{50} value of lodoxamide were 7.8 for GRK2, 7.6 for GRK3, 8.3 for GRK5, 8.5 for GRK6 and 7.9 for mutated GRK5 (Figure 6.17(i)).

After using the recommended concentration of the GRK2/3 inhibitor, compound 101, for 30 min and then a constant amount of lodoxamide (100 nM, 5 min), the luminescence for GRK2 and GRK3 did not significantly alter (Figure 7.15 (ii)). Nevertheless, when the prescribed dose of the GRK5/6 inhibitor, compound 19, was given for 30 min, followed by a fixed concentration of lodoxamide (100 nM, 5 min), there was a sharp increase of luminescence for GRK5 and moderate increase for GRK6. Most importantly, for mutated GRK5, there was a very marginal increase (Figure 6.17(ii)).

As it is difficult to interpret the result with the raw data, I planned to analyse the data in a different way. When I considered the fold change over vehicle mode for GRK5 and GRK5 (mutated), their signals were almost the same, and they still moved in a downward direction. This strongly suggested that signal reduction was not because of plasma membrane localisation. It may be because of the pre-coupling of the GRK5 with the receptor GPR35 and that is why there is always a high basal signal. The high signal again reduced with the increasing concentration of ligand, suggesting that the ligand mediated effects disrupted this pre-coupling (Figure 6.17(iii)).

When I also looked at the fold change over vehicle values of the inhibitors with different GRKs, I noticed that the signal generated by mutated GRK5 was the highest. This finding is very significant because, in this case, mutated GRK5 can be directly comparable to cytosolic GRK2 and GRK3, as mutated GRK5 is no longer in the plasma membrane. The high signal generated by mutated GRK5 also supports the predominant role of GRK5 in GPR35 phosphorylation and arrestin recruitment (Chapter 5). As I have previously found that GRK6 is also equally important for GPR35 phosphorylation and subsequent recruitment of arrestin, I anticipate the idea that if mutated GRK6 with LgBiT can be generated, this would also yield a similar high signal to mutated GRK5 in the luciferase complementation assay (Figure 6.17 ((iv)).

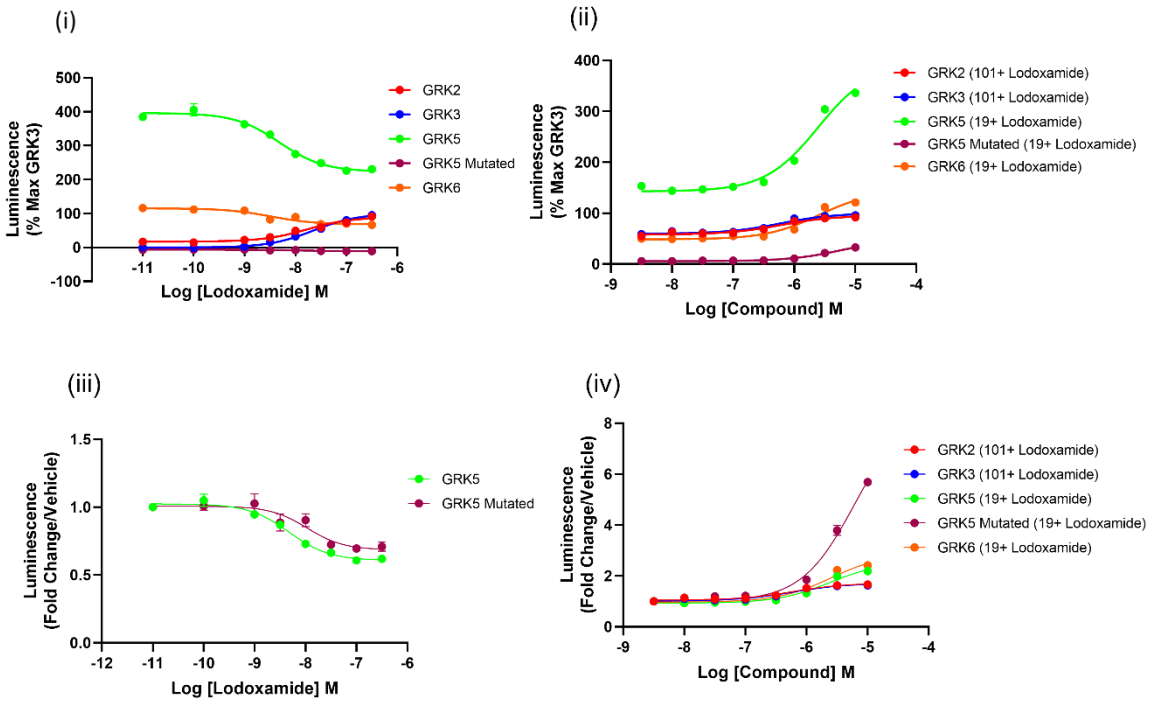

Figure 6.17 Comparison of luminescence between full length versus mutated GRK5 LgBiT with hGPR35a SmBiT

Studies akin to Figure 6.3, ΔGRK2/3/5/6 cells were transfected to co-express either hGPR35a SmBiT and GRK 2 (red circles),3 (blue circles),5 (green circles), mutated 5 (maroon circles) and 6 (orange circles) each tagged with LgBiT. (i) Cells were exposed to the indicated concentrations of lodoxamide for 5 min and after substrate addition luminescence was measured. (ii) Prior to the addition of lodoxamide (100 nM, 5 min) cells were pre-treated for 30 min with varying concentrations of either compound 19 (GRK5, mutated GRK5 and GRK6) or compound 101 (GRK2 and GRK3). (iii) Fold change over vehicle luminescence value of GRK5 and mutated GRK5. (iv) Fold change over vehicle luminescence value of kinase inhibitor compounds for (GRK2,3,5, mutated 5 and 6). Data are presented as % of the effect of lodoxamide (300 nM) in GRK3 co-transfected cells. The experiment was performed once only (n=1).

6.3 Discussion

The precise contribution of various G protein-coupled receptor kinases (GRKs) has frequently been understudied and poorly defined, even though it is generally recognised that they are crucial for the phosphorylation and control of several GPCRs (Sulon and Benovic, 2021). As GPR35 is a therapeutically important orphan GPCR and a potential target for lower gut inflammation to non-alcoholic steatohepatitis (Milligan, 2023), a thorough comprehension of how GRK isoforms regulate GPR35 is essential. As multiple GRK isoforms are often routinely co-expressed and there is an obvious scarcity of well-characterised small molecules kinase inhibitors, a battery of complementary approaches, including the creation of genome-edited cell lines devoid of expression of GRK2, GRK3, GRK5, and GRK6, the ubiquitously expressed GRK isoforms (Drube et al., 2022), development and

utilisation of both selective small molecule GRK inhibitors (Uehling et al., 2021, Varney et al., 2022), generation of phosphorylation-specific antisera that identify GPR35 phosphorylation-regulated locations have been applied successfully and ultimately found that GRK5 and 6 are the key mediators of both the phosphorylation and arrestin recruitment for GPR35. Although the study of the role of a single or multiple GRKs in the phosphorylation of GPR35 has been greatly benefited from all these new tools and innovative methodologies, a standardised method to reveal the GPR35-GRK interaction pattern directly and methodically is still required. For this, in this chapter, the direct and systematic profiling of GPR35-GRK interaction was carried out using the split nanoluciferase-based complementation assay.

This system is based on two small subunits, large BiT (LgBiT) and small BiT (SmBiT), of the very bright NanoLuc® luciferase (Hall et al., 2012). The LgBiT and SmBiT subunits are expressed as fusions to target proteins of interest and have each been individually optimised for stability and minimal self-association (Dixon et al., 2016). Target protein interaction makes it easier for subunit complementation to recreate a luminescent enzyme.

At first, this technique was applied to investigate the direct interaction between human GPR35 and different GRKs in a parental 293 derived cell line that is genome edited to lack expression of all the ubiquitous GRKs. The reason for using ΔGRK2/3/5/6 293 cells is to eliminate the possibility of interference by endogenous GRKs. From this study, it was found that, initially, the basal signal was low for GRK2 and 3, but the signal increased modestly in an agonist mediated manner. On the other hand, the basal signal was very high for GRK5 and 6 but there was a marked concentration dependent reduction of signal upon the addition of ligand. Upon applying selective kinase inhibitors, the signal was almost unchanged for GRK2 and 3, but the signal increased significantly for GRK5 and 6. As all the kinase inhibitors like compound 101 (GRK2 and 3) and compound 19 (GRK5 and 6) target the ATP for their inhibitory action, they have no direct relation or antagonism with the agonist of GPR35. For this reason, for GRK2 and GRK3, there were no effects produced by compound 101. After carefully observing the data of compound 19, it was found that the increasing trend of the signal is obvious although it was almost reverse to the agonist mediated response curve.

The probable reason for this is possible pre-coupling of GRK5 and 6 with GPR35 initially and subsequent agonist mediated disruption of such interaction and thereby signal reduction with increasing agonist concentration. As hGPR35 has two isoforms (hGPR35a and hGPR35b), I found almost similar results for the long isoforms compared to the short one, although the intensity of the signal is lower for hGPR35b with different GRKs

The same set of experiments were also conducted in the parental 293 cell line. As the receptor hGPR35 is tagged with SmBiT and different GRKs are tagged with LgBiT, again complementation worked between the two protein subunits upon adding luciferase substrate. Here, similar results were obtained, although the raw luminescence values were significantly lower in HEK 293 cells compared to genome edited cells. These may be because of the possible interference of the endogenous kinase to the introduced GRKs. The signal difference between the two isoforms of hGPR35 was maintained in the parental 293 cell line.

When I made the phosphodeficient version of this receptor to interact with GRKs, I found the similar outcome compared to the wild type form of the receptor. The possible reason behind this is in the PDM mutant of the hGPR35, all five amino acids (4 serine and 1 threonine) in the C-terminal chain have been mutated to alanine only. But from my recent study (Ganguly et al., 2023), when I attempted to predict the GPR35-GRK interaction using the 'Alphafold' deep learning algorithm (Jumper et al., 2021, Mirdita et al., 2022), this approach suggests that GRK5 and GRK6's extreme N-terminal regions reside in the same methionine pocket as the Ga_{13} C-terminal helix (Duan et al., 2022). As GRK5 and 6 do not interact with the C-terminal chain of GPR35, the response generated by the PDM form of the receptor is alike to the wild type GPR35.

As there are some reports that totally phosphorylation deficient mutant of receptor can still recruit arrestin protein and thereby can be internalised (Sánchez-Fernández et al., 2013), I used a cell line that is deliberately genome edited to lack expression of both arrestin-2 and arrestin-3. This was done to rule out a single possibility of phosphorylation, internalisation, and therefore, signal reduction. But unfortunately, the outcomes did not change.

As described above, in the split luciferase system, the LgBiT can be tagged with GRKs in both N-terminal and C-terminal. After switching the LgBiT tag from N to C-terminal, I found almost no luminescence for GRK2 and 3 and the GRK6 signal is slightly greater than GRK5 for both wild type and PDM version of hGPR35. These outcomes were different from the previous study and might be because of the conformational change of the LgBiT fragments in GRKs, thereby, affecting interaction between GRKs and GPR35.

As there are some published reports where genome edited knock down of G_q cause signal increase of GRK5 and GRK6 (Kawakami et al., 2022), I attempted to use a parental 293 derived cell line that is genome edited to lack expression of G_q, G_{11}, G_{12} and G_{13}. As GPR35 signals through G_{12} and G_{13} (Quon et al., 2020), the hypothesis was that probably G_{12} and G_{13} cause signal reduction of GRK5 and GRK6. However, the results from the experiment did not match the hypothesis, and signals generated by GRK5 and GRK6 still were in a downward direction.

After that, I decided to use a partial agonist of GPR35 known as pamoic acid instead of the full agonist lodoxamide. After analysing the data, I found that there was still a signal reduction of GRK5 and GRK6 although the reduction intensity was less than lodoxamide. This may be due to partial agonism of pamoic acid to hGPR35a.

I again used the partial agonist pamoic acid to measure interaction with all commonly expressed GRKs with hGPR35b. The raw luminescence levels in this series of tests, which were transfected with hGPR35b-SmBiT, were noticeably lower because it is evident that the long isoform of GPR35 produces a weaker signal. When pamoic acid was used in place of the full agonist lodoxamide, the overall raw luminescence was also reduced, as anticipated.

After using the standard agonist lodoxamide and partial agonist pamoic acid, I utilised a new potent agonist of GPR35, developed by a company called GlaxoSmithKline pharmaceutical industry company. After conducting this assay initially in ΔGq/11/12/13 cells, I did not find any different result compared to the reference agonist lodoxamide.

Then I decided to use the ΔGRK2/3/5/6 293 cell to assess the interaction between different GRKs with hGPR35a with GSK 938. I also used CID-2745687, a potent hGPR35a antagonist, in this study. After completing this experiment, I found that there is still a reduction of the signal of GRK5 and GRK6 even when utilising GSK 938 as an agonist in ΔGRK2/3/5/6 293 cells. Upon the addition of the antagonist CID-2745687, the curve generated by GSK 938 became almost reversed, justifying the potent antagonism of CID-2745687 for hGPR35a.

I also validated this assay by deliberately introducing other uncommon GRKs like (GRK1, GRK4 and GRK7) with hGPR35a. GRK5 with an LgBiT tag was also used as a reference. Lodoxamide, a standard agonist, was used in this experiment. From this assay, I did not find any interaction with all the above GRKs with hGPR35, although GRK5 still generated a signal. This experiment clearly justifies the accuracy of the luciferase-based complementation assay system for direct and systematic profiling of GPCR-GRK interaction.

As there are distinct pharmacology between the human and rodent orthologues of GPR35 (Quon et al., 2020), translation of this receptor is problematic. For this reason, I measured the interaction between mouse GPR35 with different GRKs using this complementation approach. I again used the hGPR35 specific antagonist CID-2745687 in this assay to check whether it can work in the mouse orthologue of the receptor. From the experiment results, I noticed that luminescence signal reduction of GRK5 and GRK6 were also prevalent in mouse orthologue of GPR35. In case CID-2745687, the antagonism was very poor, suggesting its human orthologue selectivity and thereby establishing the complex pharmacology of the receptor between humans and rodents.

After observing the signal reduction also in the mouse orthologue of the receptor, I employed the PDM version of this receptor. But again, there was no change of signalling in the PDM version of mouse GPR35 compared to wild type receptor. The antagonist CID-2745687 was unable to exert its antagonistic effects in this situation, validating the intricate pharmacology of the GPR35 receptor in both mice and humans.

Finally, I was very much eager to investigate the ligand mediated signal reduction of GRK5 and GRK6. After careful observation of the results and a literature search,

I studied the plasma membrane localisation of GRK5 (Ribas et al., 2007). From research from another group, I discovered that the GRK5's short C-terminal stretch of amino acids regulates plasma membrane localisation. The amino acids 546-565 of GRK5 may comprise a piece of an amphipathic helix, inferred from secondary structure calculations. On one face of the amphipathic helix, there may be a hydrophobic patch, whereas on the other, there may be hydrophilic amino acids, covered by a number of basic amino acids. Green fluorescent protein (GFP) in the cytoplasm can be directed to the plasma membrane by the amino acids 546-565 of GRK5; however, the hydrophobic amino acids are required for GFP-546-565 to be directed to the membrane (Thiyagarajan et al., 2004). As the region contained within amino acids 546–565 of GRK5 forms an amphipathic helix, I was keen to truncate this portion from the GRK5 to eliminate its membrane anchoring nature. After conducting this experiment with full-length GRK5 and truncated GRK5 with hGPR35a, I found that full-length GRK5 again generated a high signal and was decreasing with increasing concentration of ligand lodoxamide. On the other hand, the truncated version of GRK5 yielded no response. This may be because of the dissociation of truncated GRK5 from the plasma membrane. In the truncated version of GRK5, only the short C-terminal stretch of amino acids of GRK5 has been removed.

Although the truncated GRK5 is effective in its displacement from the plasma membrane, I decided to switch to mutating some amino acids of GRK5 and then run an experiment. In the mutated form GRK5, the GRK5 is still in full-length and there is no possibility of losing any function of the original full-length GRK5. Here, four basic residues that are projected to surround the hydrophobic patch (Lys 547, Lys 548, Lys 556, and Arg 557) were changed to alanines, and the resulting GRK5(basic)-GFP was found throughout the cytoplasm of cells with no discernible plasma membrane attachment (Thiyagarajan et al., 2004). For this reason, I intentionally mutated the following residues (Lys ^{547}, Lys ^{548}, Lys ^{556}, and Arg ^{557}) to alanine. In this assay, all other GRKs produced similar responses compared to previous studies, but the luminescence signal of mutated GRK5 was not at all significant from the original curve. After using the GRK5/6 specific inhibitor compound 19, for mutated GRK5, there was a very marginal increase. As it is difficult to interpret the result with the raw data, I analysed the data in a different way. When GRK5 and GRK5 (mutated) were compared in terms of fold change over

vehicle mode, their signals were nearly identical and continued to proceed in a downward way. This strongly implied that plasma membrane localisation was not the cause of the reduction of signal. There may be a pre-coupling between the GRK5 and the GPR35, as a result of which the basal signal is always strong. As ligand concentration rises, the reduction of high signal was visible, and this once more indicates that the effects of the ligand have disrupted the pre-coupling.

When I also looked at the fold change over vehicle mode values of the inhibitors with different GRKs, I noticed that the signal generated by mutated GRK5 is the highest. This observation was particularly important because, since mutant GRK5 is no longer found in the plasma membrane, it can be directly compared to cytosolic GRK2 and GRK3. The strong signal produced by mutant GRK5 further confirms that GRK5 plays a key role in arrestin recruitment and GPR35 phosphorylation (Chapter 5). As GRK6 is also essential for the phosphorylation of GPR35 and subsequent recruitment of arrestin, as I have previously discovered, I predict that if mutated GRK6 can be produced, it will similarly provide a strong signal like mutated GRK5.

Overall, from the above luciferase-based complementation assay, it was clearly proved that GRK5 (most obviously) and also GRK6 can greatly interact with GPR35. The cytosolic GRK2 and GRK3 can also interact with GPR35 to a moderate extent. These findings strongly support my previous outcomes obtained in chapter 5. In conclusion, I can claim that split luciferase-based complementation assay is a useful technique to systematically measure the GPCR-GRK interaction and for GPR35, this novel technology has accurately determined the preferential role of GRK5 and also GRK6 for receptor phosphorylation.

Chapter 7 Final discussion

Class A G protein-coupled receptor GPR35 is thought to be an orphan receptor; its exact physiological role and endogenous ligand are still uncertain (Otkur et al., 2023b, Milligan, 2023). Although GPR35 is still poorly characterised, it has great therapeutic utilities in a spectrum of conditions ranging from fatty liver diseases to inflammatory bowel disorders and different cancers (Milligan, 2023, Otkur et al., 2023b). The pharmacology of the GPR35 orthologues in humans and rodents differs substantially and in human orthologue, 2 isoforms are transcribed and translated from 3 variants of the human GPR35 gene (Quon et al., 2020). Although the 2 isoforms of human GPR35 display comparable pharmacology, the agonist response efficacy is significantly different in pharmacological assays (Quon et al., 2020). Most importantly, there are clear contradictions in findings about the isoform function between different groups (Marti-Solano et al., 2020, Schihada et al., 2022) that should be resolved. Although the role of agonist-mediated phosphorylation of GPR35 in activating GRKs and subsequent interaction with arrestin is frequently observed in the context of GPCR regulation, there is a paucity of information regarding the precise locations of these post-translational regulatory regions and the potential contribution of each altered amino acid to the outcome. A clear understanding of GPR35 phosphorylation was attained using mass spectrometry, [^{32}P] tagging, mutagenesis, and phospho-site-specific antisera (Divorty et al., 2022). It is also crucial to identify the exact role played by each GRK in the phosphorylation and regulation of this receptor. To elucidate the specific role of individual or group of GRKs, combinations of GRK subtype knock-out cell lines (Drube et al., 2022), reconstitution of function with specific GRKs, a human GPR35a-directed antiserum, and a collection of selective small molecule GRK inhibitors (Uehling et al., 2021, Varney et al., 2022) were all used in this thesis. Finally, a complementation experiment using split nanoluciferase was carried out to systematically and directly disclose the GPR35-GRK interaction pattern.

In the first result chapter of my thesis (**Chapter 3**), studies were undertaken to investigate the pharmacology of two isoforms of human GPR35. In contrast to the 31 amino acid extended version, which is known as hGPR35b or (‘GPR35 long’), the original polypeptide, which contains 309 amino acids, is called hGPR35a or (‘GPR35 short’). The $G\alpha_{13}$ activation and arrestin-3 signalling of the two isoforms were comparable, despite the longer isoform's significantly lower maximum signal

intensity. However, along both isoforms, the agonist ligand's potency remained comparable (Marti-Solano et al., 2020). After comparing the sequences of the two hGPR35 isoforms, it was shown that hGPR35b could create one more extracellular disulphide bond than hGPR35a. However, this possibility—or any potential consequences—have not yet been thoroughly investigated. Using site-directed mutagenesis, the pharmacology and function of two human GPR35 isoforms were thoroughly investigated, and the interactions of these isoforms with arrestins and G proteins were later identified.

With the pharmacological experiments followed by mutagenesis, it was found that in hGPR35a, two cysteines (position 8 and position 248) may form a disulphide bonding, and alteration of either of these cysteines can eliminate arrestin interaction capacity and G protein activation in response to ligands. In the longer isoform (hGPR35b), there might be a disulphide bond between cysteine at position 27 and 279 in addition to the hGPR35a comparable disulphide bond between cysteine at position 39 and 279. The experimental outputs again showed that mutation of either of the cysteine at position 39 or 279 of hGPR35b greatly reduced the efficacy of the agonist while alteration of the long isoform specific cysteine at position 27 increased the agonist function significantly. This clearly indicated that a second disulphide bond prevents hGPR35b agonist-induced activation. The efficacy of agonist at hGPR35b might be equalised to that of hGPR35a due to the mutation of this cysteine (position 27) to serine. To better understand the role of the N-terminal extension of the hGPR35b protein, ten additional mutants were made with cysteine in place of various residues in the Cys27Ser hGPR35b backbone. Experimental results with these additional mutants proved that their arrestin-3 recruitment potential and $G\alpha_{13}$ activation were nearly identical to the extent that was demonstrated by hGPR35b WT. None of the novel mutants could induce an arrestin-3 or $G\alpha_{13}$ response that was higher than hGPR35a WT or hGPR35b C27S. The most plausible explanation for this was the formation of additional disulphide bonds between extracellular loop 3 and various places of the hGPR35b N-terminal domain. Molecular modelling and maybe knowledge of atomic level structures are absolutely important to fully understand the relevance of the organisation of the N-terminal domain of hGPR35b.

In (**Chapter 4)**, studies were conducted to selectively detect the post-translational states of GPR35. Here, novel phospho-site-specific antibodies were created that ultimately served as activation state-specific biosensors by utilising the knowledge of the full scenario of GPR35 phosphorylation and the contribution of individual amino acids for arrestin recruitment and phosphorylation (Divorty et al., 2022).

Due to the importance of Ser^{303} (as well as Ser^{300}) in arrestin recruitment to hGPR35a, phospho-specific antibodies to these amino acid pairs in the human receptor sequence and their equivalents in the mouse orthologue of GPR35 undoubtedly detected phosphorylated GPR35 on these residues in physiologically relevant settings. Initially, for characterising the novel antisera, different cell lines were generated that can stably express human and mouse GPR35 orthologues. After validating the cell lines, several agonists were employed to stimulate the Flp-In TREx 293 cells stably expressing mGPR35-HA. The phospho specific antisera were very successful in identifying the phosphorylation signals caused by various agonists. When a similar study was carried out on mouse receptors lacking phosphorylation, mGPR35-$pSer^{298}$/$pSer^{301}$ was unable to detect anything, proving that phosphorylation is fully dependent on phospho serine and phospho threonine residues in the mouse GPR35's C-terminal tail. For investigating whether GPR35 phosphorylation is agonist-mediated or not, cell lines expressing receptors were activated with both agonist and vehicle. Here, phospho-site-specific antisera could detect only the receptors stimulated by the agonist but not the vehicle, indicating that phosphorylation of GPR35 is agonist regulated (particularly for mouse orthologues). Similar to mouse phospho antisera, hGPR35a-$pSer^{300}$/$pSer^{303}$ antisera were characterised upon treatment with different agonists, partial agonist and antagonist in cell lines stably expressing human form of GPR35. In this case, almost equivalent outcomes were found compared to mouse form of the receptor. Later, it was attempted to produce the same outcomes in an immunocytochemical assay with these antibodies after immunoblotting techniques were proven successful in characterising the phosphorylation site specific antisera for both orthologues of GPR35. Here, both the hGPR35a-$pSer^{300}$/$pSer^{303}$ and mGPR35-$pSer^{298}$/$pSer^{301}$ clearly identified phosphorylation signals of hGPR35a-HA and mGPR35-HA in an immunocytochemical based test.

Due to the use of phosphorylation site-specific antibodies to determine the post-activation status of GPR35 in immunoblot and immunocytochemical studies throughout this (**Chapter 4)**, an appropriate control was necessary to confirm that the antibodies are, in fact, recognising the $pSer^{300}$, $pSer^{303}$, or both sites. For this purpose, an enzyme known as Lambda protein phosphatase was used. This enzyme typically removes or chops phosphate groups from the receptor protein's phosphorylated serine or threonine, thereby, completely eliminating the possibility of further phosphorylation. Upon treatment with λ-PPase, hGPR35a-$pSer^{300}$-$pSer^{303}$antisera failed to detect the receptor. This clearly validated that the amino acid residues Ser^{300} and Ser^{303} need to be phosphorylated to be detected by these antisera, thereby proving their specificities.

From the overall outcomes of (**Chapter 4**), it should be noted that in both immunoblotting and immunocytochemical assays, phospho-site-specific antisera against the region encompassing Ser^{303} in human GPR35a (Ser^{301} in mouse) were useful sensors for assessing the activation status of the receptors. Additionally, these antibodies only detected fully matured forms of GPR35. It is safe to say, based on the results of all the experiments in this chapter, that these antibodies could be useful tools for evaluating target engagement in drug discovery and target validation operations.

After obtaining a comprehensive analysis of GPR35 phosphorylation and the contribution of novel phospho specific antisera as useful reagents for addressing pathophysiological roles of this receptor, I was keen to investigate the specific contribution of an individual or a sub-set of GRKs that predominantly controls the phosphorylation of the receptor and thereby promoting desensitisation and internalisation. In (**Chapter 5)** of my thesis, it was established at the outset that the involvement of one or more GRK isoforms was required for agonist-induced interactions between arrestin proteins and human GPR35a. Additionally, the existence of cell lines derived from 293 lacking expression of different GRKs showed that while the absence of both GRK2 and GRK3 did not impede agonist-induced receptor-arrestin interactions, the absence of both GRK5 and GRK6 blocked such interactions to a nearly complete extent. Furthermore, reconstitution investigations with individual GRK isoforms were made possible by the ΔGRK2/3/5/6 HEK293 cells, and these showed that GRK5 and GRK6 were

virtually equally effective. Molecular level and mechanistic study utilising the 'Alphafold' deep learning method (Jumper et al., 2021, Mirdita et al., 2022) showed that GRK5 and GRK6 interacted with hGPR35a more strongly and effectively than GRK2 and GRK3, corroborating our experimental findings. Compound 101 is a selective inhibitor of GRK2 and GRK3 that has been well studied and proved to work (Thal et al., 2011); however, there have just lately been more choices for selective small molecule inhibition of GRK5 and GRK6. Uehling et al addressed this issue by collecting quinazoline-based inhibitors (Uehling et al., 2021). Compound 19 and others from this series efficiently prevented agonist-induced interactions of human GPR35a with either arrestin-2 or arrestin-3 as well as detection of agonist-mediated phosphorylation of both the human and mouse orthologue by the hGPR35a pSer^{300}/pSer^{303} antiserum and the equivalent mouse directed antiserum in both immunoblotting and immunocytochemistry studies. Compound 101, a known inhibitor molecule, was ineffective in suppressing receptor-arrestin association or preventing GPR35 phosphorylation, respectively. This clearly justified the predominant involvement of GRK5/6 in the regulation of GPR35. For further confirmation of the direct involvement of GRK5 and GRK6 in the phosphorylation of human GPR35, I transiently introduced LgBiT-tagged versions of GRK2, GRK3, GRK5, or GRK6 coupled with hGPR35a-HA into ΔGRK2/3/5/6 293 cells. The presence of GRK5 and, in particular, GRK6, increased the phosphorylation of these sites, whereas GRK2 and GRK3 had no appreciable influence, according to immunoblotting using anti-hGPR35a pSer^{300}-pSer^{303}. It was further evident that these effects would have been entirely blocked if compound 19 had been administered to cells before being treated with agonists.

Overall, the cell-based research presented in this chapter (**Chapter 5)** showed significant roles for GRK5 and 6, with little to no contribution from GRK2 or GRK3 to either the phosphorylation of these specific locations or the interaction of GPR35 with arrestins. The findings in this chapter provide unique and thorough insights into GPR35 regulation, a receptor that plays a crucial role in colon cancer and inflammatory bowel disorders (IBD).

With the aid of a variety of complementary methods, such as the creation of genome-edited cell lines devoid of the widely expressed GRK isoforms GRK2, GRK3, GRK5 and GRK6, as well as the development and use of both selective small molecule GRK inhibitors and the production of phospho-site specific antisera that detect sites of regulated phosphorylation within GPR35, I discovered a remarkable role for GRK5 and 6 as the key mediators of both the phosphorylation and arrestin recruitment for GPR35. Even though all these cutting-edge techniques and tools are highly helpful, a standardised approach to expose the GPR35-GRK interaction pattern directly and methodically is still needed. To do this, the split nanoluciferase-based complementation assay was used in (**Chapter 6)** to profile the interaction directly and systematically between GPR35 and GRK.

This split luciferase-based assay was initially used to examine the direct interaction between human GPR35 and several GRKs in a parental 293-derived cell line that was genome edited to eliminate the expression of every common GRK. ΔGRK2/3/5/6 293 cells were employed to rule out the likelihood of interference from endogenous GRKs. According to the results of this investigation, the basal signal for GRK2 and 3 was initially weak but gradually grew via agonist-mediated mechanisms. On the other hand, the GRK5 and 6 had very strong basal signals, but the addition of the ligand resulted in a significant concentration-dependent reduction of the signal. Similar results with my experiments were also reported by (Palmer et al., 2022). For further looking into the incidence of GRK5/6 signal reduction, I undertook a series of approaches, including the use of phosphodeficient version of receptor GPR35, the use of a cell line that is deliberately genome edited to lack expression of both arrestin-2 and arrestin-3 and utilisation of cells that are genetically modified to miss the expression of G_q, G_{11}, G_{12} and G_{13}. In every experiment with the above-mentioned cell lines, agonist-mediated signal reduction of GRK5/6 continued. Initially, it was thought that as GRK5 and 6 are membrane associated protein (Ribas et al., 2007), their plasma membrane localisation is responsible for probable bystander effects and high basal signals. In order to investigate the signal reduction of GRK5 in detail, I generated a mutated version of GRK5 where four basic residues (Lys 547, Lys 548, Lys 556, and Arg 557) that are anticipated to surround the hydrophobic patch and are responsible for membrane localisation were converted to alanines (Thiyagarajan et al., 2004). As a result, it was anticipated that the ensuing mutant GRK5 would

be distributed throughout the cytoplasm of cells with no obvious plasma membrane connection. After experimental study and analysis, it was found that the signals of full-length GRK5 and mutated (cytoplasm localised GRK5) were almost similar and they both went in a downward direction. This strongly suggested that signal reduction was not due to plasma membrane localisation. The basal signal may always be strong because of a pre-coupling between the GRK5 and the GPR35. The pre-coupling has been disrupted by the impacts of the ligand, as seen by the lowering of the high signal as ligand concentration increased. Upon concentrating on the inhibitor's effects on GRKs, the signal generated by mutated GRK5 was significantly higher. This finding was particularly significant since mutant GRK5 can be directly compared to cytosolic GRK2 and GRK3 because it is no longer present in the plasma membrane. The robust signal generated by mutant GRK5 provides additional evidence that GRK5 is essential for arrestin recruitment and GPR35 phosphorylation. I previously found that GRK6 is also necessary for the phosphorylation of GPR35 and the consequent recruitment of arrestin. Thus, I predict that if mutated GRK6 can be created, it will similarly deliver a potent signal like altered GRK5.

Overall, it was demonstrated with the luciferase-based complementation assay mentioned above that GRK5 and GRK6 could interact with GPR35 significantly, with GRK5 being the most prominent example. Additionally, GPR35 could interact modestly with the cytosolic GRK2 and GRK3. These results firmly backed up my earlier findings from Chapter 5 of this thesis in every way. Finally, I can conclude that the split luciferase-based complementation assay is a practical method for measuring the GPCR-GRK interaction and that for the GPR35 receptor, this cutting-edge technology has precisely identified the predominant function of GRK5 and GRK6 for receptor phosphorylation.

In conclusion, throughout this thesis, multiple approaches like BRET, immunoblot, immunocytochemistry and luciferase complementation assays were employed to investigate the pharmacology, signalling, function, and regulation of the orphan receptor GPR35. As human GPR35 contains two isoforms, and long isoform hGPR35b is more frequently connected with carcinogenesis because of its expression in gastric and colon cancer cells, the in-depth investigation of this isoform is vital. Although I did extensive site-directed mutagenesis and pharmacological studies with this long isoform, there are still needs for accurate molecular level analysis and modelling experiments. As GPR35 is currently gaining attention for its involvement with a variety of diseases like nonalcoholic steatohepatitis, inflammatory bowel disease and colon cancers, proper knowledge of the regulation of this receptor is very crucial. From my thesis outcomes, it was evident that GRK5 and GRK6 mainly promoted phosphorylation and thereby regulated the human and mouse orthologues of GPR35. As all of my experimental protocols were based on wild type and genome-edited HEK293- derived cells, the focus of future research must now be on determining whether these changes are truly produced in physiologically relevant tissues and, if so, how they might affect the types of cells and tissue function. A summary figure is drawn at the end to outline the most important aspects of this thesis.

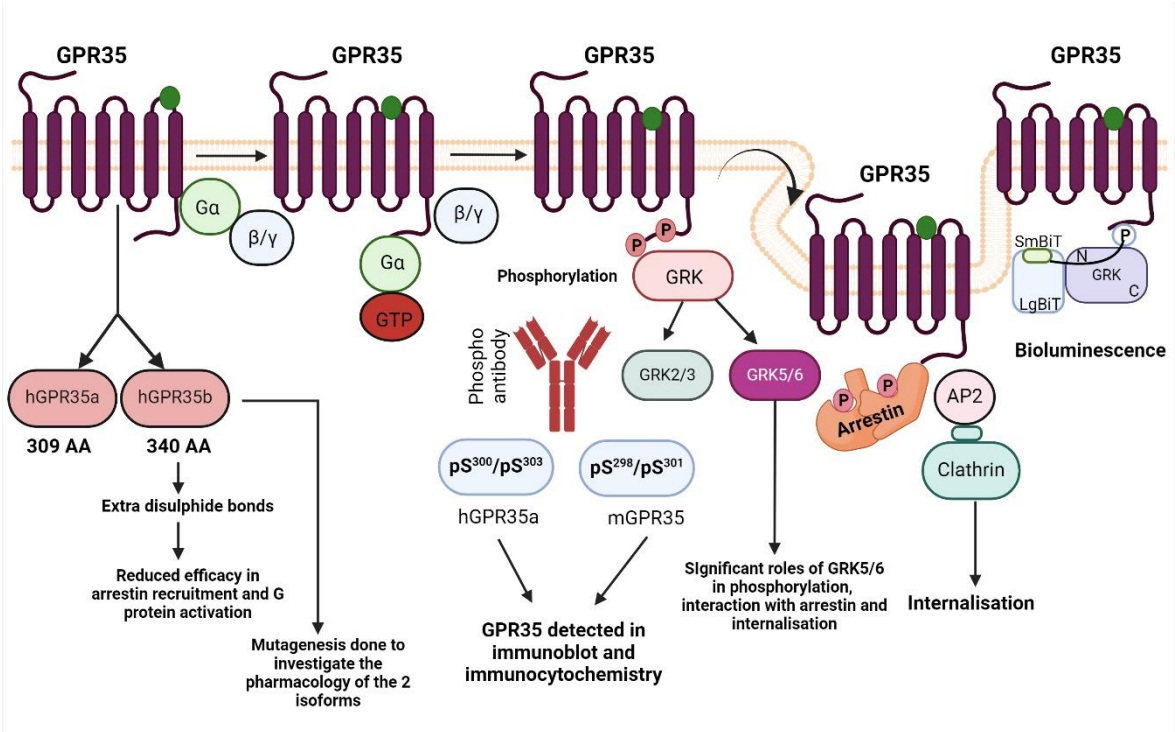

Figure 7.1 A summary figure demonstrating the mutagenesis, phosphorylation, GRK mediated regulation and nanoluciferase based pairing of GRKs with GPR35

GPR35 is a 7-TM domain orphan receptor whose human orthologue has two isoforms. As hGPR35b has an additional disulphide bond and exhibits reduced efficacy than hGPR35a in pharmacological assays, mutagenesis and functional studies were done to investigate the issues. For selectively detecting the phosphorylation states of GPR35, hGPR35a pSer^{300}/pSer^{303} and mGPR35 pSer^{298}/pSer^{301} were employed. These antibodies were useful sensors for assessing the post-translational status of GPR35 in both immunoblotting and immunocytochemical assays. GRK5/6 were proven more effective than GRK2/3 in the phosphorylation, interaction with arrestins and internalisation of GPR35 using a variety of experiments. In luciferase-based complementation assay, GPR35-GRK interaction was measured using NanoBit experiments where GPR35 was fused with SmBiT and GRKs were tagged with LgBiT. This figure was created with BioRender.com.

List of References

ALEXANDER, S. P., DAVENPORT, A. P., KELLY, E., MARRION, N., PETERS, J. A., BENSON, H. E., FACCENDA, E., PAWSON, A. J., SHARMAN, J. L. & SOUTHAN, C. 2015. The Concise Guide to PHARMACOLOGY 2015/16: G protein-coupled receptors. *British journal of pharmacology,* 172**,** 5744-5869.

ALEXANDER, S. P., CHRISTOPOULOS, A., DAVENPORT, A. P., KELLY, E., MATHIE, A., PETERS, J. A., VEALE, E. L., ARMSTRONG, J. F., FACCENDA, E. & HARDING, S. D. 2019. The Concise Guide to PHARMACOLOGY 2019/20: G protein-coupled receptors. *British journal of pharmacology,* 176**,** S21-S141.

ALI, H., ABDELMAGEED, M., OLSSON, L., ISRAELSSON, A., LINDMARK, G., HAMMARSTROM, M. L., HAMMARSTROM, S. & SITOHY, B. 2019. Utility of G protein-coupled receptor 35 expression for predicting outcome in colon cancer. *Tumour Biology,* 41**,** 1010428319858885.

ATTWOOD, T. & FINDLAY, J. 1994. Fingerprinting G-protein-coupled receptors. *Protein Engineering, Design and Selection,* 7**,** 195-203.

BALLESTEROS, J., KITANOVIC, S., GUARNIERI, F., DAVIES, P., FROMME, B. J., KONVICKA, K., CHI, L., MILLAR, R. P., DAVIDSON, J. S. & WEINSTEIN, H. 1998. Functional microdomains in G-protein-coupled receptors: the conserved arginine-cage motif in the gonadotropin-releasing hormone receptor. *Journal of Biological Chemistry,* 273**,** 10445-10453.

BARTH, M. C., AHLUWALIA, N., ANDERSON, T. J., HARDY, G. J., SINHA, S., ALVAREZ-CARDONA, J. A., PRUITT, I. E., RHEE, E. P., COLVIN, R. A. & GERSZTEN, R. E. 2009. Kynurenic acid triggers firm arrest of leukocytes to vascular endothelium under flow conditions. *Journal of Biological Chemistry,* 284**,** 19189-95.

BASITH, S., CUI, M., MACALINO, S. J., PARK, J., CLAVIO, N. A., KANG, S. & CHOI, S. 2018. Exploring G protein-coupled receptors (GPCRs) ligand space via cheminformatics approaches: impact on rational drug design. *Frontiers in pharmacology,* 9**,** 128.

BENOVIC, J., KÜHN, H., WEYAND, I., CODINA, J., CARON, M. & LEFKOWITZ, R. 1987. Functional desensitization of the isolated beta-adrenergic receptor by the beta-adrenergic receptor kinase: potential role of an analog of the retinal protein arrestin (48-kDa protein). *Proceedings of the National Academy of Sciences,* 84**,** 8879-8882.

BENOVIC, J. L., DEBLASI, A., STONE, W. C., CARON, M. G. & LEFKOWITZ, R. J. 1989. Β-Adrenergic receptor kinase: primary structure delineates a multigene family. *Science,* 246**,** 235-240.

BENOVIC, J. L. 2021. Historical perspective of the G protein-coupled receptor kinase family. *Cells,* 10**,** 555.

BERLINGUER-PALMINI, R., MASI, A., NARDUCCI, R., CAVONE, L., MARATEA, D., COZZI, A., SILI, M., MORONI, F. & MANNAIONI, G. 2013. GPR35 activation reduces Ca2+ transients and contributes to the kynurenic acid-dependent reduction of synaptic activity at CA3-CA1 synapses. *PLoS One,* 8**,** e82180.

BINTI MOHD AMIR, N. A. S., MACKENZIE, A. E., JENKINS, L., BOUSTANI, K., HILLIER, M. C., TSUCHIYA, T., MILLIGAN, G. & PEASE, J. E. 2018. Evidence for the Existence of a CXCL17 Receptor Distinct from GPR35. *Journal of Immunology,* 201**,** 714-724.

BOGUSZEWSKI, C. L. & VAN DER LELY, A. J. 2015. The role of the gastrointestinal tract in the control of energy balance. *Translational Gastrointestinal Cancer,* 4**,** 3-13.
BOLEIJ, A., FATHI, P., DALTON, W., PARK, B., WU, X., HUSO, D., ALLEN, J., BESHARATI, S., ANDERS, R. A., HOUSSEAU, F., MACKENZIE, A. E., JENKINS, L., MILLIGAN, G., WU, S. & SEARS, C. L. 2021. G-protein coupled receptor 35 (GPR35) regulates the colonic epithelial cell response to enterotoxigenic Bacteroides fragilis. *Communication Biology,* 4**,** 585.
BROWNING, A. M., WALLE, U. K. & WALLE, T. 2005. Flavonoid glycosides inhibit oral cancer cell proliferation—role of cellular uptake and hydrolysis to the aglycones. *Journal of pharmacy and pharmacology,* 57**,** 1037-1041.
BU, J., YAN, W., HUANG, Y. & LIN, K. 2023. Activation of the IL-17 signalling pathway by the CXCL17-GPR35 axis affects drug resistance and colorectal cancer tumorigenesis. *American Journal of Cancer Research,* 13**,** 2172.
BURKHARDT, A. M., TAI, K. P., FLORES-GUITERREZ, J. P., VILCHES-CISNEROS, N., KAMDAR, K., BARBOSA-QUINTANA, O., VALLE-RIOS, R., HEVEZI, P. A., ZUÑIGA, J. & SELMAN, M. 2012. CXCL17 is a mucosal chemokine elevated in idiopathic pulmonary fibrosis that exhibits broad antimicrobial activity. *The Journal of Immunology,* 188**,** 6399-6406.
BUTCHER, A. J., PRIHANDOKO, R., KONG, K. C., MCWILLIAMS, P., EDWARDS, J. M., BOTTRILL, A., MISTRY, S. & TOBIN, A. B. 2011. Differential G-protein-coupled receptor phosphorylation provides evidence for a signaling bar code. *Journal of Biological Chemistry,* 286**,** 11506-11518.
CALEBIRO, D., NIKOLAEV, V. O., GAGLIANI, M. C., DE FILIPPIS, T., DEES, C., TACCHETTI, C., PERSANI, L. & LOHSE, M. J. 2009. Persistent cAMP-signals triggered by internalized G-protein–coupled receptors. *PLoS biology,* 7**,** e1000172.
CALEBIRO, D. & GODBOLE, A. 2018. Internalization of G-protein-coupled receptors: Implication in receptor function, physiology and diseases. *Best practice & research Clinical endocrinology & metabolism,* 32**,** 83-91.
CATO, M. C., YEN, Y.-C., FRANCIS, C. J., ELKINS, K. E., SHAREEF, A., STERNE-MARR, R. & TESMER, J. J. 2021. The open question of how GPCRs interact with GPCR kinases (GRKs). *Biomolecules,* 11**,** 447.
CHENG, L., WU, H., CAI, X., ZHANG, Y., YU, S., HOU, Y., YIN, Z., YAN, Q., WANG, Q., SUN, T., WANG, G., YUAN, Y., ZHANG, X., HAO, H. & ZHENG, X. 2024. A Gpr35-tuned gut microbe-brain metabolic axis regulates depressive-like behavior. *Cell Host & Microbe*.
CHUNG, K. Y., RASMUSSEN, S. G., LIU, T., LI, S., DEVREE, B. T., CHAE, P. S., CALINSKI, D., KOBILKA, B. K., WOODS JR, V. L. & SUNAHARA, R. K. 2011. Conformational changes in the G protein Gs induced by the ß2 adrenergic receptor. *Nature,* 477**,** 611-615.
CLAPHAM, D. E. & NEER, E. J. 1997. G protein βγ subunits. *Annual review of pharmacology and toxicology,* 37**,** 167-203.
CONG, Z., ZHOU, F., ZHANG, C., ZOU, X., ZHANG, H., WANG, Y., ZHOU, Q., CAI, X., LIU, Q. & LI, J. 2021. Constitutive signal bias mediated by the human GHRHR splice variant 1. *Proceedings of the National Academy of Sciences,* 118**,** e2106606118.
COSI, C., MANNAIONI, G., COZZI, A., CARLA, V., SILI, M., CAVONE, L., MARATEA, D. & MORONI, F. 2011. G-protein coupled receptor 35 (GPR35) activation and inflammatory pain: Studies on the antinociceptive effects of kynurenic acid and zaprinast. *Neuropharmacology,* 60**,** 1227-31.
CRÉPIEUX, P., POUPON, A., LANGONNÉ-GALLAY, N., REITER, E., DELGADO, J., SCHAEFER, M. H., BOURQUARD, T., SERRANO, L. & KIEL, C. 2017. A

comprehensive view of the ß-arrestinome. *Frontiers in Endocrinology,* 8**,** 32.
DALE, N. C., JOHNSTONE, E. K., WHITE, C. W. & PFLEGER, K. D. 2019. NanoBRET: the bright future of proximity-based assays. *Frontiers in Bioengineering and Biotechnology,* 7**,** 56.
DAVENPORT, A., ALEXANDER, S., SHARMAN, J., PAWSON, A., BENSON, H., MONAGHAN, A., LIEW, W., MPAMHANGA, C., BONNER, T. & NEUBIG, R. 2013. Spedding. M. and Harmar, A. J.(2013) International union of basic and clinical pharmacology. LXXXVIII. G protein-coupled receptor list: recommendations for new pairings with cognate ligands. *Pharmacological Reviews,* 65**,** 967-986.
DE GIOVANNI, M., TAM, H., VALET, C., XU, Y., LOONEY, M. R. & CYSTER, J. G. 2022. GPR35 promotes neutrophil recruitment in response to serotonin metabolite 5-HIAA. *Cell,* 185**,** 815-830.
DE GIOVANNI, M., CHEN, H., LI, X. & CYSTER, J. G. 2023a. GPR35 and mediators from platelets and mast cells in neutrophil migration and inflammation. *Immunological Reviews,* 317**,** 187-202.
DE GIOVANNI, M., DANG, E. V., CHEN, K. Y., AN, J., MADHANI, H. D. & CYSTER, J. G. 2023b. Platelets and mast cells promote pathogenic eosinophil recruitment during invasive fungal infection via the 5-HIAA-GPR35 ligand-receptor system. *Immunity,* 56**,** 1548-1560.e5.
DE MENDOZA, A., SEBE-PEDROS, A. & RUIZ-TRILLO, I. 2014. The evolution of the GPCR signaling system in eukaryotes: modularity, conservation, and the transition to metazoan multicellularity. *Genome biology and evolution,* 6**,** 606-619.
DEWIRE, S. M., AHN, S., LEFKOWITZ, R. J. & SHENOY, S. K. 2007. ß-arrestins and cell signaling. *Annual Review of Physiology,* 69**,** 483-510.
DEWIRE, S. M., YAMASHITA, D. S., ROMINGER, D. H., LIU, G., COWAN, C. L., GRACZYK, T. M., CHEN, X.-T., PITIS, P. M., GOTCHEV, D. & YUAN, C. 2013. AG protein-biased ligand at the µ-opioid receptor is potently analgesic with reduced gastrointestinal and respiratory dysfunction compared with morphine. *Journal of Pharmacology and Experimental Therapeutics,* 344**,** 708-717.
DIVORTY, N., MACKENZIE, A. E., NICKLIN, S. A. & MILLIGAN, G. 2015. G protein-coupled receptor 35: an emerging target in inflammatory and cardiovascular disease. *Frontiers in Pharmacology,* 6**,** 41.
DIVORTY, N., MILLIGAN, G., GRAHAM, D. & NICKLIN, S. A. 2018. The Orphan Receptor GPR35 Contributes to Angiotensin II-Induced Hypertension and Cardiac Dysfunction in Mice. *American Journal of Hypertension,* 31**,** 1049-1058.
DIVORTY, N., JENKINS, L., GANGULY, A., BUTCHER, A. J., HUDSON, B. D., SCHULZ, S., TOBIN, A. B., NICKLIN, S. A. & MILLIGAN, G. 2022. Agonist-induced phosphorylation of orthologues of the orphan receptor GPR35 functions as an activation sensor. *Journal of Biological Chemistry*.
DIXON, A. S., SCHWINN, M. K., HALL, M. P., ZIMMERMAN, K., OTTO, P., LUBBEN, T. H., BUTLER, B. L., BINKOWSKI, B. F., MACHLEIDT, T. & KIRKLAND, T. A. 2016. NanoLuc complementation reporter optimized for accurate measurement of protein interactions in cells. *ACS chemical biology,* 11**,** 400-408.
DREWS, J. 2000. Drug discovery: a historical perspective. *science,* 287**,** 1960-1964.
DRUBE, J., HAIDER, R., MATTHEES, E., REICHEL, M., ZEINER, J., FRITZWANKER, S., ZIEGLER, C., BARZ, S., KLEMENT, L. & FILOR, J. 2022. GPCR kinase

knockout cells reveal the impact of individual GRKs on arrestin binding and GPCR regulation. *Nature Communications,* 13**,** 540.
DUAN, J., LIU, Q., YUAN, Q., JI, Y., ZHU, S., TAN, Y., HE, X., XU, Y., SHI, J. & CHENG, X. 2022. Insights into divalent cation regulation and G13-coupling of orphan receptor GPR35. *Cell Discovery,* 8**,** 135.
EBERINI, I., DANIELE, S., PARRAVICINI, C., SENSI, C., TRINCAVELLI, M. L., MARTINI, C. & ABBRACCHIO, M. P. 2011. In silico identification of new ligands for GPR17: a promising therapeutic target for neurodegenerative diseases. *Journal of computer-aided molecular design,* 25**,** 743-752.
EGEROD, K. L., PETERSEN, N., TIMSHEL, P. N., REKLING, J. C., WANG, Y., LIU, Q., SCHWARTZ, T. W. & GAUTRON, L. 2018. Profiling of G protein-coupled receptors in vagal afferents reveals novel gut-to-brain sensing mechanisms. *Molecular Metabolism,* 12**,** 62-75.
ELLINGHAUS, D., FOLSERAAS, T., HOLM, K., ELLINGHAUS, E., MELUM, E., BALSCHUN, T., LAERDAHL, J. K., SHIRYAEV, A., GOTTHARDT, D. N. & WEISMÜLLER, T. J. 2013. Genome-wide association analysis in primary sclerosing cholangitis and ulcerative colitis identifies risk loci at GPR35 and TCF4. *Hepatology,* 58**,** 1074-1083.
EVANS, R., O'NEILL, M., PRITZEL, A., ANTROPOVA, N., SENIOR, A., GREEN, T., ŽÍDEK, A., BATES, R., BLACKWELL, S., YIM, J., RONNEBERGER, O., BODENSTEIN, S., ZIELINSKI, M., BRIDGLAND, A., POTAPENKO, A., COWIE, A., TUNYASUVUNAKOOL, K., JAIN, R., CLANCY, E., KOHLI, P., JUMPER, J. & HASSABIS, D. 2022. Protein complex prediction with AlphaFold-Multimer. *bioRxiv*, 2021.10.04.463034.
FALLARINI, S., MAGLIULO, L., PAOLETTI, T., DE LALLA, C. & LOMBARDI, G. 2010. Expression of functional GPR35 in human iNKT cells. *Biochemical and Biophysical Research Communications,* 398**,** 420-425.
FAZIO, F., LIONETTO, L., MOLINARO, G., BERTRAND, H.-O., ACHER, F., NGOMBA, R. T., NOTARTOMASO, S., CURINI, M., ROSATI, O. & SCARSELLI, P. 2012. Cinnabarinic acid, an endogenous metabolite of the kynurenine pathway, activates type 4 metabotropic glutamate receptors. *Molecular pharmacology,* 81**,** 643-656.
FLOCK, T., RAVARANI, C. N., SUN, D., VENKATAKRISHNAN, A. J., KAYIKCI, M., TATE, C. G., VEPRINTSEV, D. B. & BABU, M. M. 2015. Universal allosteric mechanism for Gα activation by GPCRs. *Nature,* 524**,** 173-179.
FLOCK, T., HAUSER, A. S., LUND, N., GLORIAM, D. E., BALAJI, S. & BABU, M. M. 2017. Selectivity determinants of GPCR–G-protein binding. *Nature,* 545**,** 317-322.
FREDRIKSSON, R., LAGERSTRÖM, M. C., LUNDIN, L.-G. & SCHIÖTH, H. B. 2003. The G-protein-coupled receptors in the human genome form five main families. Phylogenetic analysis, paralogon groups, and fingerprints. *Molecular pharmacology,* 63**,** 1256-1272.
GANGULY, A., QUON, T., JENKINS, L., JOSEPH, B., AL-AWAR, R., CHEVIGNE, A., TOBIN, A. B., UEHLING, D. E., HOFFMANN, C., DRUBE, J. & MILLIGAN, G. 2023. G protein-receptor kinases 5/6 are the key regulators of G protein-coupled receptor 35-arrestin interactions. *Journal of Biological Chemistry,* 299.
GARLAND, S. L. 2013. Are GPCRs still a source of new targets? *Journal of biomolecular screening,* 18**,** 947-966.
GASHAW, I., ELLINGHAUS, P., SOMMER, A. & ASADULLAH, K. 2011. What makes a good drug target? *Drug discovery today,* 16**,** 1037-1043.
GIBLIN, S. P. & PEASE, J. E. 2023. What defines a chemokine?–The curious case of CXCL17. *Cytokine,* 168**,** 156224.

GIMENEZ, L. E., KOOK, S., VISHNIVETSKIY, S. A., AHMED, M. R., GUREVICH, E. V. & GUREVICH, V. V. 2012. Role of receptor-attached phosphates in binding of visual and non-visual arrestins to G protein-coupled receptors. *Journal of Biological Chemistry,* 287**,** 9028-9040.

GOLD, J. I., MARTINI, J. S., HULLMANN, J., GAO, E., CHUPRUN, J. K., LEE, L., TILLEY, D. G., RABINOWITZ, J. E., BOSSUYT, J. & BERS, D. M. 2013. Nuclear translocation of cardiac G protein-coupled receptor kinase 5 downstream of select Gq-activating hypertrophic ligands is a calmodulin-dependent process. *PloS one,* 8**,** e57324.

GOODMAN JR, O. B., KRUPNICK, J. G., SANTINI, F., GUREVICH, V. V., PENN, R. B., GAGNON, A. W., KEEN, J. H. & BENOVIC, J. L. 1996. β-Arrestin acts as a clathrin adaptor in endocytosis of the β2-adrenergic receptor. *nature,* 383**,** 447-450.

GRIGORIADIS, D. E., HOARE, S. R., LECHNER, S. M., SLEE, D. H. & WILLIAMS, J. A. 2009. Drugability of extracellular targets: discovery of small molecule drugs targeting allosteric, functional, and subunit-selective sites on GPCRs and ion channels. *Neuropsychopharmacology,* 34**,** 106-125.

GUO, J., WILLIAMS, D. J., PUHL, H. L., 3RD & IKEDA, S. R. 2008. Inhibition of N-type calcium channels by activation of GPR35, an orphan receptor, heterologously expressed in rat sympathetic neurons. *The Journal of Pharmacology and Experimental Therapeutics,* 324**,** 342-51.

GUO, S., ZHAO, T., YUN, Y. & XIE, X. 2022. Recent progress in assays for GPCR drug discovery. *American Journal of Physiology-Cell Physiology,* 323**,** C583-C594.

GUO, Y. J., ZHOU, Y. J., YANG, X. L., SHAO, Z. M. & OU, Z. L. 2017. The role and clinical significance of the CXCL17-CXCR8 (GPR35) axis in breast cancer. *Biochemical and Biophysical Research Communications,* 493**,** 1159-1167.

GUREVICH, E. V., GAINETDINOV, R. R. & GUREVICH, V. V. 2016. G protein-coupled receptor kinases as regulators of dopamine receptor functions. *Pharmacological research,* 111**,** 1-16.

GUREVICH, V. V. & GUREVICH, E. V. 2008. How and why do GPCRs dimerize? *Trends in pharmacological sciences,* 29**,** 234-240.

GUREVICH, V. V. & GUREVICH, E. V. 2019. GPCR signaling regulation: the role of GRKs and arrestins. *Frontiers in pharmacology,* 10**,** 125.

HAIDER, R. S., MATTHEES, E. S., DRUBE, J., REICHEL, M., ZABEL, U., INOUE, A., CHEVIGNÉ, A., KRASEL, C., DEUPI, X. & HOFFMANN, C. 2022. β-arrestin1 and 2 exhibit distinct phosphorylation-dependent conformations when coupling to the same GPCR in living cells. *Nature communications,* 13**,** 5638.

HAJIZADEH, F., OKOYE, I., ESMAILY, M., CHALESHTARI, M. G., MASJEDI, A., AZIZI, G., IRANDOUST, M., GHALAMFARSA, G. & JADIDI-NIARAGH, F. 2019. Hypoxia inducible factors in the tumor microenvironment as therapeutic targets of cancer stem cells. *Life sciences,* 237**,** 116952.

HALL, M. P., UNCH, J., BINKOWSKI, B. F., VALLEY, M. P., BUTLER, B. L., WOOD, M. G., OTTO, P., ZIMMERMAN, K., VIDUGIRIS, G. & MACHLEIDT, T. 2012. Engineered luciferase reporter from a deep sea shrimp utilizing a novel imidazopyrazinone substrate. *ACS chemical biology,* 7**,** 1848-1857.

HARMAR, A. J. 2001. Family-B G-protein-coupled receptors. *Genome biology,* 2**,** 1-10.

HASHEMI, S. F. & KHORRAMDELAZAD, H. 2023. The cryptic role of CXCL17/CXCR8 axis in the pathogenesis of cancers: a review of the latest evidence. *Journal of Cell Communication and Signaling,* 17**,** 409-422.

HAUSER, A. S., CHAVALI, S., MASUHO, I., JAHN, L. J., MARTEMYANOV, K. A., GLORIAM, D. E. & BABU, M. M. 2018. Pharmacogenomics of GPCR drug targets. *Cell,* 172**,** 41-54. e19.

HEYNEN-GENEL, S., DAHL, R., SHI, S., SAUER, M., HARIHARAN, S., SERGIENKO, E., DAD, S., CHUNG, T., STONICH, D. & SU, Y. 2010. Selective GPR35 Antagonists: Probes 1 and 2. Probe Reports from the NIH Molecular Libraries Program, Bethesda, MD. National Center for Biotechnology Information Bethesda, MD.

HOMAN, K. T. & TESMER, J. J. 2014. Structural insights into G protein-coupled receptor kinase function. *Current opinion in cell biology,* 27**,** 25-31.

HOPKINS, A. L. & GROOM, C. R. 2002. The druggable genome. *Nature reviews Drug discovery,* 1**,** 727-730.

HORIKAWA, Y., ODA, N., COX, N. J., LI, X., ORHO-MELANDER, M., HARA, M., HINOKIO, Y., LINDNER, T. H., MASHIMA, H. & SCHWARZ, P. E. 2000. Genetic variation in the gene encoding calpain-10 is associated with type 2 diabetes mellitus. *Nature genetics,* 26**,** 163-175.

HOUSLAY, M. & BAILLIE, G. 2005. ß-Arrestin-recruited phosphodiesterase-4 desensitizes the AKAP79/PKA-mediated switching of ß2-adrenoceptor signalling to activation of ERK. Portland Press Ltd.

HU, G.-M., MAI, T.-L. & CHEN, C.-M. 2017. Visualizing the GPCR network: classification and evolution. *Scientific reports,* 7**,** 15495.

IM, D.-S. 2023. Recent advances in GPR35 pharmacology; 5-HIAA serotonin metabolite becomes a ligand. *Archives of Pharmacal Research***,** 1-14.

IMIELINSKI, M., BALDASSANO, R. N., GRIFFITHS, A., RUSSELL, R. K., ANNESE, V., DUBINSKY, M., KUGATHASAN, S., BRADFIELD, J. P., WALTERS, T. D. & SLEIMAN, P. 2009. Common variants at five new loci associated with early-onset inflammatory bowel disease. *Nature genetics,* 41**,** 1335-1340.

JENKINS, L., BREA, J., SMITH, N. J., HUDSON, B. D., REILLY, G., BRYANT, N. J., CASTRO, M., LOZA, M. I. & MILLIGAN, G. 2010. Identification of novel species-selective agonists of the G-protein-coupled receptor GPR35 that promote recruitment of beta-arrestin-2 and activate Galpha13. *Biochemical Journal,* 432**,** 451-9.

JENKINS, L., ALVAREZ-CURTO, E., CAMPBELL, K., DE MUNNIK, S., CANALS, M., SCHLYER, S. & MILLIGAN, G. 2011. Agonist activation of the G protein-coupled receptor GPR35 involves transmembrane domain III and is transduced via $G\alpha_{13}$ and ß-arrestin-2. *British Journal of Pharmacology,* 162**,** 733-48.

JENKINS, L., HARRIES, N., LAPPIN, J. E., MACKENZIE, A. E., NEETOO-ISSELJEE, Z., SOUTHERN, C., MCIVER, E. G., NICKLIN, S. A., TAYLOR, D. L. & MILLIGAN, G. 2012. Antagonists of GPR35 display high species ortholog selectivity and varying modes of action. *Journal of Pharmacology and Experimental Therapeutics,* 343**,** 683-95.

JOISTEN, N., RUAS, J. L., BRAIDY, N., GUILLEMIN, G. J. & ZIMMER, P. 2021. The kynurenine pathway in chronic diseases: a compensatory mechanism or a driving force? *Trends in Molecular Medicine,* 27**,** 946-954.

JUMPER, J., EVANS, R., PRITZEL, A., GREEN, T., FIGURNOV, M., RONNEBERGER, O., TUNYASUVUNAKOOL, K., BATES, R., ŽÍDEK, A. & POTAPENKO, A. 2021. Highly accurate protein structure prediction with AlphaFold. *Nature,* 596**,** 583-589.

KAPOLKA, N., TAGHON, G., ROWE, J., MORGAN, W., ENTEN, J., LAMBERT, N. & ISOM, D. 2020. DCyFIR: a high-throughput CRISPR platform for multiplexed G protein-coupled receptor profiling and ligand discovery. *Proceedings of the National Academy of Sciences,* 117**,** 13117-13126.

KARNAM, P. C., VISHNIVETSKIY, S. A. & GUREVICH, V. V. 2021. Structural basis of arrestin selectivity for active phosphorylated g protein-coupled receptors. *International Journal of Molecular Sciences,* 22**,** 12481.
KATRITCH, V., CHEREZOV, V. & STEVENS, R. C. 2012. Diversity and modularity of G protein-coupled receptor structures. *Trends in pharmacological sciences,* 33**,** 17-27.
KAWAKAMI, K., YANAGAWA, M., HIRATSUKA, S., YOSHIDA, M., ONO, Y., HIROSHIMA, M., UEDA, M., AOKI, J., SAKO, Y. & INOUE, A. 2022. Heterotrimeric Gq proteins act as a switch for GRK5/6 selectivity underlying β-arrestin transducer bias. *Nature communications,* 13**,** 487.
KAYA, B., DONAS, C., WUGGENIG, P., DIAZ, O. E., MORALES, R. A., MELHEM, H., SWISS, I. B. D. C. I., HERNANDEZ, P. P., KAYMAK, T., DAS, S., HRUZ, P., FRANC, Y., GEIER, F., AYATA, C. K., VILLABLANCA, E. J. & NIESS, J. H. 2020. Lysophosphatidic Acid-Mediated GPR35 Signaling in CX3CR1(+) Macrophages Regulates Intestinal Homeostasis. *Cell Reports,* 32**,** 107979.
KAYA, B., MELHEM, H. & NIESS, J. H. 2021. GPR35 in Intestinal Diseases: From Risk Gene to Function. *Frontiers in Immunology,* 12**,** 717392.
KENAKIN, T. 2019. Biased receptor signaling in drug discovery. *Pharmacological reviews,* 71**,** 267-315.
KIM, C., KIM, Y., LIM, J. Y., KIM, M., ZHENG, H., KIM, M. & HWANG, S. W. 2023. Pamoic acid-induced peripheral GPR35 activation improves pruritus and dermatitis. *British Journal of Pharmacology,* 180**,** 3059-3070.
KIM, L. C., SONG, L. & HAURA, E. B. 2009. Src kinases as therapeutic targets for cancer. *Nature reviews Clinical oncology,* 6**,** 587-595.
KIM, M. J., PARK, S. J., NAM, S. Y. & IM, D. S. 2019. Lodoxamide Attenuates Hepatic Fibrosis in Mice: Involvement of GPR35. *Biomolecules & Therapeutics (Seoul)*, 92-97.
KIM, T. H., YANG, Y. M., HAN, C. Y., KOO, J. H., OH, H., KIM, S. S., YOU, B. H., CHOI, Y. H., PARK, T.-S. & LEE, C. H. 2018. Gα 12 ablation exacerbates liver steatosis and obesity by suppressing USP22/SIRT1-regulated mitochondrial respiration. *The Journal of clinical investigation,* 128**,** 5587-5602.
KOBILKA, B. & SCHERTLER, G. F. 2008. New G-protein-coupled receptor crystal structures: insights and limitations. *Trends in pharmacological sciences,* 29**,** 79-83.
KOBILKA, B. K. 2007. G protein coupled receptor structure and activation. *Biochimica et Biophysica Acta (BBA)-Biomembranes,* 1768**,** 794-807.
KOLAR, G. R., GROTE, S. M. & YOSTEN, G. L. 2017. Targeting orphan G protein-coupled receptors for the treatment of diabetes and its complications: C-peptide and GPR 146. *Journal of internal medicine,* 281**,** 25-40.
KOMOLOV, K. E. & BENOVIC, J. L. 2018. G protein-coupled receptor kinases: Past, present and future. *Cellular signalling,* 41**,** 17-24.
KUC, D., ZGRAJKA, W., PARADA-TURSKA, J., URBANIK-SYPNIEWSKA, T. & TURSKI, W. 2008. Micromolar concentration of kynurenic acid in rat small intestine. *Amino Acids,* 35**,** 503-505.
KUNISHIMA, N., SHIMADA, Y., TSUJI, Y., SATO, T., YAMAMOTO, M., KUMASAKA, T., NAKANISHI, S., JINGAMI, H. & MORIKAWA, K. 2000. Structural basis of glutamate recognition by a dimeric metabotropic glutamate receptor. *Nature,* 407**,** 971-977.
LANDER, E. S. 2011. Initial impact of the sequencing of the human genome. *Nature,* 470**,** 187-197.
LAPORTE, S. A., OAKLEY, R. H., ZHANG, J., HOLT, J. A., FERGUSON, S. S., CARON, M. G. & BARAK, L. S. 1999. The β2-adrenergic receptor/βarrestin

complex recruits the clathrin adaptor AP-2 during endocytosis. *Proceedings of the National Academy of Sciences,* 96**,** 3712-3717.
LECCA, D. & ABBRACCHIO, M. P. 2008. Deorphanisation of G protein-coupled receptors: A tool to provide new insights in nervous system pathophysiology and new targets for psycho-active drugs. *Neurochemistry international,* 52**,** 339-351.
LEE, W.-Y., WANG, C.-J., LIN, T.-Y., HSIAO, C.-L. & LUO, C.-W. 2013. CXCL17, an orphan chemokine, acts as a novel angiogenic and anti-inflammatory factor. *American Journal of Physiology-Endocrinology and Metabolism,* 304**,** E32-E40.
LEFKOWITZ, R. 2007. Seven transmembrane receptors: something old, something new. *Acta physiologica,* 190**,** 9-19.
LEONARD, J. & CHU, Z. L. 2007. GPR35 and modulators thereof for the treatment of metabolic-related disorders. Google Patents.
LEVOYE, A., DAM, J., AYOUB, M. A., GUILLAUME, J. L. & JOCKERS, R. 2006. Do orphan G-protein-coupled receptors have ligand-independent functions? New insights from receptor heterodimers. *EMBO reports,* 7**,** 1094-1098.
LI, H., NGUYEN, H., VENKATA, S. P. M., KOH, J. Y., KOWLURU, A., LI, L., ROSSI, N. F., CHEN, W. & WANG, J.-M. 2021. Novel Role of GPR35 (G-Protein–Coupled Receptor 35) in the Regulation of Endothelial Cell Function and Blood Pressure. *Hypertension,* 78**,** 816-830.
LI, Z., QIU, Q., GENG, X., YANG, J., HUANG, W. & QIAN, H. 2016. Free fatty acid receptor agonists for the treatment of type 2 diabetes: drugs in preclinical to phase II clinical development. *Expert opinion on investigational drugs,* 25**,** 871-890.
LIGGETT, S. B. 2011. Phosphorylation barcoding as a mechanism of directing GPCR signaling. *Science signaling,* 4**,** pe36-pe36.
LIN, L.-C., QUON, T., ENGBERG, S., MACKENZIE, A. E., TOBIN, A. B. & MILLIGAN, G. 2021. G Protein-Coupled Receptor GPR35 Suppresses Lipid Accumulation in Hepatocytes. *ACS Pharmacology & Translational Science,* 4**,** 1835-1848.
LITOSCH, I. 2016. Decoding Gαq signaling. *Life sciences,* 152**,** 99-106.
LOHSE, M. J. 1993. Molecular mechanisms of membrane receptor desensitization. *Biochimica et Biophysica Acta (BBA)-Molecular Cell Research,* 1179**,** 171-188.
LOWE, J. D., SANDERSON, H. S., COOKE, A. E., OSTOVAR, M., TSISANOVA, E., WITHEY, S. L., CHAVKIN, C., HUSBANDS, S. M., KELLY, E. & HENDERSON, G. 2015. Role of G protein–coupled receptor kinases 2 and 3 in μ-opioid receptor desensitization and internalization. *Molecular pharmacology,* 88**,** 347-356.
LUNDSTROM, K. 2009. An overview on GPCRs and drug discovery: structure-based drug design and structural biology on GPCRs. *G protein-coupled receptors in drug discovery***,** 51-66.
LUTTRELL, L. M. & LEFKOWITZ, R. J. 2002. The role of ß-arrestins in the termination and transduction of G-protein-coupled receptor signals. *Journal of cell science,* 115**,** 455-465.
LUTTRELL, L. M. & GESTY-PALMER, D. 2010. Beyond desensitization: physiological relevance of arrestin-dependent signaling. *Pharmacological reviews,* 62**,** 305-330.
LUTTRELL, L. M., MAUDSLEY, S. & BOHN, L. M. 2015. Fulfilling the promise of" biased" G protein–coupled receptor agonism. *Molecular pharmacology,* 88**,** 579-588.

MA, J., CHEN, P., DENG, B. & WANG, R. 2023. Kynurenic acid promotes osteogenesis via the Wnt/ß-catenin signaling. *In Vitro Cellular & Developmental Biology-Animal*, 1-10.
MACKENZIE, A., LAPPIN, J., TAYLOR, D., NICKLIN, S. & MILLIGAN, G. 2011. GPR35 as a novel therapeutic target. *Frontiers in endocrinology,* 2, 68.
MACKENZIE, A. E., CALTABIANO, G., KENT, T. C., JENKINS, L., MCCALLUM, J. E., HUDSON, B. D., NICKLIN, S. A., FAWCETT, L., MARKWICK, R., CHARLTON, S. J. & MILLIGAN, G. 2014. The antiallergic mast cell stabilizers lodoxamide and bufrolin as the first high and equipotent agonists of human and rat GPR35. *Molecular Pharmacology,* 85, 91-104.
MACKENZIE, A. E. & MILLIGAN, G. 2017. The emerging pharmacology and function of GPR35 in the nervous system. *Neuropharmacology,* 113, 661-671.
MACKENZIE, A. E., QUON, T., LIN, L. C., HAUSER, A. S., JENKINS, L., INOUE, A., TOBIN, A. B., GLORIAM, D. E., HUDSON, B. D. & MILLIGAN, G. 2019. Receptor selectivity between the G proteins Galpha(12) and Galpha(13) is defined by a single leucine-to-isoleucine variation. *The FASEB Journal,* 33, 5005-5017.
MACKIEWICZ, T., WLODARCZYK, J., ZIELINSKA, M., WLODARCZYK, M., DURCZYNSKI, A., HOGENDORF, P., DZIKI, L. & FICHNA, J. 2023. Increased GPR35 expression in human colorectal and pancreatic cancer samples: A preliminary clinical validation of a new biomarker. *Advances in Clinical and Experimental Medicine,* 32, 783-789.
MAEDA, S. & SCHERTLER, G. F. 2013. Production of GPCR and GPCR complexes for structure determination. *Current opinion in structural biology,* 23, 381-392.
MANGGE, H., SUMMERS, K. L., MEINITZER, A., ZELZER, S., ALMER, G., PRASSL, R., SCHNEDL, W. J., REININGHAUS, E., PAULMICHL, K. & WEGHUBER, D. 2014. Obesity-related dysregulation of the Tryptophan–Kynurenine metabolism: Role of age and parameters of the metabolic syndrome. *Obesity,* 22, 195-201.
MARAVILLAS-MONTERO, J. L., BURKHARDT, A. M., HEVEZI, P. A., CARNEVALE, C. D., SMIT, M. J. & ZLOTNIK, A. 2015. Cutting edge: GPR35/CXCR8 is the receptor of the mucosal chemokine CXCL17. *The Journal of Immunology,* 194, 29-33.
MARCHESE, A. & TREJO, J. 2013. Ubiquitin-dependent regulation of G protein-coupled receptor trafficking and signaling. *Cellular signalling,* 25, 707-716.
MARKOVIC, D. & CHALLISS, R. J. 2009. Alternative splicing of G protein-coupled receptors: physiology and pathophysiology. *Cellular and molecular life sciences,* 66, 3337-3352.
MARSANGO, S., WARD, R. J., JENKINS, L., BUTCHER, A. J., AL MAHMUD, Z., DWOMOH, L., NAGEL, F., SCHULZ, S., TIKHONOVA, I. G. & TOBIN, A. B. 2022. Selective phosphorylation of threonine residues defines GPR84–arrestin interactions of biased ligands. *Journal of Biological Chemistry,* 298, 101932.
MARTI-SOLANO, M., CRILLY, S. E., MALINVERNI, D., MUNK, C., HARRIS, M., PEARCE, A., QUON, T., MACKENZIE, A. E., WANG, X., PENG, J., TOBIN, A. B., LADDS, G., MILLIGAN, G., GLORIAM, D. E., PUTHENVEEDU, M. A. & BABU, M. M. 2020. Combinatorial expression of GPCR isoforms affects signalling and drug responses. *Nature,* 587, 650-656.

MATTHEES, E. S., HAIDER, R. S., HOFFMANN, C. & DRUBE, J. 2021. Differential regulation of GPCRs—are GRK expression levels the key? *Frontiers in Cell and Developmental Biology,* 9**,** 687489.
MAUDSLEY, S., MARTIN, B. & LUTTRELL, L. M. 2005. The origins of diversity and specificity in G protein-coupled receptor signaling. *Journal of Pharmacology and Experimental Therapeutics,* 314**,** 485-494.
MCCALLUM, J. E., MACKENZIE, A. E., DIVORTY, N., CLARKE, C., DELLES, C., MILLIGAN, G. & NICKLIN, S. A. 2015. G-Protein-Coupled Receptor 35 Mediates Human Saphenous Vein Vascular Smooth Muscle Cell Migration and Endothelial Cell Proliferation. *Journal of Vascular Research,* 52**,** 383-95.
MILLIGAN, G. 2011. Orthologue selectivity and ligand bias: translating the pharmacology of GPR35. *Trends in Pharmacological Sciences,* 32**,** 317-25.
MILLIGAN, G. 2023. GPR35: from enigma to therapeutic target. *Trends in Pharmacological Sciences,* 44**,** 263-273.
MIN, K. D., ASAKURA, M., LIAO, Y., NAKAMARU, K., OKAZAKI, H., TAKAHASHI, T., FUJIMOTO, K., ITO, S., TAKAHASHI, A., ASANUMA, H., YAMAZAKI, S., MINAMINO, T., SANADA, S., SEGUCHI, O., NAKANO, A., ANDO, Y., OTSUKA, T., FURUKAWA, H., ISOMURA, T., TAKASHIMA, S., MOCHIZUKI, N. & KITAKAZE, M. 2010. Identification of genes related to heart failure using global gene expression profiling of human failing myocardium. *Biochemical and Biophysical Research Communications,* 393**,** 55-60.
MINNEMAN, K. P. 2001. Splice variants of GPCRs. *Molecular interventions,* 1**,** 108.
MINUTELLO, K. & GUPTA, V. 2020. Cromolyn sodium.
MIRDITA, M., SCHÜTZE, K., MORIWAKI, Y., HEO, L., OVCHINNIKOV, S. & STEINEGGER, M. 2022. ColabFold: making protein folding accessible to all. *Nature Methods,* 19**,** 679-682.
MIYAMOTO, K., SUJINO, T., HARADA, Y., ASHIDA, H., YOSHIMATSU, Y., YONEMOTO, Y., NEMOTO, Y., TOMURA, M., MELHEM, H., NIESS, J. H., SUZUKI, T., SUZUKI, T., SUZUKI, S., KODA, Y., OKAMOTO, R., MIKAMI, Y., TERATANI, T., TANAKA, K. F., YOSHIMURA, A., SATO, T. & KANAI, T. 2023. The gut microbiota-induced kynurenic acid recruits GPR35-positive macrophages to promote experimental encephalitis. *Cell Reports,* 42**,** 113005.
MORONI, F., COZZI, A., SILI, M. & MANNAIONI, G. 2012. Kynurenic acid: a metabolite with multiple actions and multiple targets in brain and periphery. *Journal of Neural Transmission* 119**,** 133-139.
NAKAMURA, S., ITABASHI, T., OGAWA, D. & OKADA, T. 2013. Common and distinct mechanisms of activation of rhodopsin and other G protein-coupled receptors. *Scientific Reports,* 3**,** 1-6.
NAKASHIMA, F., QI LOH, W., WAKABAYASHI, M., SHIMOMURA, S., HATTORI, H., KITA, M., INOUE, A., UCHIDA, K. & SHIBATA, T. 2023. Eriodictyol and thymonin act as GPR35 agonists. *Bioscience, Biotechnology, and Biochemistry,* 87**,** 1514-1522.
NAM, S. Y., PARK, S. J. & IM, D. S. 2019. Protective effect of lodoxamide on hepatic steatosis through GPR35. *Cellular Signalling,* 53**,** 190-200.
NASRI, I., CHAWECH, R., GIRARDI, C., MAS, E., FERRAND, A., VERGNOLLE, N., FABRE, N., MEZGHANI-JARRAYA, R. & RACAUD-SULTAN, C. 2017. Anti-inflammatory and anticancer effects of flavonol glycosides from Diplotaxis harra through GSK3β regulation in intestinal cells. *Pharmaceutical biology,* 55**,** 124-131.

NEETOO-ISSELJEE, Z., MACKENZIE, A. E., SOUTHERN, C., JERMAN, J., MCIVER, E. G., HARRIES, N., TAYLOR, D. L. & MILLIGAN, G. 2013. High-throughput identification and characterization of novel, species-selective GPR35 agonists. *The Journal of Pharmacology and Experimental Therapeutics,* 344**,** 568-578.

NEUBIG, R. R. 2010. Mind your salts: when the inactive constituent isn't. *Molecular Pharmacology,* 78**,** 558-559.

NGO, T., KUFAREVA, I., COLEMAN, J. L., GRAHAM, R. M., ABAGYAN, R. & SMITH, N. J. 2016. Identifying ligands at orphan GPCRs: current status using structure-based approaches. *British journal of pharmacology,* 173**,** 2934-2951.

NOBLES, K. N., XIAO, K., AHN, S., SHUKLA, A. K., LAM, C. M., RAJAGOPAL, S., STRACHAN, R. T., HUANG, T.-Y., BRESSLER, E. A. & HARA, M. R. 2011. Distinct phosphorylation sites on the β2-adrenergic receptor establish a barcode that encodes differential functions of β-arrestin. *Science signaling,* 4**,** ra51-ra51.

O'DOWD, B. F., NGUYEN, T., MARCHESE, A., CHENG, R., LYNCH, K. R., HENG, H. H., KOLAKOWSKI, L. F., JR. & GEORGE, S. R. 1998. Discovery of three novel G-protein-coupled receptor genes. *Genomics,* 47**,** 310-3.

OHSHIRO, H., TONAI-KACHI, H. & ICHIKAWA, K. 2008. GPR35 is a functional receptor in rat dorsal root ganglion neurons. *Biochemical and Biophysical Research Communications,* 365**,** 344-348.

OKA, S., OTA, R., SHIMA, M., YAMASHITA, A. & SUGIURA, T. 2010. GPR35 is a novel lysophosphatidic acid receptor. *Biochemical and Biophysical Research Communications,* 395**,** 232-237.

OKUMURA, S., BABA, H., KUMADA, T., NANMOKU, K., NAKAJIMA, H., NAKANE, Y., HIOKI, K. & IKENAKA, K. 2004. Cloning of a G-protein-coupled receptor that shows an activity to transform NIH3T3 cells and is expressed in gastric cancer cells. *Cancer Science,* 95**,** 131-135.

OTKUR, W., LIU, X., CHEN, H., LI, S., LING, T., LIN, H., YANG, R., XIA, T., QI, H. & PIAO, H.-L. 2023a. GPR35 antagonist CID-2745687 attenuates anchorage-independent cell growth by inhibiting YAP/TAZ activity in colorectal cancer cells. *Frontiers in Pharmacology,* 14**,** 1126119.

OTKUR, W., WANG, J., HOU, T., LIU, F., YANG, R., LI, Y., XIANG, K., PEI, S., QI, H. & LIN, H. 2023b. Aminosalicylates target GPR35, partly contributing to the prevention of DSS-induced colitis. *European Journal of Pharmacology***,** 175719.

OXENKRUG, G., CORNICELLI, J., VAN DER HART, M., ROESER, J. & SUMMERGRAD, P. 2016. Kynurenic acid, an aryl hydrocarbon receptor ligand, is elevated in serum of Zucker fatty rats. *Integrative molecular medicine,* 3**,** 761.

OXENKRUG, G. & NAVROTSKA, V. 2023. Extension of life span by down-regulation of enzymes catalyzing tryptophan conversion into kynurenine: Possible implications for mechanisms of aging. *Experimental Biology and Medicine***,** 15353702231179411.

PALCZEWSKI, K., BUCZYŁKO, J., KAPLAN, M., POLANS, A. & CRABB, J. 1991. Mechanism of rhodopsin kinase activation. *Journal of Biological Chemistry,* 266**,** 12949-12955.

PALCZEWSKI, K., KUMASAKA, T., HORI, T., BEHNKE, C. A., MOTOSHIMA, H., FOX, B. A., TRONG, I. L., TELLER, D. C., OKADA, T. & STENKAMP, R. E. 2000. Crystal structure of rhodopsin: AG protein-coupled receptor. *science,* 289**,** 739-745.

PALMER, C. B., D'UONNOLO, G., LUÍS, R., MEYRATH, M., UCHAŃSKI, T., CHEVIGNÉ, A. & SZPAKOWSKA, M. 2022. Nanoluciferase-based

complementation assay for systematic profiling of GPCR-GRK interactions. *Methods in Cell Biology*. Academic Press.
PALUSZKIEWICZ, P., ZGRAJKA, W., SARAN, T., SCHABOWSKI, J., VALVERDE PIEDRA, J. L., FEDKIV, O., RENGMAN, S., PIERZYNOWSKI, S. G. & TURSKI, W. A. 2009. High concentration of kynurenic acid in bile and pancreatic juice. *Amino Acids,* 37**,** 637-641.
PARK, S. J., LEE, S. J., NAM, S. Y. & IM, D. S. 2018. GPR35 mediates lodoxamide-induced migration inhibitory response but not CXCL17-induced migration stimulatory response in THP-1 cells; is GPR35 a receptor for CXCL17? *British Journal of Pharmacology,* 175**,** 154-161.
PENELA, P., RIBAS, C. & MAYOR JR, F. 2003. Mechanisms of regulation of the expression and function of G protein-coupled receptor kinases. *Cellular signalling,* 15**,** 973-981.
PHAM, T. H., KIM, E. N., TRANG, N. M. & JEONG, G. S. 2023. Gallic acid induces osteoblast differentiation and alleviates inflammatory response through GPR35/GSK3β/β-catenin signaling pathway in human periodontal ligament cells. *Journal of Periodontal Research*.
PRIHANDOKO, R., BRADLEY, S. J., TOBIN, A. B. & BUTCHER, A. J. 2015. Determination of GPCR phosphorylation status: establishing a phosphorylation barcode. *Current Protocols in Pharmacology,* 69**,** 2.13. 1-2.13. 26.
PRIHANDOKO, R., ALVAREZ-CURTO, E., HUDSON, B. D., BUTCHER, A. J., ULVEN, T., MILLER, A. M., TOBIN, A. B. & MILLIGAN, G. 2016. Distinct Phosphorylation Clusters Determine the Signaling Outcome of Free Fatty Acid Receptor 4/G Protein–Coupled Receptor 120. *Molecular pharmacology,* 89**,** 505-520.
PRÖMEL, S., LANGENHAN, T. & ARAÇ, D. 2013. Matching structure with function: the GAIN domain of adhesion-GPCR and PKD1-like proteins. *Trends in pharmacological sciences,* 34**,** 470-478.
QUON, T., LIN, L.-C., GANGULY, A., TOBIN, A. B. & MILLIGAN, G. 2020. Therapeutic opportunities and challenges in targeting the orphan G protein-coupled receptor GPR35. *ACS Pharmacology & Translational Science,* 3**,** 801-812.
RASK-ANDERSEN, M., ALMÉN, M. S. & SCHIÖTH, H. B. 2011. Trends in the exploitation of novel drug targets. *Nature reviews Drug discovery,* 10**,** 579-590.
RASMUSSEN, S., DEVREE, B., ZOU, Y., KRUSE, A., CHUNG, K., KOBILKA, T., THIAN, F., CHAE, P., PARDON, E. & CALINSKI, D. 2011. Crystal structure of the β2 adrenergic receptor–Gs protein complex. *Nature,* 477**,** 549-555.
RASMUSSEN, S. G., CHOI, H.-J., ROSENBAUM, D. M., KOBILKA, T. S., THIAN, F. S., EDWARDS, P. C., BURGHAMMER, M., RATNALA, V. R., SANISHVILI, R. & FISCHETTI, R. F. 2007. Crystal structure of the human β2 adrenergic G-protein-coupled receptor. *Nature,* 450**,** 383-387.
REICHEL, M., WEITZEL, V., KLEMENT, L., HOFFMANN, C. & DRUBE, J. 2022. Suitability of GRK antibodies for individual detection and quantification of GRK isoforms in western blots. *International Journal of Molecular Sciences,* 23**,** 1195.
REN, X.-R., REITER, E., AHN, S., KIM, J., CHEN, W. & LEFKOWITZ, R. J. 2005. Different G protein-coupled receptor kinases govern G protein and β-arrestin-mediated signaling of V2 vasopressin receptor. *Proceedings of the National Academy of Sciences,* 102**,** 1448-1453.
RIBAS, C., PENELA, P., MURGA, C., SALCEDO, A., GARCÍA-HOZ, C., JURADO-PUEYO, M., AYMERICH, I. & MAYOR JR, F. 2007. The G protein-coupled

receptor kinase (GRK) interactome: role of GRKs in GPCR regulation and signaling. *Biochimica et Biophysica Acta (BBA)-Biomembranes,* 1768**,** 913-922.
ROJEWSKA, E., CIAPALA, K. & MIKA, J. 2019. Kynurenic acid and zaprinast diminished CXCL17-evoked pain-related behaviour and enhanced morphine analgesia in a mouse neuropathic pain model. *Pharmacological Reports,* 71**,** 139-148.
RONKAINEN, V. P., TUOMAINEN, T., HUUSKO, J., LAIDINEN, S., MALINEN, M., PALVIMO, J. J., YLA-HERTTUALA, S., VUOLTEENAHO, O. & TAVI, P. 2014. Hypoxia-inducible factor 1-induced G protein-coupled receptor 35 expression is an early marker of progressive cardiac remodelling. *Cardiovascular Research,* 101**,** 69-77.
ROTH, W., ZADEH, K., VEKARIYA, R., GE, Y. & MOHAMADZADEH, M. 2021. Tryptophan metabolism and gut-brain homeostasis. *International journal of molecular sciences,* 22**,** 2973.
ROVATI, G. E., CAPRA, V. & NEUBIG, R. R. 2007. The highly conserved DRY motif of class AG protein-coupled receptors: beyond the ground state. *Molecular pharmacology,* 71**,** 959-964.
SAKURAI, T., AMEMIYA, A., ISHII, M., MATSUZAKI, I., CHEMELLI, R. M., TANAKA, H., WILLIAMS, S. C., RICHARDSON, J. A., KOZLOWSKI, G. P. & WILSON, S. 1998. Orexins and orexin receptors: a family of hypothalamic neuropeptides and G protein-coupled receptors that regulate feeding behavior. *Cell,* 92**,** 573-585.
SALLESE, M., MARIGGIO, S., COLLODEL, G., MORETTI, E., PIOMBONI, P., BACCETTI, B. & DE BLASI, A. 1997. G protein-coupled receptor kinase GRK4: molecular analysis of the four isoforms and ultrastructural localization in spermatozoa and germinal cells. *Journal of Biological Chemistry,* 272**,** 10188-10195.
SAMS-DODD, F. 2005. Target-based drug discovery: is something wrong? *Drug discovery today,* 10**,** 139-147.
SÁNCHEZ-FERNÁNDEZ, G., CABEZUDO, S., GARCÍA-HOZ, C., TOBIN, A. B., MAYOR JR, F. & RIBAS, C. 2013. ERK5 activation by Gq-coupled muscarinic receptors is independent of receptor internalization and ß-arrestin recruitment. *PLoS One,* 8**,** e84174.
SANTOS, R., URSU, O., GAULTON, A., BENTO, A. P., DONADI, R. S., BOLOGA, C. G., KARLSSON, A., AL-LAZIKANI, B., HERSEY, A. & OPREA, T. I. 2017. A comprehensive map of molecular drug targets. *Nature reviews Drug discovery,* 16**,** 19-34.
SCHIHADA, H., KLOMPSTRA, T. M., HUMPHRYS, L. J., CERVENKA, I., DADVAR, S., KOLB, P., RUAS, J. L. & SCHULTE, G. 2022. Isoforms of GPR35 have distinct extracellular N-termini that allosterically modify receptor-transducer coupling and mediate intracellular pathway bias. *Journal of Biological Chemistry,* 298**,** 102328.
SCHNEDITZ, G., ELIAS, J. E., PAGANO, E., ZAEEM CADER, M., SAVELJEVA, S., LONG, K., MUKHOPADHYAY, S., ARASTEH, M., LAWLEY, T. D., DOUGAN, G., BASSETT, A., KARLSEN, T. H., KASER, A. & KANEIDER, N. C. 2019. GPR35 promotes glycolysis, proliferation, and oncogenic signaling by engaging with the sodium potassium pump. *Science Signaling,* 12.
SCHUMACHER, S. M., GAO, E., ZHU, W., CHEN, X., CHUPRUN, J. K., FELDMAN, A. M., G. TESMER, J. J. & KOCH, W. J. 2015. Paroxetine-mediated GRK2 inhibition reverses cardiac dysfunction and remodeling after myocardial infarction. *Science translational medicine,* 7**,** 277ra31-277ra31.

SCHWARCZ, R., BRUNO, J. P., MUCHOWSKI, P. J. & WU, H.-Q. 2012. Kynurenines in the mammalian brain: when physiology meets pathology. *Nature Reviews Neuroscience,* 13**,** 465-477.
SEIBOLD, A., WILLIAMS, B., HUANG, Z.-F., FRIEDMAN, J., MOORE, R. H., KNOLL, B. J. & CLARK, R. B. 2000. Localization of the sites mediating desensitization of the ß2-adrenergic receptor by the GRK pathway. *Molecular pharmacology,* 58**,** 1162-1173.
SHARMIN, O., ABIR, A. H., POTOL, A., ALAM, M., BANIK, J., RAHMAN, A. T., TARANNUM, N., WADUD, R., HABIB, Z. F. & RAHMAN, M. 2020. Activation of GPR35 protects against cerebral ischemia by recruiting monocyte-derived macrophages. *Scientific Reports,* 10**,** 9400.
SHENOY, S. K., DRAKE, M. T., NELSON, C. D., HOUTZ, D. A., XIAO, K., MADABUSHI, S., REITER, E., PREMONT, R. T., LICHTARGE, O. & LEFKOWITZ, R. J. 2006. ß-Arrestin-dependent, G protein-independent ERK1/2 activation by the ß2 adrenergic receptor. *Journal of Biological Chemistry,* 281**,** 1261-1273.
SIEHLER, S. 2009. Regulation of RhoGEF proteins by G12/13-coupled receptors. *British journal of pharmacology,* 158**,** 41-49.
SONG, Z., LU, D., SUN, J., YE, Y., FANG, J., WANG, K., GUO, S., ZHANG, Q., HE, X. & XIE, X. 2023. Discovery of a novel GPR35 agonist with high and equipotent species potency for oral treatment of IBD. *Bioorganic & Medicinal Chemistry,* 96**,** 117511.
SPRANG, S. R., CHEN, Z. & DU, X. 2007. Structural basis of effector regulation and signal termination in heterotrimeric Gα proteins. *Advances in protein chemistry,* 74**,** 1-65.
SRIRAM, K. & INSEL, P. A. 2018. G protein-coupled receptors as targets for approved drugs: how many targets and how many drugs? *Molecular pharmacology,* 93**,** 251-258.
STANDFUSS, J., EDWARDS, P. C., D'ANTONA, A., FRANSEN, M., XIE, G., OPRIAN, D. D. & SCHERTLER, G. F. 2011. The structural basis of agonist-induced activation in constitutively active rhodopsin. *Nature,* 471**,** 656-660.
STEVENS, R. C., CHEREZOV, V., KATRITCH, V., ABAGYAN, R., KUHN, P., ROSEN, H. & WÜTHRICH, K. 2013. The GPCR Network: a large-scale collaboration to determine human GPCR structure and function. *Nature reviews Drug discovery,* 12**,** 25-34.
STRATHMANN, M. P. & SIMON, M. I. 1991. G alpha 12 and G alpha 13 subunits define a fourth class of G protein alpha subunits. *Proceedings of the National Academy of Sciences,* 88**,** 5582-5586.
SULON, S. M. & BENOVIC, J. L. 2021. Targeting G protein–coupled receptor kinases to G protein–coupled receptors. *Current opinion in endocrine and metabolic research,* 16**,** 56-65.
SUN, Y. V., BIELAK, L. F., PEYSER, P. A., TURNER, S. T., SHEEDY, P. F., 2ND, BOERWINKLE, E. & KARDIA, S. L. 2008. Application of machine learning algorithms to predict coronary artery calcification with a sibship-based design. *Genetic Epidemiology,* 32**,** 350-360.
SZCZEPEK, M., BEYRIÈRE, F., HOFMANN, K. P., ELGETI, M., KAZMIN, R., ROSE, A., BARTL, F. J., VON STETTEN, D., HECK, M. & SOMMER, M. E. 2014. Crystal structure of a common GPCR-binding interface for G protein and arrestin. *Nature communications,* 5**,** 4801.
TANG, X.-L., WANG, Y., LI, D.-L., LUO, J. & LIU, M.-Y. 2012. Orphan G protein-coupled receptors (GPCRs): biological functions and potential drug targets. *Acta Pharmacologica Sinica,* 33**,** 363-371.

TANIGUCHI, Y., TONAI-KACHI, H. & SHINJO, K. 2006. Zaprinast, a well-known cyclic guanosine monophosphate-specific phosphodiesterase inhibitor, is an agonist for GPR35. *FEBS Letter,* 580**,** 5003-5008.

TELLER, D. C., OKADA, T., BEHNKE, C. A., PALCZEWSKI, K. & STENKAMP, R. E. 2001. Advances in determination of a high-resolution three-dimensional structure of rhodopsin, a model of G-protein-coupled receptors (GPCRs). *Biochemistry,* 40**,** 7761-7772.

TESMER, V. M., KAWANO, T., SHANKARANARAYANAN, A., KOZASA, T. & TESMER, J. J. 2005. Snapshot of activated G proteins at the membrane: the Gαq-GRK2-Gßγ complex. *Science,* 310**,** 1686-1690.

THAL, D. M., YEOW, R. Y., SCHOENAU, C., HUBER, J. & TESMER, J. J. 2011. Molecular mechanism of selectivity among G protein-coupled receptor kinase 2 inhibitors. *Molecular pharmacology,* 80**,** 294-303.

THIYAGARAJAN, M. M., STRACQUATANIO, R. P., PRONIN, A. N., EVANKO, D. S., BENOVIC, J. L. & WEDEGAERTNER, P. B. 2004. A predicted amphipathic helix mediates plasma membrane localization of GRK5. *Journal of Biological Chemistry,* 279**,** 17989-17995.

THOMPSON, M. D., COLE, D. E., CAPRA, V., SIMINOVITCH, K. A., ROVATI, G. E., BURNHAM, W. M. & RANA, B. K. 2014. Pharmacogenetics of the G protein-coupled receptors. *Pharmacogenomics in Drug Discovery and Development***,** 189-242.

THOMSEN, A. R., PLOUFFE, B., CAHILL III, T. J., SHUKLA, A. K., TARRASCH, J. T., DOSEY, A. M., KAHSAI, A. W., STRACHAN, R. T., PANI, B. & MAHONEY, J. P. 2016. GPCR-G protein-β-arrestin super-complex mediates sustained G protein signaling. *Cell,* 166**,** 907-919.

THORBURN, A. N., MACIA, L. & MACKAY, C. R. 2014. Diet, metabolites, and "western-lifestyle" inflammatory diseases. *Immunity,* 40**,** 833-42.

TOBIN, A. 2008. G-protein-coupled receptor phosphorylation: Where, when and by whom. *British journal of pharmacology,* 153**,** S167-S176.

TSVETANOVA, N. G. & VON ZASTROW, M. 2014. Spatial encoding of cyclic AMP signaling specificity by GPCR endocytosis. *Nature chemical biology,* 10**,** 1061-1065.

TURSKI, M. P., TURSKA, M., PALUSZKIEWICZ, P., PARADA-TURSKA, J. & OXENKRUG, G. F. 2013. Kynurenic acid in the digestive system--new facts, new challenges. *International Journal of Tryptophan Research,* 6**,** IJTR. S12536.

UEHLING, D. E., JOSEPH, B., CHUNG, K. C., ZHANG, A. X., LER, S., PRAKESCH, M. A., PODA, G., GROULEFF, J., AMAN, A. & KIYOTA, T. 2021. Design, synthesis, and characterization of 4-aminoquinazolines as potent inhibitors of the G protein-coupled receptor kinase 6 (GRK6) for the treatment of multiple myeloma. *Journal of medicinal chemistry,* 64**,** 11129-11147.

VARNEY, M. J., STEYAERT, W., COUCKE, P. J., DELANGHE, J. R., UEHLING, D. E., JOSEPH, B., MARCELLUS, R., AL-AWAR, R. & BENOVIC, J. L. 2022. G protein–coupled receptor kinase 6 (GRK6) regulates insulin processing and secretion via effects on proinsulin conversion to insulin. *Journal of Biological Chemistry,* 298.

VENTER, J. C., ADAMS, M. D., MYERS, E. W., LI, P. W., MURAL, R. J., SUTTON, G. G., SMITH, H. O., YANDELL, M., EVANS, C. A. & HOLT, R. A. 2001. The sequence of the human genome. *science,* 291**,** 1304-1351.

VÖGLER, O., BARCELÓ, J. M., RIBAS, C. & ESCRIBÁ, P. V. 2008. Membrane interactions of G proteins and other related proteins. *Biochimica et Biophysica Acta (BBA)-Biomembranes,* 1778**,** 1640-1652.

VULPETTI, A. & BOSOTTI, R. 2004. Sequence and structural analysis of kinase ATP pocket residues. *Il farmaco,* 59**,** 759-765.
WACHTER, S. B. & GILBERT, E. M. 2012. Beta-adrenergic receptors, from their discovery and characterization through their manipulation to beneficial clinical application. *Cardiology,* 122**,** 104-112.
WALCZAK, K., DĄBROWSKI, W., LANGNER, E., ZGRAJKA, W., PIŁAT, J., KOCKI, T., RZESKI, W. & TURSKI, W. A. 2011. Kynurenic acid synthesis and kynurenine aminotransferases expression in colon derived normal and cancer cells. *Scandinavian journal of gastroenterology,* 46**,** 903-912.
WALKER, J., GAINETDINOV, R., FELDMAN, D., MCFAWN, P., CARON, M., LEFKOWITZ, R., PREMONT, R. & FISHER, J. 2004. G protein-coupled receptor kinase 5 regulates airway responses induced by muscarinic receptor activation. *American Journal of Physiology-Lung Cellular and Molecular Physiology,* 286**,** L312-L319.
WANG, D., WANG, W., BING, X., XU, C., QIU, J., SHEN, J., HUANG, J., LI, J., LIU, P. & XIE, B. 2023. GPR35-mediated kynurenic acid sensing contributes to maintenance of gut microbiota homeostasis in ulcerative colitis. *FEBS Open Bio,* 13**,** 1415-1433.
WANG, J., SIMONAVICIUS, N., WU, X., SWAMINATH, G., REAGAN, J., TIAN, H. & LING, L. 2006. Kynurenic acid as a ligand for orphan G protein-coupled receptor GPR35. *Journal of Biological Chemistry,* 281**,** 22021-22028.
WANG, J., CHEN, L., QU, L., LI, K., ZHAO, Y., WANG, Z., LI, Y., ZHANG, X., JIN, Y. & LIANG, X. 2019. Isolation and bioactive evaluation of flavonoid glycosides from Lobelia chinensis Lour using two-dimensional liquid chromatography combined with label-free cell phenotypic assays. *Journal of Chromatography A,* 1601**,** 224-231.
WANG, W., HAN, T., TONG, W., ZHAO, J. & QIU, X. 2018. Overexpression of GPR35 confers drug resistance in NSCLC cells by beta-arrestin/Akt signaling. *Onco Targets and Therapy,* 11**,** 6249-6257.
WEI, H., AHN, S., SHENOY, S. K., KARNIK, S. S., HUNYADY, L., LUTTRELL, L. M. & LEFKOWITZ, R. J. 2003. Independent ß-arrestin 2 and G protein-mediated pathways for angiotensin II activation of extracellular signal-regulated kinases 1 and 2. *Proceedings of the National Academy of Sciences,* 100**,** 10782-10787.
WEI, X., YIN, F., WU, M., XIE, Q., ZHAO, X., ZHU, C., XIE, R., CHEN, C., LIU, M. & WANG, X. 2023. G protein-coupled receptor 35 attenuates nonalcoholic steatohepatitis by reprogramming cholesterol homeostasis in hepatocytes. *Acta Pharmaceutica Sinica B,* 13**,** 1128-1144.
WETTSCHURECK, N. & OFFERMANNS, S. 2005. Mammalian G proteins and their cell type specific functions. *Physiological reviews,* 85**,** 1159-1204.
WHALEN, E. J., RAJAGOPAL, S. & LEFKOWITZ, R. J. 2011. Therapeutic potential of ß-arrestin-and G protein-biased agonists. *Trends in molecular medicine,* 17**,** 126-139.
WOODARD, G. E., JARDIN, I., BERNA-ERRO, A., SALIDO, G. M. & ROSADO, J. A. 2015. Regulators of G-protein-signaling proteins: negative modulators of G-protein-coupled receptor signaling. *International review of cell and molecular biology,* 317**,** 97-183.
WORZFELD, T., WETTSCHURECK, N. & OFFERMANNS, S. 2008. G12/G13-mediated signalling in mammalian physiology and disease. *Trends in pharmacological sciences,* 29**,** 582-589.
WU, B., CHIEN, E., MOL, C., FENALTI, G., LIU, W., KATRITCH, V., ABAGYAN, R. & BROOUN, A. 2010. 2266 Wells P, Bi FC, Hamel DJ, Kuhn P, Handel TM, Cherezov V, Stevens RC. 2267 Structures of the CXCR4 chemokine GPCR

with small-molecule and cyclic peptide 2268 antagonists. *Science,* 330**,** 2269.
WU, X., CHEN, S., YAN, Q., YU, F., SHAO, H., ZHENG, X. & ZHANG, X. 2023a. Gpr35 shapes gut microbial ecology to modulate hepatic steatosis. *Pharmacological Research,* 189**,** 106690.
WU, Y., ZHANG, P., FAN, H., ZHANG, C., YU, P., LIANG, X. & CHEN, Y. 2023b. GPR35 acts a dual role and therapeutic target in inflammation. *Frontiers in Immunology,* 14.
XIANG, Q., ZHOU, D., XIANG, X., LE, X., DENG, C., SUN, R., LI, C., PANG, H., HE, J. & ZHENG, Z. 2023. Neuroglobin plays as tumor suppressor by disrupting the stability of GPR35 in colorectal cancer. *Clinical Epigenetics,* 15**,** 57.
YANG, D., ZHOU, Q., LABROSKA, V., QIN, S., DARBALAEI, S., WU, Y., YULIANTIE, E., XIE, L., TAO, H. & CHENG, J. 2021. G protein-coupled receptors: structure-and function-based drug discovery. *Signal transduction and targeted therapy,* 6**,** 7.
YANG, Y., LU, J. Y., WU, X., SUMMER, S., WHORISKEY, J., SARIS, C. & REAGAN, J. D. 2010. G-protein-coupled receptor 35 is a target of the asthma drugs cromolyn disodium and nedocromil sodium. *Pharmacology,* 86**,** 1-5.
YANG, Z., YANG, F., ZHANG, D., LIU, Z., LIN, A., LIU, C., XIAO, P., YU, X. & SUN, J.-P. 2017. Phosphorylation of G protein-coupled receptors: from the barcode hypothesis to the flute model. *Molecular pharmacology,* 92**,** 201-210.
YE, X. & CHUN, J. 2010. Lysophosphatidic acid (LPA) signaling in vertebrate reproduction. *Trends in Endocrinology & Metabolism,* 21**,** 17-24.
YUE, J., GUO, H., XU, P., MA, J. & WU, Y. 2023. Activation of the GPR35 on ILC2 drives immunosuppression to promote lung cancer progression. *American Journal of Cancer Research,* 13**,** 2426.
ZAMBROWICZ, B. P. & SANDS, A. T. 2003. Knockouts model the 100 best-selling drugs—will they model the next 100? *Nature reviews Drug discovery,* 2**,** 38-51.
ZHANG, D., ZHAO, Q. & WU, B. 2015. Structural studies of G protein-coupled receptors. *Molecules and cells,* 38**,** 836.
ZHANG, J., BARAK, L. S., ANBORGH, P. H., LAPORTE, S. A., CARON, M. G. & FERGUSON, S. S. 1999. Cellular trafficking of G protein-coupled receptor/β-arrestin endocytic complexes. *Journal of Biological Chemistry,* 274**,** 10999-11006.
ZHANG, T., SUO, C., ZHENG, C. & ZHANG, H. 2019. Hypoxia and metabolism in metastasis. *Hypoxia and cancer metastasis***,** 87-95.
ZHANG, Y., SHI, T. & HE, Y. 2021. GPR35 regulates osteogenesis via the Wnt/GSK3beta/beta-catenin signaling pathway. *Biochemical and Biophysical Research Communications,* 556**,** 171-178.
ZHAO, P., SHARIR, H., KAPUR, A., COWAN, A., GELLER, E. B., ADLER, M. W., SELTZMAN, H. H., REGGIO, P. H., HEYNEN-GENEL, S., SAUER, M., CHUNG, T. D., BAI, Y., CHEN, W., CARON, M. G., BARAK, L. S. & ABOOD, M. E. 2010. Targeting of the orphan receptor GPR35 by pamoic acid: a potent activator of extracellular signal-regulated kinase and beta-arrestin2 with antinociceptive activity. *Molecular Pharmacology,* 78**,** 560-568.
ZHOU, X. E., HE, Y., DE WAAL, P. W., GAO, X., KANG, Y., VAN EPS, N., YIN, Y., PAL, K., GOSWAMI, D. & WHITE, T. A. 2017. Identification of phosphorylation codes for arrestin recruitment by G protein-coupled receptors. *Cell,* 170**,** 457-469. e13.
ZHUO, S., CLEMENS, J., HAKES, D., BARFORD, D. & DIXON, J. 1993. Expression, purification, crystallization, and biochemical characterization of a

recombinant protein phosphatase. *Journal of Biological Chemistry,* 268**,** 17754-17761.